



University of Venda
Creating Future Leaders

FACULTY OF SCIENCE, ENGINEERING AND AGRICULTURE

**COMPUTATIONAL AND ADSORPTION INVESTIGATION OF
SOME QUINOXALINE DERIVATIVES ON SELECTED METALS IN
ACIDIC MEDIA**

GIFT MOSES MASUKU

B.Sc (UNIVEN), B.Sc (Hons) (UNIVEN)

A dissertation submitted in fulfilment of the requirements of the degree of Master of Science
in the

DEPARTMENT OF CHEMISTRY

Supervisor

Dr. L.C. MURULANA

Co-supervisor

Prof. M.M. KABANDA

Co-supervisor

Prof. W. NXUMALO

2022

DECLARATION

I **Gift Moses Masuku** declare that this research project in this dissertation is the results of the work carried out originally by me under the guidance and supervision of Dr L.C. Murulana, Prof. M.M Kabanda, and Prof. W. Nxumalo. This work is being I fulfillment of Master of Science in Chemistry at the University of Venda and has not been submitted before for any degree or examination at any other university for any degree and examination. The information derived from literature have been appropriately acknowledged in text and a list of references provided.

Date: ...6/5/2022.....

Signature



DEDICATION

This dissertation is dedicated to **MYSELF**

TABLE OF CONTENTS

NO	CONTENTS	PAGE NO
	Acknowledgements	I
	Abstract	ii
	List of Abbreviations	iv
	List of figures	viii
	List of tables	xxvii
1	INTRODUCTION	1
1.1	Background of the study	2
1.2	Justification of the study	3
1.3	Problem statement	4
1.4	Aims and Objectives of the Study	5
2	LITERATURE REVIEW	6
2.1	Definition of Corrosion	7
2.1.1	The electrochemical origin of corrosion	8
2.1.2	Classification of corrosion	13
2.1.3	Corrosive environment	15
2.1.4	Forms of corrosion	19
2.1.5	Corrosion thermodynamics	30
2.1.6	Corrosion kinetics	35
2.1.7	Rate of corrosion	38
2.1.8	Effects of corrosion	45
2.2	Corrosion control measures	49
2.2.1	Material selection	49
2.2.2	Proper design	49
2.2.3	Protection coating	50

2.2.4	Cathodic protection	51
2.2.5	Corrosion inhibitors	52
2.3	Corrosion inhibitors and inhibition mechanism	53
2.3.1	Definition of corrosion inhibitors	53
2.3.2	Classification of corrosion inhibitors	54
2.3.3	The synergistic effects	57
2.3.4	Inhibition mechanism	57
2.3.5	Adsorption isotherm	59
2.4	Corrosion of metals	62
2.4.1	Aluminium (Al)	62
2.4.2	Zinc (Zn)	64
2.4.3	Mild steel (MS)	67
2.5	Quinoxalines	68
2.5.1	Properties of quinoxalines	69
2.5.2	Development and synthesis of quinoxalines	69
2.5.3	Quinoxalines used as corrosion inhibitors	71
2.6	Molecular simulations techniques	72
2.6.1	Introduction	72
2.6.2	The Schrödinger equation	73
2.6.3	Density Function Theory (DFT)	76
2.6.4	Software program selected for performing calculation: Material studio	79
3	EXPERIMENTAL DETAILS	82
3.1	Metal specimens	83
3.2	Preparation of solutions	83
3.3	Other equipment and apparatus utilized	84
3.4	Inhibitors used	84
3.5	Electrochemical analysis	87
3.5.1	Host computer	88
3.5.2	Corrosion cell	88

3.5.3	Potentiodynamic Polarization	90
3.5.4	Electrochemical Impedance Spectroscopy (EIS)	91
3.6	Atomic Absorption Spectroscopy (AAS)	92
3.7	Fourier Transform Infrared Spectroscopy (FTIR)	93
3.8	Computational analysis	94
4	RESULTS AND DISCUSSION	95
4.1	Blank tests	96
4.1.1	Weight loss in the absence of corrosion inhibitors	96
4.2	Mild Steel	103
4.2.1	Weight in the absence and presence of corrosion inhibitors	103
4.2.2	Corrosion rate and inhibition efficiency	111
4.2.3	Impact of temperature and kinetic parameters	125
4.2.4	Adsorption isotherms and thermodynamic parameters	136
4.2.5	Potentiodynamic Polarization (PDP)	154
4.2.6	Electrochemical Impedance Spectroscopy (EIS)	164
4.2.7	Atomic absorption spectroscopy (AAS)	176
4.2.8	Fourier Transform Infrared Spectroscopy (FTIR)	179
4.3	Zinc	185
4.3.1	Weight in the absence and presence of corrosion inhibitors	185
4.3.2	Corrosion rate and inhibition efficiency	193
4.3.3	Impact of temperature and kinetic parameters	207
4.3.4	Adsorption isotherms and thermodynamic parameters	217
4.3.5	Potentiodynamic Polarization (PDP)	234
4.3.6	Electrochemical Impedance Spectroscopy (EIS)	244
4.3.7	Atomic absorption spectroscopy (AAS)	256
4.3.8	Fourier Transform Infrared Spectroscopy (FTIR)	258

4.4	Aluminium	263
4.4.1	Potentiodynamic Polarization (PDP)	263
4.4.2	Electrochemical Impedance Spectroscopy (EIS)	266
4.4.3	Adsorption isotherm	272
5	THEORETICAL ANALYSIS	277
5.1	Validation of the method	278
5.2	Results of the study on the interaction between selected quinoxaline derivatives on the Al surface	282
5.3	Results of the study on the interaction between selected quinoxaline derivatives on the Zn surface	286
6	CONCLUSSIONS AND RECOMMENDATIONS	292
6.1	Conclusions	293
6.2	Recommendation	295
	REFERENCES	296

ACKNOWLEDGEMENTS

All the praises, thanks and adorations are due to God, the Almighty, for His shower of blessings throughout the course and completion of this research study.

Throughout the writing of this work, I have received tremendous deal of support. I am overwhelmed in all humbleness and gratefulness to acknowledge my depth of gratitude to all those who have offered their assistance in putting these ideas into something concrete. I would like to express my deep and sincere gratitude to my supervisor, and mentor **Dr. L.C. Murulana**, who offered me the golden opportunity to do this wonderful study. Sir! You offered advice and encouragement with a perfect blend of insight and humor. I'm proud, and grateful for my time working you. You are the best supervisor of all time.

I owe a deep sense of thanks to my co-supervisor **Prof. M.M. Kabanda** for his keen interest in me at every stage of this research and sharing his deep knowledge of computational chemistry. I acknowledge **Prof. W. Nxumalo** for his expertise in organic synthesis. My special thanks are also due **Mr. T. Nesane** who was also instrumental in performing a number of experiments, gathering and arranging data prior to the completion of this study. Thank you whoNesane, I will never forget you. I acknowledge the support and contributions of all members of Dr. Murulana's research group (Univen corrosion science research group). I would like to acknowledge my former physics HOD **Dr. N.E. Maluta** for always welcoming me in us office whenever we needed help, thank you Sir!

Enormous heartfelt gratitude is also sent to my brother, colleague, and friend **Consol Kubayi** for all of your support you have contributed to my life and into this work. Thank you buddy, may God forever bless you. All the members of "Place called home", I am humbled with your support and encouragements, I thank you all. I pray to God that our little but humongous home should never crack its foundation. Any attempt at any level can never be satisfactorily complete without the support of my partner, **Mabatho**, special thanks to you for not only be emotionally and spiritually supportive but you were also hands-on in this work from day one. I thank you so much "sweet". To my best friend **Fortune Ravhuanzwo**, my thanks are so inferior as compared to you great controbution not only supprting me throughout this study but my life at large, I really appreciate you Nkabi'yam. Lastly, I would like to thank my family for being patient and supporting throughout this whole study.

ABSTRACT

This research study reports the inhibition of mild steel (MS), zinc (Zn) in 1.0 M HCl and 1.0 M H₂SO₄, and the inhibition of aluminium (Al) in 0.5 M HCl by three selected quinoxaline derivatives namely, quinoxalone-6-carboxylic acid (Q6CA), 3-hydroxy-2-quinoxaline carboxylic acid (H2QCA), and Methyl quinoxaline-6-carboxylate (MQ6CA) at 303 – 333 K. The corrosion inhibition characteristics including corrosion mechanism, corrosion inhibition efficiencies, and inhibitor-metal adsorption/desorption behavior were analyzed using gravimetric analysis, electrochemical impedance spectroscopy (EIS), and potentiodynamic polarization (PDP). Fourier transform infrared spectroscopy (FTIR) was utilized to give more insight into the functional groups that formed or disappeared during the adsorption/desorption of the studied quinoxaline molecules on the metal surfaces. Atomic absorption spectroscopy (AAS) was employed to determine the amount of MS and Zn ions that remained in the solutions after gravimetric analysis. Density functional theory (DFT) was utilized to compute all theoretical studies.

The gravimetric analysis for mild steel show that the inhibition efficiency increased with the increase in the concentrations of the studied quinoxalines and decreased with the increase in temperature of the corrosive environment, whereas for zinc the inhibition efficiency increased with the increase in the temperature of the corrosive environment for all the quinoxaline compounds. The compounds inhibited the mild steel and zinc corrosion by adsorption on the active sites on the surfaces without altering the mechanism of the adsorption process. The studied compounds obeyed the Langmuir isotherm, and this isotherm indicated the adsorption mechanism which was mixed-typed adsorption with chemisorption dominant for both mild and zinc. The trend of inhibition efficiency for both mild steel and zinc varied in the order: MQ6CA>Q6CA>H2QCA.

PDP results indicated that the studied quinoxalines shifted the polarization curves towards the region of low current densities as compared to the uninhibited system, which suggested that the inhibitor molecules reduced the anodic dissolution of mild steel, zinc, and aluminium and also suppressed the hydrogen evolution reaction. The obtained potentiodynamic polarization parameters revealed that all three inhibitors studied acted as mixed-type inhibitors, that is, anodic and cathodic inhibitor that protected the mild steel, zinc, and aluminium surfaces through spontaneous adsorption. Moreover, the increase in the concentration of the inhibitors increased the inhibition efficiency.

EIS results showed that the studied quinoxalines retarded the rate of corrosion of mild steel, zinc, and aluminium surfaces through the adsorption process. For all the investigated metals the charge transfer resistance values increased with the increase in concentration of the inhibitors.

The AAS analysis revealed a decrease in the concentration of iron and zinc ions in the presence of the studied inhibitors as compared to the blank solutions. The inhibition efficiency increased with an increase in the concentration of the inhibitors. The FTIR spectra confirmed the formation of the inhibitor-Fe²⁺ and inhibitor-Zn²⁺ complexes. The obtained adsorption energies from the DFT results revealed that the studied quinoxalines exhibit a mixed-type adsorption mechanism, with the domination of the chemisorption process.

Keywords: Corrosion inhibition efficiency, adsorption/desorption, quinoxalines, Langmuir isotherm, chemisorption

LIST OF ABBREVIATIONS

PGM	Platinum and gold group metals
MS	Mild steel
Zn	Zinc
Al	Aluminium
GDP	Gross Domestic Product
Q6CA	Quinoxaline-6-carboxylic acid
H2QCA	3-hydroxy-2-quinoxaline carboxylic acid
MQ6CA	Methyl quinoxaline-6-carboxylate
PDP	Potentiodynamic polarization
EIS	Electrochemical Impedance Spectroscopy
FTIR	Fourier Transform Infrared Spectroscopy
AAS	Atomic Absorption Spectroscopy
DFT	Density functional theory
FAC	Flow-assisted corrosion
SO₂	Sulfur oxide
HCl	Hydrochloric Acid
H₂SO₄	Sulfuric acid
US	United states
SCC	Stress corrosion cracking
SHE	Standard hydrogen electrode
emf	Electromotive series
LPR	Linear Polarization Resistance
CPR	Control Penetration Rate
ipy	Inch penetration/year

mpy	Mils penetration/year
CP	Cathodic protection
OCP	Open Circuit Potential
NANO₂	Sodium nitrite
VPIs	Volatile corrosion inhibitors
MM	Molecular mechanics
MMFF	Merck molecular force field
UFF	Universal force field
MNDO	Modified Neglect of Diatomic Differential
AM1	Austin model 1
PM3	Parameterized model number 3
LDA	Local density approximation
LSDA	Local spin density approximation
GGA	Generalized gradient approximation
PBE	Burke-Enzerhof
BLYP	Parr exchange
HF	Hartree-Fock
CASTEP	Cambridge Serial Total Energy Package
DFTB+	Density Functional-based Tight Binding
ONETEP	Order-N Electronic Total Energy Package
IUPAC	International Union of Pure and Applied Chemistry
IE	Inhibition efficiency
WE	Working electrode
RE	Reference electrode
OCP	Open Circuit Potential
DNP	Double numeric plus polarization

KI	Potassium iodide
C_R	Corrosion rate
E_a	Activation Energy
R_P	Polarization resistance
C_{dl}	Double layer capacitance
CPE	Constant phase element
R_{ct}	Charge transfer resistance
R_s	Solution resistance
GFAAS	Graphite furnace atomic absorption spectroscopy
MQ6CA-MS	Methyl quinoxaline-6-carboxylate-Mild steel
Q6CA-MS	Quinoxaline-6-carboxylic acid-Mild steel
H2QCA-MS	3-hydroxy-2-quinoxaline carboxylic acid-Mild steel
MQ6CA-Zn	Methyl quinoxaline-6-carboxylate-Zinc
Q6CA-Zn	Quinoxaline-6-carboxylic acid-Zinc
H2QCA-Zn	3-hydroxy-2-quinoxaline carboxylic acid-Zinc

LIST OF FIGURES

No	DESCRIPTION	PAGE No
2.1	Pits resulted from corrosion of carbon metal	7
2.2	Illustration of the processes involved in metallurgy	8
2.3	Schematic representation of an anodic reaction	9
2.4	Schematic representation of a cathodic reaction	10
2.5	Heterogeneous surface of metal crystal showing different types of imperfections	12
2.6	Schematic representation of the overall corrosion process of iron metal cathodic reaction in an acidic aqueous environment	12
2.7	A general scheme for the classification of corrosion	14
2.8	Major constituents of sea water	18
2.9	An example of uniform corrosion	20
2.10	Shapes associated with pitting corrosion	21
2.11	corrosion of dissimilar metals in seawater	23
2.12	An example of SCC	24
2.13	Representation of crevice corrosion	25
2.14	The failure at a pipe elbow due to erosion-corrosion	26
2.15	An example of fretting corrosion	27
2.16	An example of selective corrosion	28
2.17	schematic diagram of the SHE	32
2.18	Pourbaix diagram for the Fe–H ₂ O system at 398 K showing (a) indicating three different corrosion regions (b) considering Fe, Fe ₃ O ₄ , and Fe ₂ O ₃ as the only solid substances	34
2.19	Schematic Evans diagram for the corrosion of metal M by an acid	37
2.20	Effect of temperature on open and closed corrosion system iron in water	41

	containing dissolved oxygen	
2.21	The effect of pH on the measure corrosion rate of aluminum and iron	42
2.22	The effect of relative humidity on the corrosion rate of iron	43
2.23	Different states of an oxide-surface film behavior as liquid velocity or surface shear stresses are increased	44
2.24	Illustration of (a) a dental implant and (b) a knee implant using metals	47
2.25	1984 India chemical plant after exploding	48
2.26	A picture of ferry “Princess Ashika” under the sea	48
2.27	Sacrificial protection offered by zinc coating to steel surface	50
2.28	An example of impress-current cathodic protection system setup	52
2.29	A schematic representation of the Al metal with the oxide film formed on the surface	63
2.30	Schematic representation of Al corrosion mechanism in aqueous medium	64
2.31	List of various applications of zinc and its alloys employed as protective coating	65
2.32	Schematic representation of Zn corrosion mechanism in the solution of HCl	66
2.33	Molecular structure of quinoxaline	68
2.34	Structures isomeric with quinoxaline	68
3.1	System Used for the gravimetric analysis	86
3.2	Typical electrochemical experiment set-up showing the electrochemical glass cell and electrodes	87
3.3	The picture of a typical a metal specimen (WE) used for the experiments in this study	88
3.4	The Struers Labosystem instrument used for pre-cleaning metal specimens	88
3.5	Complete system set up for the electrochemical experiments	90
3.6	Atomic absorption spectrometer utilized in this study	91

3.7	Fourier transform infrared spectrometer utilized in this study	92
4.1	The plot of weight loss of zinc as a function of the concentration of HCl in the absence of a corrosion inhibitor	96
4.2	The plot of weight loss of mild steel as a function of the concentration of HCl in the absence of a corrosion inhibitor	96
4.3	The plot of weight loss of zinc as a function of the concentration of H ₂ SO ₄ in the absence of a corrosion inhibitor	97
4.4	The plot of weight loss of mild steel as a function of the concentration of H ₂ SO ₄ in the absence of a corrosion inhibitor	97
4.5	The graph showing the weight loss measurements of mild steel in the absence and presence of MQ6CA in 1.0 M HCl	102
4.6	The graph showing the weight loss measurements of mild steel in the absence and presence of Q6CA in 1.0 M HCl	103
4.7	The graph showing the weight loss measurements of mild steel in the absence and presence of H2QCA without KI in 1.0 M HCl	103
4.8	The graph showing the weight loss measurements of mild steel in the absence and presence of H2QCA with KI in 1.0 M HCl	104
4.9	The graph showing the weight loss measurements of mild steel in the absence and presence of MQ6CA in 1.0 M H ₂ SO ₄	106
4.10	The graph showing the weight loss measurements of mild steel in the absence and presence of Q6CA in 1.0 M H ₂ SO ₄	106
4.11	The graph showing the weight loss measurements of mild steel in the absence and presence of H2QCA without KI in 1.0 M H ₂ SO ₄	107
4.12	The graph showing the weight loss measurements of mild steel in the absence and presence of H2QCA with KI in 1.0 M H ₂ SO ₄	107
4.13	The variation of percentage inhibition efficiency with various concentration of MQ6CA at various temperatures in 1.0 M HCl	110
4.14	The variation of percentage inhibition efficiency with various concentration	111

	of Q6CA at various temperatures in 1.0 M HCl	
4.15	The variation of percentage inhibition efficiency with various concentration of H2QCA without KI at various temperatures in 1.0 M HCl	111
4.16	The variation of percentage inhibition efficiency with various concentration of H2QCA with KI at various temperatures in 1.0 M HCl	112
4.17	The variation of percentage inhibition efficiency with various concentration of MQ6CA at various temperatures in 1.0 M H ₂ SO ₄	116
4.18	The variation of percentage inhibition efficiency with various concentration of Q6CA at various temperatures in 1.0 M H ₂ SO ₄	117
4.19	The variation of percentage inhibition efficiency with various concentration of H2QCA without KI at various temperatures in 1.0 M H ₂ SO ₄	117
4.20	The variation of percentage inhibition efficiency with various concentration of H2QCA with KI at various temperatures in 1.0 M H ₂ SO ₄	118
4.21	Arrhenius plots for mild steel corrosion in 1.0 M HCl solution in the absence and presence of different concentrations of MQ6CA	125
4.22	Arrhenius plots for mild steel corrosion in 1.0 M HCl solution in the absence and presence of different concentrations of Q6CA	125
4.23	Arrhenius plots for mild steel corrosion in 1.0 M HCl solution in the absence and presence of different concentrations of H2QCA with KI	126
4.24	Arrhenius plots for mild steel corrosion in 1.0 M H ₂ SO ₄ solution in the absence and presence of different concentrations of MQ6CA	126
4.25	Arrhenius plots for mild steel corrosion in 1.0 M H ₂ SO ₄ solution in the absence and presence of different concentrations of Q6CA	127
4.26	Arrhenius plots for mild steel corrosion in 1.0 M H ₂ SO ₄ solution in the absence and presence of different concentrations of H2QCA with KI	127
4.27	Transition state plots for mild steel corrosion in 1.0 M HCl solution in the absence and presence of different concentrations of MQ6CA	128
4.28	Transition state plots for mild steel corrosion in 1.0 M HCl solution in the	129

	absence and presence of different concentrations of Q6CA	
4.29	Transition state plots for mild steel corrosion in 1.0 M HCl solution in the absence and presence of different concentrations of H2QCA with KI	129
4.30	Transition state plots for mild steel corrosion in 1.0 M H ₂ SO ₄ solution in the absence and presence of different concentrations of MQ6CA	130
4.31	Transition state plots for mild steel corrosion in 1.0 M H ₂ SO ₄ solution in the absence and presence of different concentrations of Q6CA	130
4.32	Transition state plots for mild steel corrosion in 1.0 M H ₂ SO ₄ solution in the absence and presence of different concentrations of H2QCA with KI	131
4.33	Langmuir adsorption isotherm plot for the adsorption of various concentrations of MQ6CA on the surface of mild steel in 1.0 M HCl at various temperatures	137
4.34	Langmuir adsorption isotherm plot for the adsorption of various concentrations of Q6CA on the surface of mild steel in 1.0 M HCl at various temperatures	137
4.35	Langmuir adsorption isotherm plot for the adsorption of various concentrations of H2QCA with KI on the surface of mild steel in 1.0 M HCl at various temperatures	138
4.36	Frumkin adsorption isotherm plot for the adsorption of various concentrations of MQ6CA on the surface of mild steel in 1.0 M HCl at various temperatures	138
4.37	Frumkin adsorption isotherm plot for the adsorption of various concentrations of Q6CA on the surface of mild steel in 1.0 M HCl at various temperatures	139
4.38	Frumkin adsorption isotherm plot for the adsorption of various concentrations of H2QCA with KI on the surface of mild steel in 1.0 M HCl at various temperatures	139
4.39	Freundlich adsorption isotherm plot for the adsorption of various concentrations of MQ6CA on the surface of mild steel in 1.0 M HCl at	140

	various temperatures	
4.40	Freundlich adsorption isotherm plot for the adsorption of various concentrations of Q6CA on the surface of mild steel in 1.0 M HCl at various temperatures	140
4.41	Freundlich adsorption isotherm plot for the adsorption of various concentrations of H2QCA with KI on the surface of mild steel in 1.0 M HCl at various temperatures	141
4.42	Temkin adsorption isotherm plot for the adsorption of various concentrations of MQ6CA on the surface of mild steel in 1.0 M HCl at various temperatures	141
4.43	Temkin adsorption isotherm plot for the adsorption of various concentrations of Q6CA on the surface of mild steel in 1.0 M HCl at various temperatures	142
4.44	Temkin adsorption isotherm plot for the adsorption of various concentrations of H2QCA with KI on the surface of mild steel in 1.0 M HCl at various temperatures	142
4.45	Langmuir adsorption isotherm plot for the adsorption of various concentrations of MQ6CA on the surface of mild steel in 1.0 M H ₂ SO ₄ at various temperatures	144
4.46	Langmuir adsorption isotherm plot for the adsorption of various concentrations of Q6CA on the surface of mild steel in 1.0 M H ₂ SO ₄ at various temperatures	144
4.47	Langmuir adsorption isotherm plot for the adsorption of various concentrations of H2QCA with KI on the surface of mild steel in 1.0 M H ₂ SO ₄ at various temperatures	145
4.48	Frumkin adsorption isotherm plot for the adsorption of various concentrations of MQ6CA on the surface of mild steel in 1.0 M H ₂ SO ₄ at various temperatures	145
4.49	Frumkin adsorption isotherm plot for the adsorption of various	146

	concentrations of Q6CA on the surface of mild steel in 1.0 M H ₂ SO ₄ at various temperatures	
4.50	Frumkin adsorption isotherm plot for the adsorption of various concentrations of H ₂ QCA with KI on the surface of mild steel in 1.0 M H ₂ SO ₄ at various temperatures	146
4.51	Freundlich adsorption isotherm plot for the adsorption of various concentrations of MQ6CA on the surface of mild steel in 1.0 M H ₂ SO ₄ at various temperatures	147
4.52	Freundlich adsorption isotherm plot for the adsorption of various concentrations of Q6CA on the surface of mild steel in 1.0 M H ₂ SO ₄ at various temperatures	147
4.53	Freundlich adsorption isotherm plot for the adsorption of various concentrations of H ₂ QCA with KI on the surface of mild steel in 1.0 M H ₂ SO ₄ at various temperatures	148
4.54	Temkin adsorption isotherm plot for the adsorption of various concentrations of MQ6CA on the surface of mild steel in 1.0 M H ₂ SO ₄ at various temperatures	148
4.55	Temkin adsorption isotherm plot for the adsorption of various concentrations of Q6CA on the surface of mild steel in 1.0 M H ₂ SO ₄ at various temperatures	149
4.56	Temkin adsorption isotherm plot for the adsorption of various concentrations of H ₂ QCA with KI on the surface of mild steel in 1.0 M H ₂ SO ₄ at various temperatures	149
4.57	Tafel plots for mild steel in 1.0 M HCl in the absence and presence of various concentrations of MQ6CA at 303 K	154
4.58	Tafel plots for mild steel in 1.0 M HCl in the absence and presence of various concentrations of Q6CA at 303 K	154
4.59	Tafel plots for mild steel in 1.0 M HCl in the absence and presence of various concentrations of H ₂ QCA without KI at 303 K	155

4.60	Tafel plots for mild steel in 1.0 M HCl in the absence and presence of various concentrations of H ₂ QCA with KI at 303 K	155
4.61	Tafel plots for mild steel in 1.0 M H ₂ SO ₄ in the absence and presence of various concentrations of MQ6CA at 303 K	158
4.62	Tafel plots for mild steel in 1.0 M H ₂ SO ₄ in the absence and presence of various concentrations of Q6CA at 303 K	158
4.63	Tafel plots for mild steel in 1.0 M H ₂ SO ₄ in the absence and presence of various concentrations of H ₂ QCA without KI at 303 K	159
4.64	Tafel plots for mild steel in 1.0 M H ₂ SO ₄ in the absence and presence of various concentrations of H ₂ QCA with KI at 303 K	159
4.65	Nyquist plot of mild steel in 1.0 M HCl in the presence and absence of various concentrations of MQ6CA	164
4.66	Bode plot of mild steel in 1.0 M HCl in the presence and absence of various concentrations of MQ6CA	164
4.67	Nyquist plot of mild steel in 1.0 M HCl in the presence and absence of various concentrations of Q6CA	165
4.68	Bode plot of mild steel in 1.0 M HCl in the presence and absence of various concentrations of Q6CA	165
4.69	Nyquist plot of mild steel in 1.0 M HCl in the presence and absence of various concentrations of H ₂ QCA without KI	166
4.70	Nyquist plot of mild steel in 1.0 M HCl in the presence and absence of various concentrations of H ₂ QCA with KI	167
4.71	Bode plot of mild steel in 1.0 M HCl in the presence and absence of various concentrations of H ₂ QCA with KI	167
4.72	Nyquist plot of mild steel in 1.0 M H ₂ SO ₄ in the presence and absence of various concentrations of MQ6CA	168
4.73	Bode plot of mild steel in 1.0 M H ₂ SO ₄ in the presence and absence of various concentrations of MQ6CA	168
4.74	Nyquist plot of mild steel in 1.0 M H ₂ SO ₄ in the presence and absence of	170

	various concentrations of Q6CA	
4.75	Bode plot of mild steel in 1.0 M H ₂ SO ₄ in the presence and absence of various concentrations of Q6CA	170
4.76	Nyquist plot of mild steel in 1.0 M H ₂ SO ₄ in the presence and absence of various concentrations of H ₂ QCA without KI	171
4.77	Nyquist plot of mild steel in 1.0 M H ₂ SO ₄ in the presence and absence of various concentrations of H ₂ QCA with KI	172
4.78	Bode plot of mild steel in 1.0 M H ₂ SO ₄ in the presence and absence of various concentrations of H ₂ QCA with KI	172
4.79	Equivalent circuit utilized to fit the impedance spectra obtained for mild steel corrosion in 1.0 M HCl and 1.0 M H ₂ SO ₄ in the absence and presence of various concentrations of the studied quinoxalines	174
4.80	Calibration curve for mild steel	176
4.81	FTIR spectra of pure MQ6CA and the adsorption film formed on mild steel surface in 1.0 M HCl in the presence of MQ6CA	178
4.82	FTIR spectra of pure Q6CA and the adsorption film formed on mild steel surface in 1.0 M HCl in the presence of Q6CA	179
4.83	FTIR spectra of pure H ₂ QCA and the adsorption film formed on mild steel surface in 1.0 M HCl in the presence of H ₂ QCA	179
4.84	FTIR spectra of pure MQ6CA and the adsorption film formed on mild steel surface in 1.0 M H ₂ SO ₄ in the presence of MQ6CA	180
4.85	FTIR spectra of pure Q6CA and the adsorption film formed on mild steel surface in 1.0 M H ₂ SO ₄ in the presence of Q6CA	181
4.86	FTIR spectra of pure H ₂ QCA and the adsorption film formed on mild steel surface in 1.0 M H ₂ SO ₄ in the presence of H ₂ QCA	181
4.87	The graph showing the weight loss measurements of zinc in the absence and presence of MQ6CA in 1.0 M HCl	184
4.88	The graph showing the weight loss measurements of zinc in the absence	185

	and presence of Q6CA in 1.0 M HCl	
4.89	The graph showing the weight loss measurements of zinc in the absence and presence of H ₂ QCA without KI in 1.0 M HCl	185
4.90	The graph showing the weight loss measurements of zinc in the absence and presence of H ₂ QCA with KI in 1.0 M HCl	186
4.91	The graph showing the weight loss measurements of zinc in the absence and presence of MQ ₆ CA in 1.0 M H ₂ SO ₄	188
4.92	The graph showing the weight loss measurements of zinc in the absence and presence of Q ₆ CA in 1.0 M H ₂ SO ₄	188
4.93	The graph showing the weight loss measurements of zinc in the absence and presence of H ₂ QCA without KI in 1.0 M H ₂ SO ₄	189
4.94	The graph showing the weight loss measurements of zinc in the absence and presence of H ₂ QCA with KI in 1.0 M H ₂ SO ₄	189
4.95	The variation of percentage inhibition efficiency with various concentration of MQ ₆ CA at various temperatures in 1.0 M HCl	192
4.96	The variation of percentage inhibition efficiency with various concentration of Q ₆ CA at various temperatures in 1.0 M HCl	193
4.97	The variation of percentage inhibition efficiency with various concentration of H ₂ QCA without KI at various temperatures in 1.0 M HCl	193
4.98	The variation of percentage inhibition efficiency with various concentration of H ₂ QCA with KI at various temperatures in 1.0 M HCl	194
4.99	The variation of percentage inhibition efficiency with various concentration of MQ ₆ CA at various temperatures in 1.0 M H ₂ SO ₄	198
4.100	The variation of percentage inhibition efficiency with various concentration of Q ₆ CA at various temperatures in 1.0 M H ₂ SO ₄	199
4.101	The variation of percentage inhibition efficiency with various concentration of H ₂ QCA without KI at various temperatures in 1.0 M H ₂ SO ₄	199
4.102	The variation of percentage inhibition efficiency with various concentration	200

	of H ₂ QCA with KI at various temperatures in 1.0 M H ₂ SO ₄	
4.103	Arrhenius plots for zinc corrosion in 1.0 M HCl solution in the absence and presence of different concentrations of MQ6CA	206
4.104	Arrhenius plots for zinc corrosion in 1.0 M HCl solution in the absence and presence of different concentrations of Q6CA	207
4.105	Arrhenius plots for zinc corrosion in 1.0 M HCl solution in the absence and presence of different concentrations of H ₂ QCA with KI	207
4.106	Arrhenius plots for zinc corrosion in 1.0 M H ₂ SO ₄ solution in the absence and presence of different concentrations of MQ6CA	208
4.107	Arrhenius plots for zinc corrosion in 1.0 M H ₂ SO ₄ solution in the absence and presence of different concentrations of Q6CA	208
4.108	Arrhenius plots for zinc corrosion in 1.0 M H ₂ SO ₄ solution in the absence and presence of different concentrations of H ₂ QCA with KI	209
4.109	Transition state plots for zinc corrosion in 1.0 M HCl solution in the absence and presence of different concentrations of MQ6CA	210
4.110	Transition state plots for zinc corrosion in 1.0 M HCl solution in the absence and presence of different concentrations of Q6CA	210
4.111	Transition state plots for zinc corrosion in 1.0 M HCl solution in the absence and presence of different concentrations of H ₂ QCA with KI	211
4.112	Transition state plots for zinc corrosion in 1.0 M H ₂ SO ₄ solution in the absence and presence of different concentrations of MQ6CA	211
4.113	Transition state plots for zinc corrosion in 1.0 M H ₂ SO ₄ solution in the absence and presence of different concentrations of Q6CA	212
4.114	Transition state plots for zinc corrosion in 1.0 M H ₂ SO ₄ solution in the absence and presence of different concentrations of H ₂ QCA with KI	212
4.115	Langmuir adsorption isotherm plot for the adsorption of various concentrations of MQ6CA on the surface of zinc in 1.0 M HCl at various temperatures	216

4.116	Langmuir adsorption isotherm plot for the adsorption of various concentrations of Q6CA on the surface of zinc in 1.0 M HCl at various temperatures	217
4.117	Langmuir adsorption isotherm plot for the adsorption of various concentrations of H2QCA with KI on the surface of zinc in 1.0 M HCl at various temperatures	217
4.118	Frumkin adsorption isotherm plot for the adsorption of various concentrations of MQ6CA on the surface of zinc in 1.0 M HCl at various temperatures	218
4.119	Frumkin adsorption isotherm plot for the adsorption of various concentrations of Q6CA on the surface of zinc in 1.0 M HCl at various temperatures	218
4.120	Frumkin adsorption isotherm plot for the adsorption of various concentrations of H2QCA with KI on the surface of zinc in 1.0 M HCl at various temperatures	219
4.121	Freundlich adsorption isotherm plot for the adsorption of various concentrations of MQ6CA on the surface of zinc in 1.0 M HCl at various temperatures	219
4.122	Freundlich adsorption isotherm plot for the adsorption of various concentrations of Q6CA on the surface of zinc in 1.0 M HCl at various temperatures	220
4.123	Freundlich adsorption isotherm plot for the adsorption of various concentrations of H2QCA with KI on the surface of zinc in 1.0 M HCl at various temperatures	220
4.124	Temkin adsorption isotherm plot for the adsorption of various concentrations of MQ6CA on the surface of zinc in 1.0 M HCl at various temperatures	221
4.125	Temkin adsorption isotherm plot for the adsorption of various concentrations of Q6CA on the surface of zinc in 1.0 M HCl at various	221

	temperatures	
4.126	Temkin adsorption isotherm plot for the adsorption of various concentrations of H ₂ QCA with KI on the surface of zinc in 1.0 M HCl at various temperatures	222
4.127	Langmuir adsorption isotherm plot for the adsorption of various concentrations of MQ ₆ CA on the surface of zinc in 1.0 M H ₂ SO ₄ at various temperatures	224
4.128	Langmuir adsorption isotherm plot for the adsorption of various concentrations of Q ₆ CA on the surface of zinc in 1.0 M H ₂ SO ₄ at various temperatures	224
4.129	Langmuir adsorption isotherm plot for the adsorption of various concentrations of H ₂ QCA with KI on the surface of zinc in 1.0 M H ₂ SO ₄ at various temperatures	225
4.130	Frumkin adsorption isotherm plot for the adsorption of various concentrations of MQ ₆ CA on the surface of zinc in 1.0 M H ₂ SO ₄ at various temperatures	225
4.131	Frumkin adsorption isotherm plot for the adsorption of various concentrations of Q ₆ CA on the surface of zinc in 1.0 M H ₂ SO ₄ at various temperatures	226
4.132	Frumkin adsorption isotherm plot for the adsorption of various concentrations of H ₂ QCA with KI on the surface of zinc in 1.0 M H ₂ SO ₄ at various temperatures	226
4.133	Freundlich adsorption isotherm plot for the adsorption of various concentrations of MQ ₆ CA on the surface of zinc in 1.0 M H ₂ SO ₄ at various temperatures	227
4.134	Freundlich adsorption isotherm plot for the adsorption of various concentrations of Q ₆ CA on the surface of zinc in 1.0 M H ₂ SO ₄ at various temperatures	227
4.135	Freundlich adsorption isotherm plot for the adsorption of various	228

	concentrations of H ₂ QCA with KI on the surface of zinc in 1.0 M H ₂ SO ₄ at various temperatures	
4.136	Temkin adsorption isotherm plot for the adsorption of various concentrations of MQ6CA on the surface of zinc in 1.0 M H ₂ SO ₄ at various temperatures	228
4.137	Temkin adsorption isotherm plot for the adsorption of various concentrations of Q6CA on the surface of zinc in 1.0 M H ₂ SO ₄ at various temperatures	229
4.138	Temkin adsorption isotherm plot for the adsorption of various concentrations of H ₂ QCA with KI on the surface of zinc in 1.0 M H ₂ SO ₄ at various temperatures	230
4.139	Tafel plots for zinc in 1.0 M HCl in the absence and presence of various concentrations of MQ6CA at 303 K	233
4.140	Tafel plots for zinc in 1.0 M HCl in the absence and presence of various concentrations of Q6CA at 303 K	234
4.141	Tafel plots for zinc in 1.0 M HCl in the absence and presence of various concentrations of H ₂ QCA without KI at 303 K	234
4.142	Tafel plots for zinc in 1.0 M HCl in the absence and presence of various concentrations of H ₂ QCA with KI at 303 K	235
4.143	Tafel plots for zinc in 1.0 M H ₂ SO ₄ in the absence and presence of various concentrations of MQ6CA at 303 K	238
4.144	Tafel plots for zinc in 1.0 M H ₂ SO ₄ in the absence and presence of various concentrations of Q6CA at 303 K	238
4.145	Tafel plots for zinc in 1.0 M H ₂ SO ₄ in the absence and presence of various concentrations of H ₂ QCA without KI at 303 K	239
4.146	Tafel plots for zinc in 1.0 M H ₂ SO ₄ in the absence and presence of various concentrations of H ₂ QCA with KI at 303 K	239
4.147	Nyquist plot of zinc in 1.0 M HCl in the presence and absence of various concentrations of MQ6CA	244

4.148	Bode plot of zinc in 1.0 M HCl in the presence and absence of various concentrations of MQ6CA	244
4.149	Nyquist plot of zinc in 1.0 M HCl in the presence and absence of various concentrations of Q6CA	245
4.150	Bode plot of zinc in 1.0 M HCl in the presence and absence of various concentrations of Q6CA	245
4.151	Nyquist plot of zinc in 1.0 M HCl in the presence and absence of various concentrations of H2QCA without KI	246
4.152	Nyquist plot of zinc in 1.0 M HCl in the presence and absence of various concentrations of H2QCA with KI	247
4.153	Bode plot of zinc in 1.0 M HCl in the presence and absence of various concentrations of H2QCA with KI	247
4.154	Nyquist plot of zinc in 1.0 M H ₂ SO ₄ in the presence and absence of various concentrations of MQ6CA	249
4.155	Bode plot of zinc in 1.0 M H ₂ SO ₄ in the presence and absence of various concentrations of MQ6CA	249
4.156	Nyquist plot of zinc in 1.0 M H ₂ SO ₄ in the presence and absence of various concentrations of Q6CA	250
4.157	Bode plot of zinc in 1.0 M H ₂ SO ₄ in the presence and absence of various concentrations of Q6CA	250
4.158	Nyquist plot of zinc in 1.0 M H ₂ SO ₄ in the presence and absence of various concentrations of H2QCA without KI	251
4.159	Nyquist plot of zinc in 1.0 M H ₂ SO ₄ in the presence and absence of various concentrations of H2QCA with KI	252
4.160	Bode plot of zinc in 1.0 M H ₂ SO ₄ in the presence and absence of various concentrations of H2QCA with KI	252
4.161	Equivalent circuit utilized to fit the impedance spectra obtained for zinc corrosion in 1.0 M HCl and 1.0 M H ₂ SO ₄ in the absence and presence of	254

	various concentrations of the studied quinoxalines	
4.162	Calibration curve for zinc	255
4.163	FTIR spectra of pure MQ6CA and the adsorption film formed on zinc surface in 1.0 M HCl in the presence of MQ6CA	257
4.164	FTIR spectra of pure Q6CA and the adsorption film formed on zinc surface in 1.0 M HCl in the presence of Q6CA	258
4.165	FTIR spectra of pure H2QCA and the adsorption film formed on zinc surface in 1.0 M HCl in the presence of H2QCA	258
4.166	FTIR spectra of pure MQ6CA and the adsorption film formed on zinc surface in 1.0 M H ₂ SO ₄ in the presence of MQ6CA	259
4.167	FTIR spectra of pure Q6CA and the adsorption film formed on zinc surface in 1.0 M H ₂ SO ₄ in the presence of Q6CA	260
4.168	FTIR spectra of pure H2QCA and the adsorption film formed on zinc surface in 1.0 M H ₂ SO ₄ in the presence of H2QCA	260
4.169	Tafel plots for zinc in 0.5 M HCl in the absence and presence of various concentrations of MQ6CA at 303 K	262
4.170	Tafel plots for zinc in 0.5 M HCl in the absence and presence of various concentrations of Q6CA at 303 K	263
4.171	Tafel plots for zinc in 0.5 M HCl in the absence and presence of various concentrations of H2QCA with KI at 303 K	263
4.172	Nyquist plot of aluminium in 0.5 M HCl in the presence and absence of various concentrations of MQ6CA	266
4.173	Bode plot of aluminium in 0.5 M HCl in the presence and absence of various concentrations of MQ6CA	266
4.174	Nyquist plot of aluminium in 0.5 M HCl in the presence and absence of various concentrations of Q6CA	267
4.175	Bode plot of aluminium in 0.5 M HCl in the presence and absence of various concentrations of Q6CA	267

4.176	Nyquist plot of aluminium in 0.5 M HCl in the presence and absence of various concentrations of H ₂ QCA with KI	268
4.177	Bode plot of aluminium in 0.5 M HCl in the presence and absence of various concentrations of H ₂ QCA with KI	268
4.178	Equivalent circuit utilized to fit the impedance spectra obtained for aluminium corrosion in 0.5 M HCl in the absence and presence of various concentrations of the studied quinoxalines	270
4.179	Langmuir adsorption isotherm plot for the adsorption of various concentrations of MQ ₆ CA on the aluminium in 0.5 M HCl at 303 K (a) PDP and (b) EIS	272
4.180	Langmuir adsorption isotherm plot for the adsorption of various concentrations of Q ₆ CA on the aluminium in 0.5 M HCl at 303 K (a) PDP and (b) EIS	273
4.181	Langmuir adsorption isotherm plot for the adsorption of various concentrations of Q ₆ CA on the aluminium in 0.5 M HCl at 303 K (a) PDP and (b) EIS	274
4.182	Selected molecules with different orientation studied for the verification the method utilized	279
4.183	Selected molecules to be studied with atom numbering	280
4.184	Selected structure, bond lengths and binding energy at different positions for Al (111) interacting with 3-Hydroxy-2-quinoxalinecarboxylic acid. The structures are arranged in order of decreasing binding energies	282
4.185	Selected structure, bond distances and binding energy at different positions for Al (111) interacting with 6-Nitro-2,3-dihydroxyquinoxaline	282
4.186	Selected structures, bond distances and binding energy at different positions for Al (111) interacting with quinoxaline-6-carboxylic acid	283
4.187	Selected structures, bond distances and binding energy at different positions for Al (111) interacting with methyl quinoxaline-6-carboxylate	283

4.188	Selected structure, bond lengths and binding energy at different positions for Zn interacting with 3-Hydroxy-2-quinoxalinecarboxylic acid	286
4.189	Selected structure, bond lengths and binding energy at different positions for Zn interacting with 6-Nitro-2,3-dihydroxyquinoxaline	287
4.190	Selected structure, bond lengths and binding energy at different positions for Zn interacting with quinoxaline-6-carboxylic acid	288
4.191	Selected structure, bond lengths and binding energy at different positions for Zn interacting with methyl quinoxaline-6-carboxylate	289

LIST OF TABLES

No	DESCRIPTION	PAGE No
2.1	Galvanic series of some commercial metal and alloys in seawater	22
2.2	Alloy/environment system causing SCC	24
2.3	Combinations of alloys and corrosive environment selective leaching	29
2.4	Standard reduction half-cell potentials	34
2.5	Some units commonly used to express corrosion rates	39
2.6	Interconversion of corrosion units	39
2.7	Direct and indirect corrosion cost in US	45
2.8	National corrosion costs in UK	46
2.9	Distinctions between physisorption and chemisorption	58
2.10	Adsorption isotherms to characterize the adsorption of inhibitors on the metal surface	61
3.1	Molecular structures, formulae, name and masses of the quinoxalines used as corrosion inhibitors in this study	84
4.1	Weight loss measurements and corrosion rate of zinc in various concentration of HCl, in the absence of the corrosion inhibitors	98
4.2	Weight loss measurements and corrosion rate of mild steel in various concentration of HCl, in the absence of the corrosion inhibitors	99
4.3	Weight loss measurements and corrosion rate of zinc in various concentration of H ₂ SO ₄ in the absence of the corrosion inhibitors	100
4.4	Weight loss measurements and corrosion rate of mild steel in various concentration of H ₂ SO ₄ in the absence of the corrosion inhibitors	101
4.5	Weight loss measurements of mild steel in the absence and presence of MQ6CA, Q6CA and H ₂ QCA in 1.0 M HCl	105
4.6	Weight loss measurements of mild steel in the absence and presence of MQ6CA, Q6CA and H ₂ QCA in 1.0 M H ₂ SO ₄	108
4.7	The corrosion parameters for mild steel in 1.0 M HCl in the absence and presence of various concentrations of MQ6CA obtained from weight loss	113

	measurements at 303 – 333 K	
4.8	The corrosion parameters for mild steel in 1.0 M HCl in the absence and presence of various concentrations of Q6CA obtained from weight loss measurements at 303 – 333 K	114
4.9	The corrosion parameters for mild steel in 1.0 M HCl in the absence and presence of various concentrations of H2QCA with and without KI obtained from weight loss measurements at 303 – 333 K	115
4.10	The corrosion parameters for mild steel in 1.0 M H ₂ SO ₄ in the absence and presence of various concentrations of MQ6CA obtained from weight loss measurements at 303 – 333 K	119
4.11	The corrosion parameters for mild steel in 1.0 M H ₂ SO ₄ in the absence and presence of various concentrations of Q6CA obtained from weight loss measurements at 303 – 333 K	120
4.12	The corrosion parameters for mild steel in 1.0 M H ₂ SO ₄ in the absence and presence of various concentrations of H2QCA with and without KI obtained from weight loss measurements at 303 – 333 K	121
4.13	Arrhenius and transition parameters for mild steel in 1.0 M HCl in the absence and presence of various concentrations of the studied quinoxalines	133
4.14	Arrhenius and transition parameters for mild steel in 1.0 M H ₂ SO ₄ in the absence and presence of various concentrations of the studied quinoxalines	134
4.15	The regression coefficient values obtained from different adsorption isotherms for mild steel in 1.0 M HCl at various temperatures for the studied quinoxaline	143
4.16	The regression coefficient values obtained from different adsorption isotherms for mild steel in 1.0 M H ₂ SO ₄ at various temperatures for the studied quinoxaline	150
4.17	Langmuir adsorption parameters for corrosion of mild steel in 1.0 M HCl at various temperatures in the presence of the studied quinoxalines	152
4.18	Langmuir adsorption parameters for corrosion of mild steel in 1.0 M H ₂ SO ₄ at various temperatures in the presence of the studied quinoxalines	153

4.19	Potentiodynamic Polarization (PDP) parameters such as corrosion current density (i_{corr}), corrosion potential (E_{corr}), polarization resistance (R_p), and anodic (β_a) and cathodic (β_c) Tafel slopes utilizing the studied quinoxalines in 1.0 M HCl	156
4.20	Potentiodynamic Polarization (PDP) parameters such as corrosion current density (i_{corr}), corrosion potential (E_{corr}), polarization resistance (R_p), and anodic (β_a) and cathodic (β_c) Tafel slopes utilizing the studied quinoxalines in 1.0 M H ₂ SO ₄	160
4.21	Electrochemical impedance parameters such as the resistance of charge transfer (R_{ct}), constant phase element (CPE) and the CPE exponent (n) of mild steel in the absence and presence of various concentrations of the studied quinoxalines in 1.0 M HCl	168
4.22	Electrochemical impedance parameters such as the resistance of charge transfer (R_{ct}), constant phase element (CPE) and the CPE exponent (n) of mild steel in the absence and presence of various concentrations of the studied quinoxalines in 1.0 M H ₂ SO ₄	173
4.23	Amount of dissolved mild steel present in 1.0 M HCl in the absence and presence of the studied quinoxalines	177
4.24	Amount of dissolved mild steel present in 1.0 M H ₂ SO ₄ in the absence and presence of the studied quinoxalines	177
4.25	Peaks and identification from FTIR spectra of the studied quinoxalines and adsorption film formed on the mild steel in 1.0 M HCl	180
4.26	Peaks and identification from FTIR spectra of the studied quinoxalines and adsorption film formed on the mild steel in 1.0 M H ₂ SO ₄	182
4.27	Weight loss measurements of in the absence and presence of MQ6CA, Q6CA and H2QCA in 1.0 M HCl	187
4.28	Weight loss measurements of zinc in the absence and presence of MQ6CA, Q6CA and H2QCA in 1.0 M H ₂ SO ₄	190
4.29	The corrosion parameters for zinc in 1.0 M HCl in the absence and presence of various concentrations of MQ6CA obtained from weight loss measurements at 303 – 333 K	195

- 4.30 The corrosion parameters for zinc in 1.0 M HCl in the absence and 196
presence of various concentrations of Q6CA obtained from weight loss
measurements at 303 – 333 K
- 4.31 The corrosion parameters for zinc in 1.0 M HCl in the absence and 197
presence of various concentrations of H2QCA with and without KI
obtained from weight loss measurements at 303 – 333 K.
- 4.32 The corrosion parameters for zinc in 1.0 M H₂SO₄ in the absence and 201
presence of various concentrations of MQ6CA obtained from weight loss
measurements at 303 – 333 K
- 4.33 The corrosion parameters for zinc in 1.0 M H₂SO₄ in the absence and 202
presence of various concentrations of Q6CA obtained from weight loss
measurements at 303 – 333 K
- 4.34 The corrosion parameters for zinc in 1.0 M H₂SO₄ in the absence and 203
presence of various concentrations of H2QCA with and without KI
obtained from weight loss measurements at 303 – 333 K
- 4.35 Arrhenius and transition parameters for zinc in 1.0 M HCl in the absence 214
and presence of various concentrations of the studied quinoxalines
- 4.36 Arrhenius and transition parameters for zinc in 1.0 M H₂SO₄ in the absence 215
and presence of various concentrations of the studied quinoxalines
- 4.37 The regression coefficient values obtained from different adsorption 223
isotherms for zinc in 1.0 M HCl at various temperatures for the studied
quinoxaline
- 4.38 The regression coefficient values obtained from different adsorption 230
isotherms for zinc in 1.0 M H₂SO₄ at various temperatures for the studied
quinoxaline
- 4.39 Langmuir adsorption parameters for corrosion of zinc in 1.0 M HCl at 232
various temperatures in the presence of the studied quinoxalines
- 4.40 Langmuir adsorption parameters for corrosion of zinc in 1.0 M H₂SO₄ at 232
various temperatures in the presence of the studied quinoxalines
- 4.41 Potentiodynamic Polarization (PDP) parameters such as corrosion current 236
density (i_{corr}), corrosion potential (E_{corr}), polarization resistance (R_p), and

- anodic (β_a) and cathodic (β_c) Tafel slopes utilizing the studied quinoxalines in 1.0 M HCl
- 4.42 Potentiodynamic Polarization (PDP) parameters such as corrosion current density (i_{corr}), corrosion potential (E_{corr}), polarization resistance (R_p), and anodic (β_a) and cathodic (β_c) Tafel slopes utilizing the studied quinoxalines in 1.0 M H₂SO₄ 240
- 4.43 Electrochemical impedance parameters such as the resistance of charge transfer (R_{ct}), constant phase element (CPE) and the CPE exponent (n) of zinc in the absence and presence of various concentrations of the studied quinoxalines in 1.0 M HCl 248
- 4.44 Electrochemical impedance parameters such as the resistance of charge transfer (R_{ct}), constant phase element (CPE) and the CPE exponent (n) of zinc in the absence and presence of various concentrations of the studied quinoxalines in 1.0 M H₂SO₄ 253
- 4.45 Amount of dissolved zinc present in 1.0 M HCl in the absence and presence of the studied quinoxalines 256
- 4.46 Amount of dissolved zinc present in 1.0 M H₂SO₄ in the absence and presence of the studied quinoxalines 257
- 4.47 Peaks and identification from FTIR spectra of the studied quinoxalines and adsorption film formed on the Zinc in 1.0 M HCl 259
- 4.48 Peaks and identification from FTIR spectra of the studied quinoxalines and adsorption film formed on the zinc in 1.0 M H₂SO₄ 261
- 4.49 Potentiodynamic Polarization (PDP) parameters such as corrosion current density (i_{corr}), corrosion potential (E_{corr}), polarization resistance (R_p), and anodic (β_a) and cathodic (β_c) Tafel slopes utilizing the studied quinoxalines in 0.5 M HCl 264

- 4.50 Electrochemical impedance parameters such as the resistance of charge transfer (R_{ct}), constant phase element (CPE) and the CPE exponent (n) of aluminium in the absence and presence of various concentrations of the studied quinoxalines in 0.5 M HCl 269
- 4.51 Langmuir adsorption parameters for corrosion of aluminium in 0.5 M HCl at 303 K in the presence of the studied quinoxalines 275
- 4.52 Binding energies for selected molecules on the Al (111) surface built with three layers, two on the bottom fixed and one on top relaxed 277

CHAPTER 1: INTRODUCTION

The work in this dissertation entitled “ COMPUTATIONAL AND ADSORPTION INVESTIGATION OF SOME QUINOXALINE DERIVATIVES ON SELECTED METALS IN ACIDIC MEDIA” is partitioned into five chapters with several sections and subsections in every chapter.

This Chapter present an overview on the background of the corrosion phenomenon, the importance of undertaking the study of corrosion of metals. The existing gaps of knowledge in the field of corrosion and corrosion mitigations are also outlined in this chapter. The aim and objectives of this project are also outlined.

1.1 Background of the study

Humans live in a society where many items are produced from metals. Different types of metal are used successfully in engineering (in bridges, automobiles, ships, trains, etc.) and commercial applications (office buildings, medical centers, hotels, malls, retail stores, etc.) [1]. These items are made of versatile material of metals that comes with varying strengths and durability. However, all metals and their end-use products except for gold and platinum group metals (PGM), are unstable, and consequently when they are subjected to their environments they revert to their original and stable state by which they were found, that is, naturally occurring minerals and ores at different rates [1, 2, 3]. This process is referred to as corrosion [1]. Corrosion of metallic material is perceived as a universal phenomenon that is widely and constantly experienced. It is there in every environment that we encounter, and its effects have been an unavoidable part of human experience for thousands of years [4].

The word corrosion is as old as our planet earth and it was derived from the Latin word *corrodere*, which means “to eat away”. This phenomenon is known by many as “rust” [4]. Corrosion of metallic materials leads to the degradation of metals and consequently metals losing their strength, durability, and efficiency. The impact of corrosion has elevated in complexity and diversity of materials systems, which include not only metallic materials but also ceramics, polymers, and composites, which are, as well, subjected to this natural and destruction process [5]. Over the years, the industrial negative impact of corrosion has increased. The industrial consequences of corrosion lead to challenges such as production plants shutdowns, product contaminations, loss of efficiency, and loss of productivity [6]. Corrosion also possesses a significant negative impact on human health and safety [7].

A significant framework of evidence concerning corrosion has been brought forward from time to time by many scientists, writers, and philosophers [6, 7]. It was the Greek philosopher Plato (427-347 B.C.) who documented the first description of corrosion in his work, where he defined rust as “the earthly component segregating out the metal” [4]. A Roman philosopher by the name of Pliny the elder (23–79 AD) wrote about the degradation of iron in his essay entitled “Ferrum Corrupitar” [6, 8]. The studies of corrosion at that time were limited in the prevention measures but not much on the mechanism. A stunning discovery was made by Thenard (1819) where he suggested that corrosion is an electrochemical phenomenon [3]. One of the most significant essays

was made by Michael Faraday (1791–1867) who discovered a quantitative relationship between chemical action and electric current. It is through Faraday's first and second laws that the basic calculation of the deterioration rates of metals was established [6, 9]. A modern understating of the causes and control of corrosion was later proposed by U.R. Evans in 1923 through his classical electrochemical theory [6]. Till to date, many scientific discoveries on the understanding of corrosion mechanisms have been published and have tremendously improved the field of corrosion.

1.2 JUSTIFICATION/SIGNIFICANCE OF THE STUDY

There are three main concerns of corrosion and reasons to undertake the study of corrosion, which are: (i) the cost of corrosion, (ii) human life and safety, and (iii) conservation of materials. The economies of nations have taken a massive toll due to this unwanted destruction of metals and these losses are encountered domestically and industrially. Domestic losses include the replacement of rusting automobile parts, water pipes, zinc roofing, etc. [10]. Losses encountered by industries and by governments amount to many billions of dollars annually due to the fact that vast industrial pieces of equipment are largely made from metals [7, 10]. The corrosion of those pieces of equipment may result in losses which may have the following consequences: [1, 6, 7, 10, 15]

- **Contamination of product:** A huge loss may result when products such as chemicals, food, pharmaceuticals, etc. need to be replaced because of being tempered by corrosion product (rust) and this will require a lot of money.
- **Loss of product:** Corroded pipe systems, oil transportation lines, and fuel tanks cause a massive loss of product and at times may enter cause an explosion and severe injuries which may cause even additional loss. Leakage of containers may go a very long time unnoticed and during that time there is a huge loss of product.
- **Shutdown:** The failure of equipment due to corrosion may lead to contamination and loss of product which can result in unplanned shutdowns of power plants and manufacturing plants and consequently loss of profit.
- **Loss of efficiency:** e.g., overdesign and corrosion products decrease the heat-transfer rate in heat exchangers.

- **Overdesign:** Equipment is often designed with additional thickness or many times heavier than normal make condition. This is done in most cases when the corrosion effect of the system is known, and it requires extra costs.

In addition to the economic corrosion cost mentioned above, according to The Worldwide Corrosion Authority, corrosion has an annual cost approximated to 2.5 trillion US dollars, which is about 3.4% of the global GDP [16]. In South Africa, research conducted by the council for mineral technology (MINTEK) group has found that the economy directly succumbs at about R130-billion per annum. A similar study in 2005 was conducted by the University of the Witwatersrand estimated about R154-billion is directly lost due to corrosion per year, which is even high than MINTEK's figure [7, 17, 18]. If these corrosion concerns are not attended for an extended period, the estimated figures above can double up or even more badly. Therefore, this implies that more intensive research in measures of preventing and controlling corrosion is needed.

1.3 PROBLEM STATEMENT

In one way or the other, metals play a huge part in human's daily lives. They pose various properties such as being lustrous, sonorous, reactivity, malleability, and high melting point which allows them to be used at a very wide range that also contribute enormously to the world's economy. With the recent advanced technology, the use of metals has even broadened greatly. Besides metals being the major component in the construction industry, they also have some important roles and some of them are listed below;

- Metals are used in human bodies as artificial organ replacements.
- Mobile cellphones and computers used in our daily lives are made of metals and it is already difficult to imagine the modern life without them.
- Most of the kitchen utensils such as spoons, forks, etc., are made from metals.
- Almost all kinds of transport used daily are made entirely from metals.
- Metals also find their uses in the military where they are used to manufacture weapons and ammunition.

The list is endless; however, the problem is that all these metals and their end products when they react with various surrounding, they behave in a way that allows them to return to their more stable oxidized state, and that is, they undergo gradual deterioration. With ample knowledge of corrosion

more effective strategies to protect and prolong their lifespan can be established. Therefore, this motivates a need to accumulate scientific knowledge in understanding corrosion mechanisms and their application to corrosion protection. The economy of South Africa suffers 5.2% of the GDP from the direct cost of corrosion [7], hence, it is clear in a foregoing that if a study of this area is done the government can then channel some needed fund from corrosion cost to combat the high rate of poverty in South Africa [19].

1.4 AIM AND OBJECTIVES OF THE STUDY

The aim of the study is to investigate the inhibition potential of some quinoxaline derivatives namely: quinoxalone-6-carboxylic acid (Q6CA), 3-hydroxy-2-quinoxaline carboxylic acid (H2QCA), and Methyl quinoxaline-6-carboxylate (MQ6CA) on aluminum, mild steel, and zinc in sulphuric and hydrochloric acids as corrosive media.

The specific objectives of this study are to:

- evaluate the inhibition efficiency of Q6CA, H2QCA, MQ6CA on mild steel and zinc in sulphuric and hydrochloric acids by weight loss analysis at varying temperatures 303K, 313K, 323K and 333K,
- propose the type of adsorption mechanism and adsorption isotherm for corrosion inhibition,
- evaluate the interaction of the inhibitor with the aluminum, mild steel and zinc surfaces by electrochemical techniques such as electrochemical impedance spectroscopy (EIS) and potentiodynamic polarization (PDP),
- utilize Fourier Transform Infrared spectrometry (FTIR) to determine the mode of interfacial reactions and the functional groups which interacted between the quinoxaline derivatives and the mild steel and zinc surface,
- utilize atomic absorption spectroscopy (AAS) to determine the concentration of mild steel and zinc for the uninhibited and inhibited processes, and
- utilize quantum chemical/theoretical techniques e.g. density functional theory (DFT) in order to estimate molecular properties of the inhibitor as well as the binding energies between the inhibitor and the metal surface.

CHAPTER 2: LITERATURE REVIEW

This Chapter consist of general aspect review of corrosion, its classification and types, its prevention, and factors that affect the rate of corrosion. The chapter also unpacks ways in which corrosion can be measured. It also provides details on the impact and consequences that corrosion imposes to human life. A brief review on the corrosion of mild steel, zinc, and aluminium and the use of organic compounds as corrosion inhibitors. The types, mechanism and the use of quinoxalines as corrosion inhibitors. It also gives a brief review on some the of available computational methods, their advantages and disadvantages.

2.1 DEFINITION OF CORROSION

Corrosion appears in various forms; however, they all share one formation mechanism. For instance, when a car or a metal coin is left exposed to moist weather for a longer period, a corrosion product, or what is often referred to as rust spot is observed. This corrosion product is formed because of the interaction between the metal and the environment it is exposed to. Moreover, the rate at which the corrosion product will be observed will differ from the car and the metal coin, but usually, for both, it will be slow [5]. Rust is not always the resultant product of corrosion. Sometimes cracks on the metal surface can be observed. The cracks are formed as a result of the metal reacting with its environment. These environments can be aqueous in nature or sustained tensile stress [5, 6]. Another good example are the tiny holes or pits that are observed on carbon (figure 2.1). In figure 2.1 below, pits are observed on the carbon surfaces instead of rust. The pits have developed because the metal has reacted with its environment [7].



Figure 2.1: Pits resulted from corrosion of carbon metal [7].

The common feature among the three examples above is that for corrosion to occur the metal has to react with the particular environment it is exposed to. Thus, generally, corrosion can be defined as the gradual attack of materials, usually metals, by its reaction with the environment [23]. However, a more comprehensive definition of corrosion is that it is the chemical or electrochemical destruction of metals by interaction with their surrounding [1–27]. Fontana also described corrosion as the extractive metallurgy in reverse [5,24], which makes good sense since metals are less stable in their temporary existence in metallic form than in their compound forms as minerals and ores [3].

2.1.1 THE ELECTROCHEMICAL ORIGIN OF CORROSION

Generally, chemical reactions are those in which elements are added or removed from a chemical species but no species in the reaction undergo a change in valence and electrochemical reactions are those which involve changes in the number of electrons in at least one species involved in the reaction when elements are added or removed from a chemical species [27]. By far, it has been established that often used metals (including alloys) are not stable against exposure to environments, like the atmosphere, hence they tend to revert to their original state which they were originally taken from the earth's crust as ores and minerals before being refined to useful material. Figure 2.2 illustrate the processes involved in metallurgy.

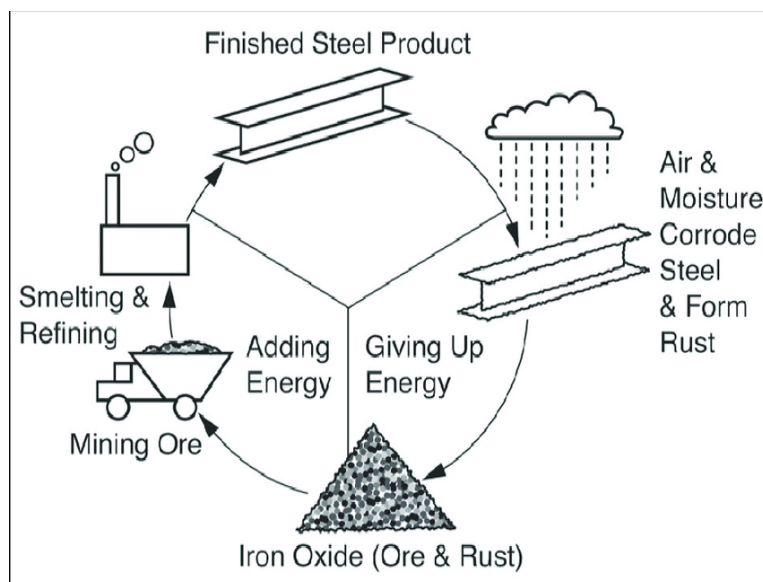


Figure 2.2: Illustration of the processes involved in metallurgy [28].

These changes illustrated in figure 2.2 above are electrochemical reaction that follow thermodynamics laws [27–31]. The process of corrosion occurs through the behavior of coupled electrochemical half-cell reactions [1]. These processes require a formation of a corrosion cell which is made up of four components and they are key to corrosion control. It is also important to note that if any of these factors to successful corrosion process is altered, the process will not occur. These components are as following: an anode, a cathode, electrolyte, and metallic pathway [5, 32–34]. These are briefly discussed below.

2.1.1.1 Anodic reaction

In most corrosion processes, the oxidation and reduction take place at separate sites on the metal's surface. The anode is the site of the electrode or metal where the degradation takes place. In the anodic site a given species undergoes oxidation, that is, it loses electrons in the process. A typical example of an anodic reaction is the dissolution of iron as shown in figure 2.3 below [33].

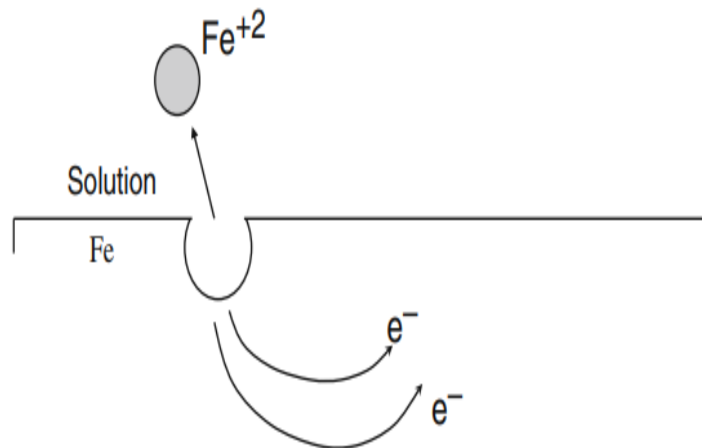


Figure 2.3: Schematic representation of an anodic reaction [1].

The half reaction at the iron electrode is as follows:



From figure 2.3 and equation (1), it is clear that the metal iron has been converted to iron ion and it has lost or given away two electrons which will then be received by a species in the reduction reaction. Thus, the metal has lost its uniformity [7, 35].

2.1.1.2 Cathodic reaction

The cathode is the site of the electrode or metal where reduction takes place. The electrons that are liberated by the anodic reaction are then consumed at the cathodic site on the surface of the metal. An example of a cathodic reaction is illustrated in figure 2.4 below. From the example, two

hydrogen ions at the metal surface were reduced to form one molecule of hydrogen gas. Thus, the cathodic half-reaction being:

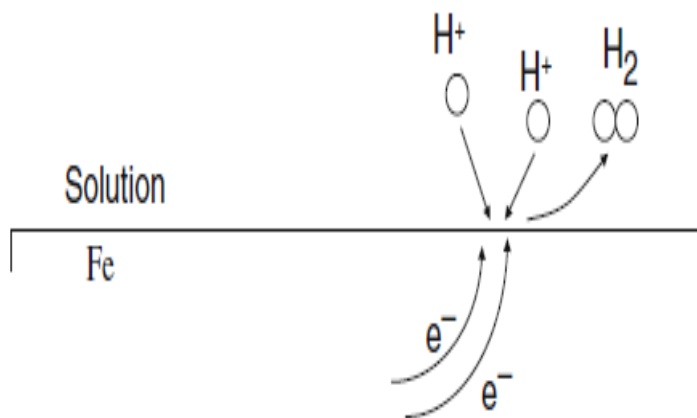


Figure 2.4: Schematic representation of a cathodic reaction [1].

Cathodic reactions are not so easy to foretell but can be classified into one of five different types of reduction reactions listed below:

Hydrogen evolution



Oxygen reduction in acids



Metal ion reduction



Metal deposition



Oxygen reduction-neutral solutions



2.1.1.3 An electrolyte

During the process of corrosion, electrons move from the anodic to the cathodic site on the surface of the metal and this movement is made possible by an electrolyte. Thus, an electrolyte is an electrically conductive solution which has dissolved ions and capable of conducting a current. This current is usually referred to as the corrosion current, i_{corr} [1, 36].

2.1.1.4 Metallic path

The anodic and cathodic electrodes are externally connected by a metallic conductor which enables the flow conventional current which is in an opposite direction is a passage for electron movement.

During the overall corrosion process, the anodic and cathodic reactions occur simultaneously and in a coupled manner at different sites on the metal surface [1, 7]. This simultaneity occurrence of the anodic and cathodic reaction is attributed to the heterogeneous nature of a metal surface (see figure 2.5) [3, 36-37]. For a successful corrosion process of iron metal in an acidic aqueous environment, the reactions illustrated by figures 2.3 and 2.4 should occur at the same time and equivalent rate.

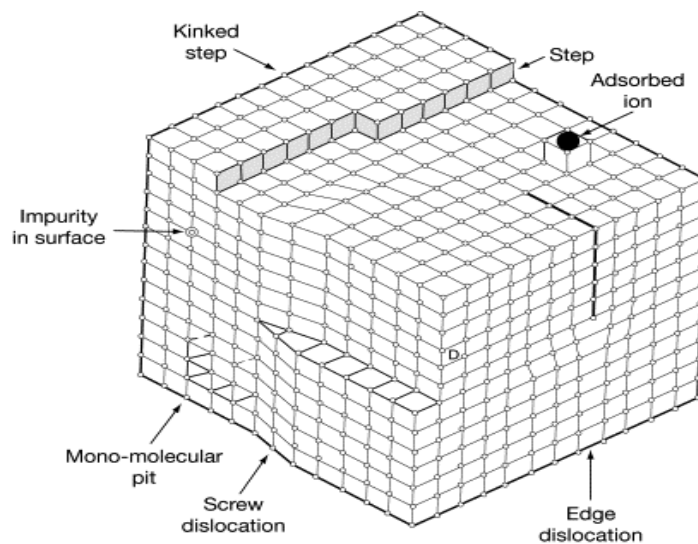


Figure 2.5: Heterogeneous surface of metal crystal showing different types of imperfections [38].

It is important to note that throughout the corrosion process, more than one reduction and one reaction may occur [5]. In the reaction in figure 2.6, the two electrons given away from the anodic site of the metal surface are instantly consumed at the cathodic site and two hydrogen ions are reduced to one H₂ molecule. Thus, the overall corrosion process is simplified in figure (2.6) and equation (8).

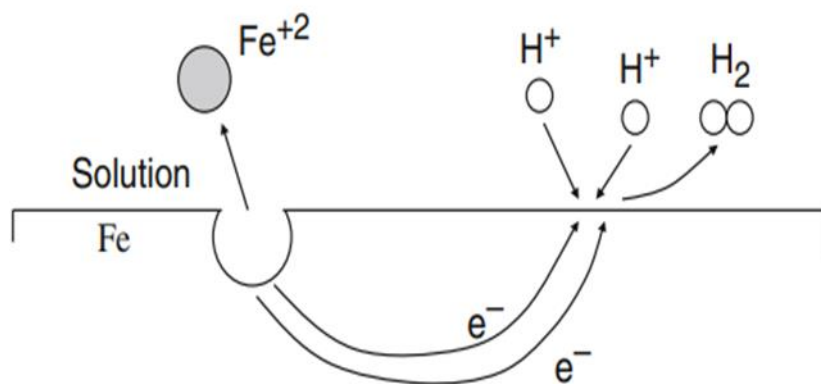


Figure 2.6: Schematic representation of the overall corrosion process of iron metal cathodic reaction in an acidic aqueous environment [1].

2.1.2 CLASSIFICATION OF CORROSION

Metallic corrosion has been classified in many ways, as low and high-temperature corrosion, electrochemical corrosion, direct oxidation, flow-assisted corrosion (FAC), chemical corrosion, bio-corrosion, etc. However, from wide perspective corrosion, can be classified based on the nature of the corrosive environment involved [7]. Thus, there are two typical categories corrosion can be based on. These are dry or wet corrosion which are briefly discussed below [7, 38–39]

2.1.2.1 Dry corrosion

Dry or chemical corrosion occurs in the surroundings that do not have any liquid phase or above the dew point of the environment. This type of corrosion involves direct attack of corrosive media, like atmospheric gases, vapor, etc. on the surface of a metal. It is classified as less prevalent and often linked with high temperature oxidation of metals [40].

2.1.2.2 Wet corrosion

Wet or electrochemical corrosion is the kind of corrosion that requires the presence of electrolyte solution or aqueous phase as the medium to occur. Unlike dry corrosion, wet corrosion is considered to be more prevalent, or it is a rapid process [40]. The classification processes are shown below in figure 2.7.

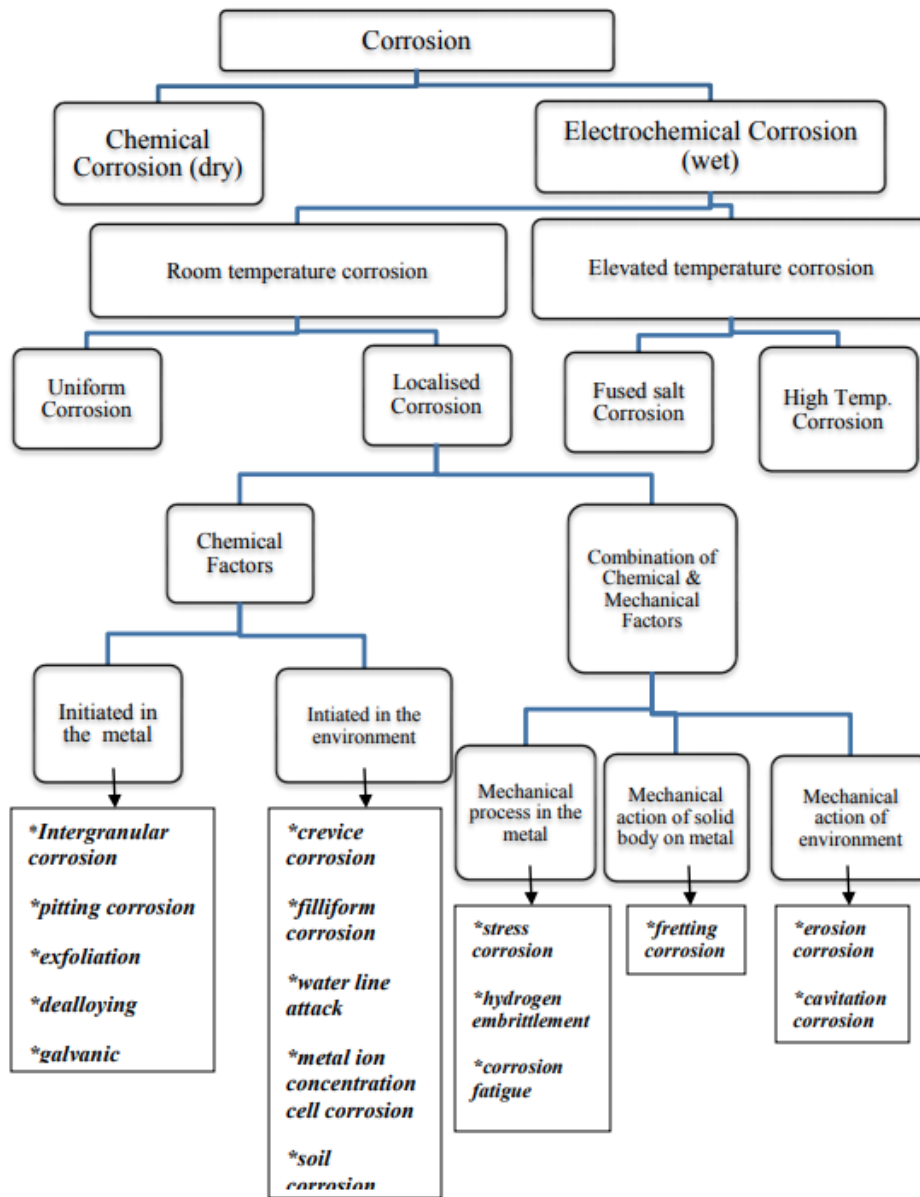


Figure 2.7: A general scheme for the classification of corrosion [40].

2.1.3 CORROSIVE ENVIRONMENT

It is almost impossible to understand the principles of the corrosion process without taking into account the nature of the environment a metal is exposed to and the type of reaction that occurs at the metal-environment interface. For instance, copper does not corrode in diluted sulfuric acid but corrodes in the presence of oxygen. Lead deteriorates very slowly in hydrochloric acid, but very fast when exposed to nitric acid. Iron corrodes very fast in oxygenated water, however, if all oxygen is removed it corrode extremely slowly [37, 41]. These examples evince that the understating of the specific environmental conditions and the corrosion behavior of metal can never be separated. Most literature suggests that to some greater or lesser extent, all the environment a metal is exposed to it is prone to corrode [6, 7, 42]. The most typical corrosive environments are discussed in the subsequent sub-sections.

2.1.3.1 Atmospheric corrosion

In this environment, metals corrode due to exposure to air, unlike being immersed in liquid. Studies show that all of the general types of corrosion processes occur in this environment [3, 43]. However, in the absence of moisture in the atmosphere to serve as an electrolyte, metals corrode at a very negligible rate. Moreover, rusting is insufficient in a climate below the freezing point of water because ice is a poor electrolytic conductor [10, 44–47]. A typical example is parts of metal left exposed in the desert air will remain rust-free for a long period [42, 45]. The weathering factors that are linked with atmospheric corrosion attack of metals does include only rainfall, temperature variations, wind velocity, etc. [44], but also the gaseous impurities that support condensation of moisture on the metal surface like SO_2 , which forms H_2SO_4 with water [48, 49]. It is important to also note that metals can resist corrosion in one atmosphere, say point A, but elsewhere (point B) lack the resistance imposed on point A; hence, the atmospheric corrosion behavior of metals varies with location. Thus, the diverse nature of atmospheric corrosion makes it complex and difficult to predict. The atmospheric corrosive environments are categorized as urban, rural, marine, and industrial [50–52].

2.1.3.1.1 Rural

The aggressiveness of rural environments is generally less towards metals and does not contain chemical contaminants, however, it does have inorganic and organic matters. In essence, rural atmospheres consist of corrosives of a little amount of sulfur oxides, carbon dioxide from different combustion products, and ammonia that results from the decomposition of farm fertilizers [53, 54].

2.1.3.1.2 Urban

The urban atmosphere is almost the same as the rural atmosphere, that is, in both there are activities (industrial) taking place. A significant difference is that the urban atmosphere has much denser pollution from a few motor vehicles, domestic combustion, dew, etc. which then result in a high increase in the amount of sulphuric acid, carbon dioxide, sulphur dioxide, and chloride that are aggressive to exposed metal surfaces [54].

2.1.3.1.3 Industrial

The industrial atmosphere is caused vigorously by sulfur dioxide from burning coal, nitrogen oxides that result from the combustion of automotive and fossil fuels in power stations. These contaminants settle in the atmosphere as microscopic droplets and they fall as acid rain which produces highly corrosive wet, acid film on exposed metal surfaces [52, 54].

2.1.3.2 Soil corrosion

Soil is a mixture of minerals, organic matter, water, and gases that is paramount to life on earth. It has been found that metal left under wet soil undergo more severe corrosion as compared to metal left under dry soil. However, soils are often wet because of rain, and in many cases lead to catastrophic damage and failure of metallic structures buried under soil [3]. Soil corrosion is of major concern globally. Across the United States (US) alone, there are more than 3.7 million kilometers of pipelines buried under soil moving different types of gases, water, and other hazardous liquids from and to different locations [10, 42, 56]. These metallic structures (pipelines) are prone to corrosion. The factors that influence the rate of corrosion in soil include aeration (porosity), electrical conductivity, pH value, microbiological activity, dissolved salts content, and moisture [3, 10].

2.1.3.3 Water corrosion

Undoubtedly water has tremendous importance in all the living things on earth, it covers a huge (three of four equal parts) surface of our planet earth, and it institutes about 60 to 70 percent of the living world [3]. However, there are some environmental concerns accompanying water corrosion due to distribution piping that contains zinc, lead, cadmium and copper in drinking water [3, 10, 20, 57]. In the concept of “water corrosion”, water is classified as fresh water and seawater. These two types of water are discussed below.

2.1.3.3.1 Freshwater

Surface water and groundwater are the two most sources of freshwater. The term freshwater refers to any natural occurring water that is sourced from rivers, lakes, glaciers, reservoirs, ponds, waterfalls, springs, wells, and even groundwater [20, 58]. Despite the importance of freshwater to life, it is limited to an extent that it only constitutes three percent of all the water on earth and only a fraction in that three percent is directly usable [20]. All water is considered to have a content of some impurities or constituents. The environmental conditions and the constituents/impurities of freshwater are what influence the aggressiveness of water towards metals they are exposed to [59–61]. The environmental conditions include temperature, water flow rate, and pH level, the constituents: dissolved gases (oxygen, nitrogen, carbon dioxide, ammonia), mineral components (salts), microorganisms (bacteria), and organic substances.

2.1.3.3.2 Seawater

The seawater environment is very complex in the concept of corrosion because almost all the elements that are found on earth are present in seawater [3, 62]. The vast amount and miscellany of dissolved gases, dissolved solids, and various species of biological matter (bacteria) make the mechanism by which metals corrode in this environment even more difficult to understand [63]. Nevertheless, from a corrosion point-of-view, some of the parameters that influence the rate of corrosion in seawater such as; salinity, dissolved oxygen concentration, pH value, and temperature have been thorough-studied for over many decades [3, 20, 61, 64]. In seawater constituents, chloride ions contribute the highest in the severity of corrosion [3]. Figure 2.8 below shows the major constituents of sea water.

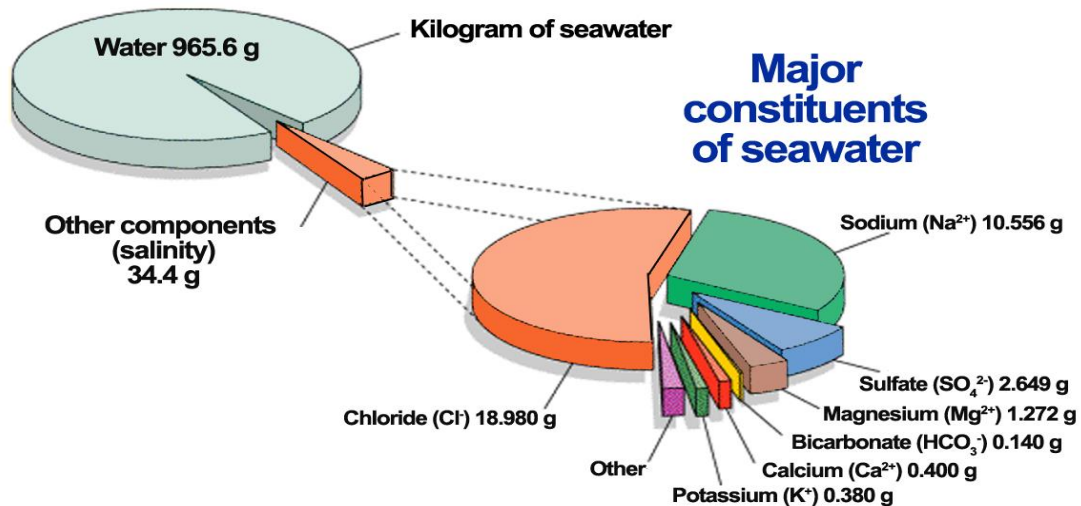


Figure 2.8: Major constituents of sea water [65].

In 1902, Forch [66] et. al. defined salinity as “the total amount of solid material in grams contained in one kilogram of seawater when all the carbonate has been converted to oxide, the bromine, and iodine replaced by chlorine, and all organic matter completely oxidized”, that in simple term is; the amount (grams) of dissolved inorganic matters per 1 kilogram of seawater [66, 67]. Seawater is typically a more aggressive environment towards metals than freshwater the high ability of chlorine ions to penetrate the metal surface and its higher conductivity [3, 20]. However, due to the dilution of fresh water and solar evaporation in some areas salinity may vary (incapacitated) as compared to others [3, 68].

2.1.4 FORMS OF CORROSION

Corrosion can manifest itself in many various ways and it can be classified accordingly. Generally, these classifications are made in visual observation of the corroded metal but at times amplification is required to correctly tell the type of corrosion [24, 69]. The most common forms of corrosion are:

- Uniform corrosion
- Pitting corrosion
- Galvanic corrosion
- Crevice corrosion
- Erosion corrosion
- Selective corrosion
- Fretting corrosion
- Stress corrosion cracking

The forms of corrosion above are listed in no particular importance and are further discussed below according to their characteristic and mechanisms.

2.1.4.1 Uniform corrosion

Uniform corrosion which is also known as general corrosion is assumed to be the most common type of corrosion [24]. This form of corrosion occurs when the metal surface is attacked at an even rate all over the entire exposed metal surface [70]. However, general corrosion is considered to be less dangerous because it is rather easy to predict. Most of the other forms of corrosion are insidious in nature and difficult to predict but uniform corrosion does not penetrate deep inside the metal, which makes it even easy to deal with at an acceptable level. Various mitigations can be employed in reducing uniform corrosion, and some of them include: the use of inhibitors and cathodic protection, these prevention measures will be well-discussed in subsequent chapters [24, 69, 70]. A commonly known example of general corrosion is rusting of steel in open-air shown in figure 2.9.

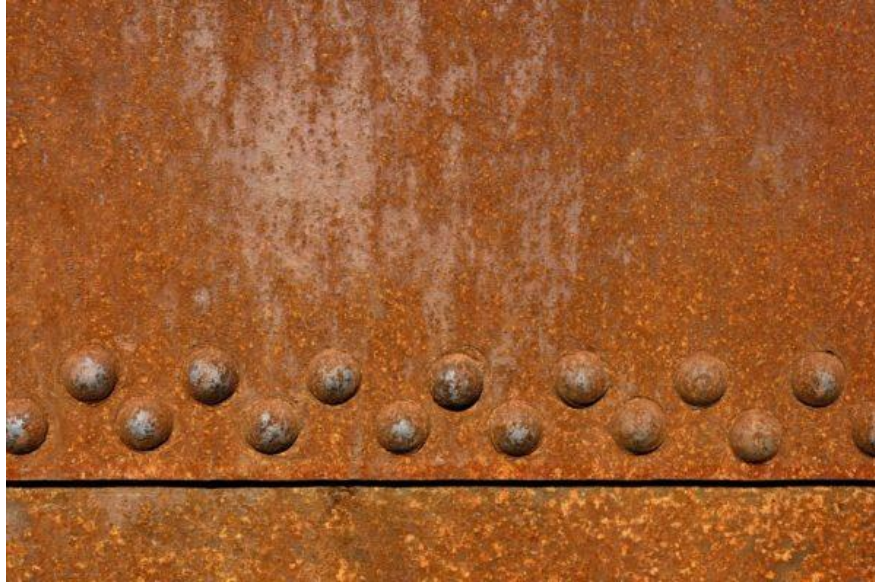


Figure 2.9: An example of uniform corrosion [71].

2.1.4.2 Pitting corrosion

Pitting corrosion is characterized by narrow pits or holes in the surface of the metal that has a radius equal to or less than the depth but generally relatively small [24]. They are sometimes separated or very close to each other that they appear as rough surface. Pitting is also regarded as an insidious and destructive localized attack; in that, the attack is limited to specific sites of metal and pits are very tiny and often covered with corrosion product, consequently, they cause undetected or unpredicted failures on metal structures [15, 24]. In addition, sometimes pits take months or even years to appear on the surface of the metal but the period depends on the metal and corrosive media involved. Moreover, once the attack has a pit pierces a metal at a non-stopping rate [24]. According to Philip A. Schweitzer [15], electrical contact between dissimilar metals is the major cause or accelerator of pitting. Carbon steels are reported to be more resistant than stainless steels, aluminum, and their alloys [15, 24, 72–74]. Pitting corrosion can result in various shapes which can only be pinpointed through metallography in the laboratory where pitted sample in cross-sectioned and examined [73]. Some of the shapes associated with pitting corrosion are illustrated in figure 2.10.

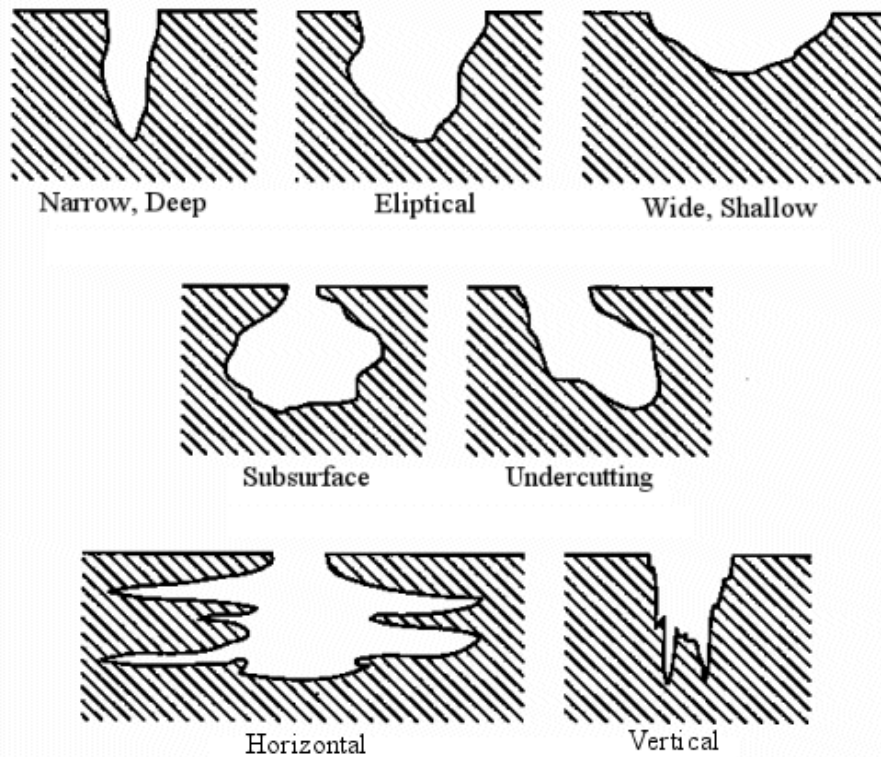


Figure 2.10: Shapes associated with pitting corrosion [73].

2.1.4.3 Galvanic corrosion

Galvanic corrosion which also known as two-metal corrosion and is sometimes referred to as dissimilar metal corrosion and occurs in the presence of an electrolyte when two different metals are electrically connected and there is a potential difference that supplies a driving force for the corrosion of the more electrically negative metal [15, 24, 72]. It is electrochemical corrosion [71–74]. In galvanic corrosion, corrosion of the more resistant (cathodic) metal is usually decreased and attack on the less resistant (anodic) metal is increased as compared to when they are not in contact [24]. Table 2.1 shows the galvanic series of metals and their alloys in seawater which distinguished nobility of some metals and alloys in seawater. In essence, the more noble metal becomes the cathode and the less noble becomes the anode [75].

Table 2.1: Galvanic series of some commercial metal and alloys in seawater [15].

Active Corroded End			
	Magnesium	Copper	
	Magnesium alloys	Aluminum bronze	
	Zinc	Composition G bronze	
	Beryllium	90-10 nickel	
	Alchid 3S	70-30 copper-nickel; low iron	
	Aluminum 3S	70-30 copper nickel; high iron	
	Aluminum 61S	Nickel	
	Aluminum 63S	Inconel, nickel-chromium	
	Aluminum 52	alloy 600 (passive)	
	Low-carbon steel	Silver	
	Alloy carbon steel	Type 410 (passive)	
	Cast iron	Type 430 (passive)	
	Type 302, 303, 321, 347, 310, 416 (active)	Type 304 (passive)	
		Type 316, (317 (passive)	
	Type 430 (active)	Monel, nickel-copper	
	Type 304 (active)	alloy 400	
	Type 316 (active)	Hastelloy alloy C	
	Ni-Resist	Titanium	
	Muntz metal	Zirconium	
	Hastelloy B (active)	Graphite	
	Yellow brass	Gold	
	Admiralty brass	Platinum	
	Aluminum brass		
	Red brass		
			Noble protected end

The position of the metal in the galvanic series is one of the major factors that affect galvanic corrosion. This is attributed by the fact that, the further apart the metals in the galvanic series, the severer the corrosion effect [15, 75]. A typical example of galvanic corrosion is when aluminum and copper are attached and submerged in seawater, the attack is expected to be quicker on aluminum, whilst copper is protected on the cathodic site. Figure 2.11 shows an example of galvanic corrosion.

Table 2.2: Alloy/environment system causing SCC [21].

Alloy	Environment
Carbon steel	Hot nitrate, hydroxide, and carbonate/bicarbonate solutions
High-strength steels	Aqueous electrolytes, particularly when containing H ₂ S
Austenitic stainless steels	Hot, concentrated chloride solutions; chloride-contaminated steam
High-nickel alloys.....	High-purity steam
α-brass	Ammoniacal solutions
Aluminum alloys	Aqueous Cl ⁻ , Br ⁻ , and I ⁻ solutions
Titanium alloys	Aqueous Cl ⁻ , Br ⁻ , and I ⁻ solutions; organic liquids; N ₂ O ₄
Magnesium alloys.....	Aqueous Cl ⁻ solutions
Zirconium alloys.....	Aqueous Cl ⁻ solutions; organic liquids; I ₂ at 350 °C (660 °F)



Figure 2.12: An example of SCC [77].

2.1.4.5 Crevice corrosion

Crevice corrosion is sometimes referred to as deposit or gasket corrosion, it is an intensive localized type of corrosion that occurs within or adjoining to narrow gaps or crevices formed by two surfaces (two metal or nonmetal-metal) that are exposed to corrosives [15, 24, 79]. This type of corrosion may occur on any metal, in any corrosive environment [24]. It is not necessary only a metallic material that is responsible for causing crevice corrosion, some other materials such as wood, rubber, wax, concrete, living organisms, and glass have been reported to have caused this attack [15, 24, 79]. It has also been reported that this attack may be a result of the concentration gradient of oxygen or ions in crevices, and it is more aggressive in chloride environments [80]. Figure 2.13 shows an example of crevices corrosion that resulted from small volumes of stagnant liquids trapped in crevices under the metallic bolt.



Figure 2.13: Representation of crevice corrosion [81].

2.1.4.6 Erosion corrosion

Erosion or abrasion corrosion is a form of metallic attack that occurs when there is a relative movement between an aqueous or gaseous corrodent and a metal surface submerged in it [15, 72, 82]. This type of corrosion is usually associated with systems where there is a high-speed movement of corrosive fluids. Some of these systems which are most commonly affected include piping systems and heat exchangers [15]. However, all equipment subjected to flowing fluids is prone to erosion-corrosion [24, 82]. Moreover, a variety of types of corrosives (e.g., organic systems, gases, aqueous solution, etc.) have the potential of causing erosion-corrosion [24]. Figure 2.14 shows an example of failure at a pipe elbow due to erosion-corrosion.



Figure 2.14: The failure at a pipe elbow due to erosion-corrosion [82].

2.1.4.7 Fretting corrosion

Fretting corrosion is also referred to as friction oxidation, it is defined as the deterioration of metals that occurs when two metal surfaces are in contact and are subjected to slight vibration or slip [24]. The vibration may vary in amplitude from less than a nanometer to about micrometers [76]. This form of metallic attacks is mostly expected in tight-fitting parts (e.g. bolted joints, automotive parts, fits, etc.) that are not manufactured to slip other, but in the presence of vibration then slip each other. Fretting corrosion very detrimental because it occurs to heavy loaded metallic surfaces that have a slight movement but frequently against each other in an atmospheric environment rather than in aqueous conditions [24]. Figure 2.15 show an example of fretting corrosion.



Figure 2.15: An example of fretting corrosion [25].

2.1.4.8 Selective corrosion

Selective corrosion is sometimes referred to as “selective leaching” occurs when one component of an alloy that is less noble than the other is removed and as a result, the alloy or material turns to be porous, with very low strength and stability [83]. “Graphite corrosion” is the term that is used for the leaching of iron from cast iron [81, 83] and “dezincification” is the term describing the leaching of zinc from brass [81]. Table 1.2 shows other combinations of alloys and corrosive environment at which they are susceptible to selective leaching. High temperatures and stagnant solutions (acidic) are some of the conditions that stimulate this form of metallic attack [15]. Moreover, it is difficult to discover or notice “selective corrosion” because sometimes the sites that are selectively attacked are covered with corrosive products [72]. Figure 2.16 shows the leaching of zinc from brass on a plumbing pipe.



Figure 2.16: An example of selective corrosion.

Table 2.3: Combinations of alloys and corrosive environment selective leaching [24].

Alloy	Environment	Element Removed
Aluminum	Hydrofluoric acid, acid chloride solutions	Aluminum
Bronzes, brasses	Many waters	Zinc
Cupronickels	High heat flux and low water velocity (in refinery condenser tubes)	Nickel
Gray iron	Soils, many waters	Iron
Gold alloys	Nitric, chromic, and sulfuric acids, human saliva	Copper or silver
High-nickel alloys	Molten salts	Chromium, iron, molybdenum, tungsten,
Iron-chromium alloys	High-temperature oxidizing atmospheres	Chromium
Medium- and high-carbon steels	Oxidizing atmospheres, hydrogen at high temperatures	Carbon
Monel	Hydrogen and other acids	Copper in some acids, nickel in others
Nickel-molybdenum alloys	Oxygen at high temperatures	Molybdenum
Silicon bronzes	High-temperature steam, acidic solution	Silicon
Tin bronzes	Hot brine, steam	Tin

2.1.5 CORROSION THERMODYNAMICS

Thermodynamics is the science that deals with the changes in energy and properties related to work and heat [24]. When evaluating metal's susceptibility to corrosion attack, thermodynamic parameters such as galvanic series, which include the reduction electrode potentials list and electromotive forces of common metals listed in standard emf are commonly mentioned or looked at [72]. It is important to note that these parameters (potentials) can be useful in determining the spontaneity of corrosion reaction, but not the rate at which corrosion occurs [7, 72]. One of the important thermodynamic state functions is that it provides information about the spontaneity of a corrosion reaction is Gibbs free energy (ΔG) and will be further discussed in subsequent sub-sections.

2.1.5.1 Gibbs free energy (ΔG)

Fontana [24], defined Gibbs free energy as “a direct measure of the work capacity or maximum electric energy available from a system. In the corrosion concept, “a system” refers to the deterioration of metal with its environment. A negative value of Gibbs free energy indicates that a corrosion reaction proceeds in a spontaneous direction and there is a loss in free energy [7, 10, 24, 42]. In principle, this means that, if there are no external forces acting on the system, the system will have a tendency to transform to its lowest energy state [24]. Moreover, a positive value of Gibbs free energy indicates that the reaction has no tendency to go or proceed at all [10]. It should be noted that the tendency of a metal/alloy to corrode does not foretell any information about the reaction rate. However, a positive value of Gibbs free energy indicates with certainty that the reaction has no tendency to go or proceed at all under given conditions unless interfered externally [10]. The value of the Gibbs free energy change for an electrochemical reaction that has all reactants and products are in their standard conditions is calculated by equation (9).

$$\Delta G^\circ = -nFE^\circ \quad (9)$$

where ΔG° is the Gibbs free energy, n is the number of electrons involved in the entire electrochemical reaction, F is the Faraday constant and E° is the emf when all the reactants and product are in their standard conditions, with all the reactants and the product at unity activity. Equation (9) can be related to the equilibrium constant (K_{eq}) by equation (10) below [3]:

$$RT \ln K_{eq} = \Delta G^\circ = -nFE^\circ \quad (10)$$

2.1.5.2 Standard electrode potentials

As shown previously (sub-section 2.1.1.3), the potential difference across an electrochemical (corrosion) cell is the potential difference measured between two electronic conductors connected to an anode and cathode electrodes. It is this potential difference between the two electrodes that causes the flow of electrons. Additionally, the movement of the electrons will be from the anodic to the cathodic site and by convention, the corrosion current will flow from cathodic to the anodic. It can also be said that in the external circuit the electrons can move from the least positive electrode to the more positive electrode. This can be attributed to the fact that the electrode potential can either be negative or positive [3]. The potential difference across the electrochemical cell can be measured using a voltmeter, however, the voltmeter cannot measure the potential difference directly for one electrode [1, 3]. Although the process is not simple, it is possible, however, to measure the potential of an electrode and electrolyte. The absolute value of the potential that will result from such a situation will depend on the temperature, pressure, and on the concentration of the electrolyte solution, and this measurement lacks precision [2]. The most classical method to correct or remove these inconsistencies was to choose a relative standard reference electrode to compare all the electrode potentials with, which will be all done under the same conditions.

The electrode that is normally used as a reference for electrode potential measurements is the standard hydrogen electrode (SHE). This electrode consists of a platinum electrode immersed in a solution of known concentration of hydrogen ions, aqueous-arsenic free hydrochloric acid, and saturated with free oxygen and carbon monoxide hydrogen gas that is bubbled to the platinum surface. For this reference electrode to be usable in comparison to other electrodes, its potential value is taken to be zero at any temperature [3, 5, 84]. Figure 2.17 displays a simplified representation of the standard hydrogen electrode.

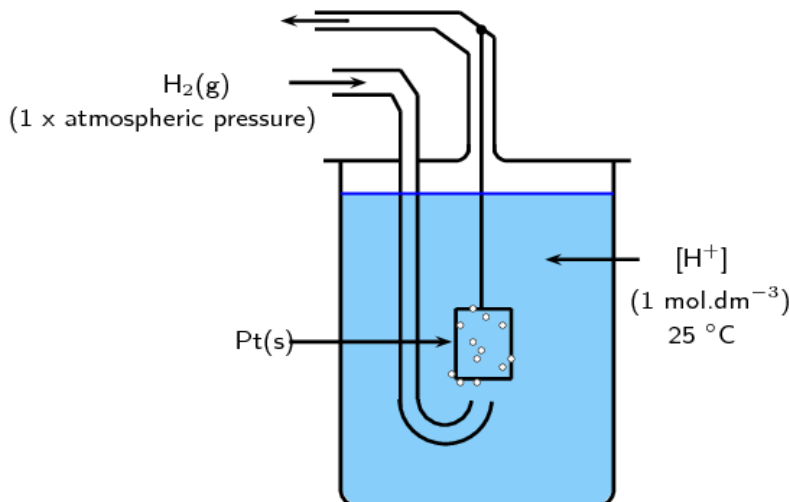


Figure 2.17: schematic diagram of the SHE [20].

The absolute potential values of various metal surfaces are not known. However, by coupling various metal's half-cells with the SHE at standard conditions, their electric potentials were measured and compared relative to the potential of SHE which was taken as zero [20, 84, 85]. This way series of potentials for electrodes were determined and represented by Table 1.4. This series is called the Electromotive (emf) series or electrochemical series. The emf series ranks metals relative to their tendency to corrode, with metals with the most positive potential values are placed at the top of the series and decreased through the potential of the SHE to potentials of the largest negative values. The metals with more positive values are also called nobles metals and possess resistance to corrosion, and the inverse is true [85]. For instance, according to the emf series zinc electrode has a potential value of -0,763 volts has a greater tendency to corrode as compared to iron with a value of -0.440 volts. Gold and platinum are among the metals with greater positive potential values; hence they are called noble metals [3, 20, 85].

In 1888, German chemist W. Nernst established a very useful relation that predicts the exact emf involved in the corrosion process of metal in terms of activities of reactants and products of a corrosion cell. This relation is given by equation (11), and it is called the Nernst equation [3, 6, 85].

$$E = E^{\circ} - \frac{RT}{nF} \ln K \quad (11)$$

Table 2.4: Standard reduction half-cell potentials [85].

Standard Rduction potential at 298 ° K on the hydrogen scale			
Sr. No.	Electrode	Reduction Half reaction Oxidising agent → Reducing agent	E ^o (volts)At 298 K
1	F ⁻ F ₂ Pt,	F ₂ + 2e ⁻ → 2F ⁻	+2.87
2	Au ⁺ Au	Au ⁺ + e ⁻ → Au	+1.68
3	Ce ⁴⁺ , Ce ³⁺ Pt,	Ce ⁴⁺ + e ⁻ → Ce ³⁺	+1.61
4	Au ³⁺ Au	Au ³⁺ + 3e ⁻ → Au	+1.50
5	Cl ⁻ Cl ₂ Pt	Cl ₂ + 2e ⁻ → 2Cl ⁻	+1.36
6	Pt ²⁺ Pt	Pt ²⁺ + 2e ⁻ → Pt	+1.20
7	Br ⁻ Br ₂ Pt	Br ₂ + 2e ⁻ → 2Br ⁻	+1.08
8	Hg ²⁺ Hg	Hg ²⁺ + 2e ⁻ → Hg	+0.854
9	Ag ⁺ Ag	Ag ⁺ + e ⁻ → Ag	+0.799
10	Hg ₂ ²⁺ Hg	Hg ₂ ²⁺ + 2e ⁻ → Hg ₂	+0.790
11	Fe ³⁺ , Fe ²⁺ Pt,	Fe ³⁺ + e ⁻ → Fe ²⁺	+0.771
12	I ⁻ I ₂ (s) Pt	I ₂ + 2e ⁻ → 2I ⁻	+0.535
13	Cu ²⁺ Cu	Cu ²⁺ + 2e ⁻ → Cu	+0.337
14	Pt Hg Hg ₂ Cl ₂ Cl ⁻	Hg ₂ Cl ₂ + 2e ⁻ → 2Hg + 2Cl ⁻	+0.242
15	Ag AgCl(s) Cl ⁻	AgCl + e ⁻ → Ag + Cl ⁻	+0.222
16	Cu ²⁺ Cu ⁺	Cu ²⁺ + e ⁻ → Cu ⁺	+0.153
17	Sn ⁴⁺ , Sn ²⁺ Pt	Sn ⁴⁺ + 2e ⁻ → Sn ²⁺	+0.15
18	H ⁺ H ₂ Pt	2H ⁺ + 2e ⁻ → H ₂ (g)	0.0 (Definition)
19	Pb ²⁺ Pb	Pb ²⁺ + 2e ⁻ → Pb	-0.126
20	Sn ²⁺ Sn	Sn ²⁺ + 2e ⁻ → Sn	-0.136
21	Ni ²⁺ Ni	Ni ²⁺ + 2e ⁻ → Ni	-0.257
22	Co ²⁺ Co	Co ²⁺ + 2e ⁻ → Co	-0.280
23	Cd ²⁺ Cd	Cd ²⁺ + 2e ⁻ → Cd	-0.403
24	Fe ²⁺ Fe	Fe ²⁺ + 2e ⁻ → Fe	-0.440
25	Cr ³⁺ Cr	Cr ³⁺ + 3e ⁻ → 3Cr	-0.740
25	Zn ²⁺ Zn	Zn ²⁺ + 2e ⁻ → Zn	-0.763
26	Al ³⁺ Al	Al ³⁺ + 3e ⁻ → 3Al	-1.66
27	Mg ²⁺ Mg	Mg ²⁺ + 2e ⁻ → Mg	-2.37
28	Na ⁺ Na	Na ⁺ + e ⁻ → Na	-2.714
29	Ca ²⁺ Ca	Ca ²⁺ + 2e ⁻ → Ca	-2.866
30	K ⁺ K	K ⁺ + e ⁻ → K	-2.925
31	Li ⁺ Li	Li ⁺ + e ⁻ → Li	-3.045

2.1.5.3 Potential-pH diagram

Potential-pH diagrams, also called Pourbaix diagrams are one of the useful concepts in interpreting thermodynamic data of the stability of any metal as a function of the potential and concentration of hydrogen ions of the aqueous solution [86]. Pourbaix diagrams are not constructed based on conducting corrosion tests experimentally, but they are generated from calculations based on the Nernst equation, equilibrium constants, and the solubility data [6, 15, 85]. Such diagrams are applicable in (a) predicting the tendency of any metal to corrode, (b) estimating the corrosion product formed, and (c) predicting any change in the environment (hydrogen ions and potential adjusting) which may reduce the corrosion attack [3, 15, 85]. A typical example of such diagrams is the E-pH diagram (Figure 2.18) for iron at 398 K which describes the general corrosion behavior of iron in the presence of water.

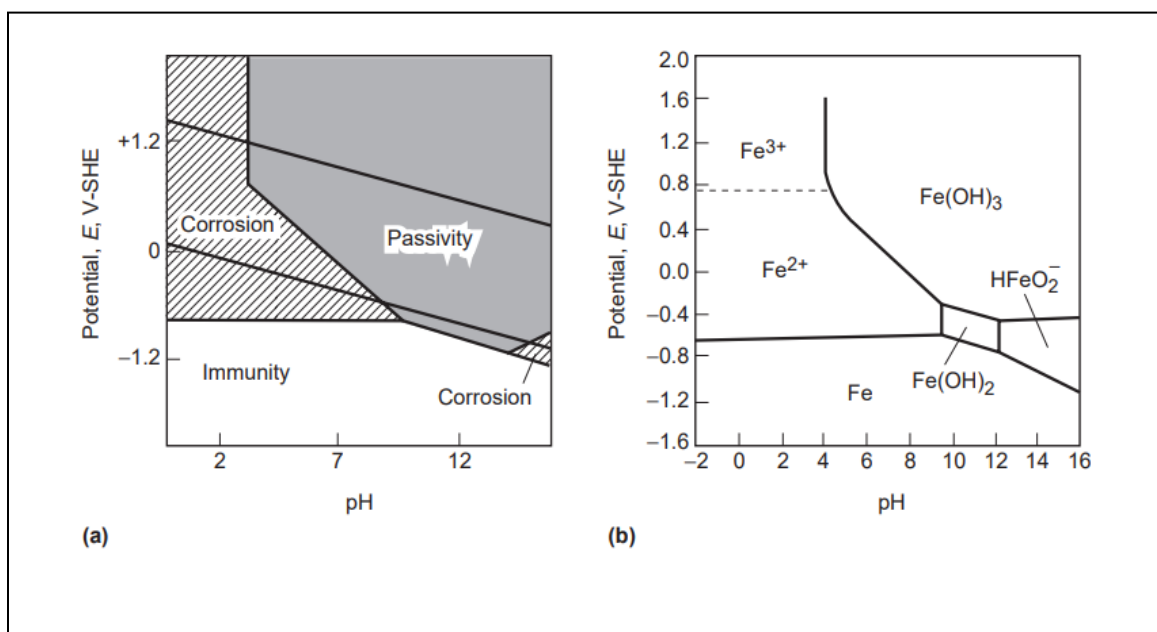


Figure 2.18: Pourbaix diagram for the Fe-H₂O system at 398 K showing (a) indicating three different corrosion regions (b) considering Fe, Fe₃O₄, and Fe₂O₃ as the only solid substances [85].

Figure 2.18 (a) indicate the simplified potential-pH diagrams for the iron-water system with the region of immunity, corrosion, and passivity which are briefly discussed described [6, 15, 85, 86]:

- **Immunity zone:** this is the region at the bottom of the diagram, and it represents conditions of potential and pH, Fe is thermodynamically stable. Any potential-pH combinations in this zone, Fe is resistant to corrosion and remains in metallic form.
- **Corrosion zone:** thermodynamic calculations show that the potential-pH combinations in this region, Fe is stable and soluble species (Fe^{2+} or Fe^{3+} or HFeO_2^-), and therefore it is prone to corrode.
- **Passive zone:** under these conditions of potential and pH, iron reacts to form a protective layer $[\text{Fe}(\text{OH})_3]$ which blocks the corrosion of Fe from further occurring.

2.1.6 CORROSION KINETICS

As seen previously, thermodynamic calculations allow the prediction of the tendency of any metal to corrode and, the conditions under which a metal is at a stable state or resistant to corrosion. Moreover, thermodynamics does not, however, convey any information about the rate at which corrosion may occur [85]. A thorough understanding of the mechanism of a corrosion reaction is necessary, hence, it is useful in foretelling if corrosion will occur and also determining the rate of corrosion reaction [20]. Thus, kinetic data is required in making such predictions. Some of the common electrochemical kinetic concepts include but are not limited to polarization and the Arrhenius equation. Polarization raises when the electrochemical equilibrium potential (E_{corr}) is altered due to the flow of current through the corrosion cell and it is expressed in terms of the resultant potential (E), and overpotential (η) [3, 87], given by equation (12).

$$\eta = E - E_{corr} \quad (12)$$

There are three different types of polarization and these independent overpotential contributors are [3, 87, 88]:

- **Activation overpotential (η_{act}):** is the difference in potential from the equilibrium for a given corrosion reaction that results if the concentration of the reactants and products at the given electrode surface are the same in the bulk solution. It is the main polarization component and always present at small currents.
- **Concentration overpotential (η_{conc}):** describe voltage losses in the corrosion cell result from to the limitation or hindrance of movement of chemical species to/from the electrodes due to mass transfer resistance between the electrode surface and the bulk electrolyte.
- **Ohmic drop (iR):** also referred to as iR ohmic potential reduction, it stems from the resistance along the current path in the corrosion cell.

It is therefore essential to know the type of polarization occurring in the corrosion reaction, since they play a tremendous role in studying the characteristic of a corrosion system of interest. For instance, The Butler-Volmer equation, equation (13), can be utilized to express the relationship for a reaction in which the rate is limited by activation overvoltage in terms of current density i , and potential E .

$$i = i_{corr} \exp\left[\frac{\alpha n F \eta_0}{RT}\right] \quad (13)$$

where α is the unitless charge transfer coefficient, with the value usually close to 0.5, but must lie between 0 and 1. n is the charge on the ion in equivalents/mol. i is the measured current density and i_{corr} is corrosion current.

Rearranging equation (13), one get the anodic and cathodic Tafel equations expressed in equation 14 and 15 respectively [87, 89, 90].

$$\eta_a = b_a \log\left(\frac{i}{i_{corr}}\right) \quad (14)$$

$$\eta_c = b_c \log\left(\frac{i}{i_{corr}}\right) \quad (15)$$

where b_a and b_c are called anodic and cathodic Tafel constants, respectively, and η_a and η_c are anodic and cathodic overpotentials, respectively. These parameters can be obtained experimentally.

The Tafel equations can be used in constructing plots, called Evans diagram, which can be further interprets corrosion kinetic data. These equations predict what is often called, Tafel slopes for the variation of logarithm of current density against potential [87]. An example of such diagram is shown in the figure 2.19.

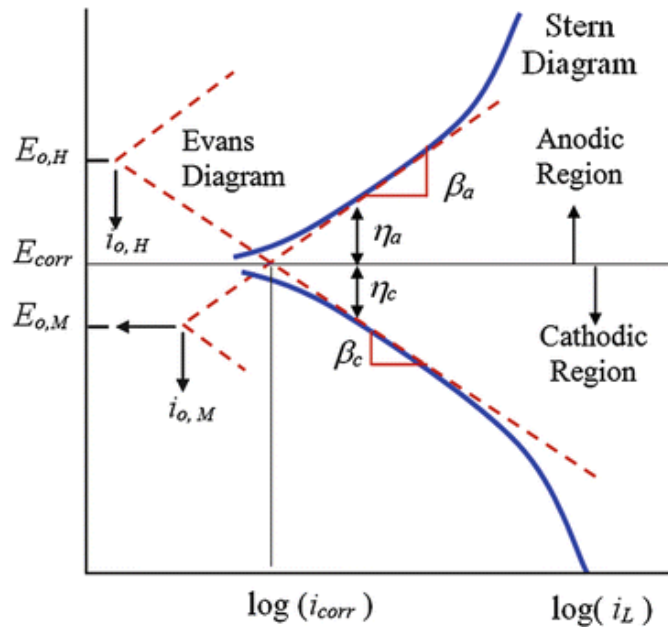


Figure 2.19: Schematic Evans diagram for the corrosion of metal by an acid [91].

Further information on corrosion rate can also be estimated from the Arrhenius equation. The Arrhenius equation relates the effect of activation energy and temperature change with the rate at which a corrosion reaction may occur, and it is expressed by the following equation [89]:

$$C_R = A \exp\left(-\frac{E_a}{RT}\right) \quad (16)$$

where C_R is the corrosion rate, A is the Arrhenius pre-exponential factor, E_a is the activation energy (J mol^{-1}), R is the universal gas constant ($8.314 \text{ J mol}^{-1} \text{ K}$), and T is the absolute temperature (K).

2.1.7 RATE OF CORROSION

A corrosion reaction of a metal/alloy result in the slow or fast degrading or dissolution of metal and consequently resulting in loss of efficiency and weight. Corrosion rate, is, therefore, the quantification of how fast the degradation of a metal/alloy may occur in a particular environment they are exposed to. The measurement of the rate of corrosion can be expressed in many different units, and the most common are [1, 15]:

- corrosion current density (mA/cm^2), this method involves the quantification of the rate of corrosion using electrochemical techniques such as potentiodynamic polarization (PDP), linear polarization resistance (LPR), and electrochemical impedance spectroscopy (EIS).
- weight loss per unit area per unit time, usually expressed in units: milligrams per square decimeter per day (mmd) or (mg/dm^2 day). This method is widely used, and it is regarded as the simplest.
- increase in corrosion depth per unit of time also known as control penetration rate (CPR), this method measures the thickness of the metal specimen as it gets thinner per unit time. It has the units, inch penetration/year (ipy), and mils penetration/year (mpy).

Some other common corrosion rate units and their interconversions are shown below in Table 1.5 and 1.6, respectively.

Table 2.5: Some units commonly used to express corrosion rates [1].

Weight loss	Penetration	Corrosion current density
$\text{g/cm}^2 \text{ h}$	ipy (inches per year)	$\mu\text{A/cm}^2$
$\text{g/cm}^2 \text{ day}$		Ma/cm^2
$\text{g/m}^2 \text{ h}$	mpy (mils per year) ^a	A/cm^2
$\text{g/m}^2 \text{ day}$	Mm/year	A/m^2
$\text{mg/m}^2 \text{ s}$	$\mu\text{m/year}$	
mdd ($\text{mg/dm}^2 \text{ day}$)		

Table 2.6: Interconversion of corrosion units [1].

	mAcm^{-2}	mmpy	mpy	$\text{gm}^{-2}\text{day}^{-1}$
mA cm^{-2}	1	3.28 M/nd	129 M/nd	8.95 M/n
mmpy	0.306 nd/M	1	3.94	2.74 d
mpy	0.0077 nd/M	0.0254	1	0.0694 d
$\text{gm}^{-2}\text{day}^{-1}$	0.112 n/M	0.365/d	14.4/d	1

2.1.7.1 Factors affecting rate of corrosion

The corrosion rate is influenced by several factors. Some of these factors are briefly discussed below [91, 92]:

2.1.7.1.1 Temperature

Generally, the rate of corrosion is highly influenced by temperature variations. In most chemical or electrochemical reactions, the increase in temperature goes along with the increase in the reaction rate due to the increase in kinetic energy [93– 95]. The dependence of corrosion rate on temperature can be experimentally linked with the rate constant through equation (16), the

Arrhenius equation [89, 93–99]. From the expression of the Arrhenius, it can be immediately seen that in a chemical reaction, the rate at which corrosion occurs exponentially rises with the increase in the temperature of the medium or surrounding.

In some corrosion reactions, water and oxygen are the two most reactants which sensitive to temperature variations [97]. Thus, corrosion reactions are also influenced by the diffusion of oxygen, that at a given concentration of oxygen the rate of corrosion is doubled for every temperature increase of 303 K [10, 97]. However, for an open corrosion system, as the temperature rises above 353 K towards the boiling point, the rate of reaction decreases drastically [10, 100–102]. This is attributed to the significant decrease of the oxygen in water which results in a marked decrease in the concentration of water and oxygen, hence the rate decreases. On a contrary, for a closed corrosion system, the rate will proceed to increase with the increase in temperature. These can be observed in figure 2.20.

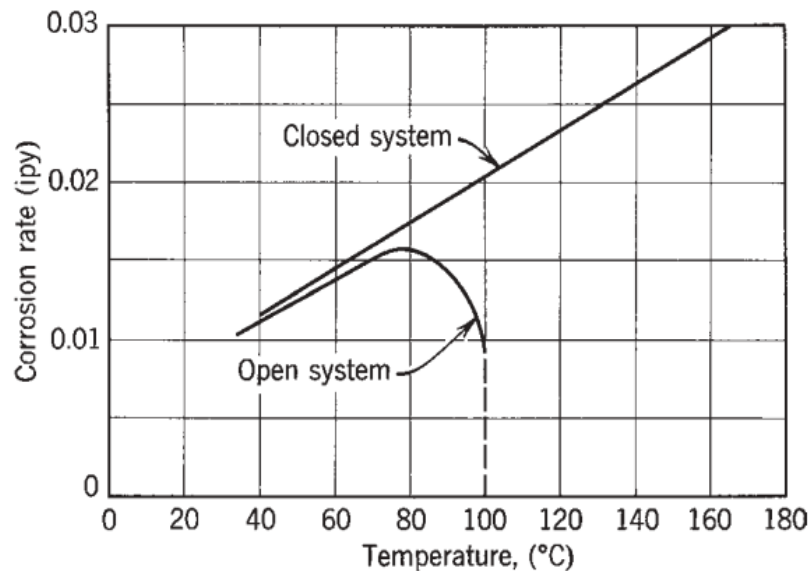


Figure 2.20: Effect of temperature on open and closed corrosion system iron in water containing dissolved oxygen [102].

2.1.7.1.2 Nature of the corrosion product

The rate at which corrosion occurs on a metal surface is sometimes largely influenced by the nature of the oxide that is formed. The oxides may form as stable and impermeable, or they may form as unstable and permeable on the metal surface. If it is stable, the oxide acts as protective layer on the metal surface which prevents corrosion from further occurring. Meanwhile, if it is unstable and permeable, it further allows oxygen easy access on the exposed metal surface, thus, enhancing the corrosion process at a constant rate. The layer that is formed on the metal surface is generally known as either film or a scale, with the term film refers to layers that are very thin (10–3 mm or less) and scale to very thin films. Examples of some of the metals in corrosion processes form oxides as protective films are aluminum, chromium, titanium, tin, lead, etc., meanwhile, metals such as zinc, iron, and magnesium, when exposed to some corrosive media are highly prone to continuous corrosion since they do not form any protective layer that act as a barrier between their surfaces and the corrosive medium [103–105].

2.1.7.1.3 pH of the corrosive environment

The rate of corrosion is generally higher in environments with lower pH value (acidic solutions) than in neutral (pH = 7) or alkaline (pH > 7) [3, 20] environment. However, the effect of pH on corrosion rate differs with metals. For instance, in the case of iron, chromium, and manganese, the rate of corrosion is very high at corrosive solutions of pH < 4, and in solutions of pH > 13.5 at temperatures above 353,15 K. Moreover, they are resistant to corrosion at solutions of pH = 9 to 13. Aluminum is known to be resistant at pH = 4.5 to 8.3, meanwhile, zinc is resistance at pH = 6.5 to 12 [20]. Figure 2.21 shows the pH effect on the corrosion rate of aluminum and iron.

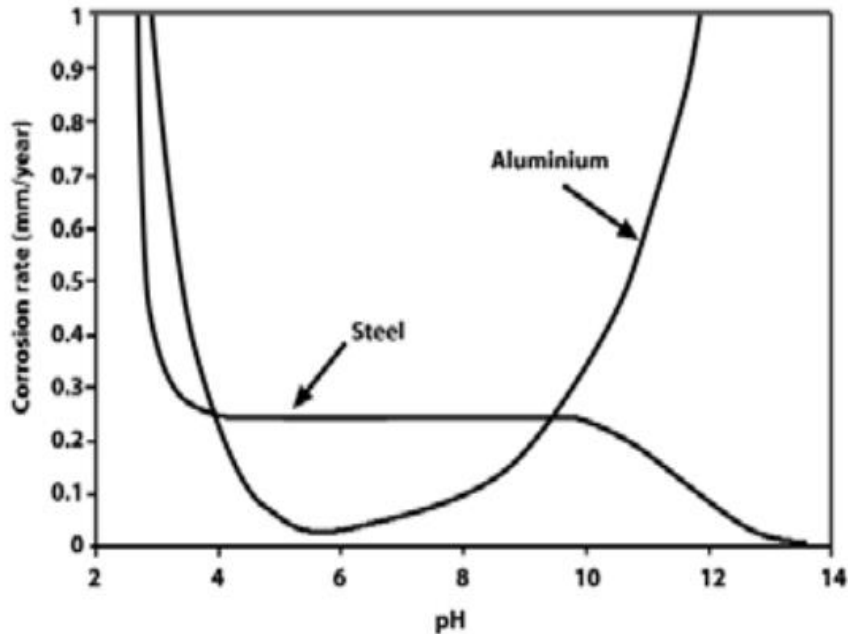


Figure 2.21: The effect of pH on the measure corrosion rate of aluminum and iron [105].

2.1.7.1.4 Humidity

Humidity has more influence on atmospheric corrosion than in dry air. For atmospheric corrosion to occur, there should be a presence of moisture on the metal surface which acts as a solvent for the oxygen in the air to supply the electrolyte that is needed for the formation of the corrosion cell. Thus, the rate of corrosion, generally, increases with increasing humidity. Moreover, below a certain value of relative humidity, the moisture film on the metal surface is so thin that the corrosion process occurring on that particular metal is considered negligible [20, 105–106]. For instance, as shown in figure 2.22, the rate of corrosion of iron significantly increases at relative humidity 60% to 80%, but below 60% the rate is rapidly declined [10, 20, 70, 107].

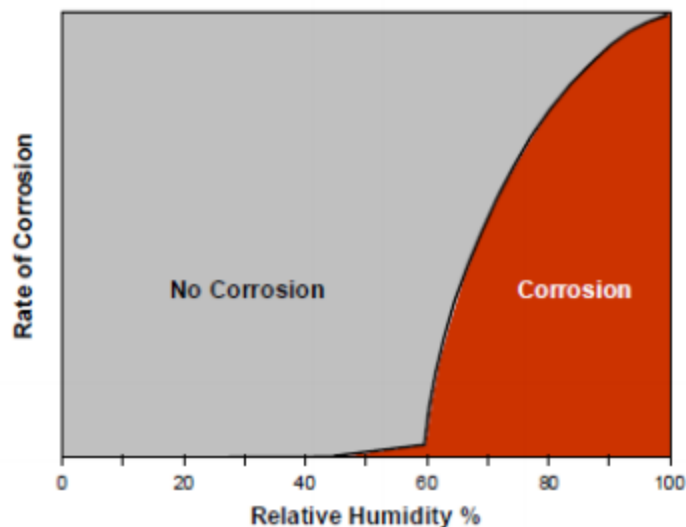


Figure 2.22: The effect of relative humidity on the corrosion rate of iron [107].

2.1.7.1.5 Purity of metal

The presence of impurities in a metal results in the creation of heterogeneity which leads to the formation of a local galvanic cell. The cell is formed in a way that the metal acts as an anodic site and the impurity as a cathodic site, thus, results in the corrosion of the metal. For different metals, there is a tolerance limit of the concentration of the impurity by which the corrosion rate can be triggered. That is, when the concentration of the impurity is higher than the tolerance limit, the corrosion rate will likely increase exponentially, whereas the corrosion rate will low or negligible below this tolerance limit [20, 108–110]. Generally, the tolerance limits of most metals are affected by the presence of other elements/metals [110]. For instance, impurities such as lead and iron in zinc result in the creation of tiny galvanic cells, hence there is a noticeable increase in the rate of corrosion of zinc around the impurities [20, 110]. In most cases, metal with a high percentage of impurities is prone to corrode and pure metals and homogenous alloys are resistant to corrosion [10, 20].

2.1.7.1.6 Effect of velocity

The protective film that formed on the metal surface during the corrosion process plays a tremendous role in minimizing the rate of corrosion of metals to some extent [111]. If this protective film is altered by and mechanical disturbances such as turbulence, abrasion, or impingent, the film can be removed, and this can lead to more attack on the underlying metal [111–115]. In essence, liquids that flow at relatively high velocity and liquid turbulence remove protective films formed by corrosion products, and consequently, increasing the rate of corrosion for exposed metals to specific corrosives. Figure 2.23 represents the different states of an oxide-surface film behavior as liquid velocity or surface shear stresses are increased.

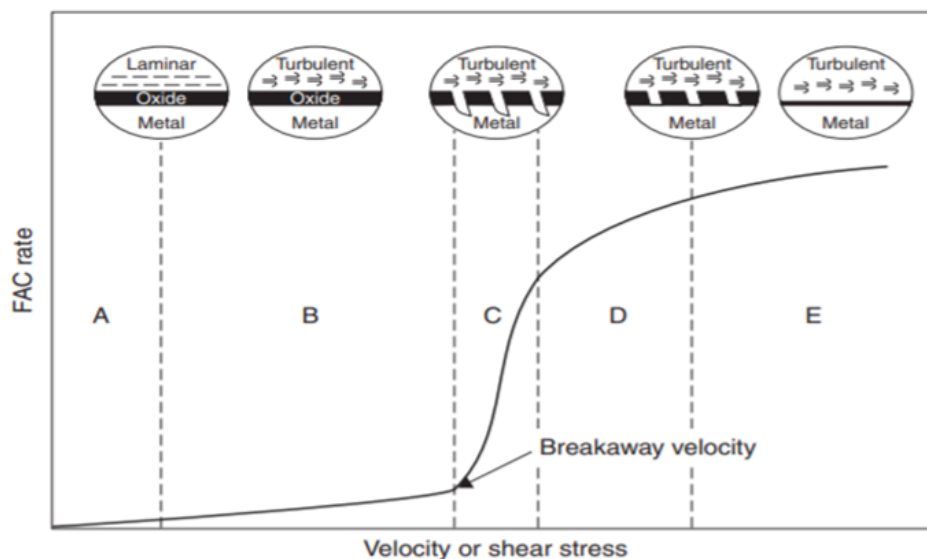


Figure 2.23: Different states of an oxide-surface film behavior as liquid velocity or surface shear stresses are increased [116].

1.2.7.1.7 Nature of the Metal

Metals that have higher electrode potentials (noble metals) such as gold, platinum, and silver do not corrode, whereas metals like zinc, aluminum, magnesium, iron, etc., with lower electrode potential, are prone to corrosion. Thus, when two dissimilar metals are in contact with a relatively large difference electrode potential, the metal with lower electrode potential will act as an anode and hence undergo an attack. The rate of corrosion increases with the increase in electrode potential of two dissimilar metals in contact [20].

2.1.8 EFFECTS OF CORROSION

The effect of corrosion in our daily lives are many and they can be direct or indirect. Moreover, these effects come with different severity from one to another. Some of these consequences of corrosion that have a negative impact on our lives are briefly discussed in the subsequent subsections below:

2.1.8.1 Economic effects

Corrosion has major economic consequences to the world's economy as it sometimes results in premature failure of industrial structures and components, which cause significant economic losses. This is a global economic crisis, even advanced-developed countries cannot escape these economic losses and the real cost of corrosion remain unmeasured [117–119]. The estimation of the economic cost for South Africa has been discussed in section 1.2. The corrosion economic costs subject has previously attracted many researchers in attempting to find methods for data and economic analysis to mitigate the extent of the severity of these losses [120]. In 1964, Uhlig [121], led a study that estimated that in the United States corrosion cost about \$5.5 billion or 2.1% of the country's GDP annually. His estimated cost value was the sum of both direct and indirect costs, and these costs are shown in Table 2.7. In 1970 [122], another report was issued by the United Kingdom (UK) committee led by Hoar. In their report, they estimated that in the UK corrosion cost about £1365 million or 3.5% of the nation's GDP in 1970, annually. Their report summarized the cost of corrosion in the industry sector, and the cost are shown in Table 1.8.

Table 2.7: Direct and indirect corrosion cost in US [121].

	Item	Cost (\$ million)	% of Total cost
Direct costs	Paint	2000	36
	Metallic coatings and electroplate	472	9
	Corrosion-resistant metals	852	15
	Boiler and other water treatment	66	1
	Underground pipe maintenance and replacement	600	11
Indirect costs	Domestic water heater replacement	225	4
	Auto engine repairs	1030	19
	Auto muffler replacement	66	1

Table 2.8: National corrosion costs in UK [122].

Industrial Sector	Estimated Corrosion Costs	
	£ x million	%
Building and construction	250	18
Food	40	3
General engineering	110	8
Government departments	55	4
Marine	280	21
Metal refining and semifabrication	15	1
Oil and chemicals	180	13
power	62	4
Transport	350	26
Water	25	2
total	£1365	100

Following Uhlig's and Hoar's study, many reports of the economic corrosion costs were published. Such reports include but are not limited to; the Japan report in 1977 [123], The Battelle-NBS report (United States) in 1978 [124], and the Kuwait report in 1995 [120].

2.1.8.2 Human life and health

Some of these consequences of corrosion are of a serious concern than just loss of mass of metal as they result in injuries and loss of life. Metals have been used in a vast application in the healthcare environment. They are used as human body parts such as hip bones [1], knee [125–127], and tooth [128] replacements [figure 2.24 (a) and (b)]. The selection of these metals requires thorough research and the highest durability and strength for the corrosion of these metals in the human body may lead to serious health issues or sometimes death may result.

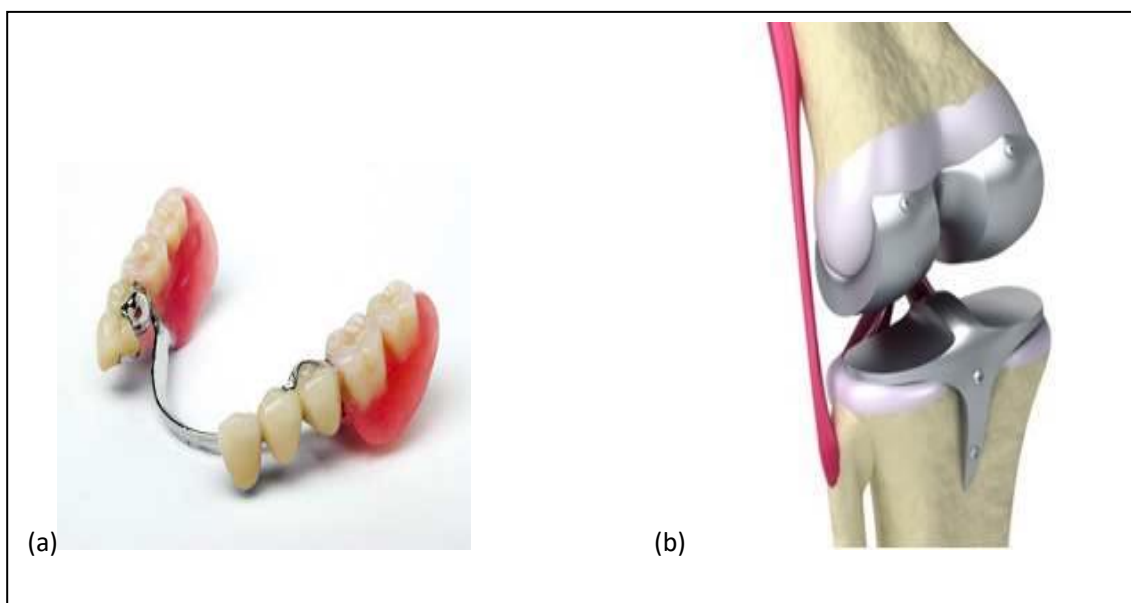


Figure 2.24: Illustration of (a) a dental implant and (b) a knee implant using metals [125–128].

There are also recorded catastrophic corrosion-related incidents that resulted in serious injuries and death. A few of these incidents are;

- The “Silver Bridge” collapsed in West Virginia, December 1967, due to stress corrosion. The incident claimed 46 lives [129].
- The chemical plant explosion (figure 2.25) in Bhopal, India in 1984, killed over 8000 people. It is reported that the explosion resulted from corroded steel pipes which leaked water into tanks containing methylisocyanate and the iron corrosion enhanced the reaction,

hence the plant blew apart and other dangerous gases escaped. Moreover, it is also estimated that since then, 500,000 others are suffering from gas-related disorders as a result of that explosion [130, 131].



Figure 2.25: 1984 India chemical plant after exploding [132].

- The most recent reported corrosion-related incident which leads to loss of life was the sinking of the ship “Princess Ashika” sinking accident in 2009 (figure 2.26). August 5th, 2009, the cargo ferry Princess Ashika sank just after taking on water and as a result, 74 people were declared dead. It is also reported that the marine engineer who was assigned to inspect the ship declared it unfit just before sailing as he presented his findings (pictures) showing the doors unable to close properly due to corrosion, but his warnings were ignored [130, 132].



Figure 2.26: A picture of ferry “Princess Ashika” under the sea [131].

2.2 CORROSION CONTROL MEASURES

There are various measures of controlling corrosion just as there are various types and causes (e.g., temperature, pH, humidity, etc.) of corrosion. These measures are aimed to eliminate or reduce these causes and they are all important in one way or the other since there is none of them which has been reported to have been effective enough for all types of corrosion [72]. Some of the most common measures of preventing corrosion are discussed below;

2.2.1 Material selection

This method involves controlling corrosion by selecting property material that does not corrode easily or a combination of materials that are favorable in minimizing the magnitude of corrosion. For instance, for a given corrosive environment, a combination of metals with a significantly small potential difference will not readily corrode as compared to a combination of metals with a big potential difference [133]. Choosing a proper material requires enough knowledge on aspects like; practical environmental conditions that can affect the material, economic considerations, and design of their end products, which must be taken to account in the final selection. However, sticking with materials that have been successfully utilized for that similar purpose before is the simplest way [133–135].

2.2.2 Proper design

This technique works together with material selection. It involves the selection of special metallic equipment for a proper design that can protect metal to some extent from corrosion when exposed to the prevailing environment. It is important that corrosion expect to be an integral part of the designing process to convey sufficient knowledge which might be useful not only in the design itself but can predict other potential corrosion-related challenges that may arise in the long run of that equipment. In many cases, equipment failures are due to the fact that more attention is paid on the selection a good corrosion-resistant material for specific environments than the design and this leads to major unnecessarily cost, which could have been easily avoided if corrosion were incorporated with design at the very early stage of manufacturing [133–135].

2.2.3 Protective coating

Protecting metal/alloys from corrosion by coatings is the most used method. The coatings applied to a metal surface to reduce the extent of corrosion attack are classified as; metallic coatings, inorganic coatings (e.g., anodizing, conversion coatings, glasses, cement, etc.), and organic coatings (e.g., chlorinated rubber, paints, plastics, varnishes, etc.). The coating and lining applied on a surface for protection may work through one or the combination of the three basic mechanisms briefly discussed below: [70, 135–137]

- **Chemical inhibition:** this protection is achieved when chemical inhibitive substances are incorporated into paint formulations, and they form a coating from one to several molecular layers which then acts as a barrier between the metal/alloy surface and the prevailing environment.
- **Barrier effect:** this protection is achieved when coating totally prevents any contact between the metal/alloy surface and the prevailing environment.
- **Sacrificial protection:** this protection is achieved by coating a surface with a more reactive metal (more active metal), this results in the coated surface acting as a cathode and the coating material being a sacrificial anode. Figure 1.27 shows an example of sacrificial

protection offered by zinc coating to a steel surface. This method is also known as cathodic protection.

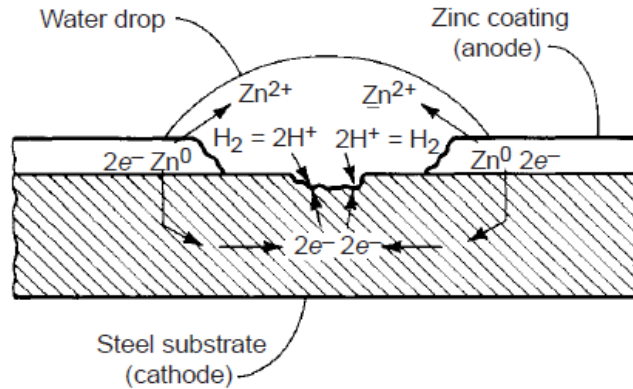


Figure 1.27: Sacrificial protection offered by zinc coating to steel surface [70].

2.2.4 Cathodic protection

The cathodic protection (CP) method has been used for over decades in protecting metals and other materials against corrosion. The main principle of this method is to modify an electrochemical cell of metal by forcing the potential difference of the metal into the immunity region, as shown in Figure 2.18, and described in sub-section 2.1.5.3 [15, 70, 85, 135–137]. CP can be further be expressed into two systems, which are the sacrificial anode and the impressed-current systems. These systems are briefly described below;

- **Sacrificial anode:** in this system a more active metal than that the one used in the structure is coupled so the structure could act as a cathode during the corrosion process. The more active metal (noble) is then being used as the protection of the structure. Hence, it is called a sacrificial anode. Some common metals used as sacrificial anodes in the protection of steel include, amongst others, zinc, aluminum, and magnesium. Sacrificial anodes are usually preferred to be sufficiently bigger in size so that they can be useable for a longer period of time. In addition, this system is typically used when current requirements are relatively low.

- **Impressed-current:** this system is used to provide protection for large structures such as underground storage tanks, ships, pipelines, etc., which galvanic anodes cannot provide sufficient current to provide protection. It uses anodes that are non-consumable and are not naturally cathodic to steel which is connected to a local power utility that involves a dc rectifier (figure 2.28). Unlike sacrificial anodes, this system involves large, complicated, and costly installation, and the anode must be corrosion resistant since in most cases it is buried under the soil or immersed under the ocean along the structure to be protected. However, once properly installed, the systems rectifier provides an easily verifiable monitoring point which reduces operating costs. Impressed-current cathodic protection systems are typically utilized for high current requirement systems.

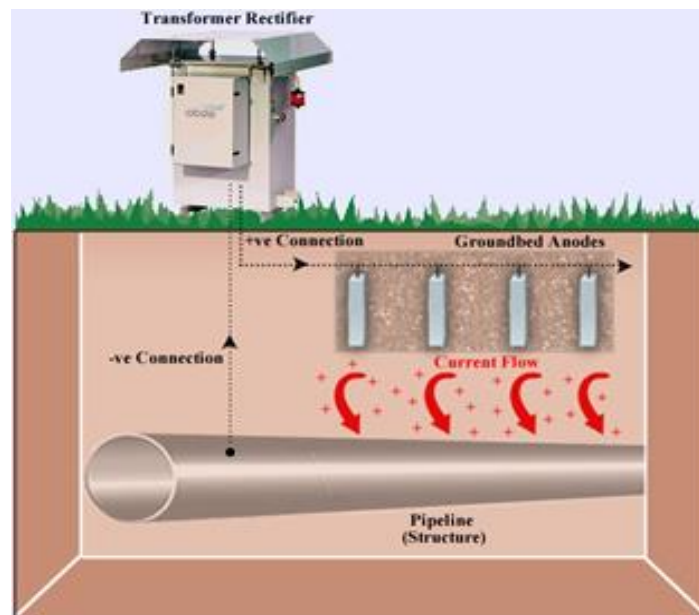


Figure 2.28: An example of impress-current cathodic protection system setup [138].

2.2.5 Corrosion inhibitors

The velocity of metallic corrosion can also be retarded by the addition of certain chemicals in an aggressive environment. These chemicals interact with the corrosive environment or/and a metallic surface to offer some protection to the metal surface. They are referred to as corrosion inhibitors [7, 139]. The use of corrosion inhibitors as a way to minimize the extent of metallic corrosion has gained extensive attention in the field of corrosion science in the past few years and it has been the most utilized method [7, 139–147]. This present study focuses only on the investigation of the use of quinoxaline derivatives as corrosion inhibitors of some selected metals in various aggressive environments. Hence more information on corrosion inhibitors is provided in detail in the following section.

2.3 CORROSION INHIBITOR AND INHIBITION MECHANISM

2.3.1 Definition of corrosion inhibitors

A corrosion inhibitor can be defined as a chemical substance or combination of substances that retard corrosion when introduced in minute concentrations to a corrosive environment [139–149]. It can also be regarded, as it were, as a negative catalyst. A large volume of these substances has been developed for various systems including, amongst others, cooling systems, steam generators, different refinery units, gas and oil reproduction, etc. [70]. However, none of them have been reported to be efficient for all the corrosive environments/systems, metallic surfaces, or types of corrosion. Thus, suggests that choosing an inhibiting substance for a particular system depends on a variety of factor which must be taken into consideration. This is because a substance can efficiently inhibit attack for a metal in a particular environment, and the same substance enhances attack for a different metal in the same environment [150]. The choice inhibitors can then be made upon organic or inorganic compounds. The recent existing data show that organic compounds are commonly used as inhibitors, and they provide efficient protection. These are compounds containing heteroatoms such as oxygen, sulphur, nitrogen, and phosphorus, π -electrons contain functional groups, electronegative functional groups, and aromatic rings in their structures [7, 17, 68, 150–155]. Furthermore, the selection of an inhibitor also depends on:

- Environmental friendliness
- Cost and availability
- Toxicity
- Stability over a lengthy period in non-stable temperature and pH environments
- Compatibility with the aggressive system

The efficiency of a corrosion inhibitor can be quantized by the following equation:

$$\%IE = \frac{CR_{uninhibited} - CR_{inhibited}}{CR_{uninhibited}} \quad (17)$$

where %IE is the inhibition percentage, $CR_{uninhibited}$ is the corrosion rate of the uninhibited system and $CR_{inhibited}$ is the corrosion rate of the inhibited system [148].

2.3.2 Classification of corrosion inhibitors

Inhibitors are classified in various ways by different authors. Some, for example, prefer to classify them according to their chemical functionalities, some according to their mechanism and seldom, some authors group them depending on the corrosion environment and the nature of the metallic surface of interest. Putilova [140] et. al. group corrosion inhibitors in three classifications, which are, (i) **class A**, forms a protective film which acts as a shield on the metal surface, (ii) **class B**, suppresses the extent of aggressiveness of the corrosion environment, and (iii) **class AB**, inhibitors that form a protective film and suppresses the extent of aggressiveness of the corrosion environment. Some of the groups of inhibitors are briefly discussed below:

2.3.2.1 Acid inhibitors

This type of inhibitors can further be divided into:

2.3.2.1.1 Organic inhibitors

Organic inhibitors are often used in aqueous media, and they are anodic, cathodic, or sometimes both anodic and cathodic effects but, as a principle, they protect a metal from an aggressive media through a process of adsorption. They are also referred to as “film-forming” inhibitors because they possess the ability to form hydrophobic films on the surface of the metal. Organic inhibitors include amongst them compounds such as carboxylic acids, alcohols, amines, extract of natural

substances, etc. and these are often oxygen, nitrogen, sulphur, and aromatic containing compound have vastly reported as good organic inhibitors [150–155]. The effectiveness of these compounds has been attributed to factors like their molecular weight, molecular structures, electron density, dipole moment, carbon-chain length, and electronegativity [7, 68].

2.3.2.1.1 Inorganic inhibitors

Inorganic inhibitors are commonly used in neutral to alkaline environments and they usually react with the metallic ions formed on the anodic reaction to produce an insoluble film on the metal surface. Despite inorganic inhibitors not being used as much as organic inhibitors, several researchers have reported on the use of these compounds [156–178]. According to Antonijevic [178] et. al., the use of inorganic inhibitors as an alternative to organic compounds is based on the possibility of degradation of organic compounds with time and temperature. Sodium nitrite (NaNO_2) has been found to be an active inhibitor in closed cooling water systems and two-phased gasoline-water systems [20]. Compounds like HNO_3 , CrO_3 , KIO_4 , MnSO_4 , and SnSO_4 have also been reported to retard the corrosion rate of copper in sulphuric acid [179].

2.3.2.2 Alkaline and neutral inhibitors

This type of inhibitors can further be divided into:

2.3.2.2.1 Anodic inhibitors

Anodic inhibitors also referred to as, passivation inhibitors, are compounds that impede only the anodic reaction in a corrosion process, that is, they block, lower the anodic reaction, and promote the natural reaction of passivation of metal surface, consequently causing a large anodic shift on the corrosion potential to a positive direction. These compounds include, amongst others, hydroxides, nitrites, chromates, carbonates, silicates, phosphates, molybdates, borates, and benzoates. Anodic inhibitors are not entirely safe. Below a certain threshold concentration, these compounds become dangerous, and they can cause even more damage (pitting corrosion) or accelerate the corrosion process to a metal surface than when an inhibitor was not introduced. This is because when the concentration of the inhibitor is not high enough in the solution the metal is likely not to be covered completely which will leave some sites of metal exposed and followed by the rapid reduction at the anodic site relative to the cathodic site. Therefore, in cases of corrosion

rate, anodic inhibitors are only safe to use when the entire reaction is governed by an anodic reaction [2].

2.3.2.2.1 Cathodic inhibitors

In contrast to anodic inhibitors, cathodic inhibitors are compounds that achieve the protection of a metal surface by either impeding the cathodic reaction in a corrosion process or by selective precipitation on cathodic sites [20]. These compounds form a film of insoluble and visible covering precipitates on the metal surface which protects it from attack. They are also regarded as safe than anodic inhibitors since they do not depend on the amount of concentration. Bockris and Conway [180] proposed that cathodic inhibitors function through a mechanism of hydrogen increase over the voltage rather than adsorption on the metal surface. Cathodic inhibitors often work by three different mechanisms as [7, 70, 180]:

- **Cathodic poisons:** these substances retard the overall rate of corrosion by suppressing the rate of hydrogen reduction. They are also referred to as hydrogen evolution poison. Arsenic antimony, and bismuth derivatives are behaving as cathodic poisons. These inhibitors have disadvantage that they cause hydrogen embrittlement due to some hydrogen that get adsorbed into the metal surface during the process of cathodic charging.
- **Oxygen scavenger:** these substances retard the rate of corrosion by reaction with dissolved oxygen, that is, they remove oxygen in the solution. Hydrazine and sodium sulfite are examples of oxygen scavengers.
- **Cathodic precipitations:** these substances retard the rate of corrosion by forming bulky precipitates on the entire metal surface, thereby forming a protective film that indirectly blocks both anodic and cathodic sites. Examples of cathodic precipitates are calcium and magnesium carbonates.

2.3.2.3 Mixed inhibitors

Mixed inhibitors are compounds that show both traits of cathodic and anodic inhibitors in slowing down the rate of corrosion. They provide protection by simultaneously indirectly suppressing the cathodic and anodic reactions in the corrosion process, thus forming precipitates that act as a protective film. Unlike anodic inhibitors, mixed inhibitors are safe to use because they do not lead

to any shift in corrosion potential and there are potential dangers of pitting corrosion occurring or corrosion being enhanced. Examples of these compounds are silicates and phosphates [187–189].

2.3.2.4 Volatile corrosion inhibitors (VCI)

VCI's also referred to as vapor phase inhibitors (VPI's) are compounds with a low vapour pressure of approximately 2×10^{-4} to 0.4 mm Hg. These compounds provide most protection by volatilizing and condensing on the metal surface, in environments with less ventilation [7, 70, 181–184]. They do so by either first dissociating and then vaporize or just vaporizing in molecular form. However, either way, these compounds adsorb in a metal surface through a chemical or physical mechanism. Some compounds that show traits of VPI's include, amongst others, ammonium benzoate, dicyclohexyl ammonium nitrite, cyclohexylamine carbonate, hydrazine carbonate, and benzotriazole [183–186]. The drawback of VPI's is that they must be used with caution because they can offer protection for one metal and accelerate corrosion for the other, for the same environment.

2.3.2.5 Ohmic inhibitor

Ohmic inhibitors, also referred to as “film forming inhibitors” are compounds that lower the rate of corrosion by lowering the movement of ions between the anodic and the cathodic site on the corroding metallic surface [70, 120]. Thus, causes the ionic conductivity to decrease, hence the decrease in the corrosion rate. Examples of Ohmic inhibitors include, amongst others, amines and sulfonates [120].

2.3.3 The synergistic effects

Inhibition compounds do not always perform as expected even though they have most of the desired properties. However, most researchers have found that reinforcing such compounds with a second or more inhibitor in small addition can improve their performance. Thus, even if the added inhibitor is less effective on its own, it can improve the inhibition effect of the other. This phenomenon is referred to as synergisms. According to Shaju et. al. [190], the synergistic effects of organic inhibitor systems can be improved by the addition of halide ions in very small concentrations to the solution. Foley [191] investigated the inhibition effects of tetraisoamyl

ammonium sulphate on iron in the presence of 4N Sulphuric acid, and he found out that the dissolution of iron was not retarded to a satisfying extent. However, when 0.005N KI was added to the inhibition solution, the dissolution of iron decreased drastically. These halides have been reported to be effective in the increasing order of $\text{Cl}^- < \text{Br}^- < \text{I}^-$ [192–194].

2.3.4 Inhibition mechanism

Universally, it has been accepted that corrosion inhibitors in an aggressive corrosive medium act through a mechanism of adsorption on a metal surface. This adsorption process is categorized into two principal types which are physical and chemical adsorption. These types of adsorptions are briefly discussed below:

2.3.4.1 Physical adsorption

These metal/inhibitor types of interactions are also referred to as physisorption or electrostatic adsorption. Physisorption results from the electrostatic attraction between the inhibitor molecule and the metal surface. These interactions requires that activation energy should be less than 80 kJ/mol [195].

2.3.4.2 Chemical adsorption

These metal/inhibitor types of interactions are also referred to as chemisorption and they result from strong chemical bonds between the inhibiting molecule and the metal surface [196]. This involves metal/inhibitor charge sharing from the presence of lone pair electrons, and π -electrons that form strong co-ordinate bonds. The strength of these interaction often increases with rise in temperature of a given system and it requires that activation energy should be at least above 80 kJ/mol [195, 196]. Further distinctions between physisorption and chemisorption are presented in Table 2.9 below.

Table 2.9: Distinctions between physisorption and chemisorption [15].

Physisorption	Chemisorption
It results due to van der Waals force.	It results due to the formation of chemical bond.
No new compounds are form in the process.	New compounds are formed at the surface of the metal.
favorable at low temperatures and decreases with rise in temperature.	Occurs at high temperature and increase with rise in temperature.
Multimolecular layers are formed.	Unimolecular layers are formed.
The enthalpy of adsorption is low. The value is in the range of 20–40 kJ/mol.	The enthalpy of adsorption is high. The value is in the range of 40–400 kJ/mol.
Processes are reversible in nature.	Processes are irreversible.
It is an instantaneous process.	It occurs very slow.

2.3.5 Adsorption isotherm

An adsorption isotherm is a mathematical equation or a graphical representation that relates the amount of the adsorbing species (inhibitor) to its surface coverage at a constant temperature [197]. Hence, it is called an *iso-therm*. These isotherms advocate the understanding of the mechanism by interpreting the adsorption behavior of a certain inhibitor on the metal surface, that is, more information on the type of adsorption process can be obtained from exploring different adsorption isotherms. Various adsorption isotherms have been exploited over years and some are briefly discussed, and more are shown in Table 2.10 [197–201]. The adsorption isotherms that were found to fit most of the organic inhibitors were Langmuir’s or Temkins’s adsorption isotherm [199–201].

2.3.5.1 Langmuir isotherm

In 1918, Irving Langmuir achieved the first scientifically based derivatives of an adsorption isotherm, and it was then referred to as Langmuir isotherm. Since from the development of this isotherm, many modified–classical models were developed, however the Langmuir isotherm remained the most popular and utilized isotherm [197–209]. This isotherm was modeled based on the following assumption:

- Adsorption of the solute molecule occurs only at selected sites on the surface.
- Each site on the surface holds an adsorbate.
- There is no interaction between neighboring adsorbed atoms or molecules.
- The enthalpy of adsorption is the same to all sites.

The Langmuir isotherm can be written in terms of the fraction (θ) of the adsorption sites to which the inhibiting molecule is adsorbed on the surface and fraction of the surface with unattached site ($1-\theta$). The expression is therefore given by the following equation:

$$K = \frac{\theta}{C(1-\theta)} \quad (18)$$

Rearranging equation (18), one gets:

$$\theta = \frac{KC}{1+KC} \quad (19)$$

where θ is the degree of surface coverage, K is adsorption equilibrium constant, and C is the concentration of the solute species.

2.3.5.1 Freundlich isotherm

The Freundlich isotherm is an adsorption isotherm that relates the concentration of solute present in the surface of an adsorbent, to the gas or liquid is in contact with. This isotherm was derived by Herbert Freundlich in 1909. He provided an empirical expression accounting for the isothermal variation of adsorption of a quantity of a gas or liquid adsorbed onto a solid surface [210]. This isotherm can be expressed as:

$$\theta = KC^{1/n} \quad (20)$$

where θ is the degree of surface coverage, K and n are positive constants for the system at a given temperature.

2.3.5.1 Temkin isotherm

This adsorption isotherm is also referred to as Slygin-Frumkin isotherm. It assumes that the more the surface of the absorbent is covered, the heat of adsorption of all the molecules in that given layer will linearly [211]. It also takes into consideration the possibility of interactions between the adsorbent and adsorbate [211, 212]. The expression for Temkin isotherm is given by the following equation:

$$\theta = \frac{1}{f} \ln KC \quad (21)$$

where θ is the degree of surface coverage, K is the constants for the system at a given temperature and f is the corrosion inhibitor interaction parameters.

Table 2.10: Adsorption isotherms to characterize the adsorption of inhibitors on the metal surface.

Name	Isotherm	Verification plot
Langmuir	$\theta = \frac{KC}{1+KC}$	$\frac{\theta}{1-\theta}$ vs log C
Temkin	$\theta = \frac{1}{f} \ln KC$	θ vs log C
Freundlich	$\theta = KC^{1/n}$	log θ vs log C
Frumkin	$\left(\frac{\theta}{1-\theta}\right) e^{f\theta} = KC$	θ vs C
BET isotherm	$\frac{1}{v\left(\frac{P_0}{P}-1\right)} = \frac{C-1}{V_m C} \left(\frac{P}{P_0}\right) + \frac{1}{V_m C}$	log $\frac{1}{v\left(\frac{P_0}{P}-1\right)}$ vs log $\frac{P}{P_0}$

Kinetic thermodynamic model	$\log \frac{\theta}{1-\theta} = \log xK + Y \log C$	$\log \frac{\theta}{1-\theta}$ vs $\log C$
Flory-Huggins adsorption isotherm	$\log \frac{\theta}{c} = \log Xk + x \log (1-\theta)$	$\log \frac{\theta}{c}$ vs $\log (1-\theta)$

where θ is the degree of surface coverage, C is the concentration of the solute species, K , Y , n are positive constants for the system at a given temperature, f is the corrosion inhibitor interaction parameters, x is the number of active sites occupied by one molecule of inhibitor molecule, P and P_0 are equilibrium and saturation pressure.

2.4 CORROSION OF METALS

2.4.1 Aluminum (Al)

Aluminum is the second most distributed element in the earth's crust and is the most extensively used metal in modern life. It first became an industrial metal after the 19th century and the lack of industrial usage before that time is attributed to the fact that it was not easy to extract it from its ore because it has always been found mixed with other elements [213–215]. Over the years, aluminum and its alloys have been involved in vast industrial applications which involves among them the manufacturing of aerospace, cooking gadgets, mirror frames, automotive, serving trays, and electrical transmission [213]. The most striking characteristics of aluminum and its alloys that attributes to its industrial wide variety usage are briefly discussed below:

- Al is a lightweight metal with density of 2.71 g/cm^3 , that is, approximately one third less than of steel (7.83 g/cm^3) and zinc (7.14 g/cm^3).
- Al has high electrical conductivity, good enough to be used as an electric conductor.
- Al possesses nontoxic characteristics which allow it to be used as cooking gadgets without any harm to humans and to be in direct contact with food products without contaminating them.
- When Al is exposed to the atmosphere, it forms a thin, invisible, passive oxide film. This Al self-protecting characteristic makes it resistant to corrosion attack, even in harsh industrial conditions that usually corrodes other metals. Moreover, this Al oxide film is

only stable in conditions of pH ranging from 4–9, below (acidic) and above (alkalic) the film dissolve and Al metal surface remain exposed to further oxidation (Section 2.1.7.1.3). Figure 2.29 show the schematic diagram of an invisible, passive oxide film that forms on the Al surface.

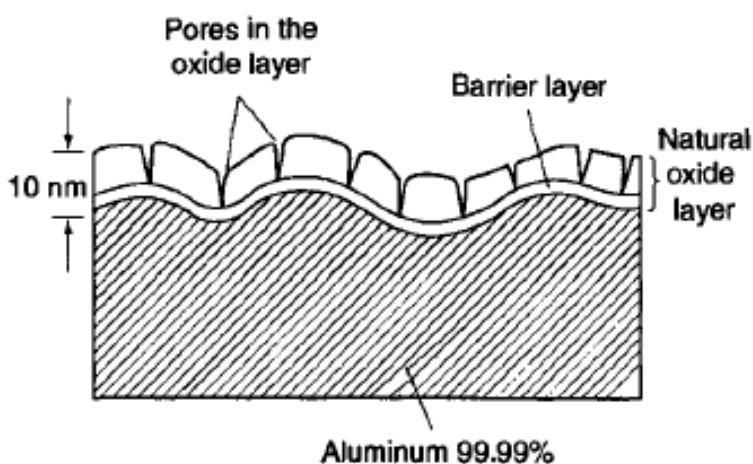


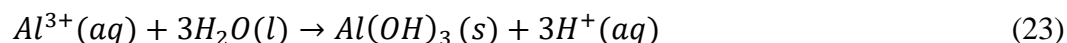
Figure 1.29: A schematic representation of the Al metal with the oxide film formed on the surface [213].

Despite Al having these all-above-mentioned characteristics which attribute for its importance and wide application in the industrial sector, it is also known to surrender to corrosion attacks when exposed to some conditions. These conditions include amongst them; diluted or concentrated HCl, H₂SO₄, seawater, mercury and mercury salts, etc. Chlorinated and Fluorinated solvents were also found to have abilities to destroy the oxide film, consequently exposing the Al to pitting corrosion [214–220]. The basic chemical reactions that are involved in corrosion of Al in aqueous medium are described below:

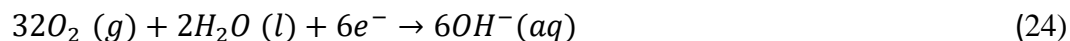
Initially, metallic Al, in oxidation state 0 is oxidized to Al³⁺ ion (loses three electrons)



This process is followed by Al³⁺ ion reacting with water, thus, Al³⁺ ions are released from the anode through an oxidation process and oxygen undergoes reduction at the cathode to form aluminum hydroxide Al(OH)₃.



the reduction of oxygen is shown by equation (24).



Finally, the overall reaction for the corrosion of Al is given by equation (25) and these processes are further elaborated by Figure 2.30 below.

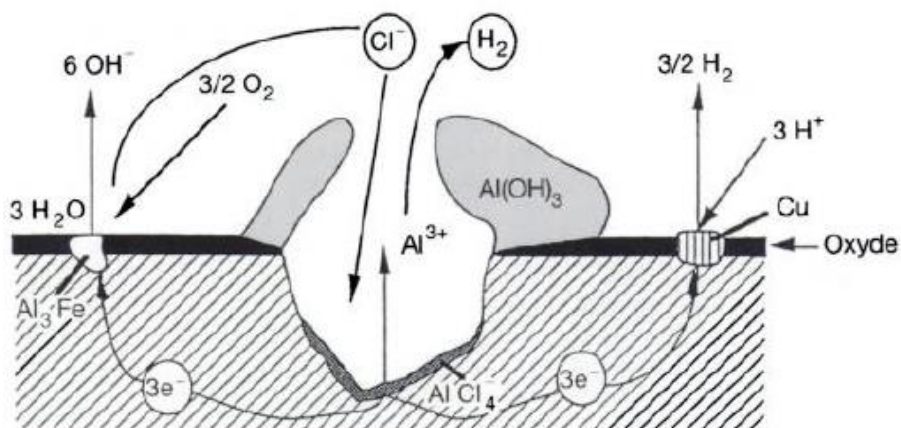
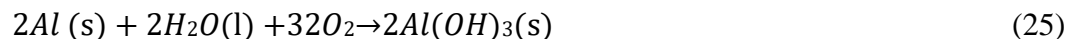


Figure 1.30: Schematic representation of Al corrosion mechanism in aqueous medium [218].

2.4.2 Zinc (Zn)

Before zinc was identified in metallic form, its ore was used for healing injured people and for making brass. The first production of zinc oxide and zinc in a metallic form was first identified in India around the 11th to the 14th century and these were followed by the production in China in the 17th century [221]. However, in 1746, the German chemist Andreas Marggraf managed to isolate the element to pure zinc, and to date, he is honored by the credit of discovering metallic zinc [221–223]. Zn currently ranks the fourth most produced and used metal worldwide after, iron, aluminum, and copper. It owes most of its application from its favorable anticorrosive properties and its relatively low price. Zinc also seen extensive use in galvanizing, thus, adding a thin layer to protect other metals such as iron and copper [223–226]. Some of the application and primary requirements of zinc and its alloys as protective coating are shown in figure 2.31.

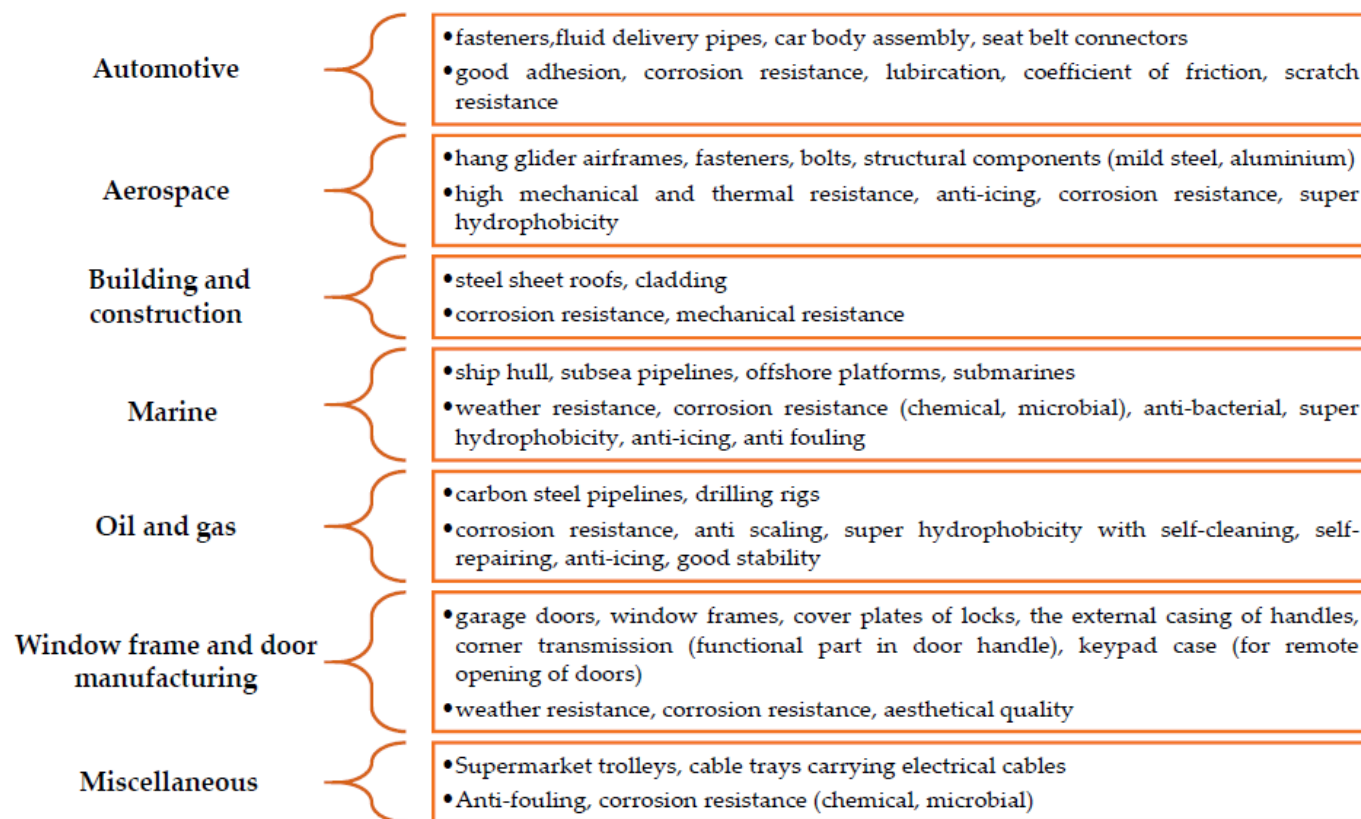


Figure 1.31: List of various applications of zinc and its alloys employed as protective coating [227].

The widespread usage of zinc coatings for the corrosion protection of iron is attributed to properties possessed by zinc such as being highly sacrificial in nature, that is, it has electrochemical potential less than that of iron. Thus, in the case of galvanic corrosion, iron becomes the cathode and does not corrode at a rate as with zinc which acts as anode does. Like aluminum, when exposed to atmospheric, aqueous, and other environments, zinc also has the ability to form a dense, protective oxide of zinc carbonate which suppresses the corrosion rate [225]. In addition, the protective oxide produced by zinc is not constant with depth, it depends on the time of exposure and also with the environment it is exposed to. In general, corrosion is dependent upon the environment upon the metal is exposed to, and the corrosion or the formation and maintenance of the oxide on zinc surface is influenced mainly by the pH of the environment. It has been reported the corrosion of zinc is severe in corrosive environment of pH below 6 and above 12.5. whereas, within the pH range of 6–12.5 the corrosion rate of zinc is relatively low [226–228].

When zinc surface comes into contact with chloride ions, it encounters pitting corrosion, and the process is explained by the half reactions below [7] and the processes are further elaborated by figure 2.32.

Initially, metallic Zn, in oxidation state 0 is oxidized to Zn^{2+} ion (loses two electrons).



This is followed by the reduction of hydrogen ion to hydrogen gas by taking up the two electrons of the oxidized zinc.



The two reactions can be combined to form the final reaction as indicated in reaction equation (27).

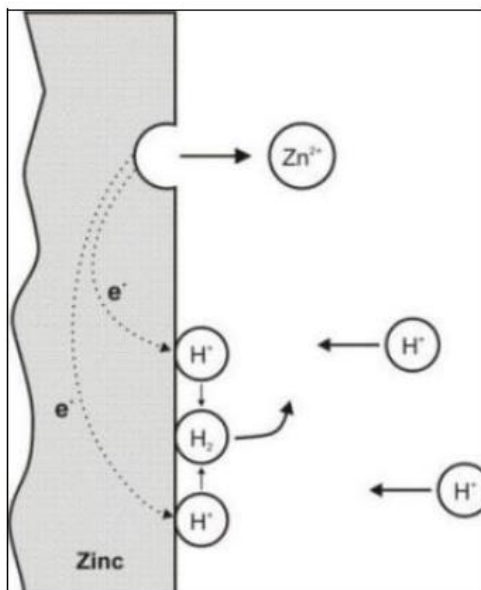


Figure 2.32: Schematic representation of Zn corrosion mechanism in the solution of HCl [7].

2.4.3 Mild steel (MS)

Mild steel (MS) is an alloy generated from iron and carbon, and also containing small quantities of other elements such as silicon, copper, Al, and manganese in providing the necessary mechanical properties. It is not all the cases MS will have the same composition, it varies with its application, however, the maximum limit of carbon content is known to be around/at about 0.29% and silicon, manganese content greater than that of carbon, having 0.6%, 1.65%, and 0.6%, respectively [229]. Like Al and Zn, iron is a naturally occurring metal found in form of oxides, which then the ore of these are refined to produce MS. Because of the special and unique properties like, good strength, hardness, and easy availability that MS chiefly possess, it has found a wide range of industrial application which amongst others include boilers, petrochemical industry, oil and gas industry, marine applications automobiles, electrical appliances, cooking gadgets, etc. When MS end products are exposed to aggressive environment, they tend to revert back to the oxide and forming what is commonly known as rust, which is a work usual used to describe the formed-reddish oxide on MS surface [230].

The corrosion mechanism of iron in the presence of an environment that has water content described in section 2.1.1 in this work is similar to the process of dissolution of MS. In a dry, clean atmosphere like in the rural area, MS is corroded by oxygen to form a thin oxide layer, and thickness of about 20 – 50 nm. This process occurs by reaction equation (28).



The layer (Fe_2O_3) acts as protection to the underlying metal against further corrosion attacks. However, the protection layer tends to breakdown and expose the metal under protection when it is introduced to an electrolyte [80].

2.5 QUINOXALINES

Quinoxaline and its derivatives are a paramount class of nitrogen-containing heterocyclic compounds, and they constitute a wide range of biological properties which are of great interest in the pharmaceutical industry [231]. They are said to have pharmacological activities like antibacterial, anticancer, antitumor, antifungal, anti-HIV, antitubercular, anti-inflammatory, antineoplastic, amongst others [231–262]. In addition, quinoxaline derivatives also find use in agriculture fields as insecticides, herbicides, and fungicides [244, 251–259]. The molecular structure of quinoxaline is shown in figure 2.33.

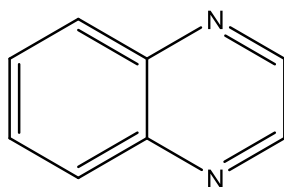


Figure 2.33: Molecular structure of quinoxaline.

As shown in figure 2.33, the unsubstituted quinoxaline is a bicyclic hetero-aromatic compound consisting of a benzene ring and a pyrazine fused together, hence, this is a reason a quinoxaline is also referred to as benzopyrazine, 1,4-benzodiazine, phenopiazine, and benzoparadiazine [263]. Quinazoline, phthalazine and cinnoline are amongst the compounds that are isomeric to quinoxaline (figure 2.34).

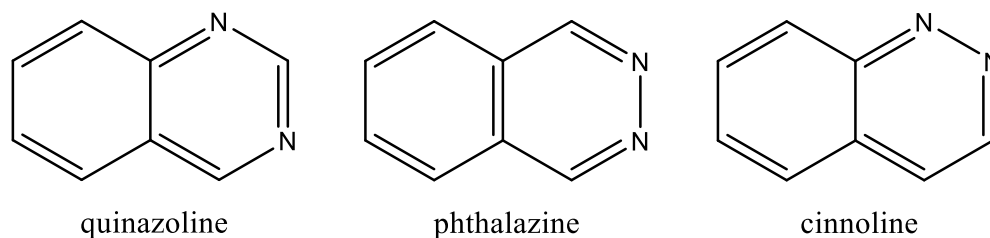


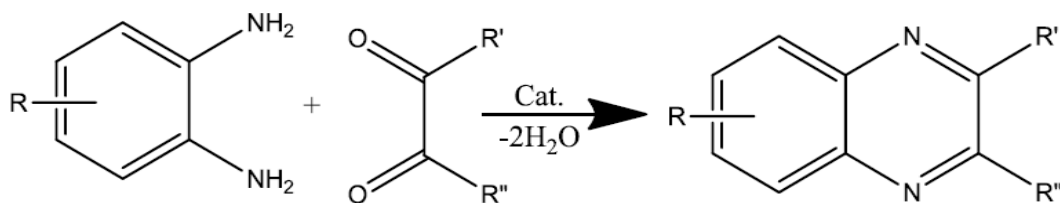
Figure 2.34: Structures isomeric with quinoxaline.

2.5.1 Some properties of quinoxalines

The unsubstituted quinoxaline compound (figure 2.33) has a molecular formula of $C_8H_6N_2$ and molecular weight of 130.15 g/mol. At standard conditions, it is a colorless crystalline powder, and it is soluble in water with melting point of 302–304 K, boiling point 493–496, and density of 1.124 g/mL [231, 264–265]. Quinoxaline is acidic with a pKa of 0.6 (much less acidic than pyrazine with pKa of 0.4) [265]. It undergoes significant di-protonation in the presence of strong acidic medium, this can be attributed to its second pKa of -5.52 [264, 265]. Under stringent conditions like undiluted HCl, at the temperature of about 363 K, quinoxaline undergoes nitration to form the mixture of 5-nitroquinoxaline and 5,7-dinitroquinoxaline [264].

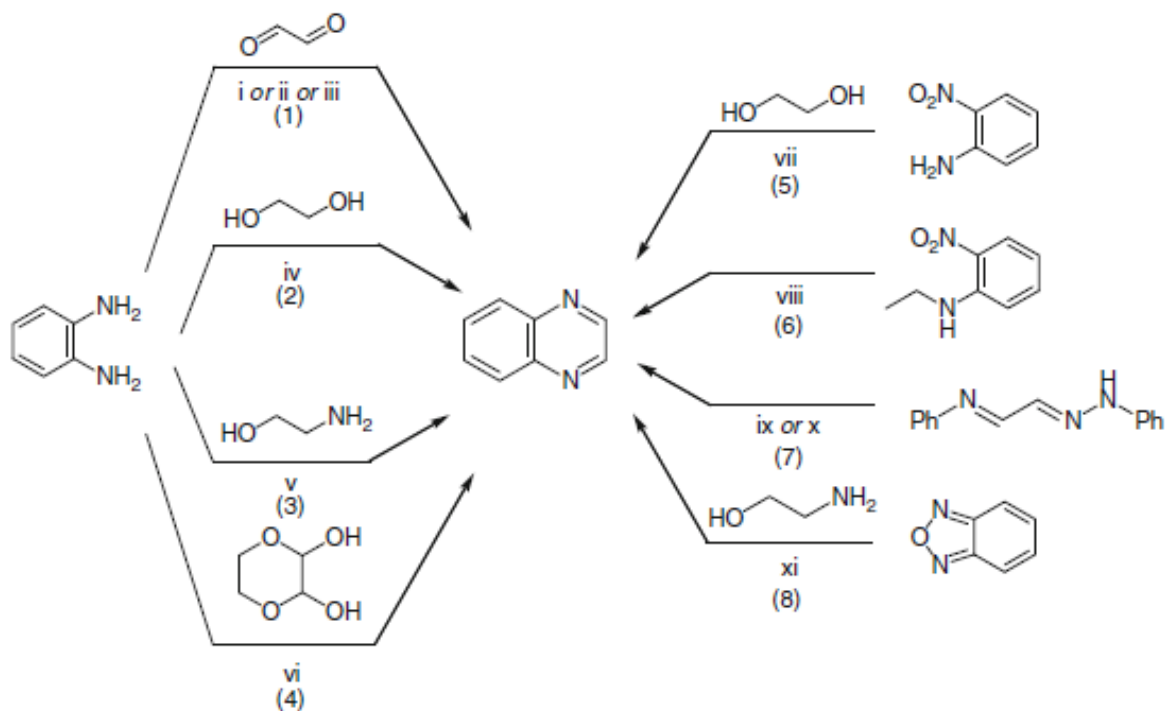
2.5.2 Development and synthesis of quinoxalines

In the year 1884, two German chemists, Daniel Hinsberg and Gottfried Körner independently discovered quinoxalines through the reaction of spontaneous condensation of 1,2-diaminobenzene with 1,2-dicarbonyl compounds [266, 267]. The general schematic reaction of the synthesis of quinoxalines is given in the Scheme 1.



Scheme 1: General schematic reaction of the synthesis of quinoxalines.

After the Hinsberg and Körner work in 1884, other synthetic ways of producing a variety of quinoxalines were developed and some of these methods are shown in Scheme 2. Some of the catalysts that have been successfully utilized in the synthesis of quinoxalines are also indicated in Scheme 2.



Scheme 2: Some available methods utilized in the synthesis of quinoxalines.

where: i = aq. HF, rt (98%)

ii = PS/AlCl₃ (10 mol%), EtOH, reflux (95%)

iii = nano-TiO₂, rt (88%)

iv = Au/CeO₂ (cat), diglime (91%)

v = CsOH, H₂O, MS, 393 K, 23 h, O₂ atmosphere (81%)

vi = EtOH, rt, 30 min (95%)

vii = FeCl₃·6H₂O, Na₂S·nH₂O, 453 K, 24 h (67%)

viii = DMAC, toluene, K₂CO₃, 438 K (5%)

ix = 600 °C, 0.01 Torr (35%)

x = 873 K, 0.007 mbar, 35 min (78%)

xi = p-TsOH, 423-443 K, 4 h (87%)

DMAC = N,N-Dimethylacetamide

PS/AlCl₃ = Polystyrene-supported aluminium chloride

2.5.3 Quinoxalines used as corrosion inhibitors

Several authors have reported quinoxaline and its derivatives as active anticorrosive compounds. Saranya et al. [268] studied corrosion inhibition potential of (3E)-3-(phenylimino)-3,4-dihydroquinoxalin-2(1H)-one, (3E)-3-[(2-methylphenyl)imino]-3,4-dihydroquinoxalin-2(1H)-one and (3E)-3-[(2-methoxy-phenyl)imino]-3,4-dihydroquinoxalin-2(1H)-One on mild steel in 1.0 M H₂SO₄ using gravimetric and electrochemical techniques and a maximum % IE of 98.69 was obtained. Using both experimental and computational techniques, Olasunkanmi and Ebenso [269] investigated 1-[3-(3-methoxyphenyl)-5-(quinoxalin-6-yl)-4,5-dihydropyrazol-1-yl]propan-1-one and 1-(3-(4-chlorophenyl)-5-(quinoxalin-6-yl)-4,5-dihydro-1H-pyrazol-1-yl)propan-1-one as inhibitors of mild steel in 1.0 M HCl. They found that both compounds exhibited mixed-type inhibitive action and showing an increase of inhibition efficiency with an increase in concentration.

In another study, Chitra et al. [270] investigated the inhibition efficiency of 3-methyl-2-phenyl quinoxaline, 2,3-diphenyl quinoxaline, 3-methyl-2(2''hydroxyphenyl)quinoxaline, 3-phenyl-2(2''hydroxyphenyl)quinoxaline for mild steel in 1.0 M H₂SO₄ using weight loss, gasometry and electrochemical techniques. Using a Tafel polarization it was evident that the compounds were mixed type inhibitors but slightly cathodic in nature and they obeyed Langmuir adsorption isotherm with the inhibition efficiency increasing with an increase in inhibitor concentration.

Rbaa et al. [271] synthesized 1,4-bis-((8-hydroxyquinolin-5-yl)-methyl)-6-methylquinoxalin-2,3-(1H,4H)-dione and 1,4-bis-((8-hydroxyquinolin-5-yl)-methyl)-quinoxalin-2,3-(1H,4H)-dione and investigated the inhibitory performance against the corrosion of mild steel in 1.0 M HCl using weight loss, Tafel polarization and electrochemical impedance spectroscopy (EIS) methods. Results obtained showed a good agreement on the inhibition efficiency values from the EIS and polarization measurements, and the compounds acted as a mixed type inhibitors but mostly anodic and adsorption of the inhibitors on the mild steel surface obeyed the Langmuir adsorption isotherm.

The corrosion inhibition potentials of 7-chloro-3-(4-methoxystyryl)quinoxalin-2(1H)-one and 7-chloro-2-(4-methoxyphenyl)thieno(3.2-b)quinoxaline was investigated in two different studies carried out by Adardour et al. [272, 273] respectively, using weight loss measurements, PDP curves and EIS techniques in 1.0 M HCl. Results from PDP studies revealed that these inhibitors

acted fundamentally as cathodic-type inhibitors and the thermodynamic studies showing that at higher temperatures the compounds maintain and increase their protective effect with spontaneous adsorption process suggested by negative values of free enthalpy. Furthermore, the study by Adardour et al. [274] compared inhibition efficiencies of 3-methylquinoxalin-2(1H)-one and 3-methylquinoxalin-2(1H)-thione at 1.0 M H₂SO₄ using weight loss, PDP, and EIS measurements. Higher corrosion inhibition efficiency of more than 99 % at 10⁻³ M was obtained. The present study therefore, is centered on the investigation of some quinoxaline derivatives which have not been discussed anywhere in the corrosion-inhibition field of study.

2.6 MOLECULAR SIMULATIONS TECHNIQUES

2.6.1 Introduction

In surface chemistry, computational methods provide important insights into molecular bonding, electronic and reactivity properties between the metal and the inhibitor molecule. Computational chemistry is a branch of chemistry that makes use of theoretical methods in-cooperated within computational software programs to determine the physical and chemical properties of molecules. There are various computation methods are employed in studying various molecular properties; the different methods can be categorized into two main types, namely; molecular and quantum mechanics approaches. These methods are briefly discussed in the subsections that follows.

2.6.1.1 Molecular mechanics (MM) approaches

Molecular mechanics techniques utilize classical physics concepts which state that a molecule consists of atoms that are connected by springs rather than the stable arrangement of nuclei and electrons [7, 269]. According to these classical physics concepts, each individual spring has its own force constant that are utilized in calculating the potential energy of the molecule. The set of the force constants related to all the springs is termed force field. Examples of force field include the Merck molecular force field (MMFF) which perform well for a wide range of organic molecules, and the universal force field (UFF) which works well in all the system containing inorganic elements, particularly transition elements. The potential energy of a molecule can be estimated using equation (29).

$$E_{FF} = E_{str} + E_{bend} + E_{tor} + E_{vdw} + E_{el} + E_{cross} \quad (29)$$

where E_{str} is the stretch energy, E_{bend} is the bending energy, E_{tor} is the torsion energy, E_{vdw} is the van der Waals energy, E_{el} is the electrostatic energy, and E_{cross} is the inversion term coupling between the first three terms.

The MM approach is associated with some advantages and disadvantages. The advantages include that it is [270];

- applicable to molecules from as small as the H₂O molecule to large molecules such as protein.
- conceptually easy to understand.
- faster and more economic.

The disadvantages include that [270];

- it does not explicitly take electronic interaction into consideration. Therefore, it is not suited to describe all molecular phenomenon that involved electronic process.
- it cannot readily be employed to systems that involve bond formation or breaking.
- the quality of calculations solely depends on the existing experimental data.

2.6.1.2 QUANTUM MECHANICS APPROACHES

This approach is different from the molecular mechanic approach in that it considers a molecule as a stable arranged electrons and nuclei, hence it assumes that the chemistry of a molecule can be completely described by the electronic interaction within the molecule. Quantum mechanics methods obtain the knowledge of a given system through solving the Schrödinger equation [269].

2.6.2 The Schrödinger equation

In quantum chemistry, all properties of a system of interest (e.g., a molecule) can be determined by simply solving the Schrödinger equation. For instance, a system of mass m , moving along the x -axis, the Schrödinger equation can be written as;

$$-\frac{\hbar^2}{2m} \frac{d^2\psi(x)}{dx^2} + V(x)\psi(x) = E\psi(x) \quad (30)$$

where $\hbar = \frac{h}{2\pi}$ is a modified Planck's constant h and it equals to 1.055×10^{-34} Js, m is the mass of the system, ψ is a wave function, $V(x)$ is the potential energy of the particle at the point x and E is the total energy of the system.

In three-dimension system, equation (30) can be expressed as shown by equation (31) below;

$$\frac{-\hbar^2}{2m} \nabla^2 \psi + V(x) \psi = E \psi \quad (31)$$

where ∇^2 is the Laplacian operator and can be expressed as below;

$$\nabla^2 = \left(\frac{\partial}{\partial x^2} + \frac{\partial}{\partial y^2} + \frac{\partial}{\partial z^2} \right) \quad (32)$$

The solutions that are obtainable from solving the Schrödinger equation provides the information such as the wave function and corresponding energy values of the system that depends entirely on the coordinates of all the particles that makes up a molecule. Other properties of the molecule such as the electric properties and magnetic properties are obtained from the energy and the geometry of the system of interest. Moreover, the most often acceptable wave function (i.e., the geometry of the molecule) and presumably the best one to utilize in computing properties of a particular system is the one with the lowest energy [271, 272]. It is worth to also mention that due to the lack of mathematical procedures, the Schrödinger equation has only been solved exact for one electron system. Therefore, it is this reason researchers opted for approximation approaches to solve the equation or to predict the behavior of any multiple electron system in a completely satisfying manner [273, 274]. The quantum mechanics methods can be subdivided into two classes; namely, semiempirical and *ab initio* methods.

2.6.2.1 Semiempirical approaches.

These methods attempt to address the problem of computational costs by neglecting some electron-electron integrals arising from the interactions between electrons in a molecule when solving the Schrödinger equation [274, 275]. Usually, it considers only the valence electrons of the molecule, and only minimal basis sets are used in the calculations [276]. A basis set is the mathematical

description of the orbitals within a system used to perform computations. A minimal basis set contains the minimum number of basic functions needed for each atom in the molecule of interest. Semiempirical methods also rely on parameterization in order to correct the errors resulting from the exclusion of some part of a molecule and to produce various results [7]. The advantage of these methods is that they are faster than methods that do not introduce approximation of the integrals during calculations and do not resort to parametrization (i.e., *ab initio* methods), and therefore, are cost-effective, especially for the study of large corrosion inhibitors molecules. However, if the molecule under study is not similar to the molecules in the database utilized to parameterize the method, the accuracy of the results can be very poor and unreliable [7, 276]. The most commonly used semiempirical methods include modified neglect of differential overlap (MNDO), Austin model 1 (AM1), Parameterized model number 3 (PM3). These semiempirical methods are briefly discussed below.

a) MNDO: this method is the modified version of Neglect of Diatomic Differential Overlap (NDDO). In this method, the two-electron integrals are evaluated using multipole-multipole interactions approach from classical electrostatics [277]. The older version MNDO only used the s and p orbital basis sets while the more recent version (MNDO/d) added d-orbital basis sets to allow the description of the transition metals. There are some setbacks that are associated with this method. These include its inability to describe the hydrogen bond due to a strong intermolecular repulsion and it is generally not reliable in predicting some properties such as heats of formation [276].

b) AM1: this method solves the two-electron integral but taking a similar approach as MNDO, however, it utilizes a modified expression for nuclear-nuclear repulsions that result in non-physical attractive forces that imitate the van der Waals interactions. Unlike MNDO, AM1 is known to be good in predicting hydrogen bonds and reliable in predicting properties such as heat of formation. There are some setbacks that are associated with this method. These include inaccuracy geometries involving phosphorus, it tends to poorly predict nitrogen pyramidalization, and it tends to produce O-Si-O bonds that are not sufficiently bent [276].

c) **PM3**: this method makes use of the equations that are very similar to AM1, however, with a modified set of parameters [276]. The modification of parameters on this method is based on reproducing a large number of molecular properties [278]. PM3 is more thermochemical accurate than MNDO or AM1. There are some setbacks that are associated with this method. These include that this method tends to predict sp^3 nitrogen as always being pyramidal and it is less good in predicting hydrogen bonds energies as compared to AM1 [276].

2.6.2.2 *Ab initio* approaches

The *Ab initio* methods solve the Schrödinger equation from pure theoretical principles without any experimental data or any parameter additions. These are approximate quantum calculations that are purely based on mathematical procedures. *Ab initio* methods provide high accurate computations than semi empirical methods since their results does not depend on the available database. However, one of the disadvantages associated with these methods is that they are usually computationally expensive. This is due to the fact that *Ab initio* methods take into consideration all the terms and integrals when computing [279]. Some of the methods that can be classified as

- *Ab initio* methods include Hartree-Fock (HF) method,
- Moller-Plesset perturbation (MP2) method,
- Coupled cluster (CC),
- quantum monte carlo method, and
- Density Functional Theory (DFT) [274].

In this present study, the DFT method was utilized for the study because of the fact that in terms of computational cost and accuracy it lies between HF and MP2 methods. It is also a preferred method when describing properties related to metal surfaces.

2.6.3 DENSITY FUNCTIONAL THEORY (DFT)

The principle behind the DFT method is that the energy, in particular, the ground-state energy of a molecule can be obtained by solving the Schrödinger equation in terms of the electron probability density parameters rather than the wave function (ψ) [280], which is the case with wavefunction based methods such as HF and MP2. DFT method determines the ground-state properties of a many-electron system using functionals. A functional is a function of a function. In other words, every ground-state property is a functional of the electron density. However, the exact density

functional is unknown. DFT takes into account the electron correlation effects, which are not largely considered in the HF method. This results in faster and a bit more computations than that of HF methods [281]. However, the exact density functionals (correlation interactions) are unknown. Although the MP2 method is known to provide more accurate results than DFT, it is also more computationally demanding than DFT. Furthermore, the DFT methods have been found by various researchers to be providing results that are very close to those obtained when using highly expensive computational methods such as the CC methods [276, 282]. Therefore, DFT methods are growingly finding application in the study of the many-electron system, such as organic corrosion inhibitors [283–290].

DFT methods are based on the mathematical proof of the first Hohenberg-Kohn theorem that stated the ground-state electronic energy of a molecule can be expressed as the function of electron density (ρ):

$$E[\rho] = E_{Ne}[\rho] + T[\rho] + E_{ee}[\rho], \quad (33)$$

where the first term $E_{Ne}[\rho] = \int \rho(\mathbf{r})V(\mathbf{r})d\mathbf{r}$ is external potential energy due to nuclei-electron attraction, the second term $T[\rho]$ is the kinetic energy of the electron, and the last term $E_{ee}(\rho)$ is the energy electron-electron repulsion term. Moreover, the electron density is also a function of position \mathbf{r} , and denoted as $\rho(\mathbf{r})$. Thus, equation (33) can further be expressed in the form;

$$E[\rho] = \int \rho(\mathbf{r})V(\mathbf{r})d\mathbf{r} + T[\rho] + E_{ee}[\rho], \quad (34)$$

The electron density is built from the occupied orbitals according to the relation in equation (35) below [7].

$$\rho(r) = \sum_{i=1}^n |\psi_i(r)|^2, \quad (35)$$

where n is the number of electrons, and it is expressed in the form;

$$n(r) = \int \rho(r)dr \quad (36)$$

The external potential energy due to nuclei-electron attraction term $V(\mathbf{r})$ in equation (33) it is the coulomb potential, and it can be expressed in the form;

$$V(\mathbf{r}) = -\sum_{\alpha} \frac{z_{\alpha}}{r_{i\alpha}} \text{ in atomic units,} \quad (37)$$

where z_{α} is the atomic charges for nuclei, and $r_{i\alpha}$ is the separation between the nucleus and electron distances.

The energy electron-electron repulsion term, $N_{ee}(\rho)$, in equation (34) is given as;

$$N_{ee}[\rho(\mathbf{r})] = \frac{1}{2} \int \frac{\rho(\mathbf{r}_1)\rho(\mathbf{r}_2)}{|\mathbf{r}_1 - \mathbf{r}_2|} d\mathbf{r}_1 d\mathbf{r}_2 + E_{XC}[\rho(\mathbf{r})], \quad (38)$$

The first term in equation (38) arises from the electron-electron interaction and the second term is the non-classical exchange-correlation energy arising from the exchange and correlation non-classical interactions. Therefore, replacing equation (39) into equation (35) the total energy function can be expressed as;

$$E[\rho(\mathbf{r})] = \int \rho(\mathbf{r})V(\mathbf{r})d\mathbf{r} + T[\rho(\mathbf{r})] + \frac{1}{2} \int \frac{\rho(\mathbf{r}_1)\rho(\mathbf{r}_2)}{|\mathbf{r}_1 - \mathbf{r}_2|} d\mathbf{r}_1 d\mathbf{r}_2 + E_{XC}[\rho(\mathbf{r})] \quad (39)$$

Here [equation (39)] we have introduced the exchange-correlation functional $E_{XC}(\rho)$ that takes in consideration the remainder of the electron-electron interaction, which itself is divided into separate correlation and exchange components. The $E_{XC}(\rho)$ functional has the mathematical form of;

$$E_{XC}(\rho) = E_X(\rho) + E_C(\rho) \quad (40)$$

where E_X is the exchange energy functional, and E_C is the correlation energy functional terms. Moreover, the speed and accuracy of DFT calculations depends on the type of functional and the basis set employed. Thus, the exact expressions for the exchange-correlation part of the total-energy functional remain unknown and must be approximated [275]. To address this problem, a variety of functional have been developed to date. Some of these density functionals are Slater and

$X\alpha$. These functionals do not involve correlation but only electron exchange. Meanwhile, other functionals provide the simplest approximation to the complete problem, that is, are based only on the electron density. Among such functions include the local density approximation (LDA) or local spin density approximation (LSDA) for high-spin systems [274]. The accuracy of LDA in predicting structural properties such as covalent bonds, metallic bonds, and ionic bonds is remarkably well when compared to HF methods [276, 277]. However, their performance is poor in molecular calculations. A typical example is that they predict binding energies that are significantly larger than experimental values [269, 276–278]. Moreover, LDA treats systems as homogenous. However, real systems are inhomogeneous.

To account for the downfalls of the LDA, a number of more complex sets of functionals that involve both the electron density and its gradient were developed. These functionals are referred to as gradient-corrected functionals or generalized gradient approximation (GGA). Such functionals include Becke correlation functional with Lee, Yang, Parr exchange (BLYP), Perdew-Burke-Enzerhof (PBE) [279]. In contrast with the LDA functionals, the GGA functionals treat the systems as a real system with inhomogeneous electron density. GGA provides an improved description of binding energies and accurate calculation for *d*-metal complexes [269, 280–282]. There are also hybrid functionals that combine functionals from other methods with pieces of HF calculation, usually the exchange integrals. The functionals include Becke 3-parameter exchange with Lee, Yang, Parr correlation (B3LYP), Becke 3-parameter exchange with Perdew correlation (B3P86), Becke 3-parameter exchange with Perdew and Wang correlation [271, 276, 283].

2.6.4 SOFTWARE PROGRAM SELECTED FOR PERFORMING CALCULATIONS: MATERIAL STUDIO

BIOVIA material studio [284], is a computational program that is widely utilized by researchers in the field of materials science and computational chemistry to predict and understand the behaviors and properties of molecular structures. The use of BIOVIA Materials Studio is not only limited to the above-mentioned fields, researchers in various fields such as pharmaceuticals, metals and alloys, polymers and composites, fuel cells, and more are making use of the program to produce better-performing materials. The advantages of this software include, but not limited to its easiness to operate, production of accurate results in shortest period of time, provides

capabilities to build, manipulate and view models of crystalline materials and molecules and it also full range of simulations and visualize outputs through graphs, tables charts, images, and animations [285].

The quantum modules that are supported by BIOVIA material studio include but not limited to;

- BIOVIA Materials Studio CAbridge Serial Total Energy Package (CASTEP)
- BIOVIA Materials Studio Cantera
- BIOVIA Materials Studio Density Functional-based Tight Binding (DFTB+)
- BIOVIA Materials Studio NMR CASTEP
- BIOVIA Materials Studio VAMP
- BIOVIA Materials Studio Order-N Electronic Total Energy Package (ONETEP)
- BIOVIA Materials Studio QMERA
- BIOVIA Materials Studio DMol3

In this present study, the DMol³ was utilized in all the computation calculations. This module can be utilized to model the properties of organic and inorganic molecules (such as, energies), metallic solids, molecular crystals and electronic structures using DFT. There are several tasks that can be found within this module. These tasks are geometry optimization, transition-state optimization, and molecular dynamic among other [285].

CHAPTER 3: *EXPERIMENTAL DETAILS*

This chapter provides details of the materials and methods that are utilized in this research. The techniques employed in this study are gravimetric analysis, potentiodynamic polarization and electrochemical impedance spectroscopy, atomic absorption spectroscopy (AAS), Fourier Transform Infrared Spectroscopy (FTIR), and computational analysis.

3.1 METAL SPECIMENS

All experimental procedures involving zinc were conducted using zinc specimens of 99.90 (wt %). All the experimental procedures involving aluminum sheets were conducted using aluminum specimens of approximately 99.00 (wt %). The mild steel utilized for all the experimental procedures has the elemental composition (wt %) of silicon (0.30), carbon (0.21), sulphur (0.03), phosphorus (0.02), molybdenum (0.01), nickel (0.039), manganese (0.37), and iron (99.32). Zinc and mild steel were utilized for all the experimental procedures and aluminum was utilized for the electrochemical procedures only. The metals used in the gravimetric test were having a surface area of 12 cm², with zinc metals weighing approximately 2.50 g and mild steel metals weighing approximately 3.30 g, both metals containing a small hole of about 2 mm diameter in the middle. All the metals specimens utilized for the electrochemical tests were cut to a size of 1 cm² surface, then were mechanically abraded on Struers Labosystem instrument (shown in figure 3.4) with emery papers (from 100, 600 and 1200) grit sizes. All the metals utilized in this study are versatile metals and they are employed tremendously in industries and in all spheres of life. Hence, their corrosion inhibition is investigated in this present study.

3.2 PREPARATION OF SOLUTIONS

The corrosive media utilized for this work were hydrochloric (32 % assay) and sulphuric acids (98 % assay) supplied by Sigma-Aldrich, South Africa. For all experiments involving zinc and mild steel, approximately 1.0 M HCl and 1.0 M H₂SO₄ corrosive solution were carefully prepared by diluting the appropriate amount of both acids (separately) with doubly distilled water. For all the experiments involving aluminum, approximately 0.5 M HCl corrosive solution were carefully prepared by diluting the appropriate amount of the acid with doubly distilled water. Stock solution of about 10×10⁻³ M for the inhibitors was prepared by weighing appropriate amounts of the inhibitors and diluting with appropriate amount of doubly distilled water to the mark of 500 ml volumetric flasks. To ensure that the inhibitors completely dissolved in the doubly distilled water, the mixture was warmed up using a hot plate and stirred with a magnetic stirrer for 2–5 minutes. From the stock solution, a series of concentrations as indicated elsewhere were prepared through dilution of appropriate amounts of doubly distilled water.

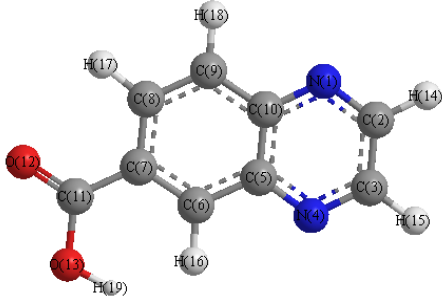
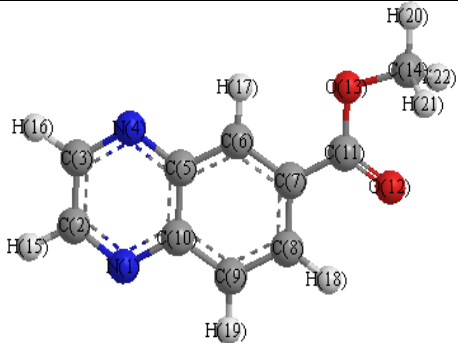
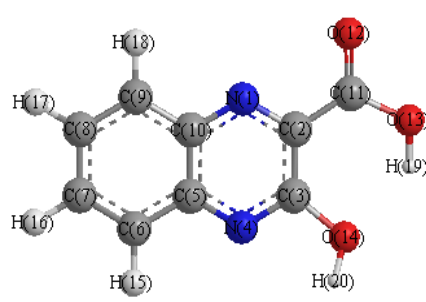
3.3 OTHER EQUIPMENT/ INSTRUMENTS AND APPARATUS UTILIZED

- Volumetric flasks (100 ml, 250 ml, 500 ml, 1000 ml, and 2000 ml)
- Thermometers: They are made of glass to measure temperature up to 373,15 K
- Desiccator
- Glass rod and hooks
- Plastic funnel
- Spatula made from stainless steel
- Pipettes
- Adam Equipment PW184 Analytical Balance, 180g x 0.0001g, 115 V was for weight loss determination and preparation of the inhibitor solutions
- Memmert thermostat water bath
- FMH magnetic stirrer, Hotplate up to 693.15 K, and powerful horseshoe magnet
- Suez Laboratory water purifier ECO
- Potassium iodide
- Paper towel

3.4 INHIBITORS USED

Three quinoxaline derivatives were utilized as corrosion inhibitors. The properties, anticorrosion, and non-toxicity of the inhibitors chosen for this study is discussed in section 2.6 of this dissertation. All the quinoxaline derivatives investigated in this study were procured commercially (at Sigma-Aldrich). Their structures, molecular formulas, IUPAC names, and molecular masses are given in Table 3.1. The studied inhibitors were chosen based on the on the constituent of heteroatoms such as nitrogen and oxygen as well as aromatic rings in their structure that have reported as major adsorption centers because they have high electron density and the inhibition potential and properties of these compounds have not been investigated or reported anywhere in literature. Furthermore, quinoxalines have been vastly reported in literature as nontoxic organic molecules.

Table 3.1: Molecular structures, formulae, name and masses of the quinoxalines used as corrosion inhibitors in this study.

Molecular structure with atom numbering	Molecular formula	IUPAC Name	Molecular mass
	C ₉ H ₆ N ₂ O ₂	quinoxalone-6-carboxylic acid Adopted acronym: Q6CA	174.16 g/mol
	C ₁₀ H ₈ N ₂ O ₂	methyl quinoxaline-6-carboxylate Adopted acronym: MQ6CA	188.19 g/mol
	C ₉ H ₆ N ₂ O ₃	3-hydroxy-2-quinoxaline carboxylic acid Adopted acronym: H2QCA	190.04 g/mol

3.4 Gravimetric Analysis

Gravimetric analysis is preferable mostly because it is more accurate and reliable. This technique is less expensive and gives high precision outcomes. Its recommendation is mainly based on its easiness for conduction [284–287]. The weight loss measurements were carried out by totally immersing each weighed metal specimens (zinc and mild steel) in the corrosive solution 1.0 M of HCl and H₂SO₄ in the absence and presence of various concentrations of all studied corrosion inhibitors at temperatures of 303K, 313K, 323K and 333K, respectively, that was maintained using the thermostat water baths. After 7 hours of exposure to the corrosion environment, the metal specimens were washed by tap water then brushed by smooth brush under running tap water to remove non-adherent corrosion products. The metals were dried with clean paper towel and reweighed to obtain the weight loss. Each run was repeated three times and for each an average weight loss values was calculated. All the weight loss data was tabulated, recorded and used to calculate the corrosion rate (ρ), surface coverage (θ), percentage inhibition efficiency (%IE) and using the equations (40), (41) and (42), respectively [284]. The system utilized for the gravimetric analysis is shown in figure 3.1.

The inhibition efficiency (% IE) was calculated from the values of corrosion rate as follows:

$$\rho = \left(\frac{\Delta w}{St} \right) \quad (41)$$

where: ρ = the corrosion rate

w = the average weight loss of the material

S = is the total surface area of the of the metal specimen

t = is the immersion time

The degree of surface coverage is given by the following equation:

$$\theta = \left(1 - \frac{w_1}{w_2} \right) \quad (42)$$

where: θ = the degree of surface coverage

w_1 = the weight loss of metal in the presence of inhibitor

w_2 = the weight of metal in the absence of inhibitor

The inhibition efficiency (% IE) is given by the following equation:

$$\% \text{IE} = \left(1 - \frac{w_1}{w_2}\right) \times 100 \quad (43)$$

where: IE = inhibition efficiency

w_1 = the weight loss of metal in the presence of inhibitor

w_2 = the weight loss of metal in the absence of inhibitor



Figure 3.1: System used for the gravimetric analysis.

3.5 Electrochemical Analysis

As discussed in sub-section 2.1.1, corrosion is an electrochemical process. Hence a pool of electrochemical techniques for corrosion monitoring have been developed and studied. The two electrochemical techniques which are mostly studied for the corrosion process of zinc, aluminum, and mild steel are the Potentiodynamic Polarization (PDP) and the Electrochemical Impedance Spectroscopy (EIS) [283–287], hence are also adopted in this study. The system and procedure are discussed in the sub-section below. The electrochemical studies were carried out using a conventional three-electrode cell SP-150 Biologic potentiostat instrument. All the electrochemical experiments were performed at room temperature.

3.5.1 Host Computer

The SP-150 Biologic potentiostat instrument was connected to an external computer (Dell type) via USB 2.0 type A male to type B male cable. The potentiostat was operated from computer software, BioLogic EC-Lab software. The software allowed remote access to an instrument, thus, abled data processing and the recording of data.

3.5.2 Corrosion Cell

A suitable titration vessel cell made of glass with 150 ml capacity, with sufficient cover openings to insert the electrode was utilized in this study, as shown in figure 3.2. The cell consisted with three electrodes, namely; the working electrode (WE) which was the metal specimens of under investigation, a saturated calomel with Ag/AgCl as a reference electrode (RE), and the counter electrode which its purpose was to provide an electron source for the working electrode. The working electrode attached to a cable was embedded in epoxy resin as shown in figure 3.3.

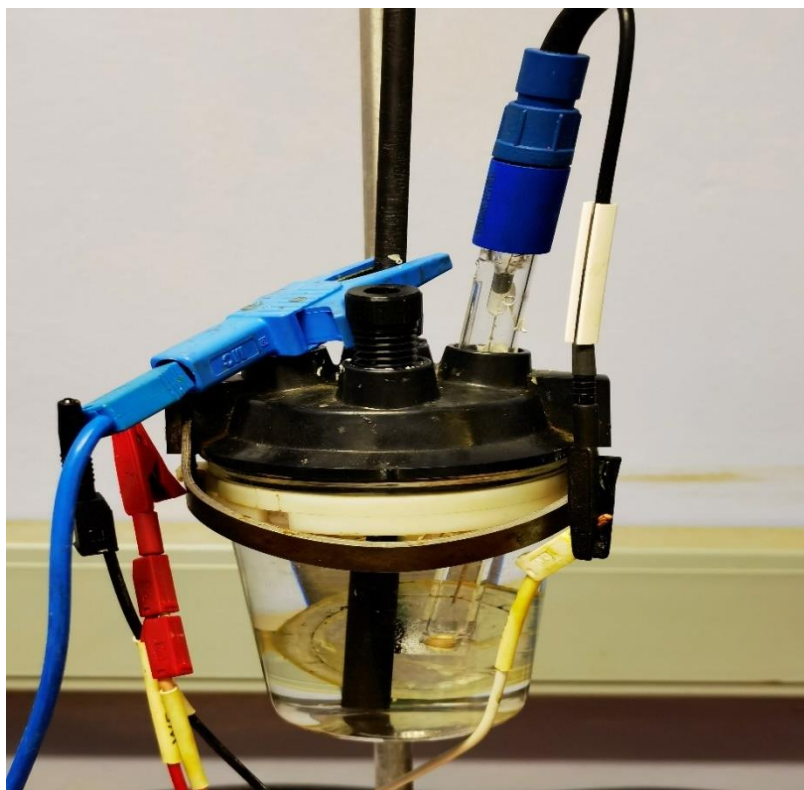


Figure 3.2: Typical electrochemical experiment set-up showing the electrochemical glass cell and electrodes.

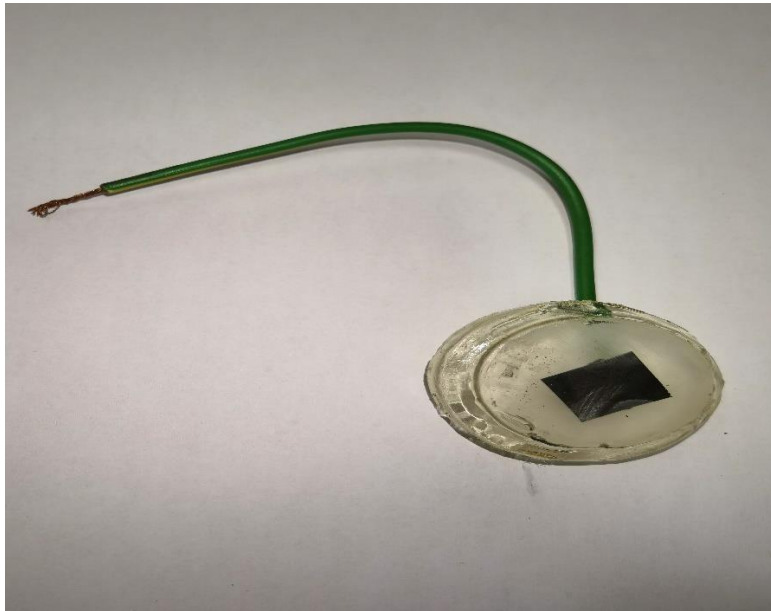


Figure 3.3: The picture of a typical a metal specimen (WE) used for the experiments in this study.



Figure 3.4: The Struers Labosystem instrument used for pre-cleaning metal specimens.

3.5.3 Potentiodynamic Polarization (PDP)

Polarization studies was carried out for all the metals under investigation in the presence and absence of inhibitors. Polarization measurements was performed to evaluate the corrosion current (i_{corr}), Tafel slope (β_a and β_c), corrosion potential (E_{corr}) and corrosion density.

The percentage inhibition efficiency in PDP will be calculated by using equation (44):

$$\%IE_{PDP} = \left(\frac{i^0_{corr} - i_{corr}}{i^0_{corr}} \right) \times 100 \quad (44)$$

where: i^0_{corr} and i_{corr} are the values of corrosion current density in the absence and presence of inhibitor, respectively

3.5.4 Electrochemical Impedance Spectroscopy (EIS)

EIS was also instrumental in studying the corrosion for all the metals under investigation in the presence and absence of inhibitors. The electrochemical parameters such as the resistance of charge transfer, capacity of double layer, the phase element constant and exponents were obtained and used to calculate the inhibition efficiency from the equation (45).

$$\%IE_{EIS} = \left(1 - \frac{R^0_{ct}}{R_{ct}} \right) \times 100 \quad (45)$$

where: R^0_{ct} is the charge transfer resistance in the absence of the inhibitor and R_{ct} is the charge transfer resistance in the presence of the inhibitor.



Figure 3.5: SP-150 Biologic potentiostat for the electrochemical experiments.

For both the PDP and EIS measurements, the metal specimens were allowed to corrode for an hour in Open Circuit Potential (OCP) until a steady corrosion potential (E_{corr}) for all the working electrodes was established. This was done so because the accuracy of PDP depends on the stability between the metal specimen and corrosive solution. The SP-150 Biologic potentiostat for the electrochemical experiments is shown in figure 3.5.

3.6 Atomic Absorption Spectrometry (AAS)

AAS is an analytical technique that measures the concentration of an element by measuring the absorbed radiation by free atoms of the element of interest. It detects elements in either liquid or solid samples through the application of characteristic wavelengths of electromagnetic radiation from a light source. The wavelength at the light is absorbed is specific for each element. For an example, in a sample containing iron together with other elements such as sulphur and chromium, when such sample exposed to the light at a wavelength for iron, only the iron atoms will absorb that light [288]. AAS is an easy, high-throughput, and less expensive technology used primarily to analyze compounds in solution, and it can measure down to parts per billion of grams. In this

study, AAS was utilized in determining the concentration of zinc and mild steel for the uninhibited and inhibited processes. After gravimetric studies, the solutions of the inhibited and uninhibited runs were preserved for concentration measurements. Figure 3.6 shows the atomic absorption spectrometer utilized in this study.



Figure 3.6: Atomic absorption spectrometer utilized in this study.

3.7 Fourier Transform Infrared Spectroscopy (FTIR)

FTIR spectroscopy is an established technique for quality control when evaluating industrially manufactured material and can often serve as the first step in the material analysis process. This technique is useful for analyzing the chemical composition of smaller particles, typically 10 – 50 microns, as well as larger areas on the surface [289]. FTIR spectroscopy was useful in determining the adsorption characteristics of the inhibitors for zinc and mild steel. After completion of the gravimetric measurements of the acidic solutions with and without the optimal concentration of the inhibitors at 303 K, zinc and mild steel specimens were rinsed with water, and dried. The layer formed on the metal surface was carefully scratched with a knife and it was subjected to FTIR studies. The pure inhibitor powder was also analyzed (FTIR). The FTIR spectra of the stretched

layer that formed on the metal surface and the pure inhibitor were compared. Perkin-Elmer FTIR spectrophotometer shown in figure 3.7 was utilized for the FTIR analysis.



Figure 3.7: Fourier transform infrared spectrometer utilized in this study.

3.8 Computational analysis

The properties of molecules under investigation were determined by optimizing the structures of the individual molecule using the density functional theory (DFT). The binding energy between the metal surface and the inhibitor molecule was estimated using a computational software, Accelrys Materials Studio [290]. The Material studio software was utilized to obtain a metal crystal structure of interest. A metal crystal structure (i.e., crystallographic information file) was imported and a unit-cell was built. A super-cell was created and subsequently, a slab of desired phase was cleaved to provide a large surface area for the interaction of the inhibitor molecule and the surface of the metal. A vacuum simulation box of certain wall thickness consisting of periodic boundary conditions for the simulation process was built. In the vacuum of the super-cell, the molecule was inserted. All the calculations in this work were calculated under the Dmol³ module with semi-core pseudopotentials and double numeric plus polarization (3DNP) basis set [291]. To describe the interactions, the generalized gradient approximation (GGA), using the functional form of Perdew-

Burke-Enzerhof (PBE) were utilized [292]. The SCF tolerance was set to 1.0×10^{-6} Hartrees. Considering the computational cost and boundary affects, all calculations were conducted on a 3-layer slab of pure Al (111) and Zn (110) (4×4 supercell) surface model, containing 64 atoms, respectively, and separated by 20 Å of vacuum along the c-axis direction. The adsorbates and the upper surface layer were relaxed, only the bottom two layers were fixed. The binding energy was estimated by subtracting the sum of the energy of the isolated metal surface and the inhibitor molecule from the energy of the complexed metal···inhibitor system [see equation (46) below].

$$E_{ads} = E_{molecule+surface} - E_{molecule} - E_{surface} \quad (46)$$

where $E_{molecule+surface}$ is the total energy of the interacting molecule of interest and the surface of interest [Al (111) and Zn (110)], $E_{molecule}$ is the energy of the isolated molecule and $E_{surface}$ is the energy of the isolated surface of interest.

CHAPTER 4

RESULTS AND

DISCUSSION

This chapter is portioned into four sections. The first section provides the results of the corrosion of mild steel and zinc in acidic media in the absence of corrosion inhibitors. The second section deals with all the experimental findings of mild steel corrosion in the absence and presence of corrosion inhibitors. The third and fourth sections unpack the experimental results for zinc and aluminum, respectively.

4.1 BLANK TESTS

4.1.1 Weight loss in the absence of corrosion inhibitors

The weight loss technique was performed by first weighing each metal specimen of zinc and mild steel, and after the metal specimens were completely immersed in the acidic solution of different concentrations at various temperatures of 303 – 333 K. After 8 hours of immersion, each metal specimen was removed from the acidic solution and re-weighed to obtain a new mass. These tests are referred to as blank tests or control tests. The weight-loss method was performed again but this time in the presence of inhibitors and a controlled 1.0 M HCl and H₂SO₄ solutions at various temperatures as those of the controlled tests. Generally, the rate of corrosion of metals is highly influenced by temperature variation, that is, the rate of reaction is directly proportional to the increase in temperature [94, 293]. The results obtained from the blank tests are graphically presented in figures 4.1 – 4.4 and in Tables 4.1 – 4.4.

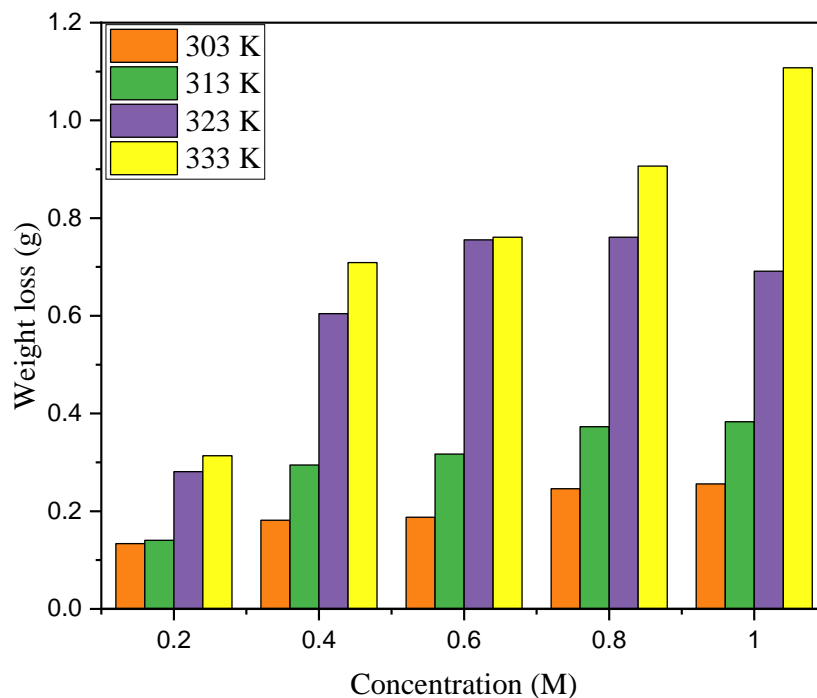


Figure 4.1: The plot of weight loss of zinc as a function of the concentration of HCl in the absence of a corrosion inhibitor.

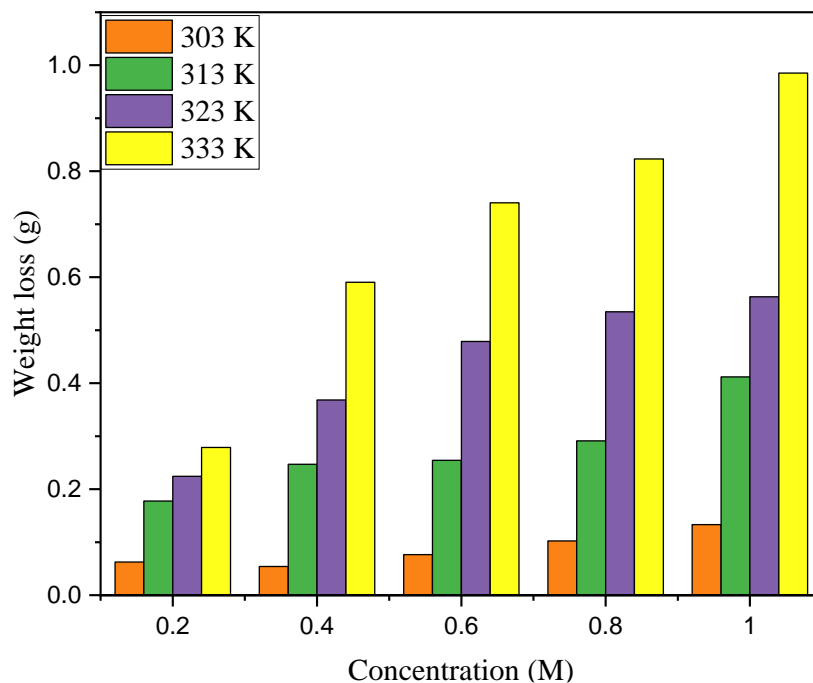


Figure 4.2: The plot of weight loss of mild steel as a function of the concentration of HCl in the absence of a corrosion inhibitor.

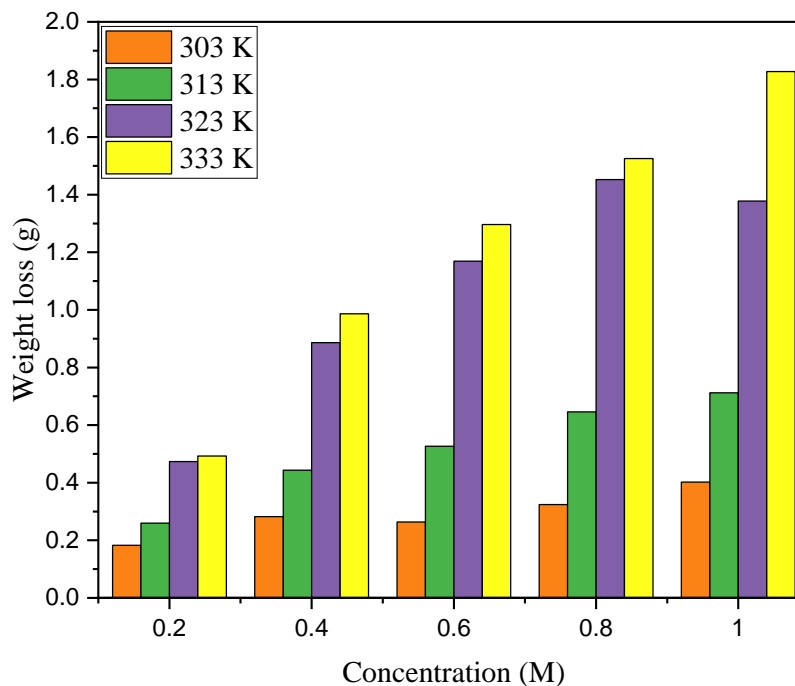


Figure 4.3: The plot of weight loss of zinc as a function of the concentration of H₂SO₄ in the absence of a corrosion inhibitor.

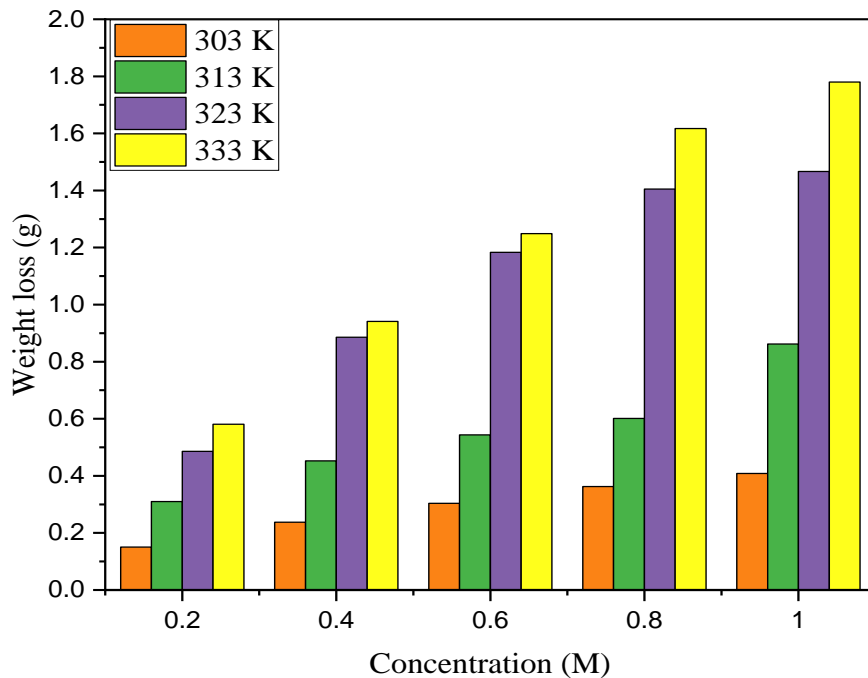


Figure 4.4: The plot of weight loss of mild steel as a function of the concentration of H_2SO_4 in the absence of a corrosion inhibitor.

Table 4.1: Weight loss measurements and corrosion rate of zinc in various concentrations of HCl, in the absence of the corrosion inhibitors.

Corrosive medium	Temperature (K)	Concentration (M)	Weight loss (g)	Corrosion rate ($\text{g}\cdot\text{cm}^{-2}\cdot\text{h}^{-1}$)
HCl	303	0.2	0.1337	0.0031833
		0.4	0.1817	0.0043261
		0.6	0.1877	0.0044690
		0.8	0.2460	0.0058571
		1.0	0.2558	0.0060904
	313	0.2	0.1406	0.0033476
		0.4	0.2947	0.0070166
		0.6	0.3170	0.0075476
		0.8	0.3729	0.0008878
		1.0	0.3823	0.0091238
	323	0.2	0.2811	0.0066928
		0.4	0.6043	0.0138809
		0.6	0.7021	0.0167166
		0.8	0.7555	0.0179880
		1.0	0.6913	0.0164590
	333	0.2	0.3127	0.0074452
		0.4	0.6088	0.0144952
		0.6	0.7607	0.0181119
		0.8	0.9063	0.0215785
		1.0	1.1077	0.0263780

Table 4.2: Weight loss measurements and corrosion rate of mild steel in various concentrations of HC in the absence of the corrosion inhibitors.

Corrosive medium	Temperature (K)	Concentration (M)	Weight loss (g)	Corrosion rate ($\text{g}\cdot\text{cm}^{-2}\cdot\text{h}^{-1}$)
HCl	303	0.2	0.0626	0.0014904
		0.4	0.0542	0.0012904
		0.6	0.0764	0.0018190
		0.8	0.1022	0.0024333
		1.0	0.1332	0.0031714
	313	0.2	0.1775	0.0042261
		0.4	0.2471	0.0058833
		0.6	0.2544	0.0060571
		0.8	0.2911	0.0069309
		1.0	0.4118	0.0098047
	323	0.2	0.2244	0.0053428
		0.4	0.3684	0.0087714
		0.6	0.4788	0.0114000
		0.8	0.5348	0.0127333
		1.0	0.5630	0.0134047
	333	0.2	0.2786	0.0066333
		0.4	0.5905	0.0140595
		0.6	0.7488	0.0178285
		0.8	0.8232	0.0196000
		1.0	0.9851	0.0234547

Table 4.3: Weight loss measurements and corrosion rate of zinc in various concentrations of H₂SO₄ in the absence of the corrosion inhibitors.

Corrosive medium	Temperature (K)	Concentration (M)	Weight loss (g)	Corrosion rate (g.cm ⁻² .h ⁻¹)
H ₂ SO ₄	303	0.2	0.1827	0.0043500
		0.4	0.2821	0.0067166
		0.6	0.2636	0.0062761
		0.8	0.3241	0.0077166
		1.0	0.4022	0.0095761
	313	0.2	0.2597	0.0061833
		0.4	0.4434	0.0105571
		0.6	0.5267	0.0125404
		0.8	0.6459	0.0153785
		1.0	0.7123	0.0169595
	323	0.2	0.4734	0.0112714
		0.4	0.8863	0.0211023
		0.6	1.1693	0.0278404
		0.8	1.4523	0.0345578
		1.0	1.3779	0.0328071
	333	0.2	0.4926	0.0117885
		0.4	0.9863	0.0234833
		0.6	1.2961	0.0308595
		0.8	1.5257	0.0363261
		1.0	1.8276	0.0435142

Table 4.4: Weight loss measurements and corrosion rate of mild steel in various concentration of H₂SO₄ in the absence of the corrosion inhibitors.

Corrosive medium	Temperature (K)	Concentration (M)	Weight loss (g)	Corrosion rate (g.cm ⁻² .h ⁻¹)
H ₂ SO ₄	303	0.2	0.1507	0.0035880
		0.4	0.2378	0.0056619
		0.6	0.3040	0.0072380
		0.8	0.3625	0.0086309
		1.0	0.4082	0.0097190
	313	0.2	0.3099	0.0073785
		0.4	0.4525	0.0107738
		0.6	0.5430	0.0129285
		0.8	0.6014	0.0143190
		1.0	0.8618	0.0205191
	323	0.2	0.4860	0.0115714
		0.4	0.8856	0.0210857
		0.6	1.1832	0.0281714
		0.8	1.4050	0.0334523
		1.0	1.4667	0.0349214
	333	0.2	0.5811	0.0138357
		0.4	0.9410	0.2240476
		0.6	1.2488	0.0297333
		0.8	1.6170	0.0385000
		1.0	1.7801	0.0423833

The variation of temperature and concentration of the corrosive medium with immersion period can be understood by assessing Tables 4.1– 4.4. In all the tables, there is a general increase in weight loss with the increase of temperature and an increase in the concentration of the corrosive medium. Moreover, from Tables 4.1 – 4.4, it can be observed that the most aggressive acid was H₂SO₄ with the weight loss of 1.828 g and 1.780 g in comparison to HCl with the weight loss of 1.107 g and 0.9851 g for zinc and mild steel, respectively, at a maximum concentration of 1.0 M and temperature of 333 K [294]. The tables also show that the corrosion rate increased with the concentration of HCl and H₂SO₄, and with the increase in the temperature. These can be attributed to the fact that the rate of corrosion is highly influenced by temperature variations, that is, due to

the kinetic energy of the atoms or/and molecules, the rate of corrosion increases along with the increases in temperature [93–95]. Similar trend was observed for both the acids and metals under study. The following sections contains results obtained when the corrosion inhibitors were introduced in the corrosive medium for each metal under study.

4.2 MILD STEEL

4.2.1 Weight loss in the absence and presence of corrosion inhibitors

The weight loss of mild steel in the absence and presence of various concentrations of MQ6CA, Q6CA, and H2QCA with and without KI in 1.0 M HCl and 1.0 M H₂SO₄ at various temperatures of 303 – 333 K were studied. The data obtained are graphically presented in figures 4.5 – 4.12 and in Tables 4.5 – 4.6. MQ6CA and Q6CA were investigated at various concentrations of 0.5×10^{-3} , 1.0×10^{-3} , 2.0×10^{-3} , 3.0×10^{-3} , and 4.0×10^{-3} M for both acids. H2QCA was investigated at various concentration of 5.0×10^{-3} , 6.0×10^{-3} , 7.0×10^{-3} , 8.0×10^{-3} , and 9.0×10^{-3} M with synergistic effect, that is, addition of potassium iodide (0.005 M) in the solution.

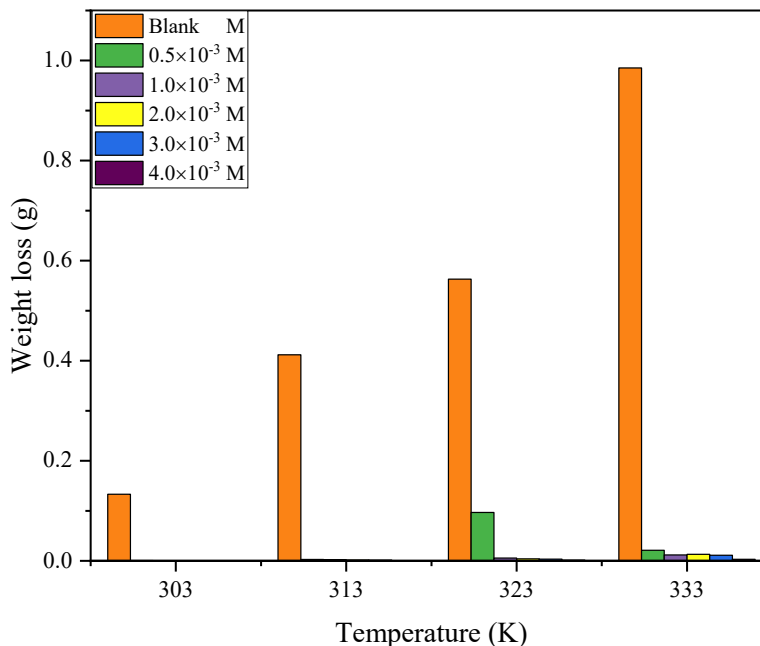


Figure 4.5: Weight loss measurements of mild steel in the absence and presence of MQ6CA in 1.0 M HCl at different temperature.

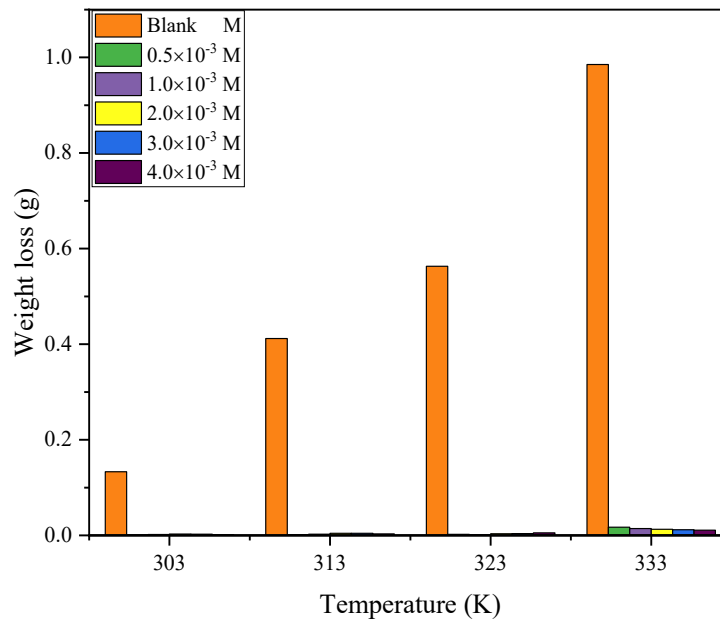


Figure 4.6: Weight loss measurements of mild steel in the absence and presence of Q6CA in 1.0 M HCl at different temperature.

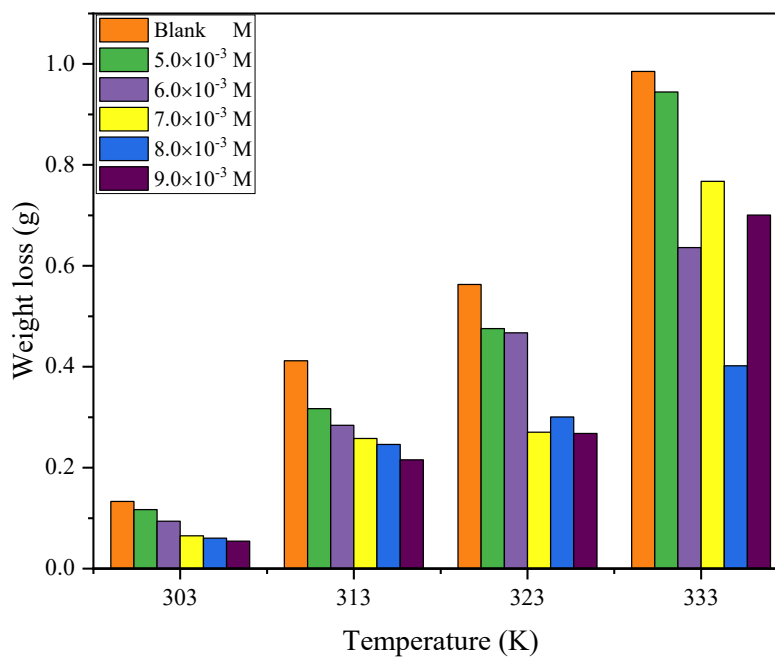


Figure 4.7: Weight loss measurements of mild steel in the absence and presence of H2QCA without KI in 1.0 M HCl at different temperature.

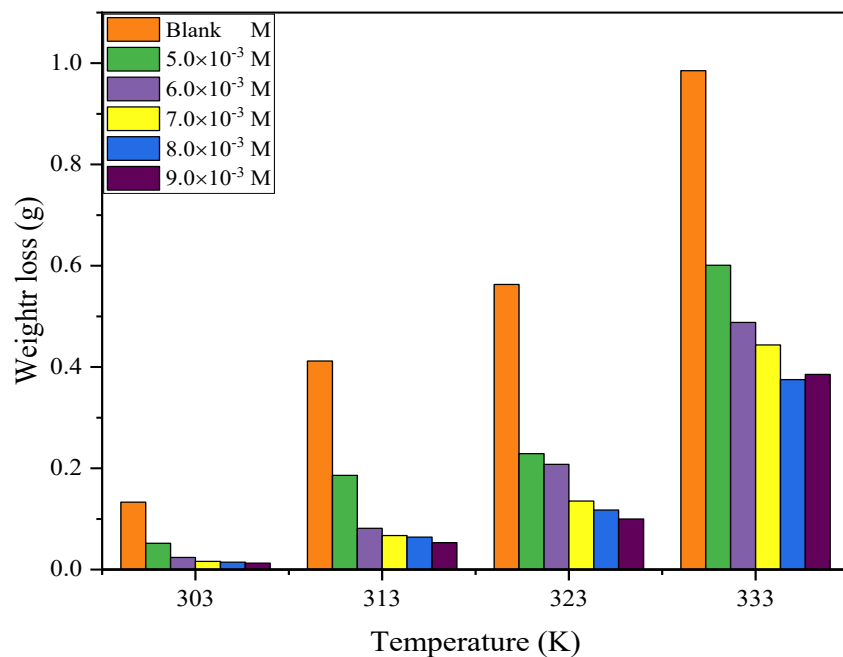


Figure 4.8: Weight loss measurements of mild steel in the absence and presence of H₂QCA with KI in 1.0 M HCl at different temperature.

Table 4.5: Weight loss measurements of mild steel in the absence and presence of MQ6CA, Q6CA and H2QCA in 1.0 M HCl obtained at different temperature.

Inhibitor	Concentration ($\times 10^{-3}$ M)	Weight loss (g)			
		303 K	313 K	323 K	333 K
	0.000	1.332	0.4118	0.5630	0.9851
MQ6CA	0.5	0.0006	0.0028	0.0966	0.0210
	1.0	0.0004	0.0026	0.0056	0.0119
	2.0	0.0004	0.0018	0.0041	0.0132
	3.0	0.0004	0.0014	0.0033	0.0111
	4.0	0.0001	0.0002	0.0016	0.0030
Q6CA	0.5	0.0005	0.0014	0.0023	0.0172
	1.0	0.0018	0.0026	0.0008	0.0142
	2.0	0.0027	0.0043	0.0034	0.0128
	3.0	0.0025	0.0044	0.0037	0.0118
	4.0	0.0014	0.0030	0.0053	0.0109
H2QCA without KI	5.0	0.1170	0.3171	0.4757	0.9445
	6.0	0.0940	0.2841	0.4672	0.6362
	7.0	0.0650	0.2580	0.2702	0.7674
	8.0	0.0602	0.2462	0.3004	0.4020
	9.0	0.0545	0.2156	0.2680	0.7005
H2QCA with KI	5.0	0.0519	0.1861	0.2290	0.6009
	6.0	0.0240	0.0814	0.2077	0.4882
	7.0	0.0163	0.0671	0.1352	0.4435
	8.0	0.0145	0.0640	0.1176	0.3752
	9.0	0.0129	0.0531	0.0999	0.3854

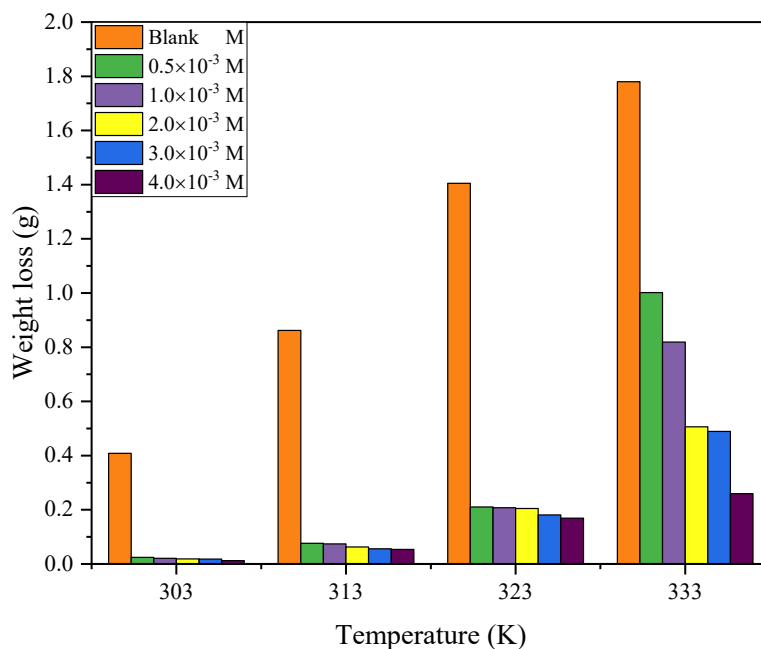


Figure 4.9: Weight loss measurements of mild steel in the absence and presence of MQ6CA in 1.0 M H₂SO₄ at different temperature.

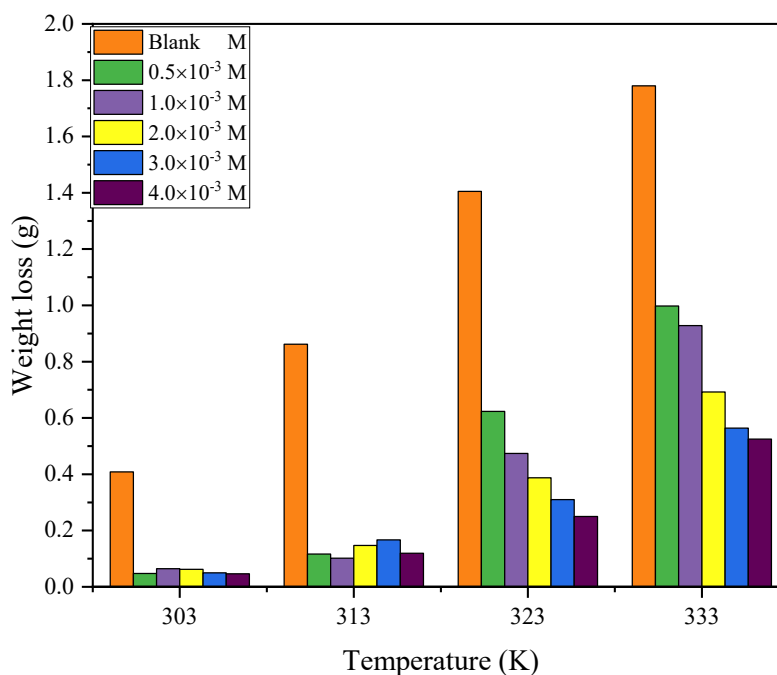


Figure 4.10: Weight loss measurements of mild steel in the absence and presence of Q6CA in 1.0 M H₂SO₄ at different temperature.

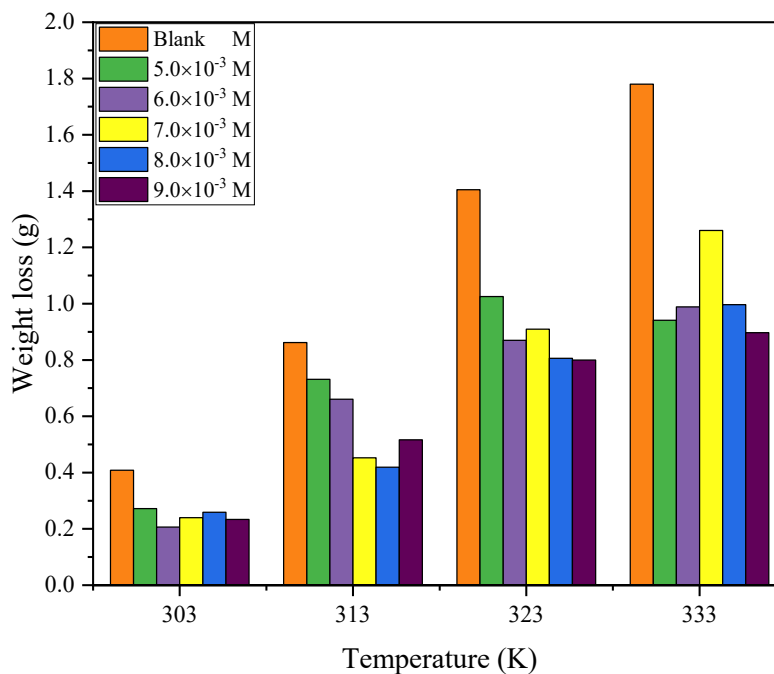


Figure 4.11: Weight loss measurements of mild steel in the absence and presence of H₂QCA without KI in 1.0 M H₂SO₄ at different temperature.

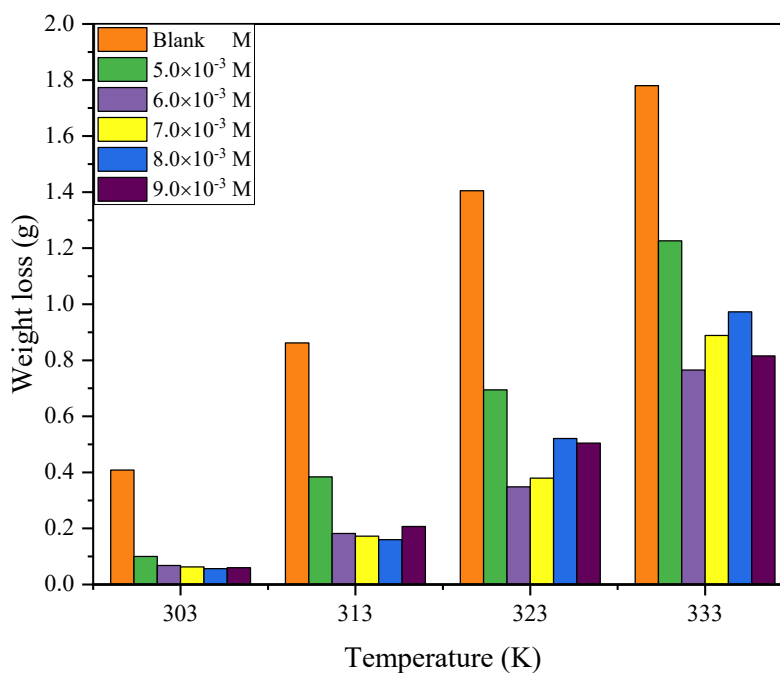


Figure 4.12: Weight loss measurements of mild steel in the absence and presence of H₂QCA with KI in 1.0 M H₂SO₄ at different temperature.

Table 4.6: Weight loss measurements of mild steel in the absence and presence of MQ6CA, Q6CA and H2QCA in 1.0 M H₂SO₄ obtained at different temperature.

Inhibitor	Concentration ($\times 10^{-3}$ M)	Weight loss (g)			
		303 K	313 K	323 K	333 K
	0.000	0.4082	0.8618	1.4050	1.7801
MQ6CA	0.5	0.2646	0.0764	0.2105	1.0018
	1.0	0.0209	0.0743	0.2078	0.8188
	2.0	0.0184	0.0630	0.2047	0.5062
	3.0	0.0180	0.0558	0.1810	0.4893
	4.0	0.0122	0.50539	0.1693	0.2594
Q6CA	0.5	0.0477	0.1163	0.6234	0.9978
	1.0	0.0264	0.1019	0.4740	0.9284
	2.0	0.0621	0.1471	0.3875	0.6924
	3.0	0.0498	0.1667	0.3099	0.5641
	4.0	0.0463	0.1194	0.2497	0.5247
H2QCA without KI	5.0	0.2722	0.7313	1.0255	1.2414
	6.0	0.2056	0.6604	0.8697	0.9885
	7.0	0.2399	0.4526	0.9093	1.2603
	8.0	0.2589	0.4189	0.8060	0.9967
	9.0	0.2337	0.5162	0.8000	0.8968
H2QCA with KI	5.0	0.1001	0.3842	0.6948	1.2260
	6.0	0.0681	0.1824	0.3482	0.7653
	7.0	0.0627	0.1723	0.3795	0.8886
	8.0	0.0568	0.1600	0.5210	0.9726
	9.0	0.0600	0.2068	0.5043	0.8158

From figures 4.5 – 4.12, it is evident that the weight loss of mild steel remarkably decreased with the increase in the concentration of the inhibitors and increased with the increase in the temperature of the corrosive environment. Upon close inspection of the data, Tables 4.5 and 4.6 show that mild steel lost weight significantly in both acid media (blank) in comparison to when the inhibitors were introduced. For instance, in Table 4.6 the weight loss of mild steel for blank tests were obtained to be 0.1332 g, 0.4118 g, 0.5630 g, and 0.9851 g at temperature of 303 K, 313 K, 323 K, and 333 K, respectively, in comparison to tests with an introduction of 0.5×10^{-3} M MQ6CA which the weight loss of mild steel was obtained to be 0.0006 g, 0.0028 g, 0.0966 g, and 0.0210 g at temperature of 303 K, 313 K, 323 K, and 333 K, respectively. The table also shows that the lowest weight loss was obtained at the highest concentration of MQ6CA (4×10^{-3} M) and temperature of 303 K. Similar trend was also observed in all the inhibitors. This observation has been reported by a number of authors [295–298]. Looking at H2QCA from both Table 4.5 and 4.6, both tables reveal that the introduction of KI in the solution tremendously reduced the weight loss of mild steel. For instance, in Table 4.5, at the concentration of 5.0×10^{-3} M H2QCA without KI, the weight loss of mild steel was found to increase from 0.1170 g, 0.3171 g, 0.4757 g, and then 0.9445 g at 303 K, 313 K, 323 K, and 333 K, respectively. However, in the presence of KI values enormously reduced to 0.0519 g, 0.1861 g, 0.2290 g, and 0.6009 g at temperature of 303 K, 313 K, 323 K, and 333 K, respectively. A similar trend was also observed in all the studied concentrations of H2QCA, and also in Table 4.6. These observations support the fact that weight loss decreases with the increases in inhibitor concentration, which consequently leads to a decrease in corrosion rate. Nkuna et al. also reported a similar observation [299]. Moreover, from the weight loss data of mild tabulated above, it is clear that H_2SO_4 was more corrosive than HCl. This may be due to the fact that H_2SO_4 possesses a relatively higher concentration than HCl [294].

4.2.2 Corrosion rate and inhibition efficiency

The corrosion rate (C_R), surface coverage (θ), and percentage inhibition efficiency (% IE) obtained from weight loss measurement of mild steel in 1.0 M HCl and 1.0 M H₂SO₄ in the absence and presence of various concentration of MQ6CA, Q6CA, and H2QCA with and without KI at temperature 303 – 333 K are presented in the Tables 4.7 – 4.12 and figures 4.13 – 4.20. It is evident from these tables that the corrosion rate in the absence of the inhibitors was relatively high at all the studied temperatures. However, with the introductory of the three quinoxalines in the corrosion medium, the corrosion rate decreased. These tables show that the lowest corrosion rate was found to be at the lowest temperature (303 K). For instance, looking at Table 4.7, the corrosion rate of mild steel at 303 K in the absence of MQ6CA was 0.003171 g.cm⁻².h⁻¹. Immediately the inhibitor was introduced a great decrease in corrosion rate (0.000014 g.cm⁻².h⁻¹) was observed. Other authors also documented the same observation [292–298].

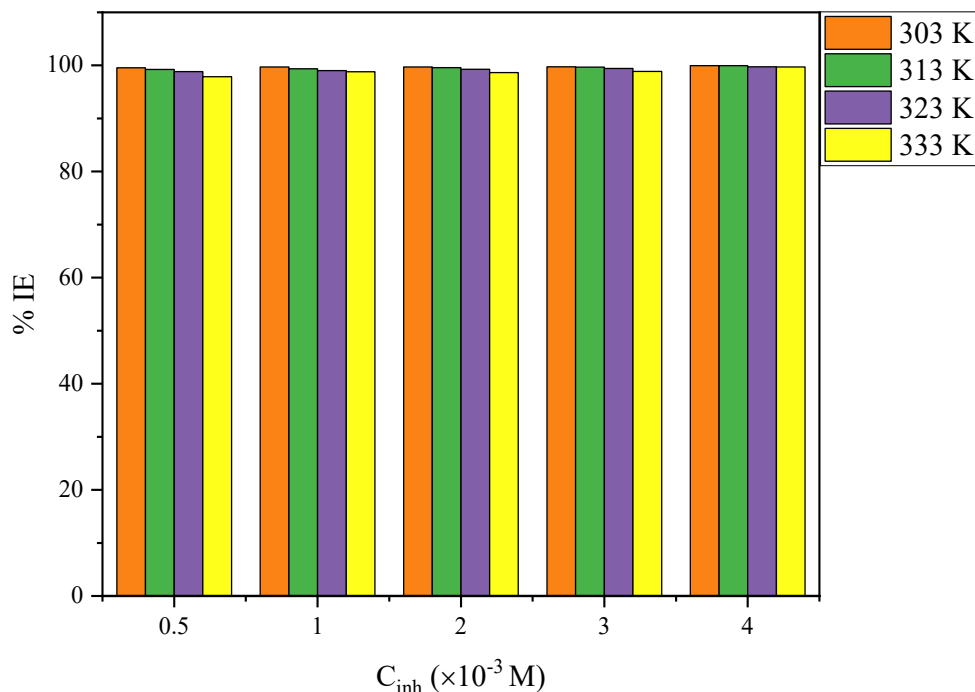


Figure 4.13: The variation of percentage inhibition efficiency with various concentration of MQ6CA at various temperatures in 1.0 M HCl.

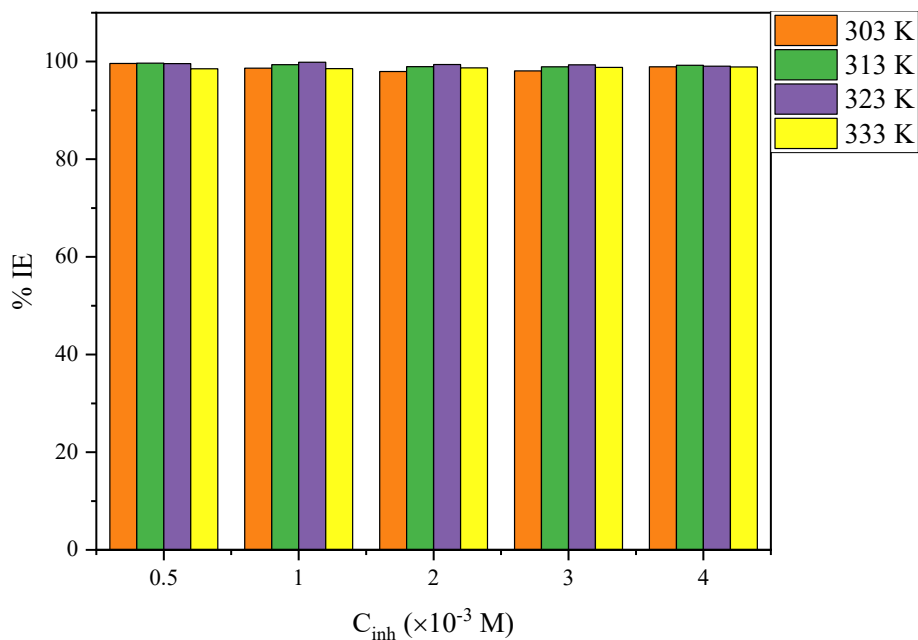


Figure 4.14: The variation of percentage inhibition efficiency with various concentration of Q6CA at various temperatures in 1.0 M HCl.

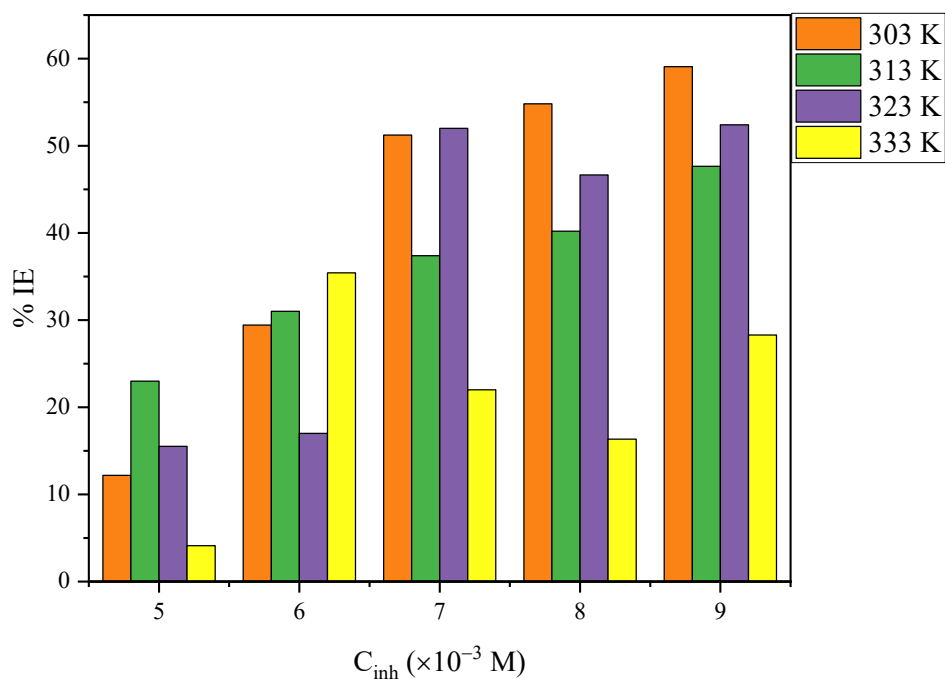


Figure 4.15: The variation of percentage inhibition efficiency with various concentration of H2QCA without KI at various temperatures in 1.0 M HCl.

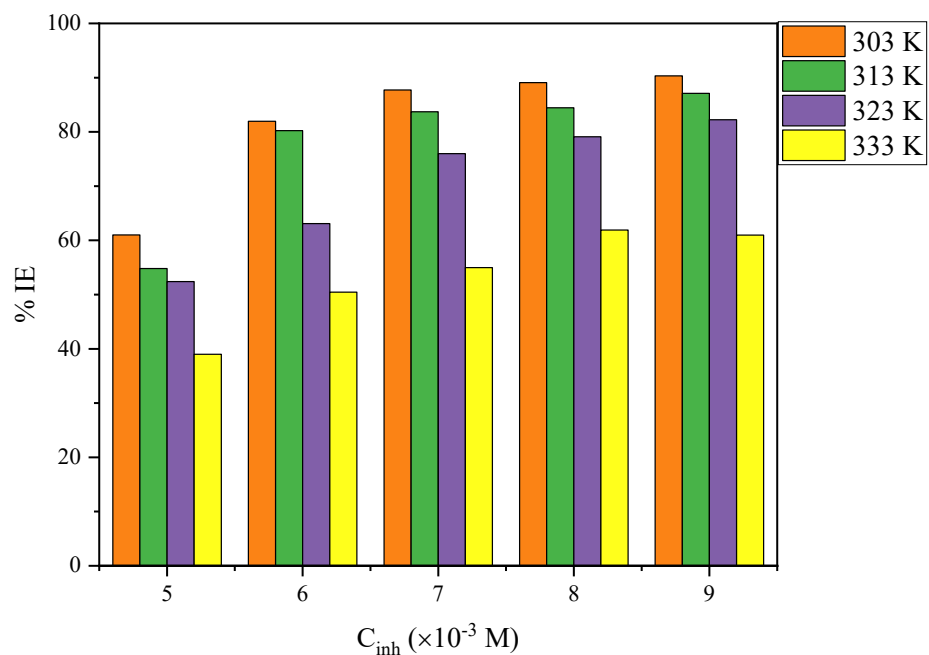


Figure 4.16: The variation of percentage inhibition efficiency with various concentration of H2QCA with KI at various temperatures in 1.0 M HCl.

Table 4.7: The corrosion parameters for mild steel in 1.0 M HCl in the absence and presence of various concentrations of MQ6CA obtained from weight loss measurements at 303 – 333 K.

Inhibitor	Temperature (K)	Inhibior concentration ($\times 10^{-3}$ M)	Corrosion rate ($\text{g.cm}^{-2}.\text{h}^{-1}$)	Surface coverage (θ)	Inhibition efficiency (%)
MQ6CA	303	-	0.0031713	-	-
		0.5	0.0000143	0.9955	99.55
		1.0	0.0000095	0.9970	99.70
		2.0	0.0000095	0.9971	99.71
		3.0	0.0000095	0.9972	99.72
		4.0	0.0000024	0.9995	99.95
	313	-	0.0098048	-	-
		0.5	0.0000667	0.9923	99.23
		1.0	0.0000619	0.9937	99.37
		2.0	0.0000429	0.9957	99.57
		3.0	0.0000333	0.9966	99.66
		4.0	0.0000048	0.9994	99.94
	323	-	0.0134078	-	-
		0.5	0.0005000	0.9883	98.83
		1.0	0.0001333	0.9901	99.01
		2.0	0.0000978	0.9927	99.27
		3.0	0.0000785	0.9941	99.41
		4.0	0.0000381	0.9972	99.72
	333	-	0.0234576	-	-
		0.5	0.0023000	0.9787	97.87
		1.0	0.0002833	0.9879	98.79
		2.0	0.0003143	0.9866	98.66
		3.0	0.0002643	0.9887	98.87
		4.0	0.0007143	0.9970	99.70

Table 4.8: The corrosion parameters for mild steel in 1.0 M HCl in the absence and presence of various concentrations of Q6CA obtained from weight loss measurements at 303 – 333 K.

Inhibitor	Temperature (K)	Inhibitor concentration ($\times 10^{-3}$ M)	Corrosion rate ($\text{g.cm}^{-2}.\text{h}^{-1}$)	Surface coverage (θ)	Inhibition efficiency (%)
Q6CA	303	-	0.0031714	-	-
		0.5	0.0000119	0.9962	0.9962
		1.0	0.0000357	0.9863	0.9863
		2.0	0.0000642	0.9795	0.9795
		3.0	0.0005952	0.9810	0.9810
		4.0	0.0000333	0.9894	0.9894
	313	-	0.0098048	-	-
		0.5	0.0000333	0.9966	99.66
		1.0	0.0000548	0.9936	99.36
		2.0	0.0001024	0.9895	98.95
		3.0	0.0001047	0.9893	98.93
		4.0	0.0000714	0.9927	99.27
	323	-	0.0134048	-	-
		0.5	0.0000548	0.9959	99.59
		1.0	0.0000190	0.9985	99.85
		2.0	0.0000810	0.9939	99.32
		3.0	0.0000880	0.9934	99.34
		4.0	0.0000013	0.9905	99.05
	333	-	0.0234760	-	-
		0.5	0.0004090	0.9853	98.53
		1.0	0.0003381	0.9855	98.55
		2.0	0.0003048	0.9870	98.70
		3.0	0.0002810	0.9880	98.80
		4.0	0.0002595	0.9889	98.89

Table 4.9: The corrosion parameters for mild steel in 1.0 M HCl in the absence and presence of various concentrations of H₂QCA with and without KI obtained from weight loss measurements at 303 – 333 K.

Inhibitor	Temperature (K)	Inhibitor concentration ($\times 10^{-3}$ M)	Corrosion rate ($\text{g.cm}^{-2}.\text{h}^{-1}$)	Surface coverage (θ)	Inhibition efficiency (%)	
H ₂ QCA without KI	303	-	0.0031741	-	-	
		5.0	0.0027857	0.1219	12.19	
		6.0	0.0022381	0.2943	29.43	
		7.0	0.0015476	0.5123	51.23	
		8.0	0.0014333	0.5481	54.81	
		9.0	0.0012976	0.5908	59.08	
	313	-	0.0098047			
		5.0	0.0075500	0.2299	22.99	
		6.0	0.0067429	0.3101	31.01	
		7.0	0.0061429	0.3739	40.21	
		8.0	0.0058619	0.4021	40.21	
		9.0	0.0051333	0.4765	47.65	
	323	-	0.0134048	-	-	
		5.0	0.0113262	0.1551	15.51	
		6.0	0.0111238	0.1701	17.01	
		7.0	0.0064333	0.5200	52.00	
		8.0	0.0071524	0.4665	46.65	
		9.0	0.0063810	0.5241	52.41	
	333	-	0.0234760	-	-	
		5.0	0.0224881	0.0412	04.12	
		6.0	0.0151479	0.3542	35.42	
		7.0	0.0182714	0.2210	22.10	
		8.0	0.0095714	0.1634	16.34	
		9.0	0.0166786	0.2889	28.89	
KI	303	-	0.0031714	-	-	
		5.0	0.0012357	0.6101	61.01	
		6.0	0.0005714	0.8195	81.95	
		7.0	0.0003881	0.8772	87.72	
		8.0	0.0003452	0.8909	89.09	
		9.0	0.0003071	0.9032	90.32	
	313	-	0.0098048	-	-	
		5.0	0.0044310	0.5481	54.81	

H2QCA with KI	313	6.0	0.0019381	0.8023	80.23
		7.0	0.0019576	0.8370	83.70
		8.0	0.0015238	0.8444	84.44
		9.0	0.0012643	0.8709	87.09
	323	-	0.0134048	-	-
		5.0	0.0054524	0.5241	52.41
		6.0	0.0049452	0.6310	63.10
		7.0	0.0032190	0.7599	75.99
		8.0	0.0028000	0.7911	79.11
		9.0	0.0023786	0.8224	82.24
	333	-	0.0234760	-	-
		5.0	0.0143071	0.3900	39.00
		6.0	0.0116238	0.5044	50.44
		7.0	0.0105595	0.5498	54.98
		8.0	0.0089333	0.6091	60.91
		9.0	0.0091761	0.6097	60.97

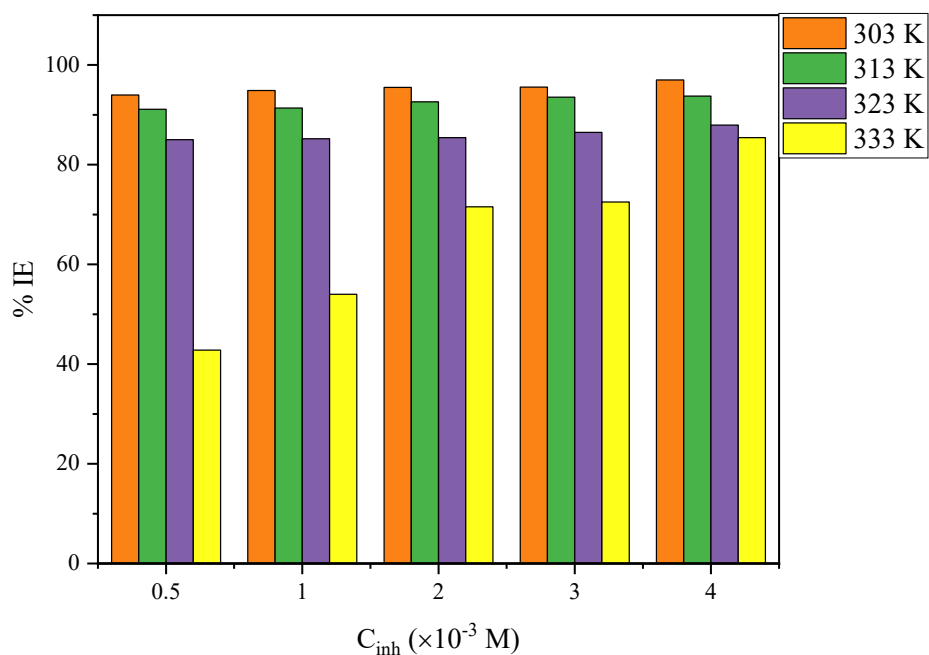


Figure 4.17: The variation of percentage inhibition efficiency with various concentration of MQ6CA at various temperatures in 1.0 M H₂SO₄.

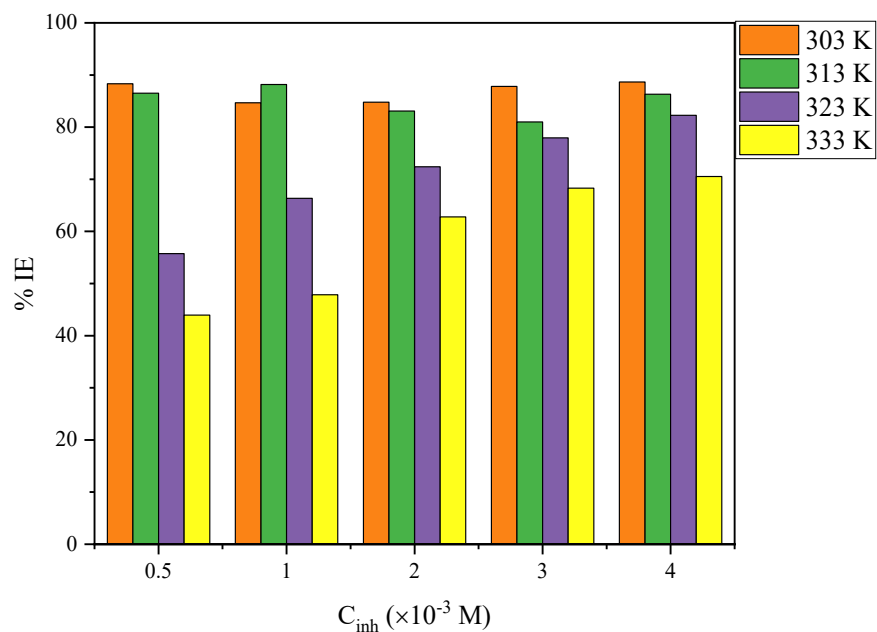


Figure 4.18: The variation of percentage inhibition efficiency with various concentration of Q6CA at various temperatures in 1.0 M H_2SO_4 .

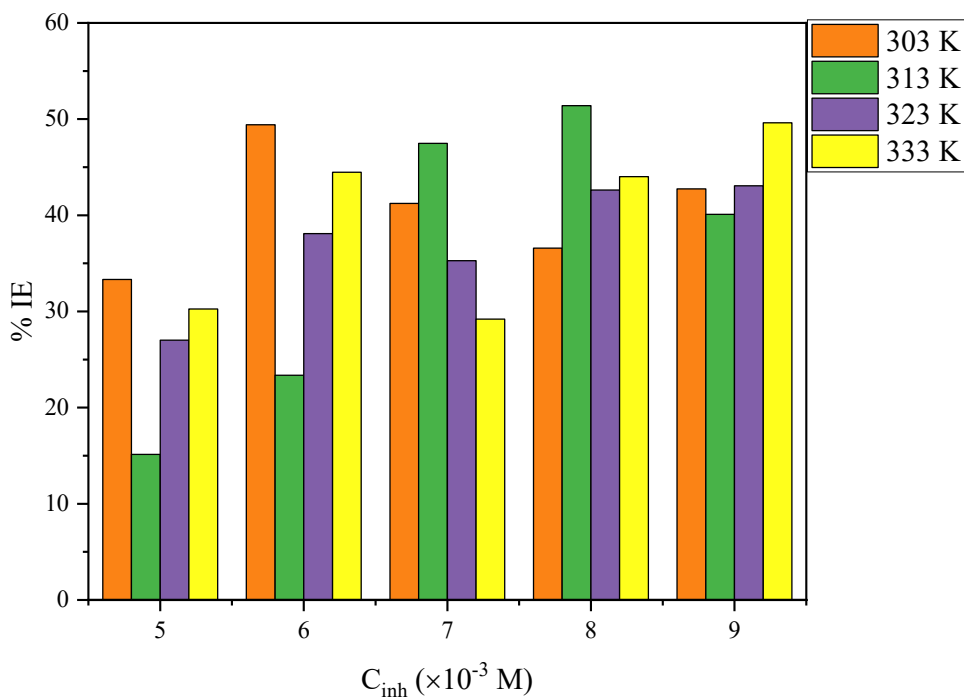


Figure 4.19: The variation of percentage inhibition efficiency with various concentration of H2QCA without KI at various temperatures in 1.0 M H_2SO_4 .

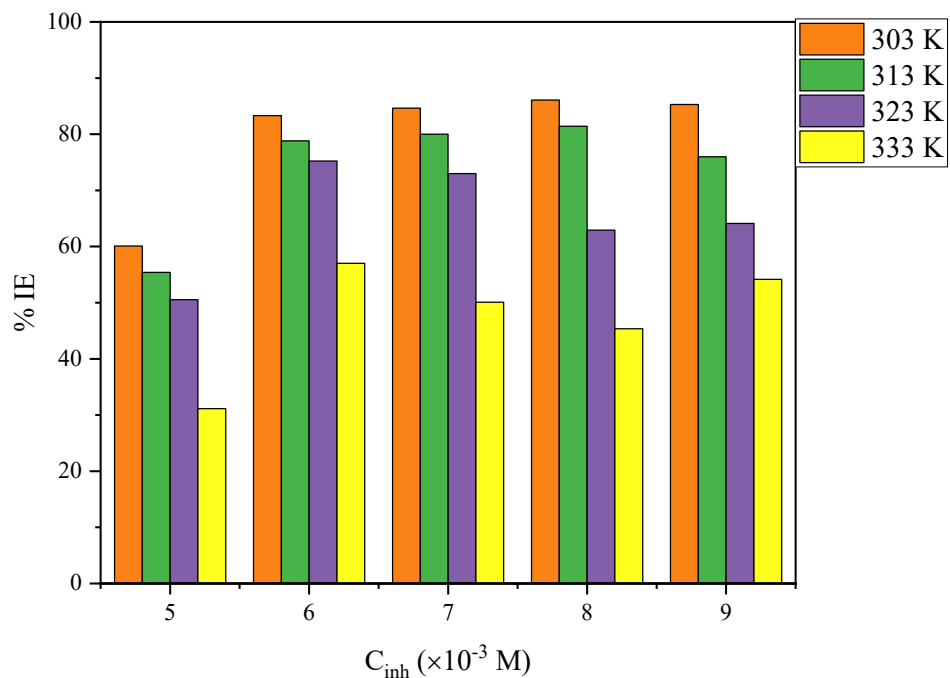


Figure 4.20: The variation of percentage inhibition efficiency with various concentration of H2QCA with KI at various temperatures in 1.0 M H₂SO₄.

Table 4.10: The corrosion parameters for mild steel in 1.0 M H₂SO₄ in the absence and presence of various concentrations of MQ6CA obtained from weight loss measurements at 303 – 333 K.

Inhibitor	Temperature (K)	Inhibior concentration ($\times 10^{-3}$ M)	Corrosion rate ($\text{g.cm}^{-2}.\text{h}^{-1}$)	Surface coverage (θ)	Inhibition efficiency (%)
MQ6CA	303	-	0.0097191	-	-
		0.5	0.0005857	0.9398	93.98
		1.0	0.0004976	0.9488	94.88
		2.0	0.0004381	0.9549	95.49
		3.0	0.0004286	0.9558	95.58
		4.0	0.0002905	0.9701	97.01
	313	-	0.0205190	-	-
		0.5	0.0018190	0.9113	91.13
		1.0	0.0017690	0.9138	91.38
		2.0	0.0015000	0.9262	92.53
		3.0	0.0013286	0.9353	93.53
		4.0	0.0012833	0.9375	93.75
	323	-	0.0334524	-	-
		0.5	0.0050119	0.8502	85.02
		1.0	0.0049476	0.8521	85.21
		2.0	0.0048738	0.8543	85.43
		3.0	0.0043095	0.8648	84.48
		4.0	0.0040309	0.8795	87.95
	333	-	0.0423833	-	-
		0.5	0.0238523	0.4279	42.79
		1.0	0.0194952	0.5400	54.00
		2.0	0.0120524	0.7156	71.56
		3.0	0.0116500	0.7251	72.51
		4.0	0.0061719	0.85433	85.43

Table 4.11: The corrosion parameters for mild steel in 1.0 M H₂SO₄ in the absence and presence of various concentrations of Q6CA obtained from weight loss measurements at 303 – 333 K.

Inhibitor	Temperature (K)	Inhibior concentration ($\times 10^{-3}$ M)	Corrosion rate ($\text{g.cm}^{-2}.\text{h}^{-1}$)	Surface coverage (θ)	Inhibition efficiency (%)
Q6CA	303	-	0.0097190	-	-
		0.5	0.0011357	0.8831	88.31
		1.0	0.0015333	0.8422	84.22
		2.0	0.0014786	0.8478	84.78
		3.0	0.0011857	0.8780	87.80
		4.0	0.0011024	0.8865	88.65
	313	-	0.0205191	-	-
		0.5	0.0027690	0.8650	86.50
		1.0	0.0024262	0.8371	83.71
		2.0	0.0035023	0.8308	83.08
		3.0	0.0039023	0.8100	81.00
		4.0	0.0028425	0.8630	86.30
	323	-	0.0334229	-	-
		0.5	0.0148429	0.5573	55.73
		1.0	0.0112857	0.6634	66.34
		2.0	0.0092262	0.7241	72.41
		3.0	0.0073786	0.7790	77.90
		4.0	0.0059452	0.8226	82.26
	333	-	0.0423833	-	-
		0.5	0.0237571	0.4394	43.94
		1.0	0.0221048	0.4784	47.84
		2.0	0.0164857	0.6278	62.78
		3.0	0.0141729	0.6831	68.31
		4.0	0.0124987	0.7052	70.52

Table 4.12: The corrosion parameters for mild steel in 1.0 M H₂SO₄ in the absence and presence of various concentrations of H₂QCA with and without KI obtained from weight loss measurements at 303 – 333 K.

Inhibitor	Temperature (K)	Inhibitor concentration ($\times 10^{-3}$ M)	Corrosion rate ($\text{g}\cdot\text{cm}^{-2}\cdot\text{h}^{-1}$)	Surface coverage (θ)	Inhibition efficiency (%)
H ₂ QCA without KI	303	-	0.0097190	-	-
		5.0	0.0064810	0.3332	33.32
		6.0	0.0049167	0.4941	49.41
		7.0	0.0057119	0.4124	41.24
		8.0	0.0061629	0.3658	36.58
		9.0	0.0055643	0.4274	42.74
	313	-	0.0205190	-	-
		5.0	0.0174119	0.1514	15.4
		6.0	0.0157238	0.2337	23.37
		7.0	0.0107762	0.4748	47.48
		8.0	0.0099738	0.5139	51.39
		9.0	0.0122905	0.4010	40.10
	323	-	0.0334238	-	-
		5.0	0.0244167	0.2701	27.01
		6.0	0.0207071	0.3810	38.10
		7.0	0.0216500	0.3528	35.28
		8.0	0.0191905	0.4263	42.63
		9.0	0.0190476	0.4306	43.06
	333	-	0.0423833	-	-
		5.0	0.0295557	0.3026	30.26
		6.0	0.0235357	0.4447	44.47
		7.0	0.0300071	0.2920	29.02
		8.0	0.0237310	0.4401	44.01
		9.0	0.0213524	0.4962	49.62
KI	303	-	0.0097190	-	-
		5.0	0.0023833	0.6010	60.10
		6.0	0.0016214	0.8332	83.32
		7.0	0.0014929	0.8465	84.65
		8.0	0.0013524	0.8609	86.09
		9.0	0.0014286	0.8530	85.30
	313	-	0.0205190	-	-
		5.0	0.0091476	0.5541	55.41

H2QCA with KI	313	6.0	0.0043429	0.7883	78.83
		7.0	0.0041024	0.8001	80.01
		8.0	0.0038095	0.8143	81.43
		9.0	0.0049238	0.7600	76.60
	323	-	0.0334238	-	-
		5.0	0.0165429	0.5055	50.55
		6.0	0.0082905	0.7522	75.22
		7.0	0.0090357	0.7299	72.99
		8.0	0.0124048	0.6292	62.92
		9.0	0.0120071	0.6411	64.11
	333	-	0.0423833	-	-
		5.0	0.0291905	0.3113	31.13
		6.0	0.0182214	0.5701	57.01
		7.0	0.0211571	0.5008	50.08
		8.0	0.0231571	0.4536	45.36
		9.0	0.0194238	0.5417	54.17

Data in Tables 4.7 and 4.10 show that percentage inhibition efficiency rises with increase in concentration of MQ6CA at all temperature. However, the inhibition efficiency of this compound is observed to decrease with increase in temperature of the corrosive environment. Table 4.7 shows that the highest inhibition efficiency for this compound was attained at highest concentration, that is, 4×10^{-3} M. Similar trend was also observed in Table 4.10. This response can be attributed that as inhibitor concentration is increased, there is a great tendency of preferential increased adsorption of the inhibitor molecules at the metal/solution interface with block the active site of mild steel from further acid attack. Furthermore, the inhibition efficiency of this compound in 1.0 M HCl was found to range from 97.87 – 99.95 %, which even the lowest attained inhibition efficiency was greatly appreciable. looking at Table 4.10, it is clear for one to observe that H_2SO_4 was more aggressive than HCl to mild steel, particularly at higher temperatures. At 333 K, the inhibition efficiency of MQ6CA in 1.0 M HCl was found to be 89.91, 90.07, 90.14, 90.73 and 90.91 % at 5×10^{-3} , 1.0×10^{-3} , 2.0×10^{-3} , 3.0×10^{-3} , and 4.0×10^{-3} M, respectively. In 1.0 M H_2SO_4 at the same temperature the inhibition efficiency of MQ6CA was attained to be 42.79, 54.00, 71.56, 72.51, and 85.43 % at 0.5×10^{-3} , 1.0×10^{-3} , 2.0×10^{-3} , 3.0×10^{-3} , and 4.0×10^{-3} M, respectively. similar findings have been observed by several researchers [300–302].

Generally, it is anticipated that increase in concentration of corrosion inhibitor will result in reduction of corrosion rate, consequently a relative high percentage inhibition efficiency [300]. However, it can be observed from Tables 4.8 and 4.11 that there was no definitive trend in the values of inhibition efficiency as the concentration of Q6CA and the temperature of the corrosive environment were increased. Although the tests were done in triplicates, no simple trend was observed. This observation can be attributed to the fact that corrosion is a highly complex process due to activities that lead to the alterations which includes the exchange of electrons and desorption of the inhibitor among others [301]. Several researchers also reported similar findings [302–304]. Nevertheless, the introduction of the inhibitor showed to have significantly retarded the rate of corrosion of mild steel in both acids. In 1.0 M HCl, the lowest inhibition efficiency was obtained to be 97.95 % at concentration of 2×10^{-3} M and temperature of 303 K. For the same corrosive medium, the highest inhibition efficiency was obtained to be 99.85 % at concentration of 1×10^{-3} M and temperature of 323 K. The lowest and the highest percentage inhibition efficiencies of Q6CA in 1.0 M HCl solution show no significant difference and they were appreciable. Despite the fact that there was no regular trend observed in the values of inhibition efficiency of Q6CA, looking closely at Table 4.11, it can be observed that inhibition efficiency values decreased with increase in temperature. At concentration of 303 K for instance, the values were obtained to be 88.31, 84.22, 84.78, 87.80, and 88.65 % at 0.5×10^{-3} , 1.0×10^{-3} , 2.0×10^{-3} , 3.0×10^{-3} , and 4.0×10^{-3} M, respectively. However, at 313 K, these values decreased to 86.50, 83.71, 83.08, 81.00, then 86.30 % at 0.5×10^{-3} , 1.0×10^{-3} , 2.0×10^{-3} , 3.0×10^{-3} , and 4.0×10^{-3} M, respectively.

Tables 4.9 and 4.12 elucidate the inhibition efficiency values of H2QCA with and without the addition of KI. From these tables it can be clearly observed that without the addition of KI in the solution of H2QCA, there was no regular trend in the inhibition efficiency values. However, after the addition of KI the inhibition efficiency values increased with increase concentration of the inhibitor and decreased with increase in temperature. A close inspection of these tables show that H2QCA without KI performed poorly in reducing the corrosion of mild steel in both acidic media. For instance, in table 4.9, at concentration of 5.0×10^{-3} M, the inhibition efficiency values were obtained to be 12.19, 22.99, 15.51, and 4.12 % at temperature 303, 313, 323, and 333 K, respectively. At the same concentration with the addition of KI in the inhibitor solution, the inhibition efficiency value improved to 61.01, 81.95, 87.72, 89.09, then 90.32 at temperature 303,

313, 323, and 333 K, respectively. Similar improvements in the inhibition efficiency values were also observed in table 4.12. Thus, it is clear that the addition of KI remarkably improved the percentage efficiency of H2QCA. The noticeable improve of the inhibition efficiency of H2QCA is due to the interaction the compound and the chemisorbed iodide [305–307]. Chitra at al. also reported similar observations [308]. The inhibition efficiency of the studied compound varied in the order: MQ6CA>Q6CA>H2QCA. As shown in the table and figures 4.13 – 4.20, all the studied quinoxalines on mild steel performed least at higher temperatures. This behaviour may be attributed to the spontaneous equilibrium that exists between the adsorption and desorption processes. At higher temperatures, the rate of desorption process tends to increase over the adsorption process until equilibrium is established again at a different value of equilibrium constants, that is, there a possible desorption of some adsorbed inhibitor molecules on mild steel surface. Thus, allows high number of H⁺ ions to attack the metal surface [309–311]. This effect is a result of physical adsorption [312].

4.2.3 Impact of temperature and kinetic parameters

As seen from section 4.2.1, temperature highly influence the corrosion of mild steel in acidic media. An increase in temperature of the corrosive environment was found to enhance the rate of corrosion of mild steel. With this regard, temperature variation can be utilized to further understand the mode of adsorption of the studied quinoxaline on mild steel surface. The Arrhenius equation is often utilized to explain the reliance of the corrosion rate of metals on the temperature of the surrounding [313]. Equation (47) shows the type of Arrhenius equation to calculate activation energy (E_a) for mild steel corrosion [314, 315]. Activation energy is the minimum energy needed for corrosion of mild steel to take place.

$$\log C_R = \log A - \frac{E_a}{2.303RT} \quad (47)$$

where C_R is the corrosion rate ($\text{g}\cdot\text{cm}^{-2}\cdot\text{h}^{-1}$), A is the Arrhenius pre-exponential factor, E_a is the corrosion activation energy, R is the gas constant ($8.3145 \text{ J}\cdot\text{K}^{-1}\cdot\text{mol}^{-1}$), and T is the absolute temperature. The values of activation energy of mild steel corrosion in the absence and presence of various concentration of the studied quinoxalines were computed from the plot of $\log C_R$ against $1/T$ (figures 4.21 – 4.26) and are presented in Tables 4.13 and 4.14.

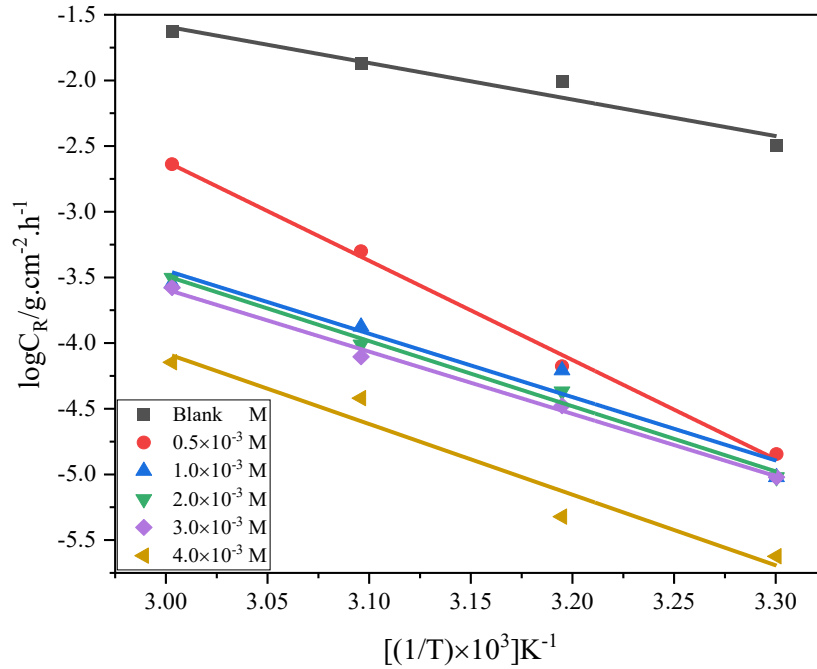


Figure 4.21: Arrhenius plots for mild steel corrosion in 1.0 M HCl solution in the absence and presence of different concentrations of MQ6CA.

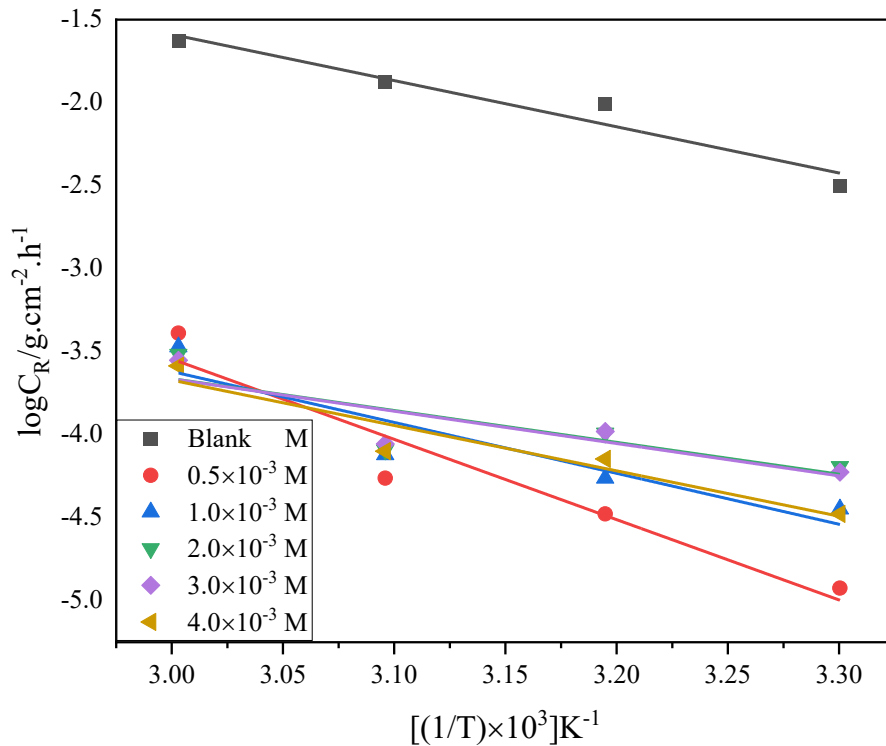


Figure 4.22: Arrhenius plots for mild steel corrosion in 1.0 M HCl solution in the absence and presence of different concentrations of Q6CA.

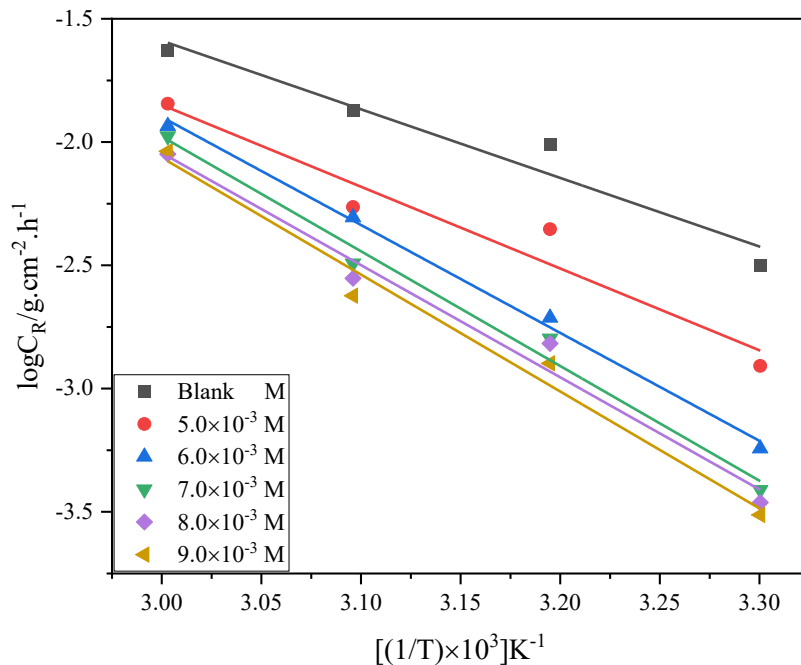


Figure 4.23: Arrhenius plots for mild steel corrosion in 1.0 M HCl solution in the absence and presence of different concentrations of H₂QCA with KI.

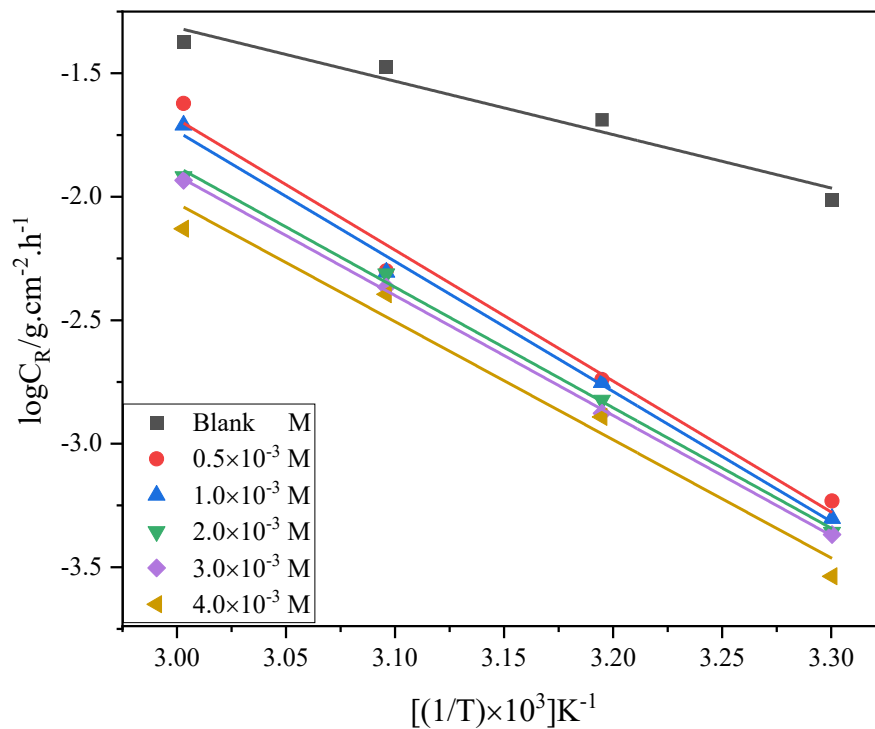


Figure 4.24: Arrhenius plots for mild steel corrosion in 1.0 M H₂SO₄ solution in the absence and presence of different concentrations of MQ6CA.

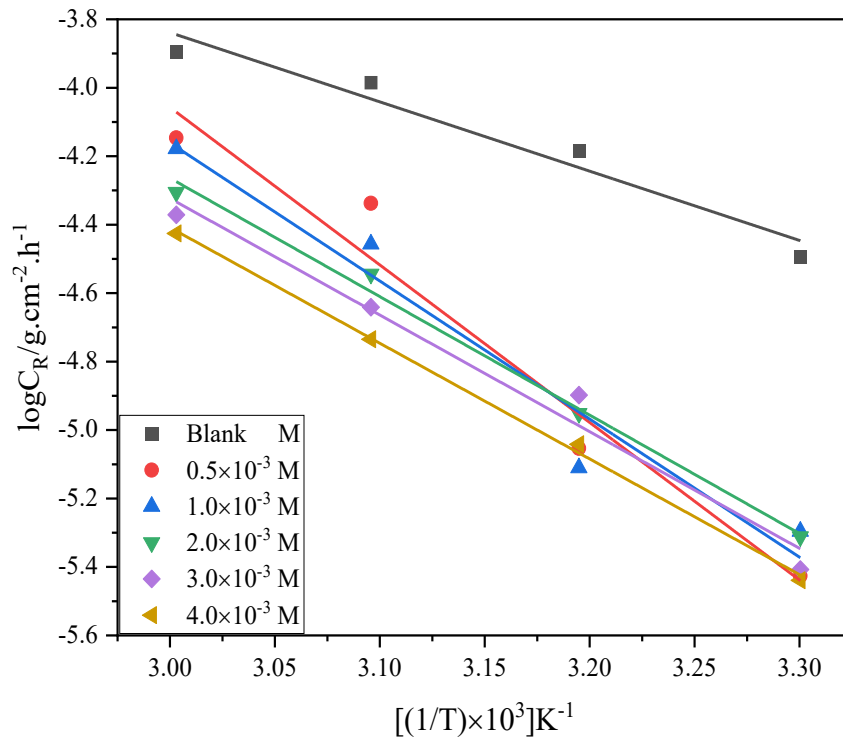


Figure 4.25: Arrhenius plots for mild steel corrosion in 1.0 M H₂SO₄ solution in the absence and presence of different concentrations of Q6CA.

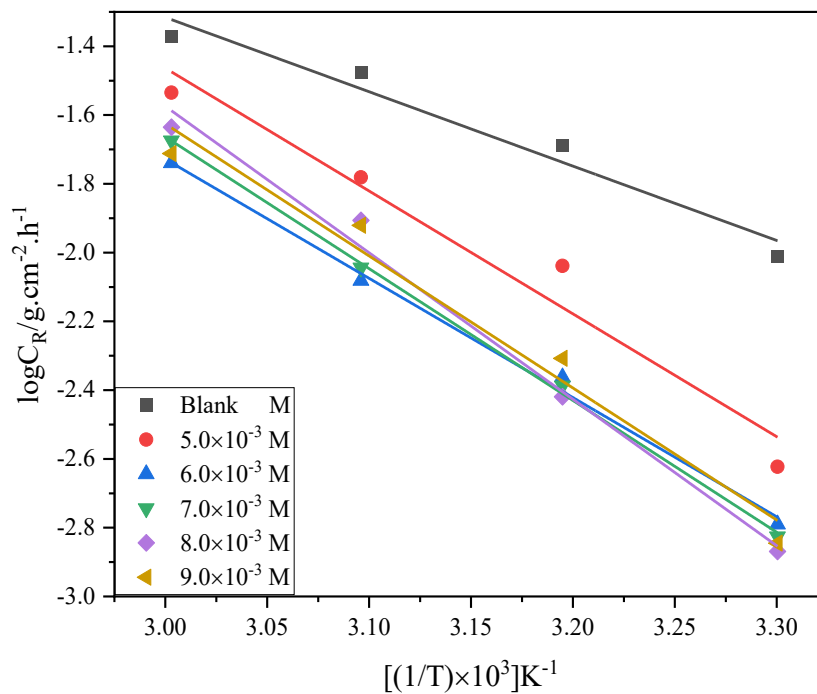


Figure 4.26: Arrhenius plots for mild steel corrosion in 1.0 M H₂SO₄ solution in the absence and presence of different concentrations of H₂QCA with KI.

More information on the impact of temperature on the corrosion rate of mild steel in 1.0 M HCl and 1.0 M H₂SO₄ can be derived from thermodynamic parameters such as enthalpy of activation (ΔH^*) and entropy of activation (ΔS^*). The rate of corrosion and temperature are related to these parameters through the transition-state equation [314, 315]:

$$\log\left(\frac{C_R}{T}\right) = \left[\log\left(\frac{R}{Nh}\right) + \left(\frac{\Delta S^*}{2.303R}\right)\right] + \left(\frac{-\Delta H^*}{2.303R}\right)\left(\frac{1}{T}\right) \quad (48)$$

where h is Planck's constant and N is the Avogadro number, 2.303 is a conversion factor from natural log to log₁₀, and T is the absolute temperature. Figures 4.27 – 4.32 present the plot of $\log(C_R/T)$ against $(1/T)$ with the data best fitted having a slope $(-\Delta H^*/2.303R)$ and an intercept $[\log(R/Nh)+(\Delta S^*/2.303R)]$ which were utilized to compute the values of the standard enthalpy (ΔH^*) and entropy of activation (ΔS^*) in the absence and presence of various concentrations of the studied quinoxalines. Their values are presented in Tables 4.13 and 4.14

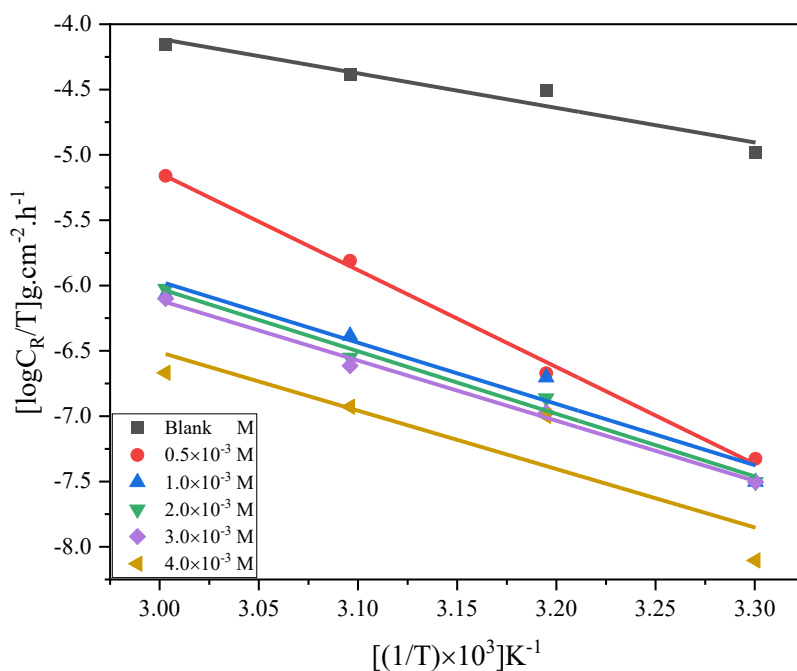
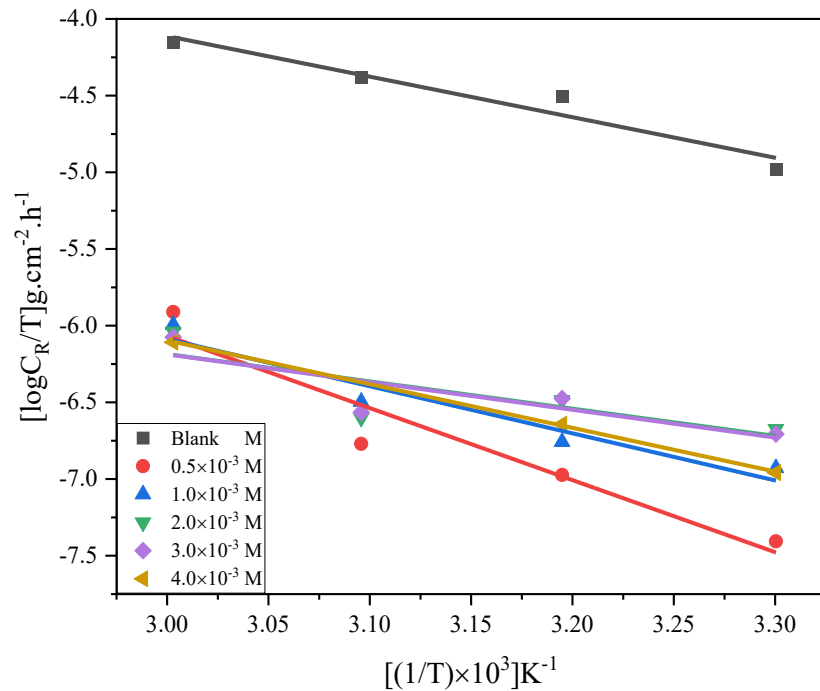


Figure 4.27: Transition state plots for mild steel corrosion in 1.0 M HCl solution in the absence and presence of different concentrations of MQ6CA.



535

Figure 4.28: Transition state plots for mild steel corrosion in 1.0 M HCl solution in the absence and presence of different concentrations of Q6CA.

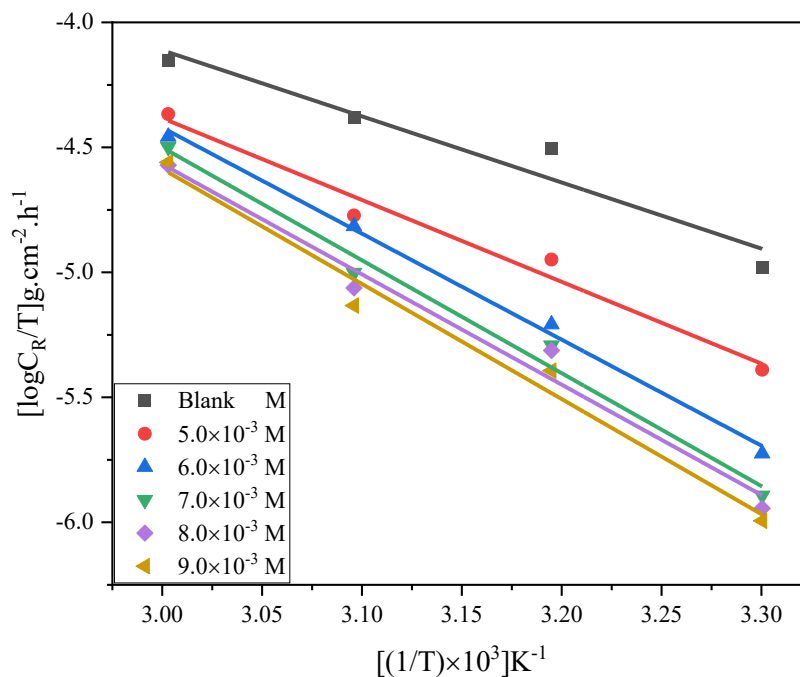


Figure 4.29: Transition state plots for mild steel corrosion in 1.0 M HCl solution in the absence and presence of different concentrations of H2QCA with KI.

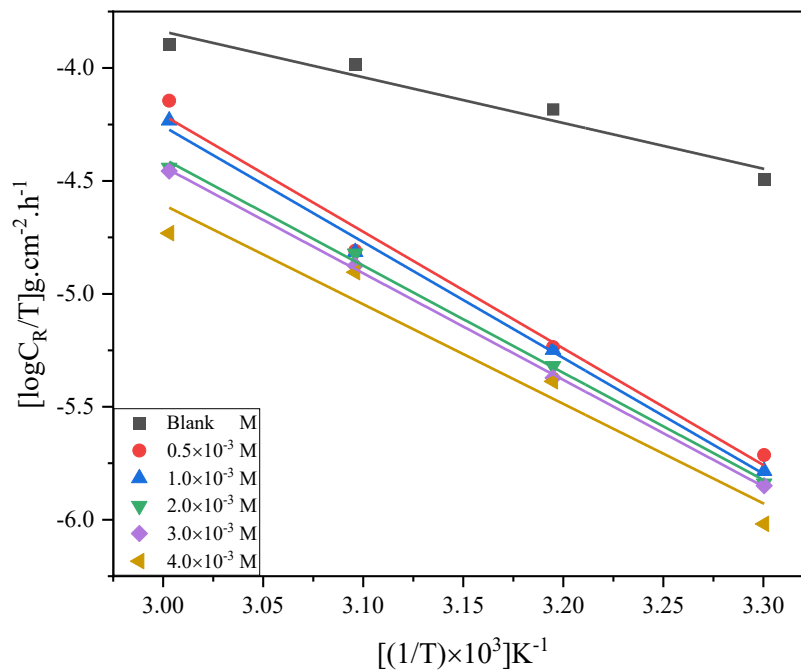


Figure 4.30: Transition state plots for mild steel corrosion in 1.0 M H₂SO₄ solution in the absence and presence of different concentrations of MQ6CA.

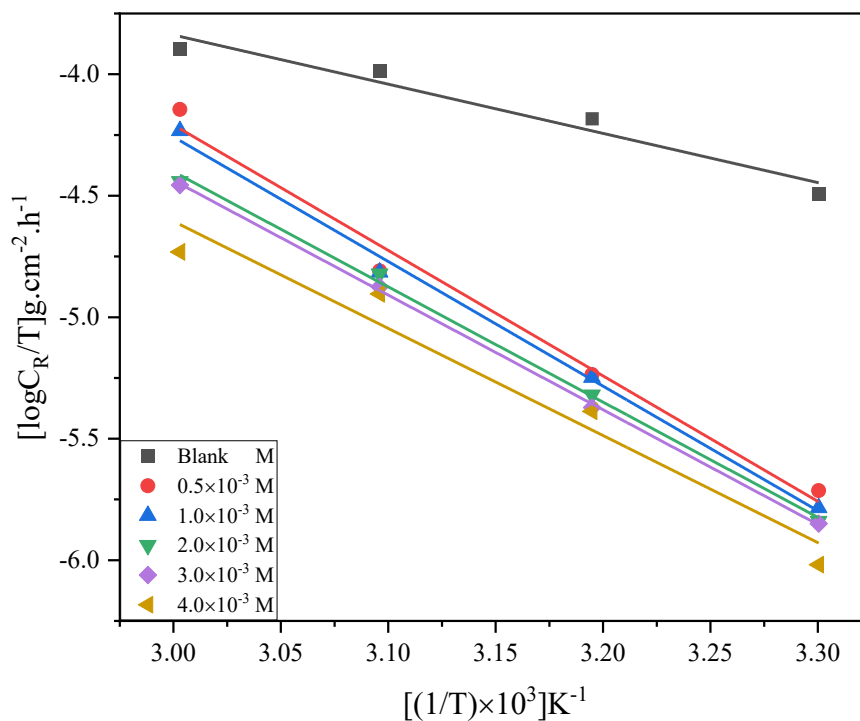


Figure 4.31: Transition state plots for mild steel corrosion in 1.0 M H₂SO₄ solution in the absence and presence of different concentrations of Q6CA.

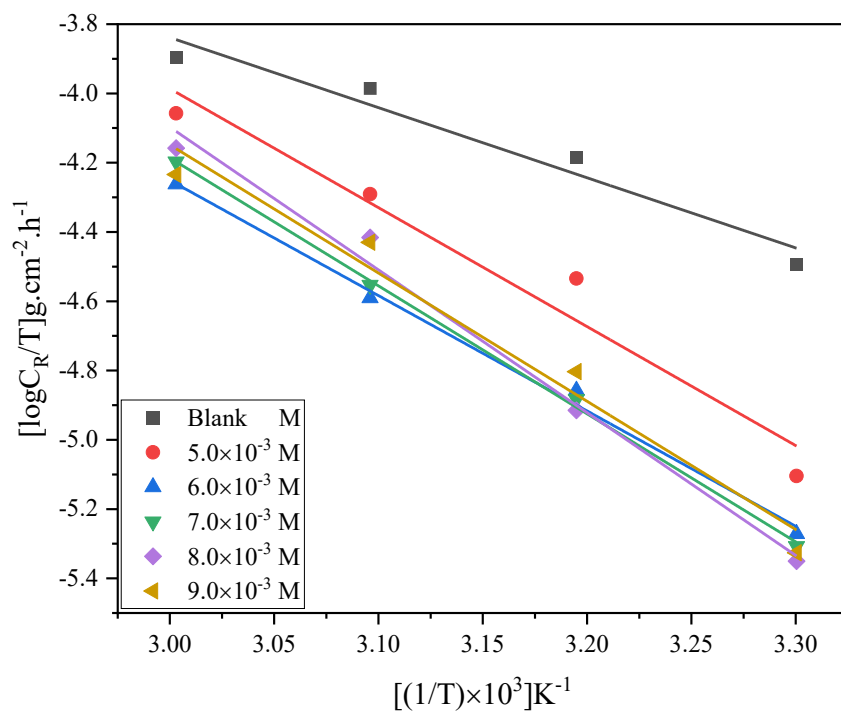


Figure 4.32: Transition state plots for mild steel corrosion in 1.0 M H₂SO₄ solution in the absence and presence of different concentrations of H₂QCA with KI.

On the report of Ojo and co-workers [316], the relationship between the temperature reliance of inhibition efficiency of an inhibitor and the activation energy can be classified into three categories which are given below:

- Inhibitors with inverse proportional relation in the inhibition efficiency and temperature of the surrounding. The activation energy value obtained is greater than that in the uninhibited solution.
- Inhibitors with inhibition efficiency values that do not change with changes in temperature of the surrounding. The activation energy value obtained is equal to the one obtained in the presence or absence of inhibitors. That is, it does not change.
- Inhibitors with direct relation to the inhibition efficiency and temperature of the surrounding. The activation energy value obtained is less than that in the uninhibited solution.

Furthermore, higher values of the activation energy of a process in the presence of an inhibitor compared to that of a process in the absence of an inhibitor are generally associated with physical adsorption, while the opposite are associated with chemical adsorption. It is clear from Tables 4.13 and 4.14 the activation values in the presence of the studied quinoxalines were obtained to be higher than in the uninhibited solution. This can be attributed to the formation of a high energy barrier by inhibitor molecules which block the acid from further attacking the metal surface [317]. This indication can be interpreted as physical adsorption. However, looking at Table 4.13, it can be seen that from the concentration of $2 \times 10^{-3} - 4 \times 10^{-3}$ M, the activation energy values of Q6CA were found to be less than that of the uninhibited solution. This interesting observation shows that at lower concentrations there are electrostatic interactions between the inhibitor molecules and the charged mild steel surface. However, as the concentration is increased the interactions might be involving the sharing of electron pairs with the vacant d-orbitals of Fe in mild steel [317]. These findings suggest that Q6CA is a mixed-type inhibitor. Furthermore, according to Dubey and co-workers [318], the values of activation energy found to be less than 80 kJ/mol and even lesser than 5 kJ/mol are associated with physical adsorption. Assessing the activation values (with a range of 36.72 – 144.72 kJ/mol) presented in Tables 4.13 and 4.14, a conclusion can be drawn the studied quinoxaline are associated with a mixed-type of adsorption of mild steel adsorption.

Table 4.13: Arrhenius and transition parameters for mild steel in 1.0 M HCl in the absence and presence of various concentrations of the studied quinoxalines.

Inhibitor	Concentration of inhibitors ($\times 10^{-3}\text{M}$)	E_a ($\text{kJ}\cdot\text{mol}^{-1}$)	ΔH^* ($\text{kJ}\cdot\text{mol}^{-1}$)	ΔS^* ($\text{J}\cdot\text{mol}^{-1}\cdot\text{K}^{-1}$)
	-	53.27	50.63	-123.99
MQ6CA	0.5	144.72	142.09	130.68
	1.0	92.38	89.72	-42.22
	2.0	95.03	91.73	-34.26
	3.0	90.81	88.23	-49.47
	4.0	103.01	85.57	-64.08
Q6CA	0.5	92.63	89.95	-193.30
	1.0	58.71	58.79	-189.09
	2.0	36.72	34.06	-197.96
	3.0	37.26	34.61	-197.88
	4.0	52.31	54.57	-194.67
H2QCA with KI	5.0	63.51	62.69	-92.99
	6.0	83.83	81.18	-38.20
	7.0	89.09	86.45	-23.91
	8.0	87.12	84.48	-31.13
	9.0	90.80	88.08	-19.81

Table 4.14: Arrhenius and transition parameters for mild steel in 1.0 M H₂SO₄ in the absence and presence of various concentrations of the studied quinoxalines.

Inhibitor	Concentration of inhibitors ($\times 10^{-3}\text{M}$)	E_a ($\text{kJ}\cdot\text{mol}^{-1}$)	ΔH^* ($\text{kJ}\cdot\text{mol}^{-1}$)	ΔS^* ($\text{J}\cdot\text{mol}^{-1}\cdot\text{K}^{-1}$)
	-	41.41	38.75	154.34
MQ6CA	0.5	101.52	98.88	17.33
	1.0	100.85	98.21	15.42
	2.0	93.44	90.79	-9.09
	3.0	93.02	90.37	-11.01
	4.0	91.59	84.40	-32.07
Q6CA	0.5	90.76	88.12	-10.43
	1.0	79.88	77.24	-45.09
	2.0	68.91	66.27	-79.94
	3.0	67.92	65.25	-84.09
	4.0	67.36	64.72	-87.40
H2QCA with KI	5.0	68.41	65.74	-76.15
	6.0	66.39	63.74	-48.98
	7.0	73.40	70.75	-64.98
	8.0	81.56	78.91	-38.80
	9.0	73.53	70.88	-63.89

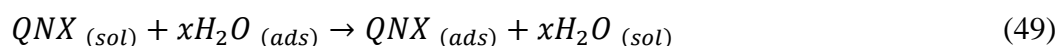
A perusal of the literature reveals that one of the requirements to achieve corrosion inhibition, there should be molecular adsorption on the metal's surface [320]. This adsorption process of mild steel and the studied quinoxaline can be categorized into either endothermic or exothermic. Moreover, an exothermic process releases energy in a form of heat and may suggest either physical

or chemical adsorption. An endothermic process requires an input of energy in a form of heat, and it suggests chemisorption entirely. From Tables 4.13 and 4.14, In both the uninhibited and inhibited solutions, the values of the enthalpy of activation were obtained to be positive. This positive enthalpy of activation values promotes about the endothermic nature of the dissolution of mild steel, which further implies that the dissolution of mild steel is slow in the presence of the studied quinoxalines. Hmamou et al. also reported a similar observation [321]. The increase in the values of enthalpy of activation of the inhibited process compared to the uninhibited process implies that adsorption took place between the surface mild steel and the studied quinoxalines. Literature has revealed that enthalpy of activation values lower than 40.86 kJ/mol indicate physical adsorption whereas enthalpy of activation values around 100.00 kJ/mol indicate chemical adsorption [322–324]. In the present study, the range of enthalpy of activation values (34.06 – 142.09 kJ/mol) further confirms that the studied quinoxalines are associated with a mixed-type of adsorption of mild steel adsorption, with chemical adsorption dominant. It is also observed from Tables 4.13 and 4.14 that the values of activation energy and enthalpy of activation varied similarly, however, the enthalpy of activation values were a bit lower than those of the activation energy. This observation was also reported in the literature [325].

The entropy of activation informs about the extent of disorder during the corrosion and inhibition process on a metal surface. Looking at Tables 4.13 and 4.14, at lower concentrations of MQ6CA, the values of entropy of activation were obtained to be positive. The positive values of entropy of activation attained can be attributed to the increase in the solvent entropy and to more positive water desorption enthalpy, that is, a driving force for an adsorption process of this inhibitor to the mild steel surface. A similar observation was reported by Kumar and co-workers [326]. An increase in the concentration of the studied quinoxalines resulted in negative values of entropy of activation. This indicated that there is a formation of an activated complex in the rate-determining step which represents association rather than dissolution of mild steel, meaning that there is more disorder in the presence of the studied quinoxalines, which may be attributed to the desorption of the molecules from mild steel surface leading to chaos. A similar observation was reported in the literature [308].

4.2.4 Adsorption isotherms and thermodynamic parameters

It is commonly accepted that for corrosion inhibition to occur, the inhibitor should adsorb on the metal surface. The mechanism of the inhibitor molecules adsorbing on a mild steel surface can be explained by understanding the process at the metal/solution interface. This adsorption mechanism can be explained through adsorption isotherm [327, 328]. Generally, adsorption of organic molecules at the metal/solution interface can occur as a result of replacement of water molecules and adsorbed organic molecules in the aqueous solution according to the hypothetical equation (49) [329].



where $QNX_{(sol)}$ is the quinoxaline corrosion inhibitor in the aqueous solution, x is the size ratio of the number of molecules replaced by adsorbed molecules, and $QNX_{(ads)}$ is the quinoxaline corrosion inhibitor adsorbed on a mild steel surface. It is imperative to determine the suitable adsorption isotherm that can give insight into the mode of adsorption of the studied quinoxalines on mild steel surfaces. The inhibition of mild steel in the presence of various concentrations of the studied quinoxalines has been attributed to their adsorption on mild steel surface. From the weight loss measurements, the values of surface coverage (θ) were obtained at various concentrations of the inhibitors. Trials were made to fit the data to different adsorption isotherms namely Langmuir, Frumkin, Freundlich, and Temkin. The plots of these adsorption isotherms are shown with descriptions in figures 4.33 – 4.56. Among all the fitted isotherms for mild steel 1.0 M HCl and 1.0 M H₂SO₄ in the absence and presence of the studied quinoxaline, the Langmuir isotherm was obtained to the description of the adsorption behavior of the investigated compounds. This judgment was based on the regression coefficient values (R^2) that were found to be at/and near the unity. The regression coefficient values obtained in all the tested isotherms for mild steel in this present study are presented in Tables 4.15 and 4.16. From this table, it is clear that the other isotherms except for Langmuir isotherm are deviating from unity.

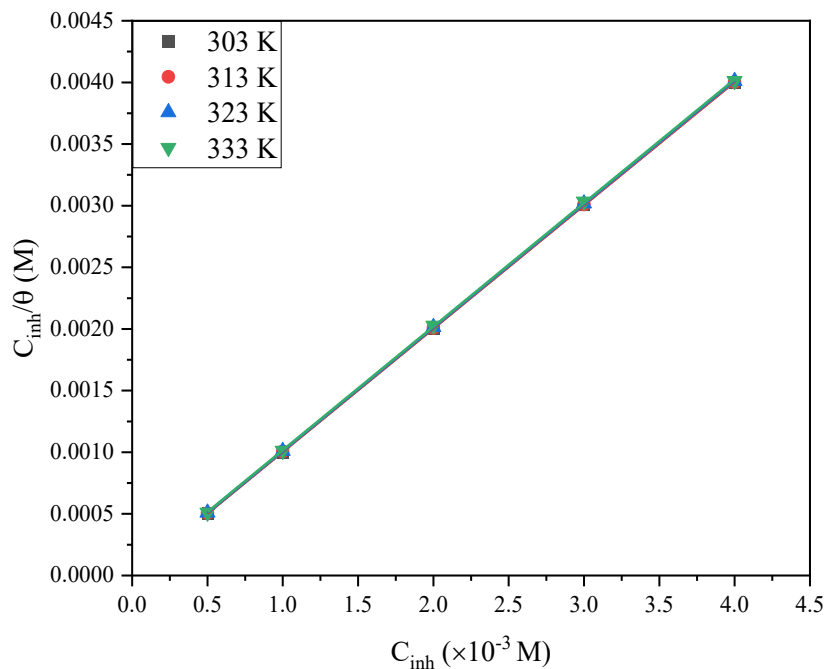


Figure 4.33: Langmuir adsorption isotherm plot for the adsorption of various concentrations of MQ6CA on the surface of mild steel in 1.0 M HCl at various temperatures.

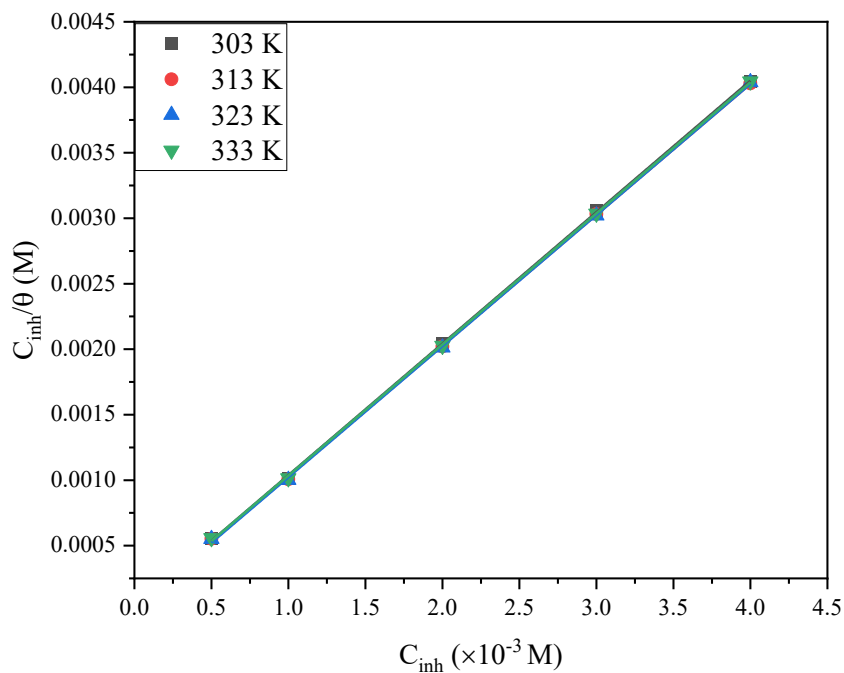


Figure 4.34: Langmuir adsorption isotherm plot for the adsorption of various concentrations of Q6CA on the surface of mild steel in 1.0 M HCl at various temperatures.

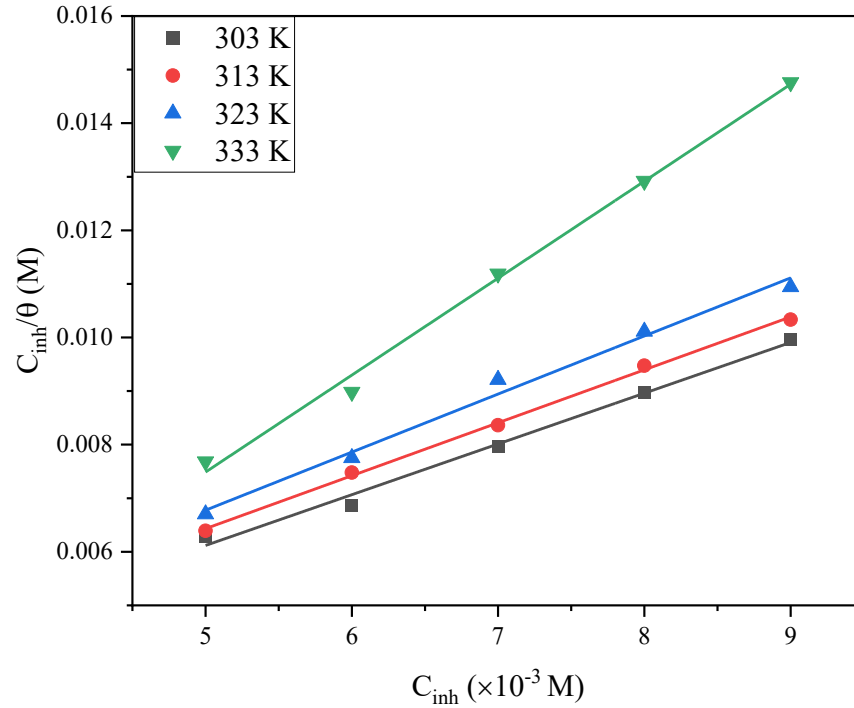


Figure 4.35: Langmuir adsorption isotherm plot for the adsorption of various concentrations of H2QCA with KI on the surface of mild steel in 1.0 M HCl at various temperatures.

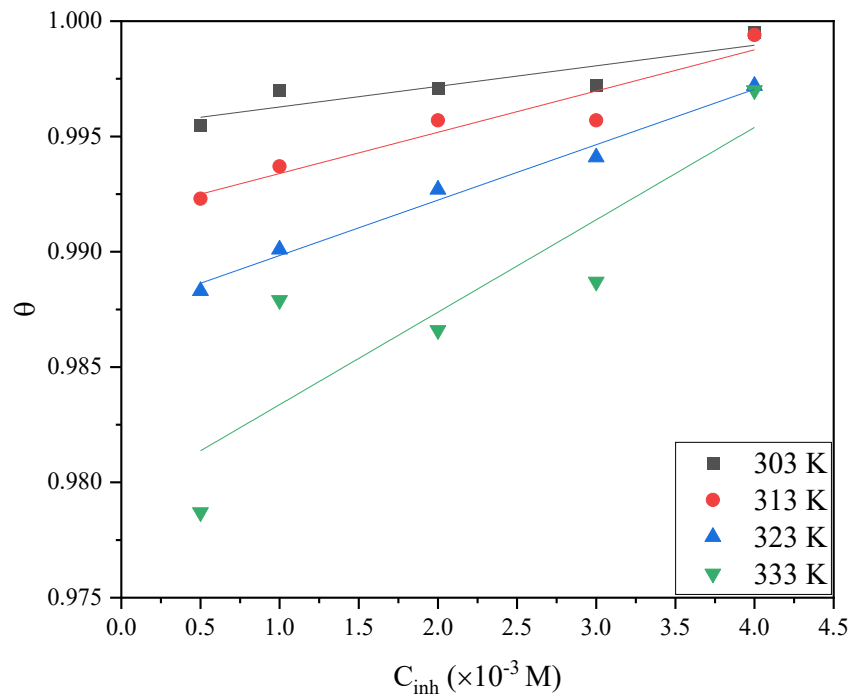


Figure 4.36: Frumkin adsorption isotherm plot for the adsorption of various concentrations of MQ6CA on the surface of mild steel in 1.0 M HCl at various temperatures.

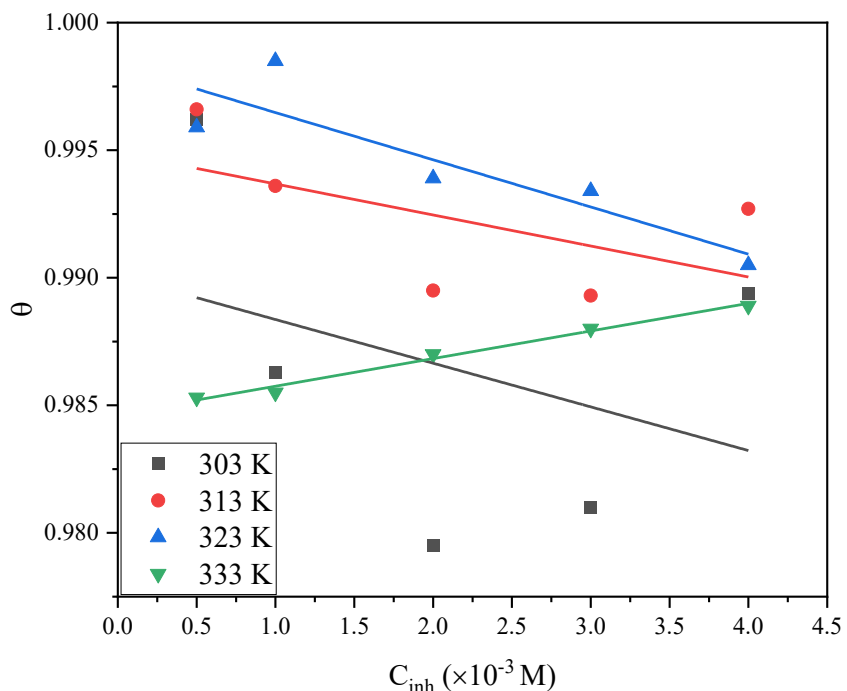


Figure 4.37: Frumkin adsorption isotherm plot for the adsorption of various concentrations of Q6CA on the surface of mild steel in 1.0 M HCl at various temperatures.

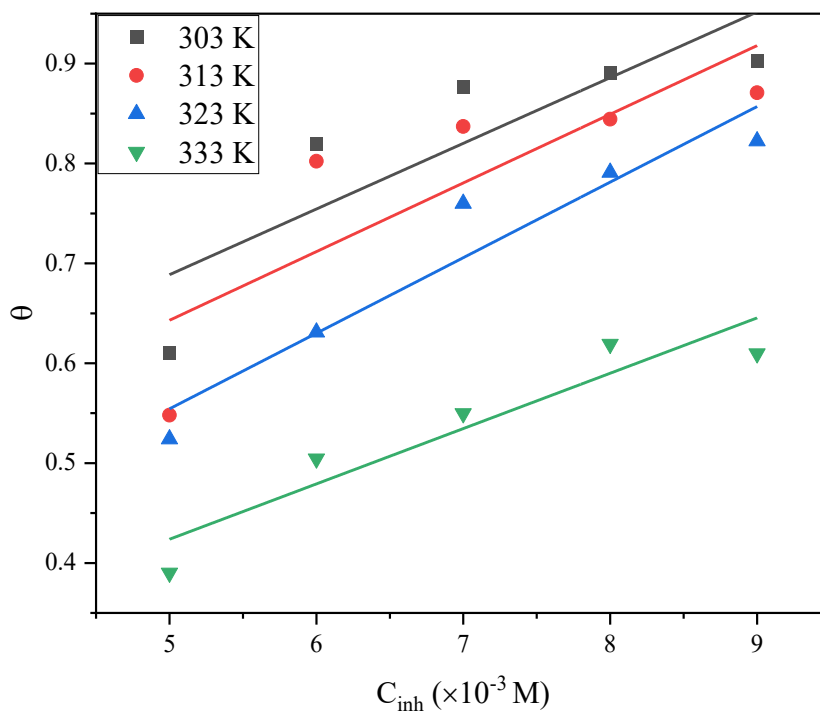


Figure 4.38: Frumkin adsorption isotherm plot for the adsorption of various concentrations of H2QCA with KI on the surface of mild steel in 1.0 M HCl at various temperatures.

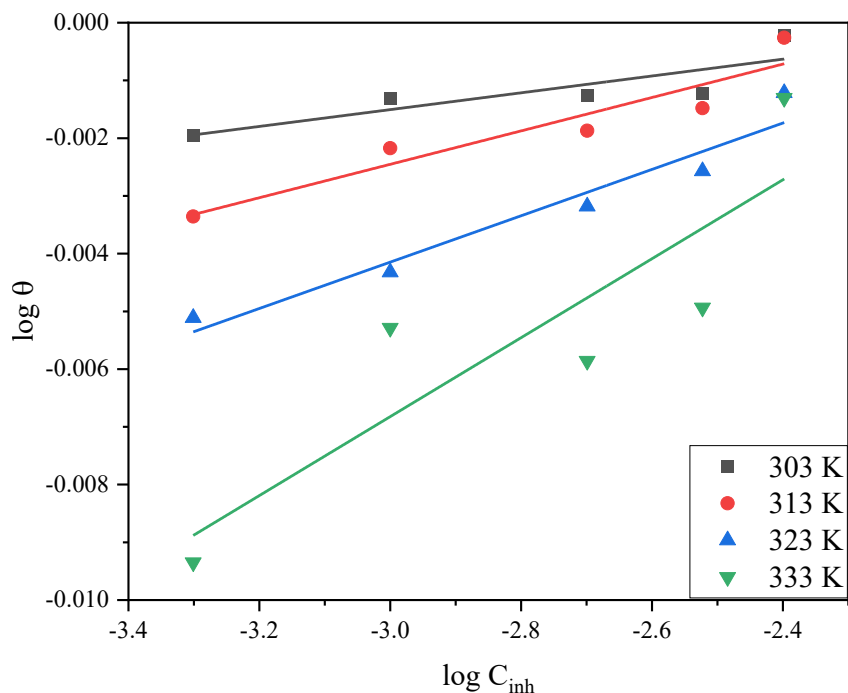


Figure 4.39: Freundlich adsorption isotherm plot for the adsorption of various concentrations of MQ6CA on the surface of mild steel in 1.0 M HCl at various temperatures.

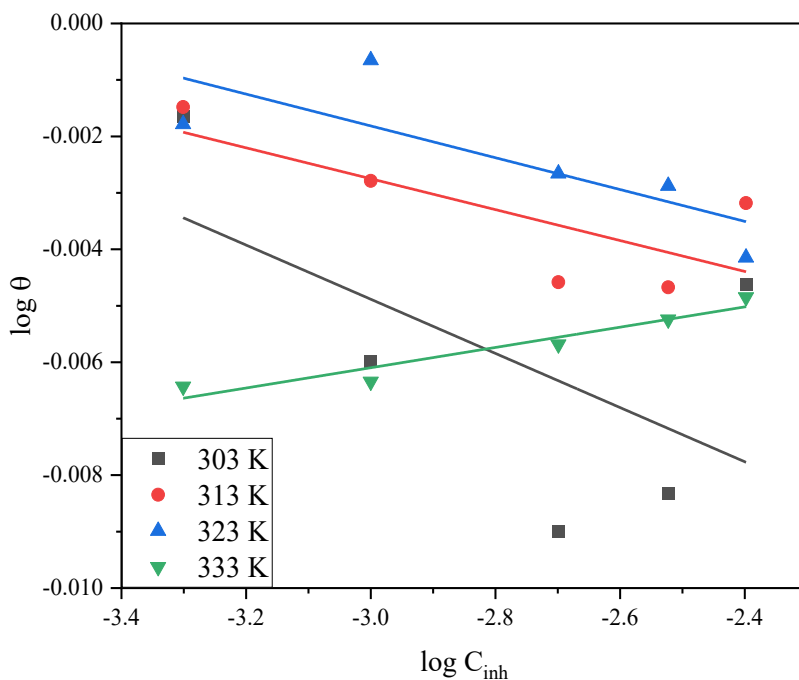


Figure 4.40: Freundlich adsorption isotherm plot for the adsorption of various concentrations of Q6CA on the surface of mild steel in 1.0 M HCl at various temperatures.

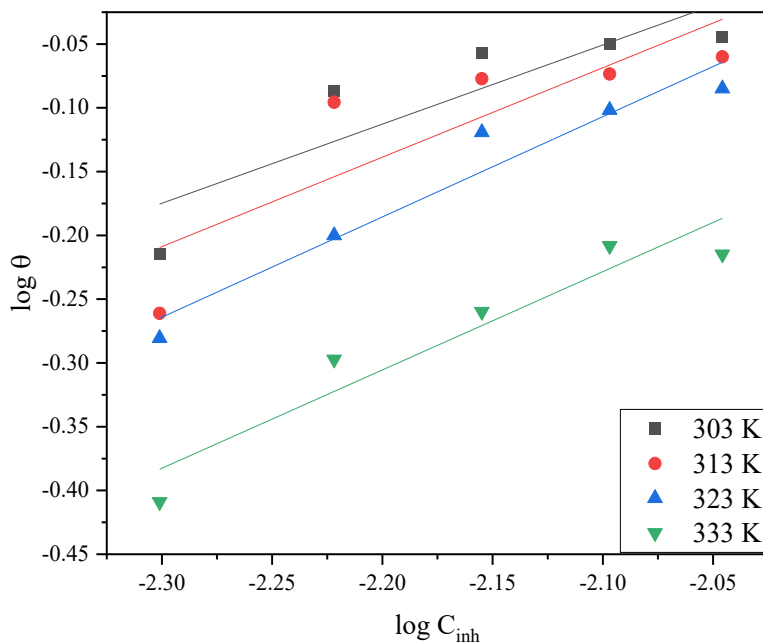


Figure 4.41: Freundlich adsorption isotherm plot for the adsorption of various concentrations of H2QCA with KI on the surface of mild steel in 1.0 M HCl at various temperatures.

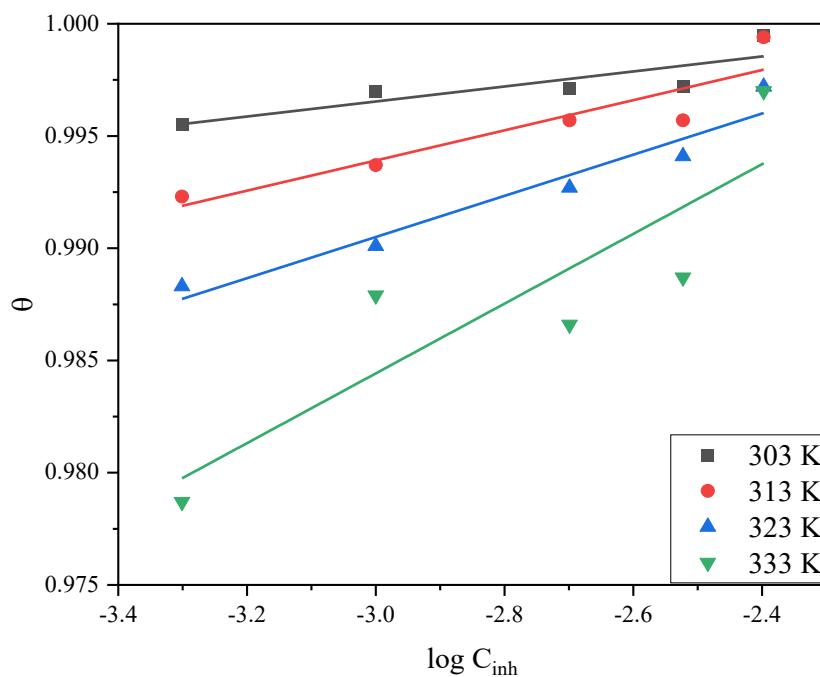


Figure 4.42: Temkin adsorption isotherm plot for the adsorption of various concentrations of MQ6CA on the surface of mild steel in 1.0 M HCl at various temperatures.

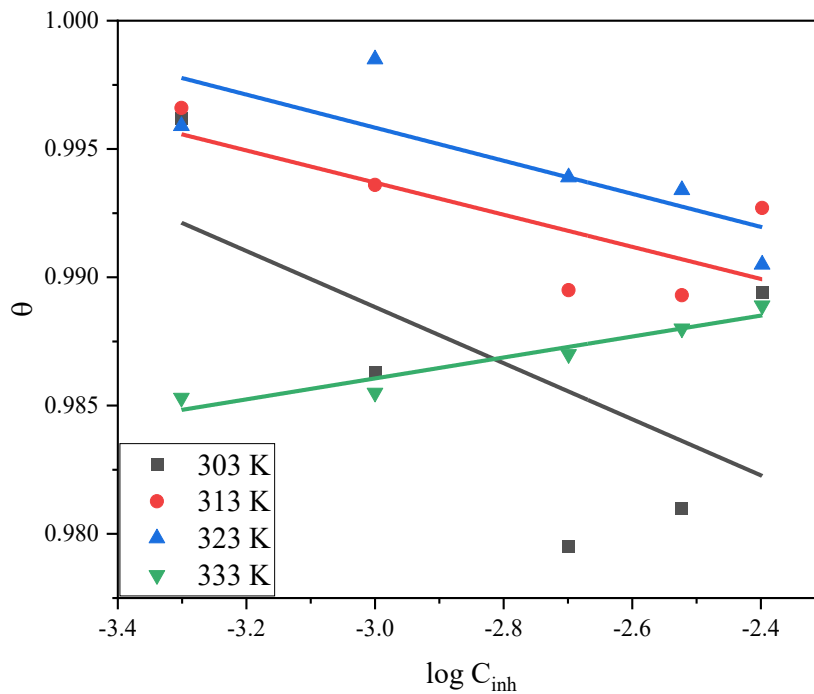


Figure 4.43: Temkin adsorption isotherm plot for the adsorption of various concentrations of Q6CA on the surface of mild steel in 1.0 M HCl at various temperatures.

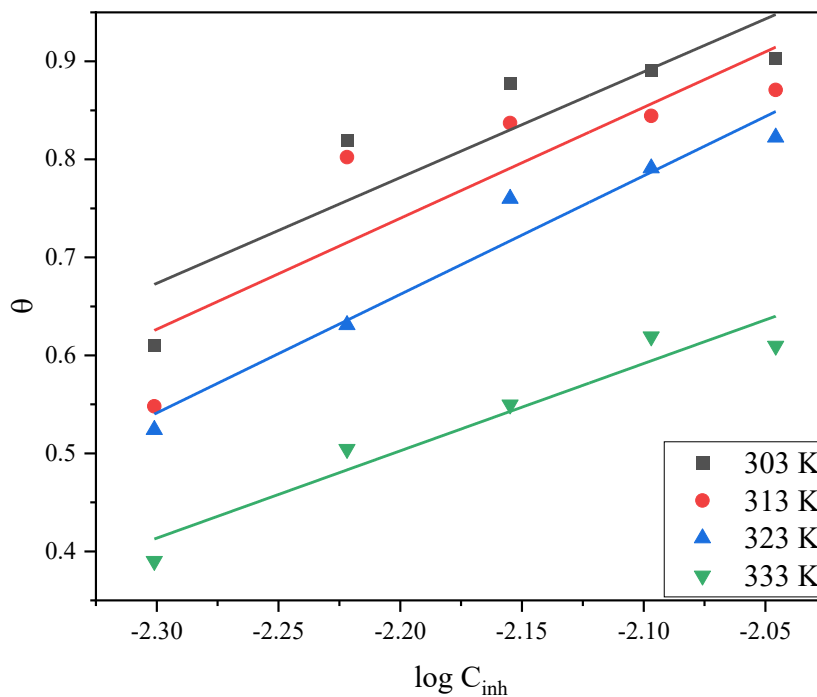


Figure 4.44: Temkin adsorption isotherm plot for the adsorption of various concentrations of H2QCA with KI on the surface of mild steel in 1.0 M HCl at various temperatures.

Table 4.15: The regression coefficient values obtained from different adsorption isotherms for mild steel in 1.0 M HCl at various temperatures for the studied quinoxaline.

Inhibitor	Temperature (K)	Correlation coefficient (R ²)			
		Langmuir	Frumkin	Freundlich	Temkin
MQ6CA	303	1.0000	0.8920	0.8572	0.8570
	313	1.0000	0.9567	0.9455	0.9210
	323	1.0000	0.9925	0.9703	0.9708
	333	0.9999	0.8809	0.8760	0.8756
Q6CA	303	0.9999	0.1322	0.3525	0.3537
	313	0.9999	0.3261	0.5674	0.5678
	323	0.9998	0.7903	0.6308	0.6299
	333	0.9999	0.9881	0.9217	0.9216
H2QCA with KI	303	0.9922	0.7295	0.7717	0.7993
	313	0.9984	0.6763	0.7176	0.7461
	323	0.9895	0.9155	0.9389	0.9554
	333	0.9956	0.8814	0.9056	0.9171

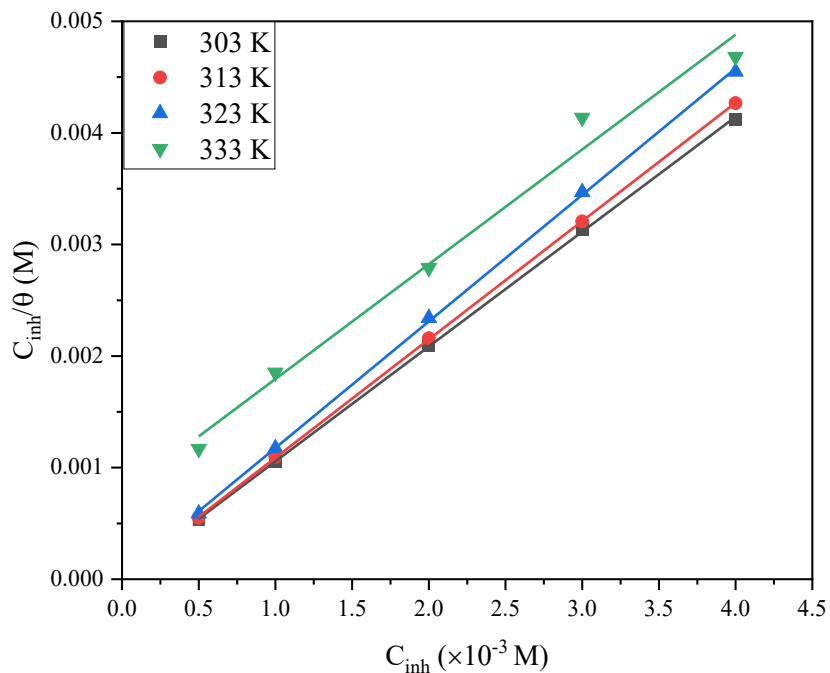


Figure 4.45: Langmuir adsorption isotherm plot for the adsorption of various concentrations of MQ6CA on the surface of mild steel in 1.0 M H₂SO₄ at various temperatures.

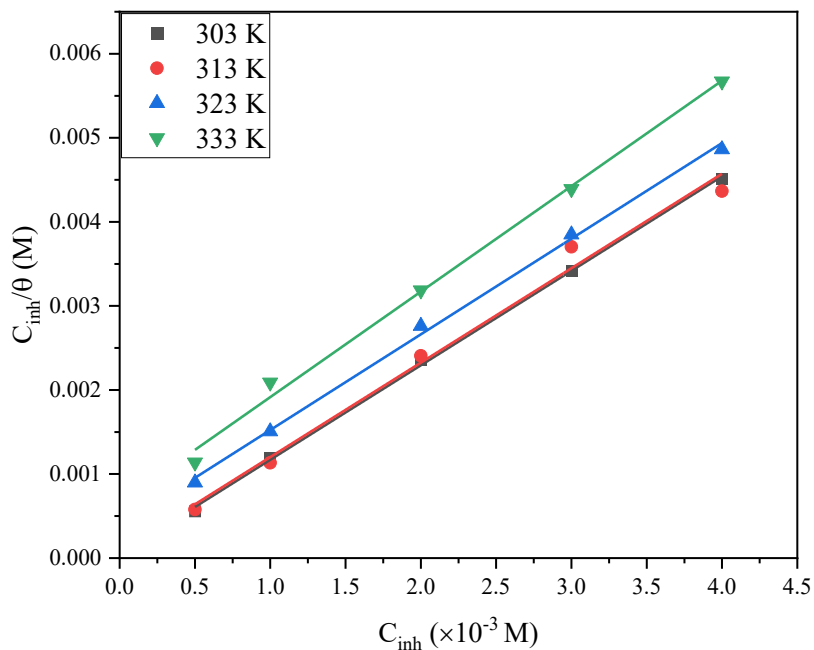


Figure 4.46: Langmuir adsorption isotherm plot for the adsorption of various concentrations of Q6CA on the surface of mild steel in 1.0 M H₂SO₄ at various temperatures.

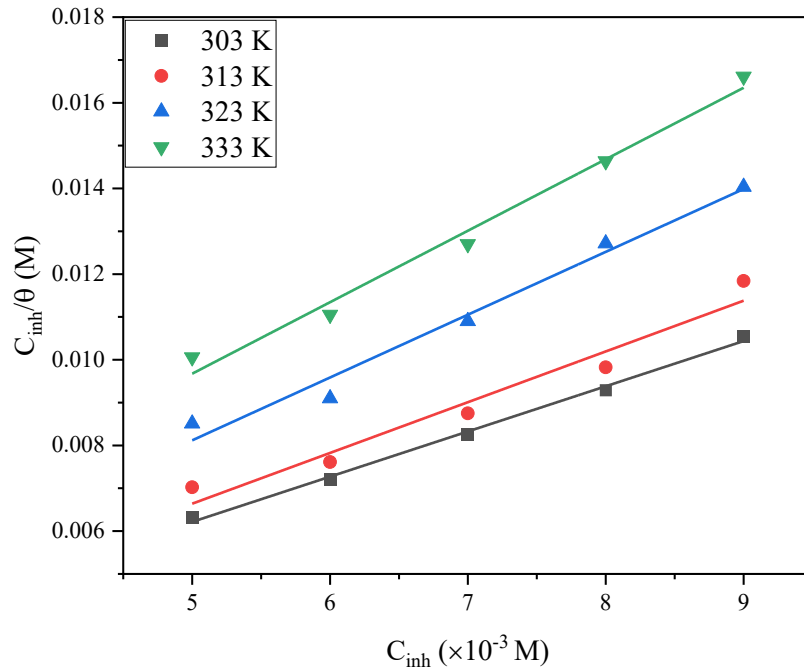


Figure 4.47: Langmuir adsorption isotherm plot for the adsorption of various concentrations of H2QCA with KI on the surface of mild steel in 1.0 M H₂SO₄ at various temperatures.

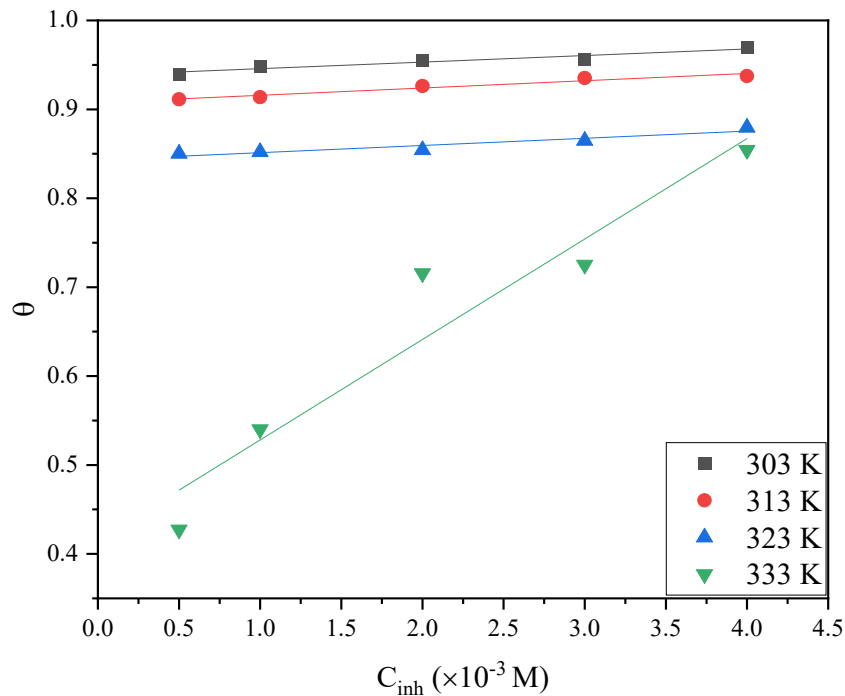


Figure 4.48: Frumkin adsorption isotherm plot for the adsorption of various concentrations of MQ6CA on the surface of mild steel in 1.0 M H₂SO₄ at various temperatures.

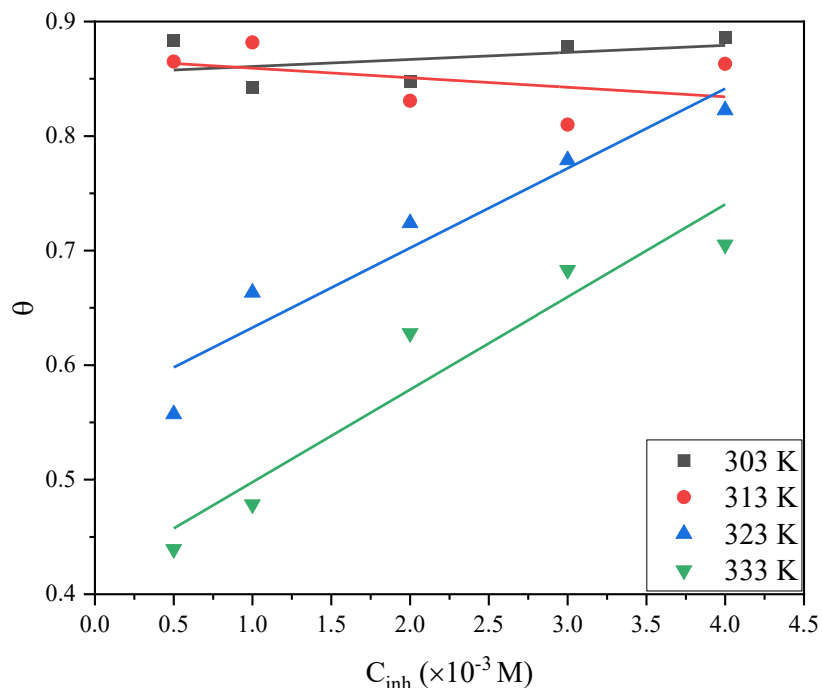


Figure 4.49: Frumkin adsorption isotherm plot for the adsorption of various concentrations of Q6CA on the surface of mild steel in 1.0 M H_2SO_4 at various temperatures.

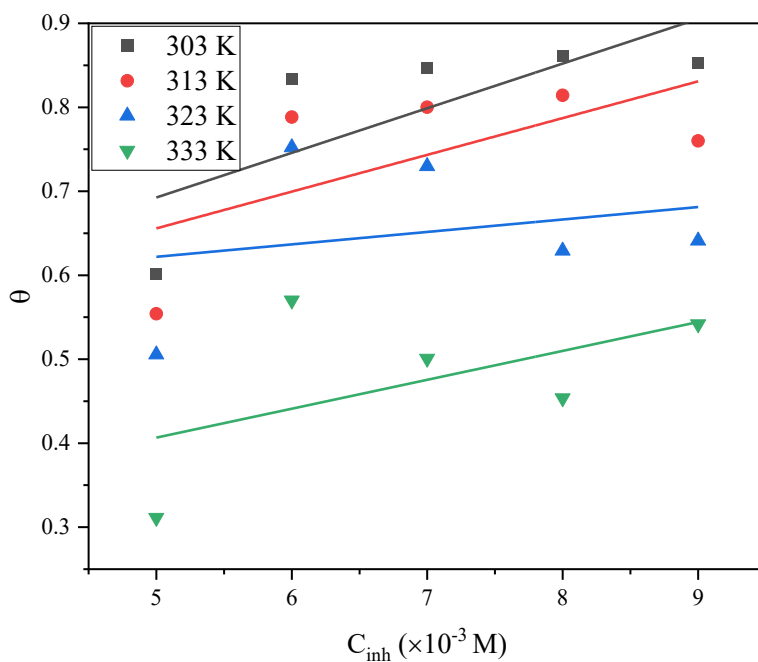


Figure 4.50: Frumkin adsorption isotherm plot for the adsorption of various concentrations of H2QCA with KI on the surface of mild steel in 1.0 M H_2SO_4 at various temperatures.

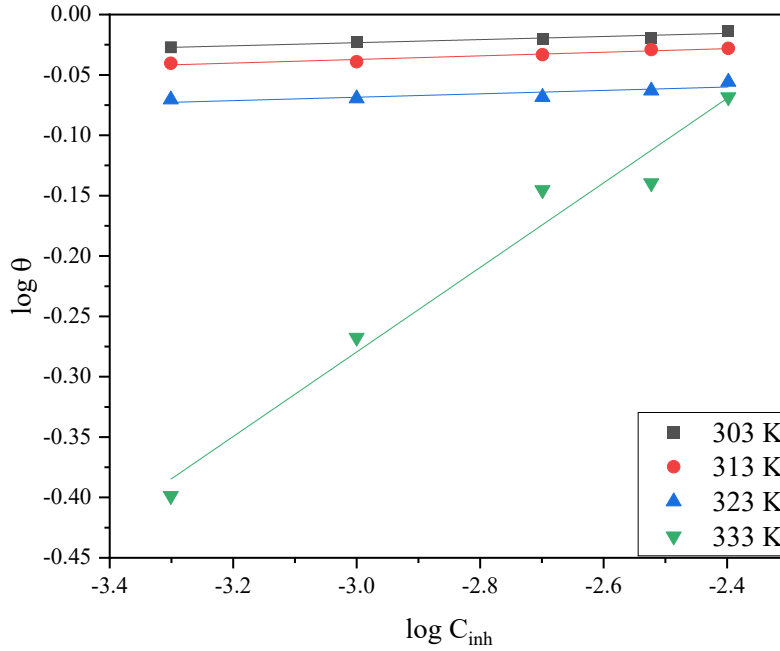


Figure 4.51: Freundlich adsorption isotherm plot for the adsorption of various concentrations of MQ6CA on the surface of mild steel in 1.0 M H₂SO₄ at various temperatures.

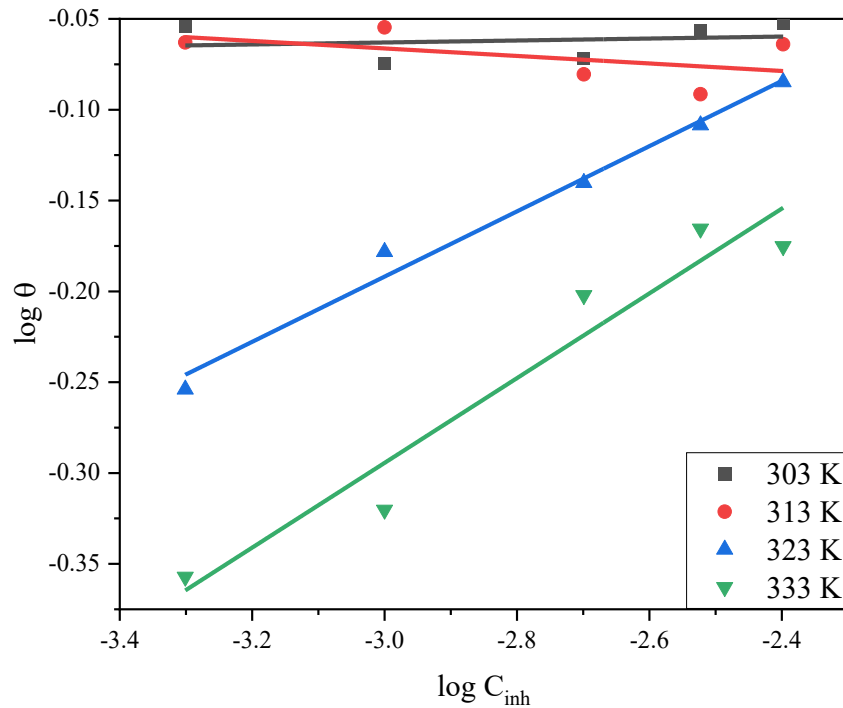


Figure 4.52: Freundlich adsorption isotherm plot for the adsorption of various concentrations of Q6CA on the surface of mild steel in 1.0 M H₂SO₄ at various temperatures.

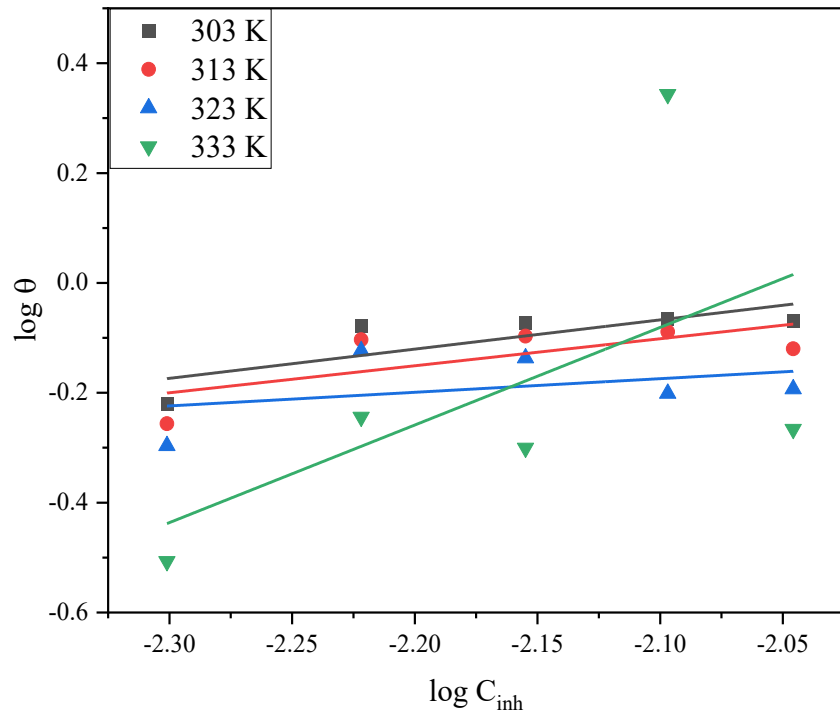


Figure 4.53: Freundlich adsorption isotherm plot for the adsorption of various concentrations of H2QCA with KI on the surface of mild steel in 1.0 M H₂SO₄ at various temperatures.

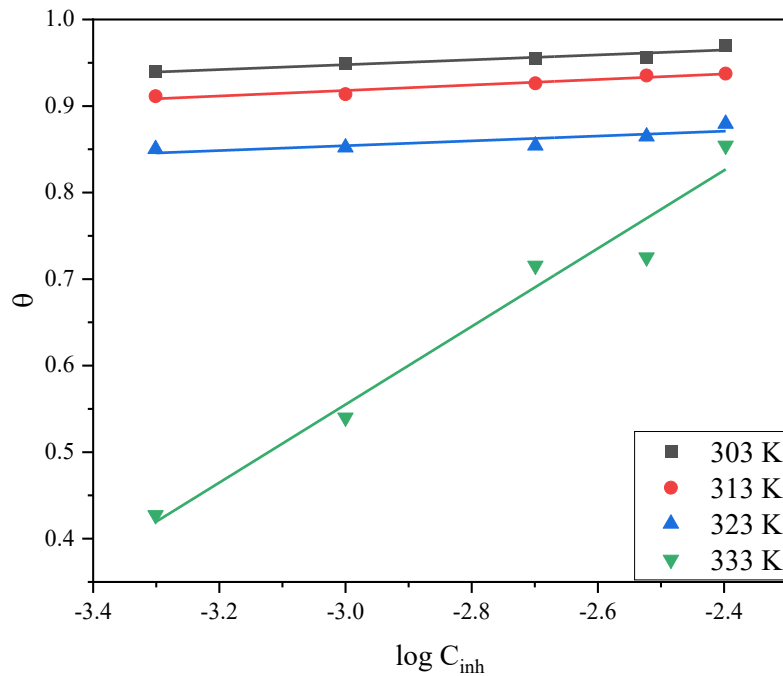


Figure 4.54: Temkin adsorption isotherm plot for the adsorption of various concentrations of MQ6CA on the surface of mild steel in 1.0 M H₂SO₄ at various temperatures.

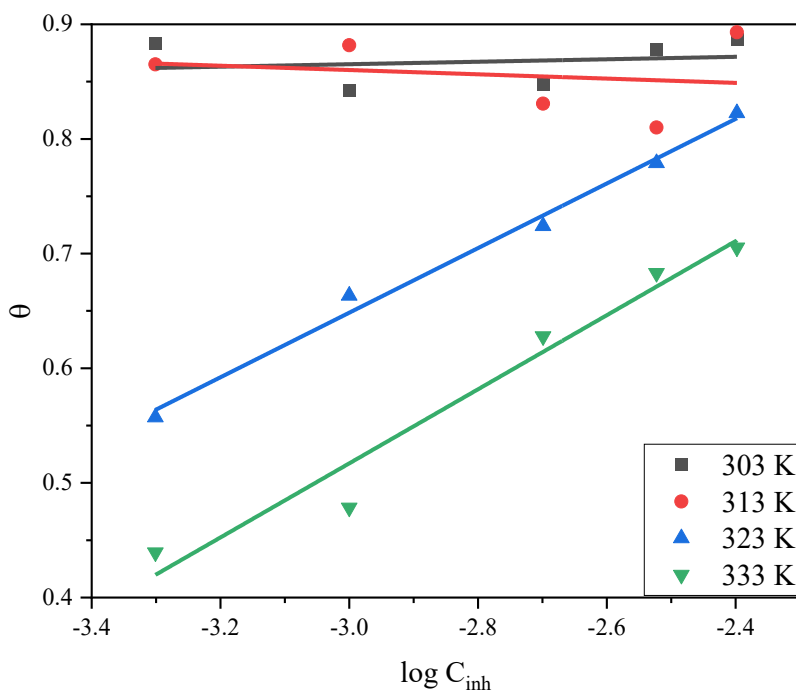


Figure 4.55: Temkin adsorption isotherm plot for the adsorption of various concentrations of Q6CA on the surface of mild steel in 1.0 M H_2SO_4 at various temperatures.

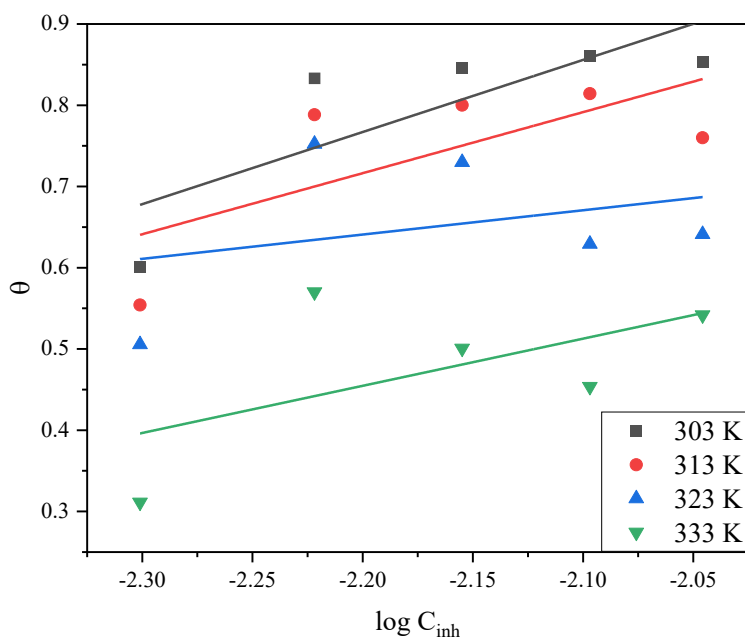


Figure 4.56: Temkin adsorption isotherm plot for the adsorption of various concentrations of H2QCA with KI on the surface of mild steel in 1.0 M H_2SO_4 at various temperatures.

Table 4.16: The regression coefficient values obtained from different adsorption isotherms for mild steel in 1.0 M H₂SO₄ at various temperatures for the studied quinoxaline.

Inhibitor	Temperature (K)	Correlation coefficient (R ²)			
		Langmuir	Frumkin	Freundlich	Temkin
MQ6CA	303	0.9999	0.9093	0.8783	0.8758
	313	0.9999	0.9532	0.9445	0.9438
	323	0.9999	0.9026	0.7134	0.7105
	333	0.9999	0.9236	0.9721	0.9674
Q6CA	303	0.9992	0.1777	0.0361	0.0359
	313	0.9883	0.1687	0.2582	0.0388
	323	0.9978	0.9195	0.9851	0.9911
	333	0.9958	0.9160	0.9370	0.9616
H2QCA with KI	303	0.9964	0.8725	0.6389	0.6495
	313	0.9582	0.4134	0.5046	0.4956
	323	0.9793	0.0575	0.1342	0.0923
	333	0.9858	0.2863	0.3167	0.3310

The degree of adsorption, that is, surface coverage (θ) of the studied quinoxaline obtained from weight loss measurements on mild steel surface and the variety of their concentration are best related by Langmuir isotherm given by equation (50):

$$\frac{\theta}{1-\theta} = K_{ads}C_{inh} \quad (50)$$

where is the K_{ads} is the adsorption/desorption constant, C_{inh} is the molar concentration of the quinoxaline inhibitors, and θ is the degree of surface coverage.

This equation can be rearranged to:

$$\frac{C_{inh}}{\theta} = \frac{1}{K_{ads}} + C_{inh} \quad (51)$$

From the aforementioned Langmuir plots, the values of K_{ads} were calculated from the intercept of the line. K_{ads} can be related to the free Gibbs energy of adsorption (ΔG°_{ads}) through equation (52).

$$K_{ads} = \frac{1}{55.5} \exp\left(-\frac{\Delta G^{\circ}_{ads}}{RT}\right) \quad (52)$$

Equation 4.1 can also be expressed as:

$$\Delta G^{\circ}_{ads} = -RT \ln (55.5K_{ads}) \quad (53)$$

where R is gas constant, T is absolute temperature in Kelvin and the value 55.5 is the molar concentration of water.

The K_{ads} and ΔG°_{ads} for mild steel in 1.0 M HCl and 1.0 M H₂SO₄ in the absence and presence of the studied quinoxalines are listed in Table 4.17 and 4.18, respectively. It has been reported that K_{ads} is representative of the strength between the inhibitor molecules and the metal's surface. Moreover, literature shows that large values of K_{ads} signifies a greater binding power [330]. The large values of K_{ads} obtained in this present study suggest a strong adsorption of the quinoxaline inhibitors on the mild steel surface. Hence appreciable inhibition efficiency obtained as reported earlier. The free Gibbs energy of adsorption gives more information on the mode interaction occurring between the inhibitors and the metal surface. As aforementioned earlier, the adsorption of organic inhibitors can be described by two main types of interaction, which are physical adsorption and chemical adsorption [195, 196]. Literature further reveals that the values of ΔG°_{ads} around -20 kJ/mol or lower are associated with physical adsorption and values of ΔG°_{ads} around -40 kJ/mol and more negative are associated with chemical adsorption [331]. In this present study, the values of ΔG°_{ads} were obtained to be negative for all the studied inhibitors which indicated that the inhibition processes were spontaneous. For MQ6CA in 1.0 M HCl the ΔG°_{ads} values for mild steel were obtained to be above -40 kJ/mol, indicating a chemical adsorption. Whereas, for the other compounds in both acids the ΔG°_{ads} were obtained to be between -20 and -40 kJ/mol,

indicating a mixed-typed of adsorption with chemisorption dominant. Similar trend was reported earlier.

Table 4.17: Langmuir adsorption parameters for corrosion of mild steel in 1.0 M HCl at various temperatures in the presence of the studied quinoxalines.

Inhibitor	Temperature (K)	K_{ads} (L/mol)	$-\Delta G^{\circ}_{ads}$ (kJ.mol ⁻¹)
MQ6CA	303	302229.85	41.51
	313	157075.72	41.59
	323	100244.30	41.71
	333	71046.44	42.05
Q6CA	303	29718.57	36.06
	313	33336.67	37.55
	323	44436.54	39.52
	333	29334.20	39.59
H2QCA with KI	303	724.63	26.71
	313	671.14	27.39
	323	735.29	28.51
	333	641.033	29.01

Table 4.18: Langmuir adsorption parameters for corrosion of mild steel in 1.0 M H₂SO₄ at various temperatures in the presence of the studied quinoxalines.

Inhibitor	Temperature (K)	K _{ads} (L/mol)	- ΔG ^o _{ads} (kJ.mol ⁻¹)
MQ6CA	303	36650.84	36.59
	313	35244.65	37.70
	323	23303.72	37.80
	333	1305.00	30.98
Q6CA	303	21595.05	35.26
	313	12811.87	35.06
	323	2594.59	31.89
	333	1515.05	31.39
H2QCA with KI	303	1064.35	27.68
	313	1398.21	29.30
	323	1274.56	30.00
	333	751.88	29.45

4.2.5 Potentiodynamic polarization (PDP)

It is imperative to mention that corrosion of mild steel is a result of simultaneous anodic and cathodic half-reactions [5]. To get more insight into this process, PDP measurements were carried out at room temperature (303 K) in 1.0 M HCl and 1.0 M H₂SO₄ in the absence and presence of the studied quinoxalines, as shown in figures 4.57 – 4.64. It can be seen from these figures that the introduction of the studied inhibitors affected both the anodic and cathodic half-reactions of the mild steel corrosion in both acids. The corresponding potentiodynamic parameters such as corrosion current density (i_{corr}), corrosion potential (E_{corr}), polarization resistance (R_p), and anodic (β_a) and cathodic (β_c) Tafel slopes were successfully evaluated from both the anodic and cathodic regions of the Tafel plots. These parameters are presented in Tables 4.19 and 4.20. The potentiodynamic polarization inhibition efficiency (%IE_{PDP}) was then evaluated from the measured i_{corr} values from equation (43).

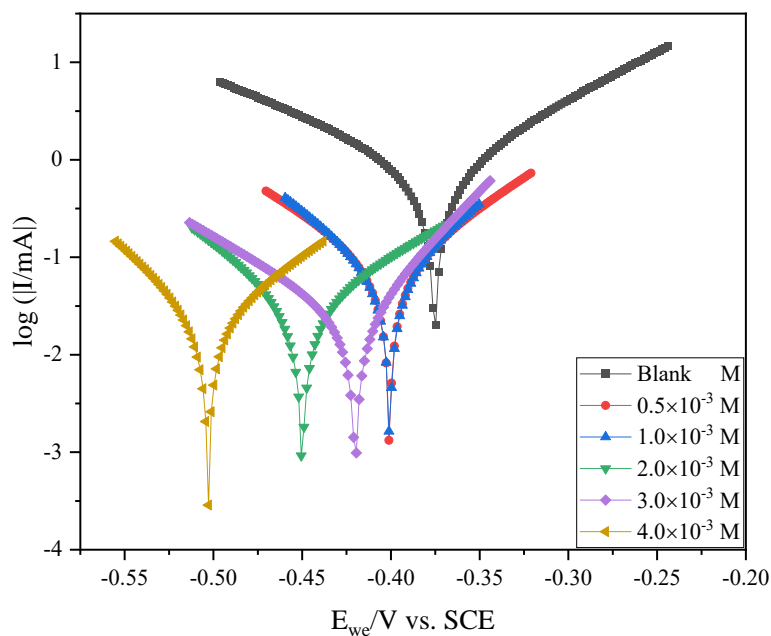


Figure 4.57: Tafel plots for mild steel in 1.0 M HCl in the absence and presence of various concentrations of MQ6CA at 303 K.

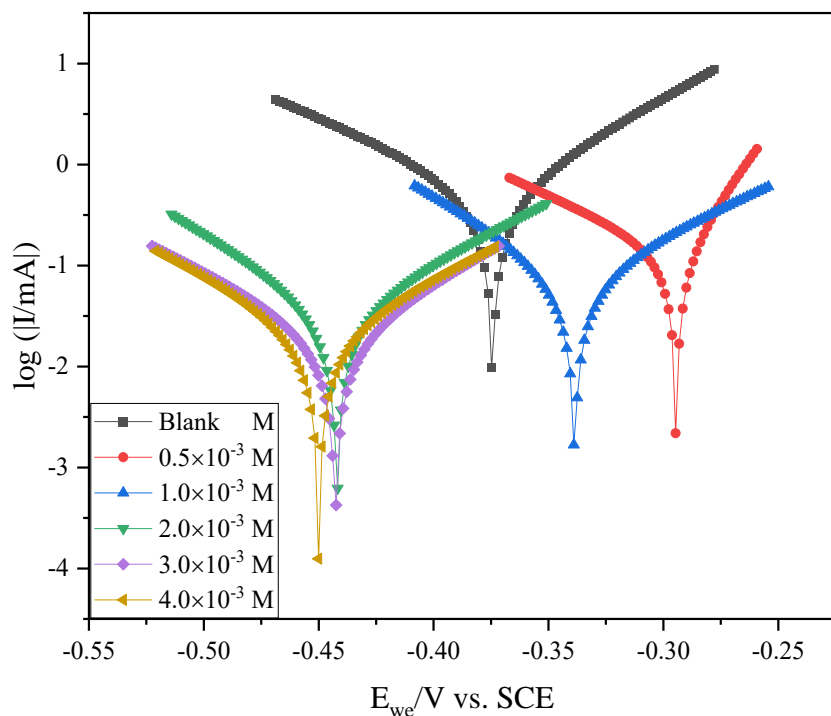


Figure 4.58: Tafel plots for mild steel in 1.0 M HCl in the absence and presence of various concentrations of Q6CA at 303 K.

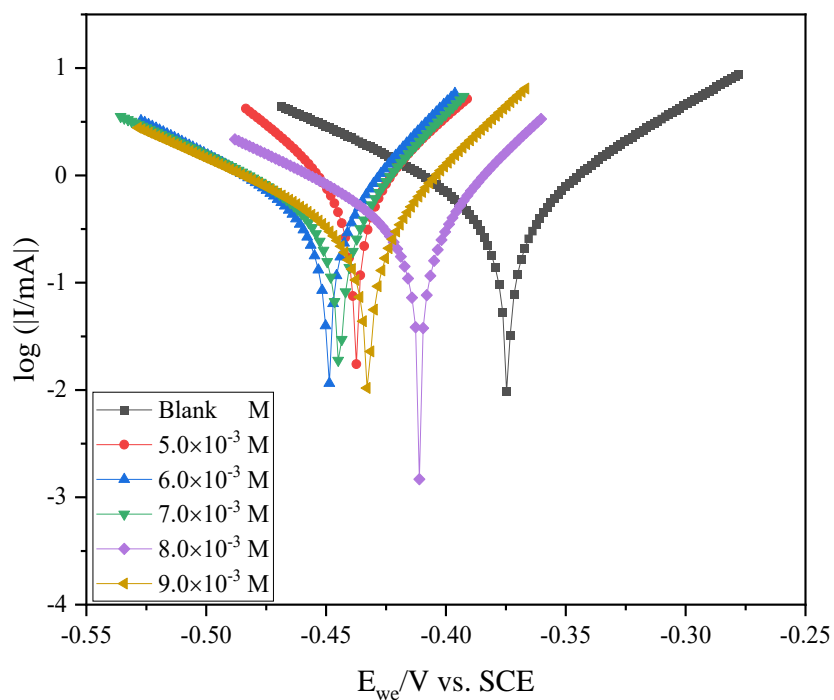


Figure 4.59: Tafel plots for mild steel in 1.0 M HCl in the absence and presence of various concentrations of H2QCA without KI at 303 K.

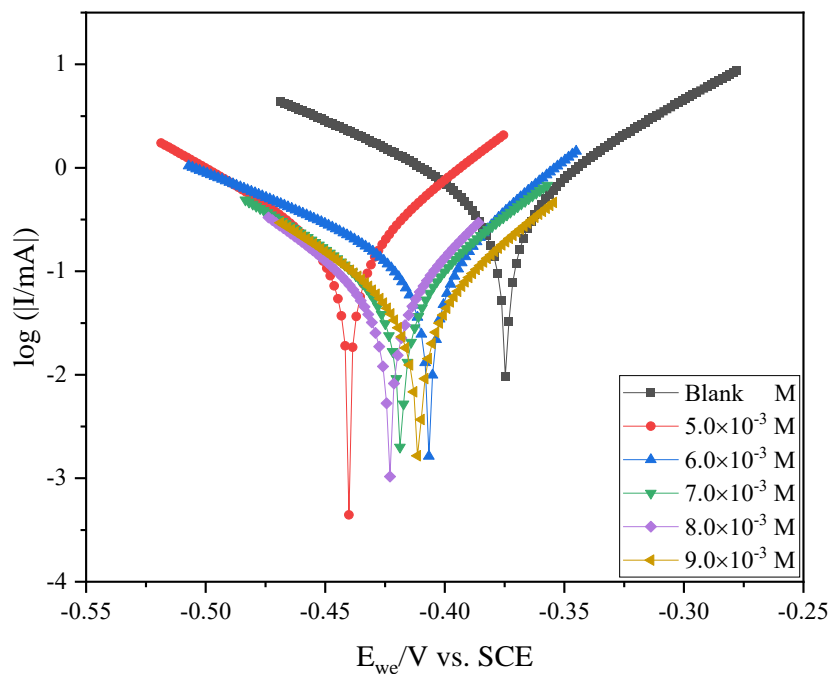


Figure 4.60: Tafel plots for mild steel in 1.0 M HCl in the absence and presence of various concentrations of H2QCA with KI at 303 K.

Table 4.19: Potentiodynamic Polarization (PDP) parameters such as corrosion current density (i_{corr}), corrosion potential (E_{corr}), polarization resistance (R_p), and anodic (β_a) and cathodic (β_c) Tafel slopes utilizing the studied quinoxalines in 1.0 M HCl.

Inhibitor	Conc. ($\times 10^{-3}$ M)	C_r /mpy	E_{corr} / mV vs. SCE	β_a / mV.dec ⁻¹	β_c / mV.dec ⁻¹	i_{corr} / μ A.cm ⁻²	R_p/Ω	%IE _{PDP}	% IE _{WL}
Blank	-	388.945	-375.342	106.1	138.6	851.634	25.1	-	
MQ6CA	0.5	39.57	-400.769	85.5	92.4	86.653	160.4	89.83	99.55
	1.0	31.02	-400.876	69.0	74.9	67.894	214.2	92.03	99.70
	2.0	16.15	-449.964	102.0	80.2	35.337	393.0	95.85	99.71
	3.0	8.357	-428.641	57.7	66.7	18.290	533.0	97.85	99.72
	4.0	8.118	-403.665	60.5	47.4	17.768	450	97.91	99.95
Q6CA	0.5	120.191	-298.114	29.6	91.4	130.000	62.30	84.50	0.9962
	1.0	65.4496	-332.807	99.4	80.2	81.760	163.00	90.40	0.9863
	2.0	21.4341	-438.742	96.9	95.7	35.795	337.00	95.79	0.9795
	3.0	21.4048	-442.562	80.2	90.3	20.707	619.00	97.57	0.9810
	4.0	13.1801	-448.475	65.7	69.5	15.530	639.00	98.18	0.9894
	5.0	358.665	-437.596	56.1	62.1	785.331	11.60	7.79	12.19
	6.0	199.862	-448.998	46.6	89.8	437.222	23.60	48.66	29.43
	7.0	184.323	-444.004	43.6	93.7	403.593	24.90	52.61	51.23

H2QCA without KI	8.0	161.451	-411.044	51.2	97.4	353.512	34.2	58.49	54.81
	9.0	154.287	-430.755	49.1	108.6	337.826	35.10	60.33	59.08
H2QCA with KI	5.0	77.92	-440.027	59.9	78.6	174.927	28.8	79.45	61.01
	6.0	49.608	-410.413	58.6	87.2	108.568	103.00	87.25	81.95
	7.0	33.250	-418.296	62.6	78.1	72.767	144.00	91.46	87.72
	8.0	24.421	-423.122	48.6	63.0	52.834	197.50	93.80	89.09
	9.0	21.482	-410.946	56.5	71.9	47.014	200.00	94.50	90.32

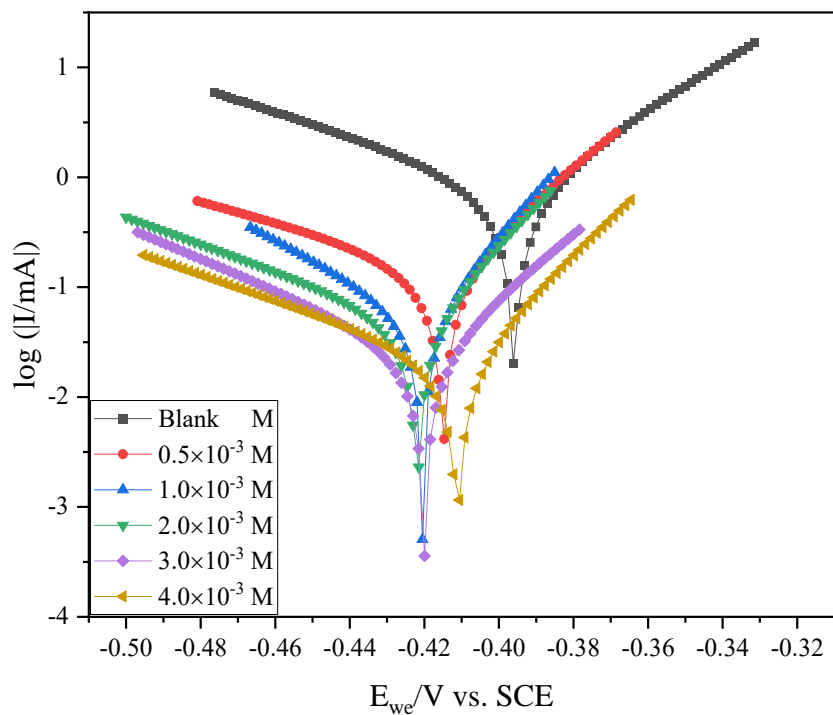


Figure 4.61: Tafel plots for mild steel in 1.0 M H₂SO₄ in the absence and presence of various concentrations of MQ6CA at 303 K.

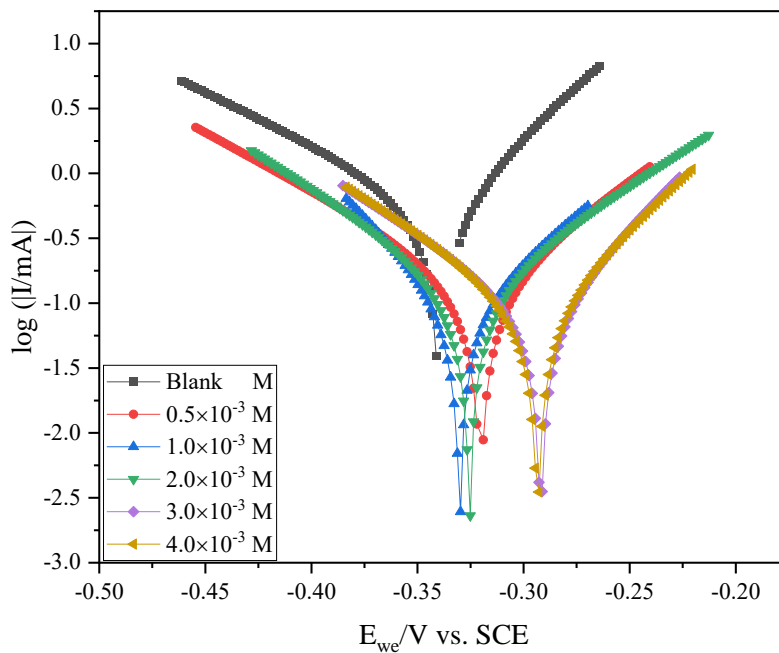


Figure 4.62: Tafel plots for mild steel in 1.0 M H₂SO₄ in the absence and presence of various concentrations of Q6CA at 303 K.

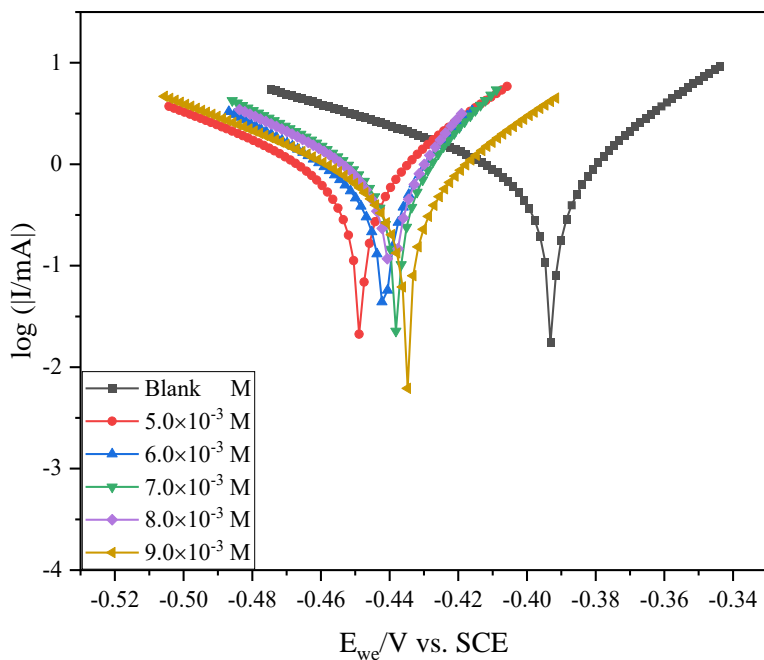


Figure 4.63: Tafel plots for mild steel in 1.0 M H_2SO_4 in the absence and presence of various concentrations of H2QCA without KI at 303 K.

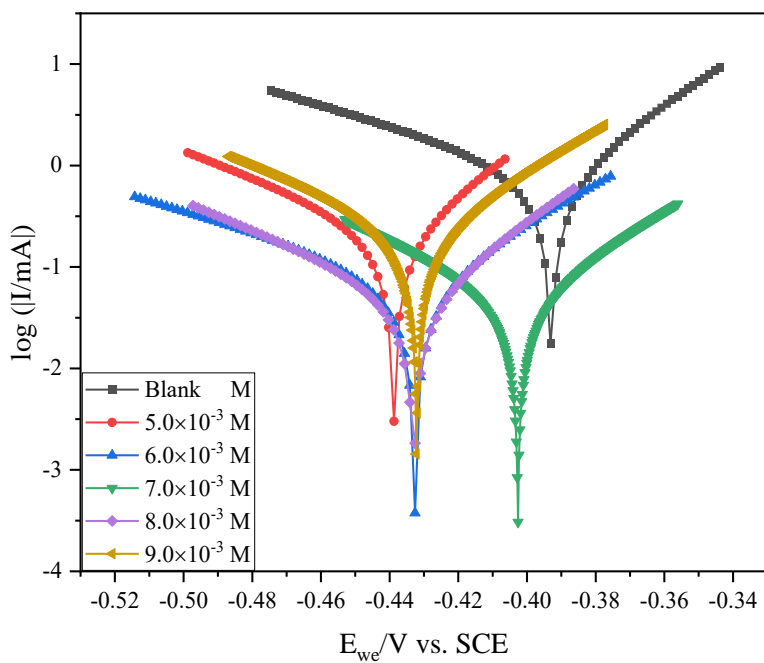


Figure 4.64: Tafel plots for mild steel in 1.0 M H_2SO_4 in the absence and presence of various concentrations of H2QCA with KI at 303 K.

Table 4.20: Potentiodynamic Polarization (PDP) parameters such as corrosion current density (i_{corr}), corrosion potential (E_{corr}), polarization resistance (R_p), and anodic (β_a) and cathodic (β_c) Tafel slopes utilizing the studied quinoxalines in 1.0 M H_2SO_4 .

Inhibitor	Conc. ($\times 10^{-3}$ M)	C_r /mpy	E_{corr} / mV vs. SCE	β_a / mV.dec $^{-1}$	β_c / mV.dec $^{-1}$	i_{corr} / $\mu A.cm^{-2}$	R_p (Ω)	%IE _{PDP}	% IE _{WL}
Blank	-	367.865	-395.802	48.6	92.8	805.067	15.2	-	-
MQ6CA	0.5	69.140	-414.974	37.4	108.0	149.589	50.4	81.42	93.98
	1.0	23.407	-420.560	26.5	55.1	51.226	102.00	93.63	94.88
	2.0	21.811	-421.935	29.6	81.4	47.733	82.00	94.07	95.49
	3.0	9.255	-420.856	38.3	52.7	20.256	339.7	97.48	95.58
	4.0	7.531	-414.825	32.6	69.0	16.48	431.0	97.95	97.01
Q6CA	0.5	66.977	-322.134	53.2	71.7	146.580	65.50	81.79	88.31
	1.0	52.627	-326.926	85.0	80.9	113.858	110.00	85.86	84.22
	2.0	42.817	-330.109	76.5	62.8	92.634	112.00	88.49	84.78
	3.0	30.856	-325.548	56.3	69.7	66.757	136.00	91.71	87.80
	4.0	11.384	-319.338	44.5	61.2	44.629	102.00	94.46	88.65
	5.0	361.091	-448.544	48.3	82.0	790.644	12.00	01.79	33.32
	6.0	247.901	-441.493	31.3	57.7	542.803	11.2	32.58	49.41
	7.0	350.282	-437.873	33.3	64.2	766.976	8.52	04.73	41.24

H2QCA without KI	8.0	349.396	-439.250	30.4	67.6	766.219	9.07	04.83	36.58
	9.0	275.299	-434.855	48.7	79.3	602.641	8.44	25.14	42.74
H2QCA with KI	5.0	104.02	-440.127	47.30	74.50	227.761	23.10	71.71	60.10
	6.0	48.317	-412.965	39.50	85.00	105.796	69.10	86.86	83.32
	7.0	24.004	-401.329	46.20	68.30	52.559	211.00	93.47	84.65
	8.0	22.611	-432.192	40.00	70.70	49.509	130.00	93.85	86.09
	9.0	15.274	-420.254	42.87	86.00	28.504	228.00	96.45	85.30

It can be seen from figures 4.57 – 4.64 that the addition of various concentrations of the three inhibitors for mild steel in 1.0 M HCl and 1.0 M H₂SO₄, the polarization curves shifted towards the region of low current region densities compared to the uninhibited system. This effect indicates that the inhibitor molecules adsorbed on the active sites mild steel surface, thus, suggests that the inhibitor molecules reduced the anodic dissolution of mild steel and also suppressed the hydrogen evolution reaction [332]. An inspection of the data in Tables 4.18 and 4.19, reveals that the inhibition efficiencies of MQ6CA, Q6CA, and H2QCA with KI increased with the increase of their concentrations, and corrosion rate decreased with increase in the inhibitor concentrations. This observation can be attributed to the increasing population of the inhibitor molecules forming a protective layer on mild steel surface. The maximum inhibition efficiency was obtained at the optimum concentration of the respective inhibitors. A similar trend was also observed in the weight loss analysis. As reported earlier, the addition of KI to the H2QCA system remarkably proved to have decreased the corrosion current density values, consequently improving the efficiency of the inhibitor. The E_{corr} values in the absence and presence of corrosion inhibitors can be utilized to classify the mode of inhibition. Based on the displacement of E_{corr} with respect to an inhibitor can be classified as cathodic, anodic or mixed-type. Moreover, a perusal of the literature reveals that an anodic or cathodic inhibitor may be assessed with E_{corr} value displacement greater than 85mV [333, 334]. In this study, the maximum displacement in E_{corr} for mild steel was found to be 77.228 mV and 76.467 in 1.0 M HCl and 1.0 M H₂SO₄, respectively. These findings imply that MQ6CA, Q6CA, and H2QCA with KI are mixed-type, that is, the studied quinoxaline retards both the anodic and cathodic half-reaction of the mild steel corrosion process. It can be observed from the tables that there was no regular trend on the values of E_{corr} of all the inhibited systems. The anodic and cathodic Tafel slope values can further be employed in conforming the mode of inhibition possessed by the studied quinoxalines. Tables 4.18 and 4.19 show that values of β_a and β_c slightly changed with the introduction of different concentrations of the inhibitors. Although there was no regular trend in the Tafel slope values with the inhibitor concentration, this observation further suggested that the inhibitors retarded both the anodic and cathodic, however, the effect was found to be more prominent on the cathodic reaction. Thus, all the three studied quinoxalines are mixed-type inhibitors on mild steel surface, however, predominantly cathodic inhibitors. Nasser and Sathiq [335], also reported similar observations. Moreover, the introduction of MQ6CA, Q6CA, and H2QCA with KI to the aggressive solution resulted in the polarization resistance (R_p). From

the tables, it is clear that the R_P values increased with the increase in the concentration of the inhibitors. According to Nesane and co-workers [336], this effect suggests that further polarization of mild steel was retarded by the barrier formed by the increasing population of the inhibitor molecules at the metal/solution interface. The %IE_{PDP} were reasonably in agreement with those of weight loss analysis.

4.2.6 Electrochemical impedance spectroscopy (EIS)

Electrochemical impedance spectroscopy is a powerful and versatile characterization technique that is mostly utilized in the corrosion field. This technique provides insight regarding the kinetics of the corrosion process and simultaneously the mechanism of inhibition. In this study, EIS was employed to investigate the behavior of mild steel corrosion in 1.0 M HCl and 1.0 M H₂SO₄ in the absence and presence of various concentrations of the studied quinoxalines at 303 K. The technique was conducted at the open-circuit voltage (OCP) after 3600s of mild steel immersion until a steady corrosion potential (E_{corr}) for all the working electrodes was established. Figures 4.65 – 4.78 show represent the obtained Nyquist plots and corresponding Bode plots. The Nyquist plots are represented by imperfect semicircles capacitive loops. Inspection of these figures, the diameter of these imperfect semicircles is observed to increase with the concentration of the inhibitors, perhaps due to an increase in the surface coverage of adsorptive quinoxalines on mild steel surface. These imperfect semicircles are indicative of a charge transfer process that presides over the mild steel corrosion in acidic medium [336].

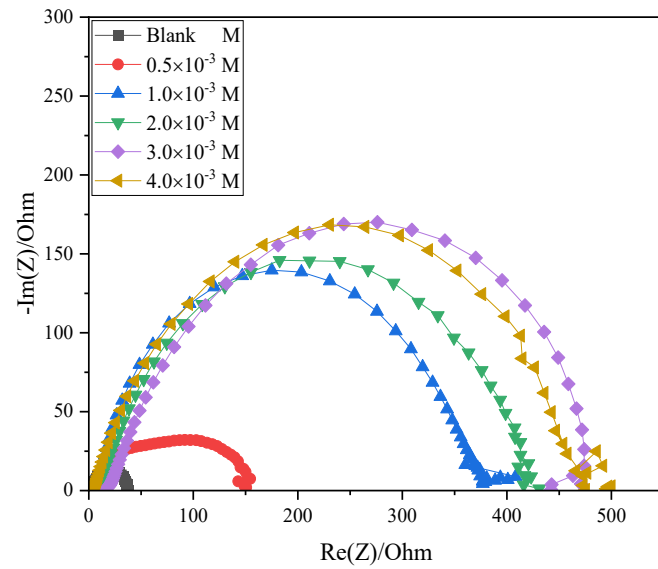


Figure 4.65: Nyquist plot of mild steel in 1.0 M HCl in the presence and absence of various concentrations of MQ6CA.

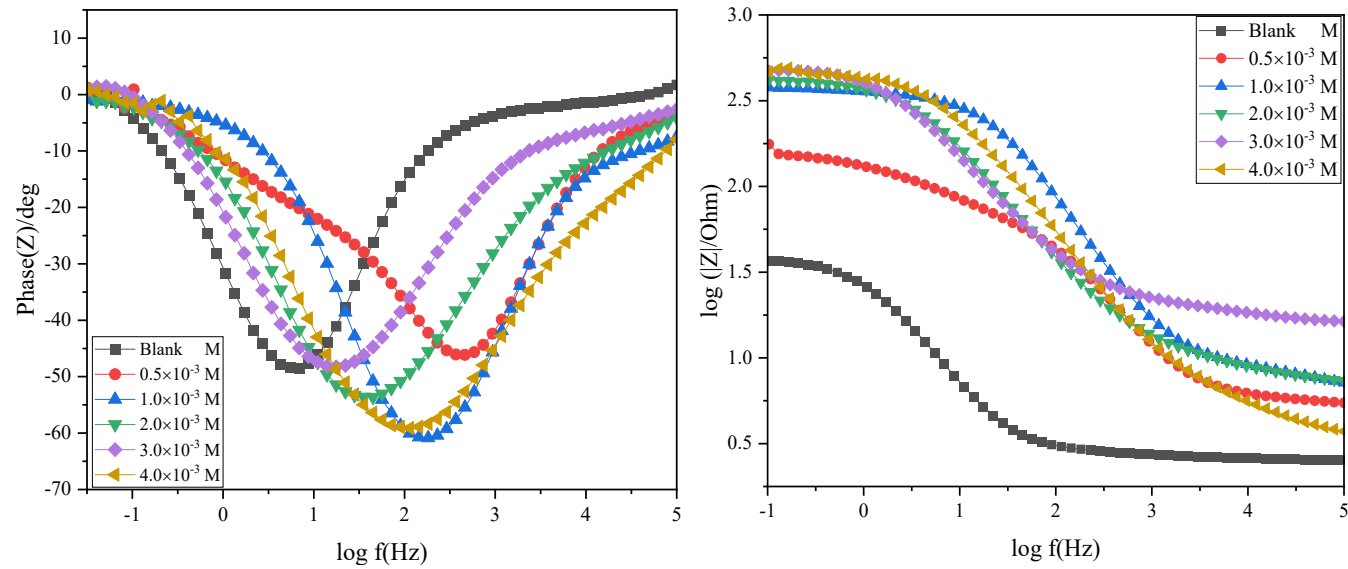


Figure 4.66: Bode plot of mild steel in 1.0 M HCl in the presence and absence of various concentrations of MQ6CA.

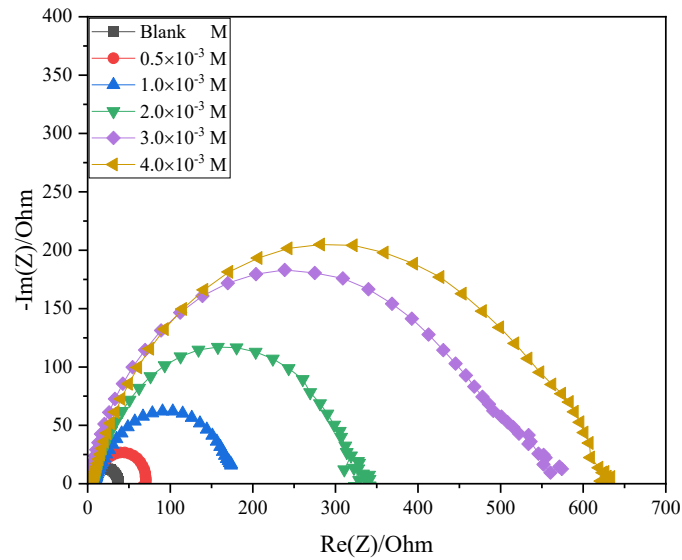


Figure 4.67: Nyquist plot of mild steel in 1.0 M HCl in the presence and absence of various concentrations of Q6CA.

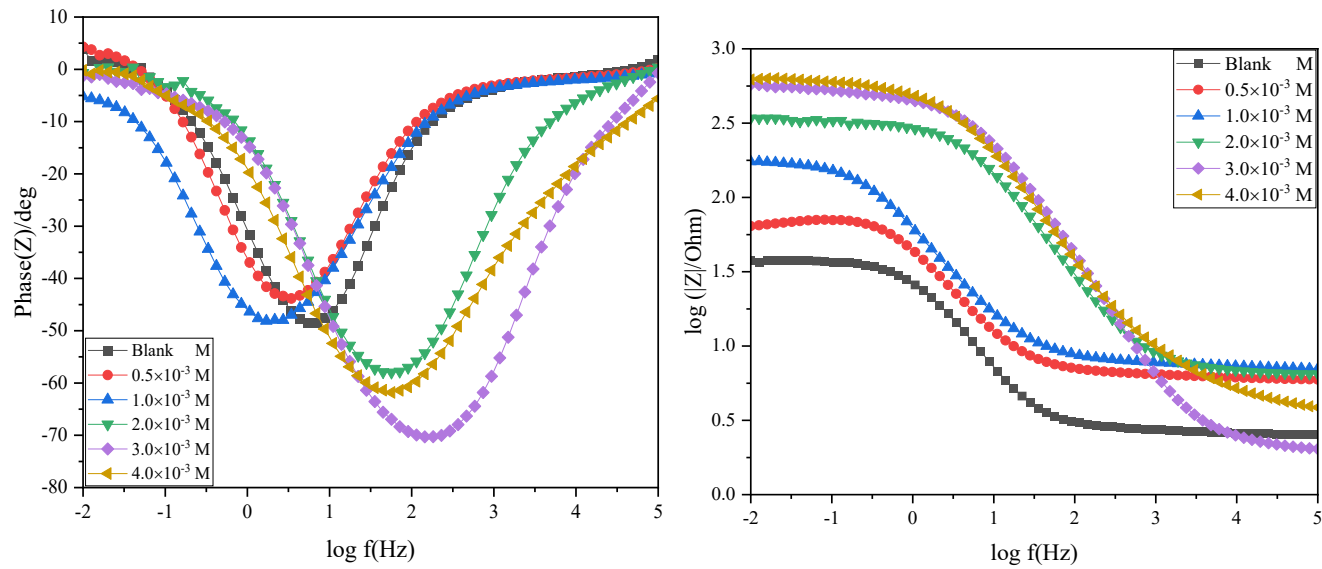


Figure 4.68: Bode plot of mild steel in 1.0 M HCl in the presence and absence of various concentrations of Q6CA

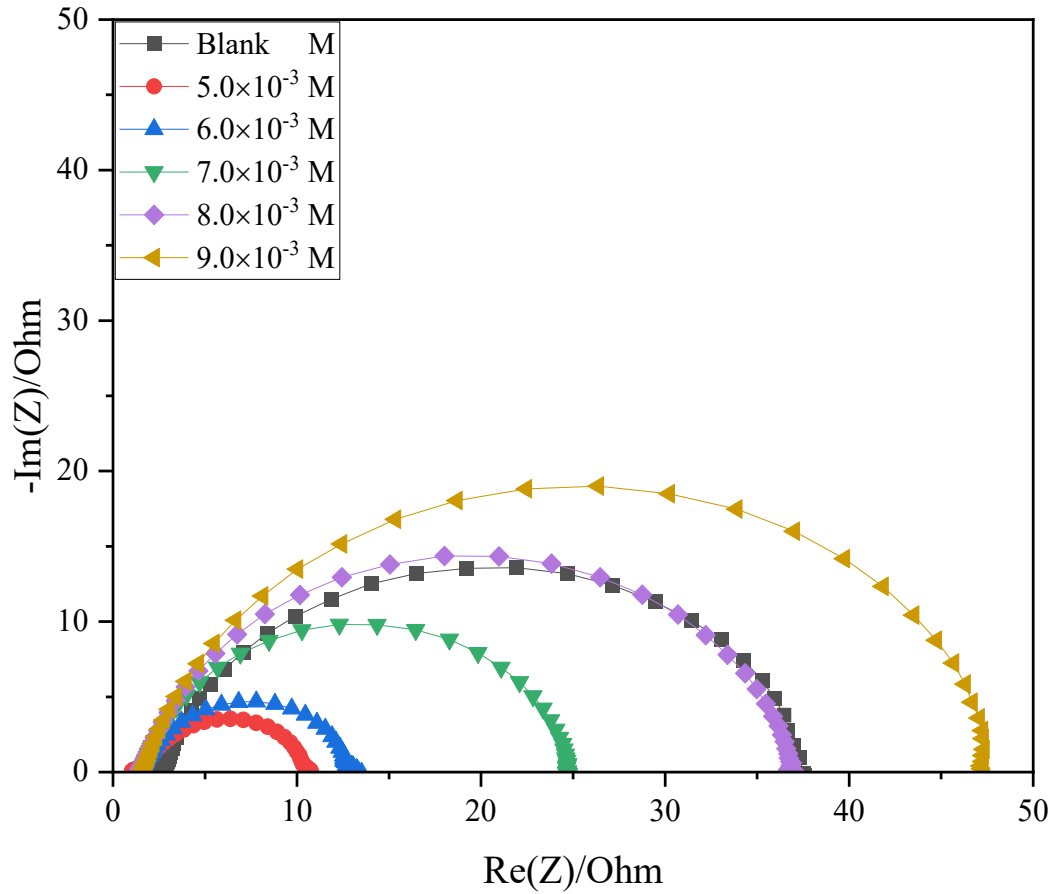


Figure 4.69: Nyquist plot of mild steel in 1.0 M HCl in the presence and absence of various concentrations of H₂QCA without KI.

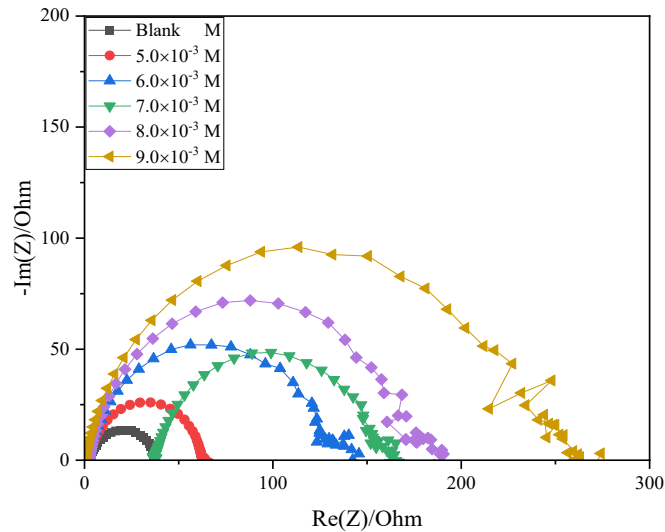


Figure 4.70: Nyquist plot of mild steel in 1.0 M HCl in the presence and absence of various concentrations of H2QCA with KI.

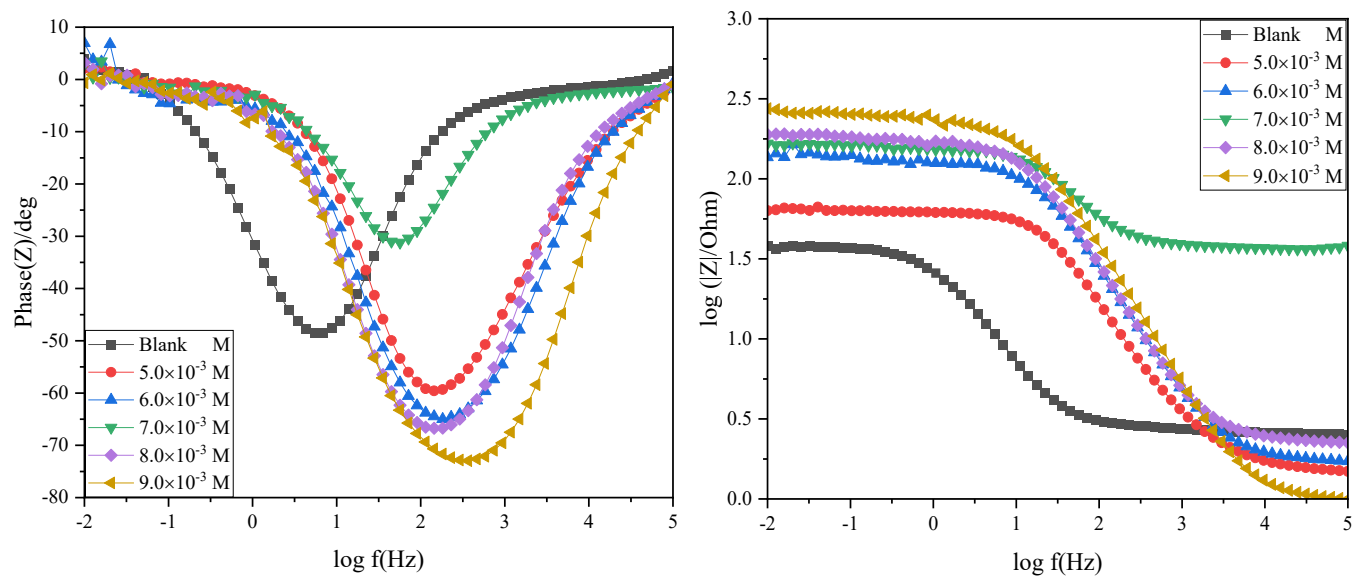


Figure 4.71: Bode plot of mild steel in 1.0 M HCl in the presence and absence of various concentrations of H2QCA with KI.

Table 4.21: Electrochemical impedance parameters such as the resistance of charge transfer (R_{ct}), constant phase element (CPE) and the CPE exponent (n) of mild steel in the absence and presence of various concentrations of the studied quinoxalines in 1.0 M HCl.

Inhibitor	Conc. ($\times 10^{-3}$ M)	R_1/Ω	$Q_2/F.s^{(a-1)}$	R_2/Ω	n	θ	%IE _{EIS}	%IE _{PDP}	%IE _{WL}
Blank	-	2.645	$5.05e^{-3}$	35.26	0.839	-	-	-	-
MQ6CA	0.5	4.867	$0.400e^{-3}$	141.00	0.638	0.7499	74.99	89.83	99.55
	1.0	7.858	$53.65e^{-3}$	367.70	0.828	0.9041	90.41	92.03	99.70
	2.0	8.036	$0.244e^{-3}$	428.60	0.727	0.9177	91.77	95.85	99.71
	3.0	17.93	$0.281e^{-3}$	468.00	0.737	0.9247	92.47	97.85	99.72
	4.0	4.033	$0.147e^{-3}$	488.00	0.739	0.9277	92.77	97.91	99.95
Q6CA	0.5	6.286	$3.688e^{-3}$	64.81	0.8215	0.4559	45.59	84.50	0.9962
	1.0	7.427	$3.643e^{-3}$	177.8	0.7485	0.8019	80.19	90.40	0.9863
	2.0	6.578	$0.196e^{-3}$	323.5	0.8066	0.8910	89.10	95.79	0.9795
	3.0	2.069	$0.110e^{-3}$	516.6	0.8396	0.9319	93.19	97.57	0.9810
	4.0	4.221	$0.205e^{-3}$	623.3	0.7452	0.9434	94.34	98.18	0.9894
H2QCA without KI	5.0	1.189	$6.157e^{-3}$	9.876	0.696	-2.5702	-270.03	7.79	12.19
	6.0	1.574	$0.226e^{-3}$	23.04	0.873	-0.5304	-53.04	48.66	29.43
	7.0	1.429	$0.174e^{-3}$	27.35	0.894	-0.2892	-28.92	52.61	51.23
	8.0	1.430	$0.218e^{-3}$	35.39	0.842	0.0034	00.34	58.49	54.81
	9.0	1.627	$0.233e^{-3}$	45.69	0.858	0.2283	22.83	60.33	59.08
H2QCA with KI	5.0	1.56	$0.251e^{-3}$	62.74	0.835	0.4380	43.80	79.45	61.01
	6.0	1.74	$0.141e^{-3}$	132.9	0.854	0.7347	73.47	87.25	81.95
	7.0	1.85	$0.132e^{-3}$	123.6	0.831	0.7147	71.47	91.46	87.72
	8.0	2.288	$0.119e^{-3}$	177.4	0.875	0.8012	80.12	93.80	89.09
	9.0	0.9931	$88.77e^{-6}$	246.3	0.881	0.8568	85.68	94.50	90.32

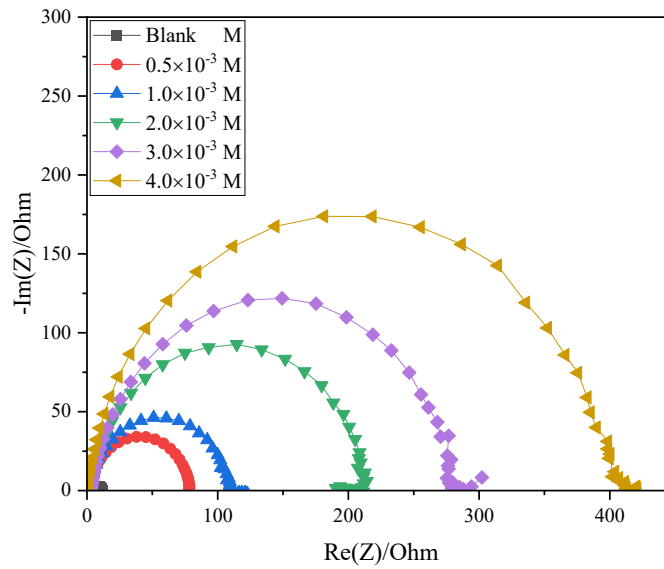


Figure 4.72: Nyquist plot of mild steel in 1.0 M H₂SO₄ in the presence and absence of various concentrations of MQ6CA.

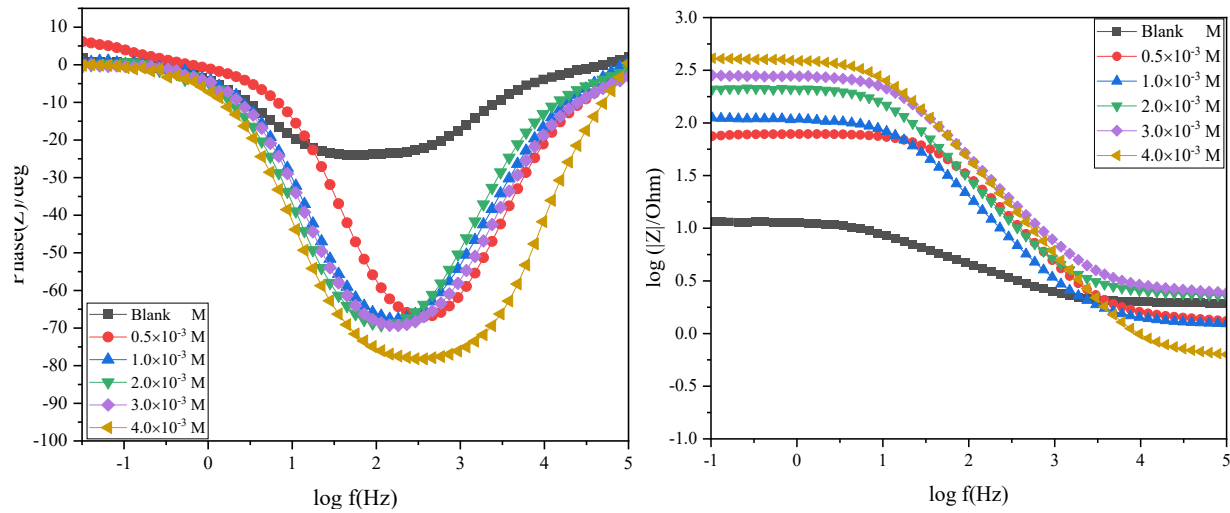


Figure 4.73: Bode plot of mild steel in 1.0 M H₂SO₄ in the presence and absence of various concentrations of MQ6CA.

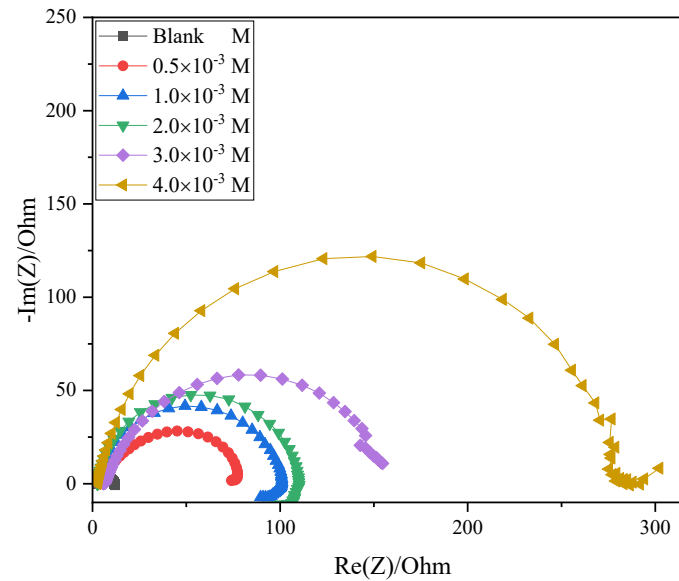


Figure 4.74: Nyquist plot of mild steel in 1.0 M H₂SO₄ in the presence and absence of various concentrations of Q6CA.

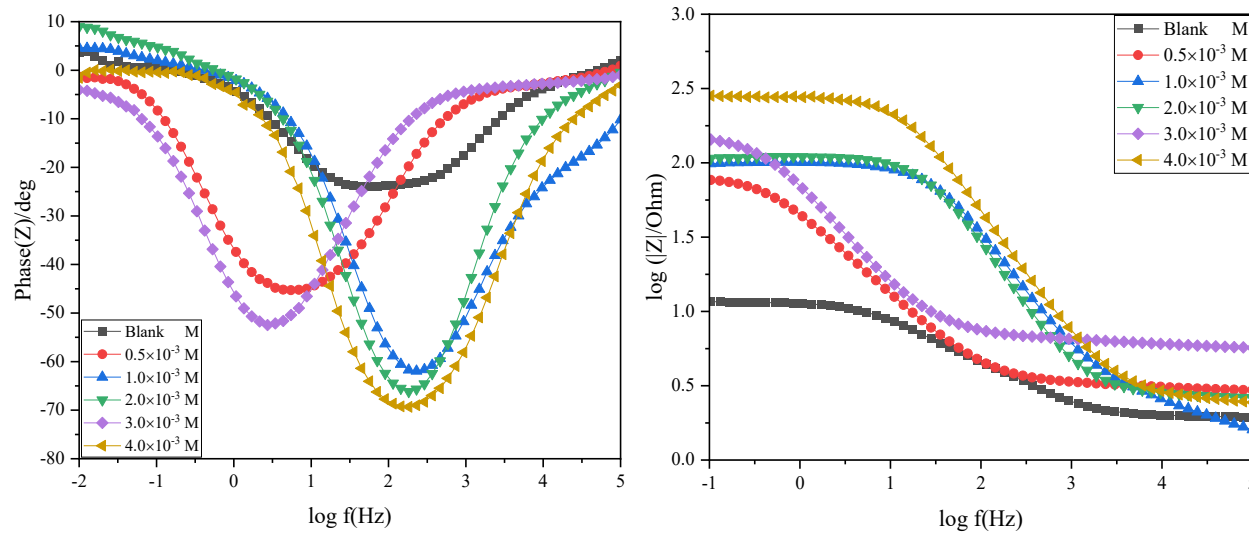


Figure 4.75: Bode plot of mild steel in 1.0 M H₂SO₄ in the presence and absence of various concentrations of Q6CA.

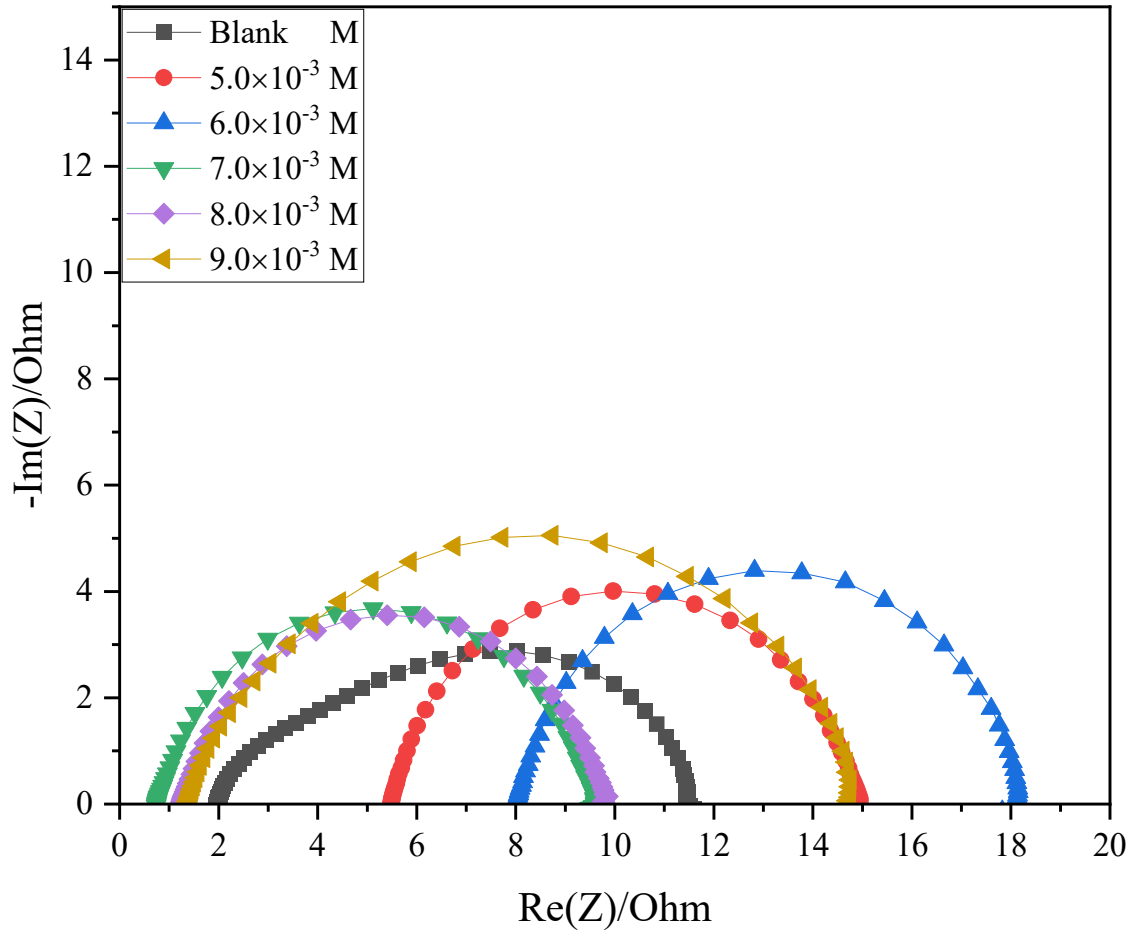


Figure 4.76: Nyquist plot of mild steel in 1.0 M H₂SO₄ in the presence and absence of various concentrations of H₂QCA without KI.

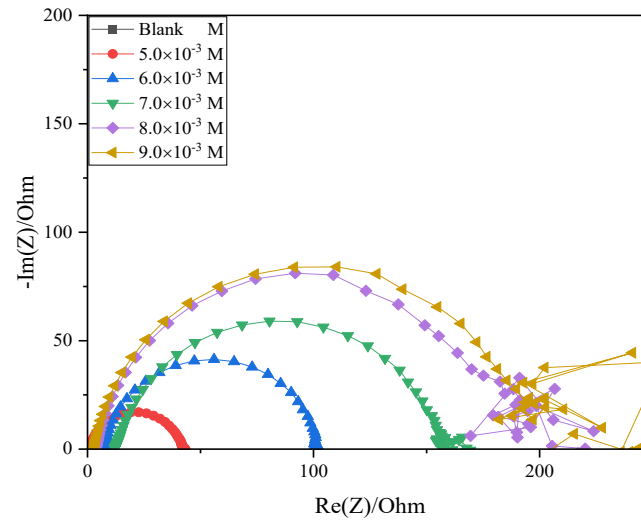


Figure 4.77: Nyquist plot of mild steel in 1.0 M H₂SO₄ in the presence and absence of various concentrations of H₂QCA with KI.

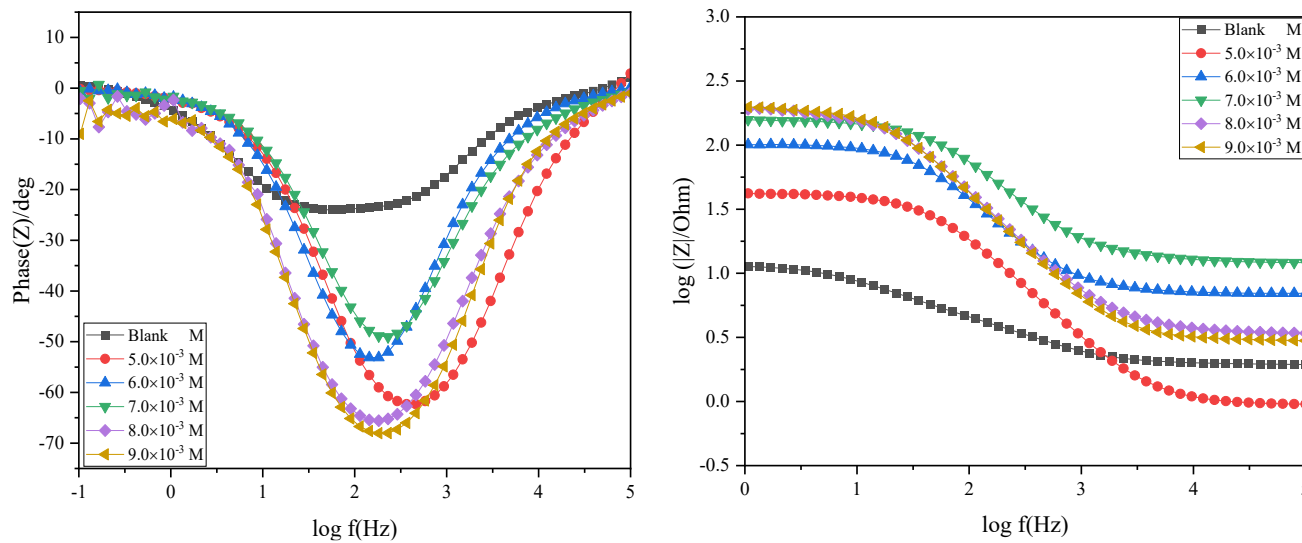


Figure 4.78: Bode plot of mild steel in 1.0 M H₂SO₄ in the presence and absence of various concentrations of H₂QCA with KI.

Table 4.22: Electrochemical impedance parameters such as the resistance of charge transfer (R_{ct}), constant phase element (CPE) and the CPE exponent (n) of mild steel in the absence and presence of various concentrations of the studied quinoxalines in 1.0 M H_2SO_4 .

Inhibitor	Conc. ($\times 10^{-3} M$)	R_1/Ω	$Q_2/F.s^{(a-1)}$	R_2/Ω	n	θ	%IE _{EIS}	%IE _{PDP}	%IE _{WL}
Blank		1.896	4.722e-3	10.06	0.628	-	-	-	-
MQ6CA	0.5	1.39	78.8e-6	72.84	0.913	0.8419	84.19	81.42	93.98
	1.0	1.278	0.170e-3	111.6	0.875	0.9099	90.99	93.63	94.88
	2.0	2.319	0.100e-3	205.4	0.898	0.9510	95.10	94.07	95.49
	3.0	2.553	67.96e-3	283.3	0.883	0.9645	96.45	97.48	95.58
	4.0	0.646	55.74e-6	406.1	0.923	0.9752	97.52	97.95	97.01
Q6CA	0.5	3.078	4.09e-3	79.25	0.772	0.8731	87.31	81.79	88.31
	1.0	1.85	0.136e-3	98.92	0.819	0.8983	89.83	85.86	84.22
	2.0	2.713	79.67e-6	100.7	0.933	0.9001	90.01	88.49	84.78
	3.0	6.176	2.831e-3	154.0	0.793	0.9347	93.47	91.71	87.80
	4.0	2.553	67.69e-6	283.3	0.883	0.9645	96.45	94.46	88.65
H2QCA without KI	5.0	5.496	0.202e-3	9.376	0.898	-0.0730	-7.23	01.79	33.32
	6.0	8.065	0.156e-3	9.808	0.923	-0.0256	-2.57	32.58	49.41
	7.0	0.762	0.255e-3	8.780	0.869	-0.1458	-14.21	04.73	41.24
	8.0	1.254	0.316e-3	8.403	0.873	-0.1972	-19.72	04.83	36.58
	9.0	1.367	0.730e-3	13.66	0.796	0.2635	26.35	25.14	42.74
H2QCA with KI	5.0	0.948	0.162e-3	41.43	0.877	0.7572	75.72	71.71	60.10
	6.0	7.06	76.99e-6	93.97	0.902	0.8929	89.29	8q6.86	83.32
	7.0	12.3	49.02e-6	146.8	0.857	0.9315	93.15	93.47	84.65
	8.0	3.474	76.04e-6	192.8	0.881	0.9478	94.78	93.85	86.09
	9.0	2.991	68.83e-6	202.4	0.900	0.9503	95.03	96.45	85.30

The Nyquist plots in this study exhibits a depressed capacitive loop at high-frequency regions. Literature has shown that the low inductive loop is related to the bulk relaxation process, whereas the capacitive loop in the high frequency is related to the charge transfer resistance and a double layer capacitance (C_{dl}) [337]. The oval-shaped semicircles observed in the Nyquist plots are a result of a phenomenon referred to as frequency dispersion of interfacial impedance which may rise due to factors such as; impurities, inhomogeneity adsorption of inhibitors, and roughness of the electrode surface [338]. Furthermore, the similar shapes of these plots indicate that the three studied inhibitors retard the rate of corrosion in a similar mechanism [336]. The model of the equivalent circuit utilized to fit the experimental data in 1.0 M HCl and 1.0 M H₂SO₄ in the presence and absence of various concentrations of the studied quinoxalines is shown in Figure 4.79. This circuit consists of a charge transfer resistance (R_{ct}), solution resistance (R_s), and constant phase element (CPE).

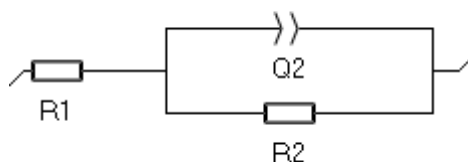


Figure 4.79: Equivalent circuit utilized to fit the impedance spectra obtained for mild steel corrosion in 1.0 M HCl and 1.0 M H₂SO₄ in the absence and presence of various concentrations of the studied quinoxalines.

where R1, R2 and Q2 are the solution resistance (R_s), charge transfer resistance (R_{ct}), and constant phase element (CPE), respectively.

It is worth mentioning that in a real acid/iron system, there is no recognized ideal capacitive behavior, hence in most cases in order to obtain more accurate results from fitting the experimental results, CPE is utilized as a substitute of a capacitor [339]. The impedance function of CPE can be defined by equation (54).

$$Z_{CPE} = \frac{1}{Y_0(j\omega)^n} \quad (54)$$

where Y_0 is the CPE proportional factor, ω is the angular frequency, j is the imaginary number, and n is the deviation parameter, and it is dependent on the surface morphology [339]. Depending on n value, the CPE can represent capacitance ($n=1$, $Y_0=C$), resistance ($n=0$, $Y_0=R$), Warburg impedance ($n=0.5$, $Y_0=W$), or inductance ($n=-1$, $Y_0=L$).

The electrochemical impedance parameters for mild steel corrosion in 1.0 M HCl and 1.0 M H₂SO₄ in the absence and presence of the studied quinoxalines are illustrated in Tables 4.21 and 4.22, respectively. The introduction of KI in the H₂QCA system tremendously improved the performance of the inhibitor. These tables show a directly proportional relation in the inhibition efficiencies of MQ6CA, Q6CA, and H₂QCA with KI and the magnitude of the R_{ct} values. This may be ascribed to the increase in the concentration of the studied inhibitors which leads to an increase in the surface coverage of adsorptive quinoxalines mild steel surface, consequently forming a protective layer that retards the extent of acid species attack. Furthermore, the tables also reveal that the decrease in the CPE values is associated with the increasing values of R_{ct} . This may be due to the decrease in local dielectric constant or perhaps an increase in the thickness of the electrical double which is indicative that the quinoxalines molecules electrostatically adsorbed on mild steel surface [325]. The values of CPE deviation exponent (n) range from 0.628 – 0.933, close to the unit, which indicates that as the concentration of the inhibitors were increased, mild steel surface became more and more homogeneous. This was also reported by Solmaz and co-workers [340]. The results obtained from EIS were reasonably in agreement with those of PDP.

4.2.6 Atomic absorption spectroscopy

Graphite furnace atomic absorption spectroscopy (GFAAS) was utilized to determine the concentration of the iron ions dissolved in the mild steel in 1.0 M HCl and 1.0 M H₂SO₄ solutions in the absence and presence of the studied quinoxalines after weight loss measurements. A calibration curve of iron ions was constructed from chosen five concentrations (2 – 10 ppm) before the analysis of the samples. Absorbance was determined at each standard concentration, which enables the construction of the calibration curve shown in figure 4.80. The concentration of all the samples containing iron ions were calculated from the absorbance values and obtained calibration curve through the relationship given by equation (55). The results obtained are presented in Tables 4.22 and 4.23.

$$Y = 0.1438X - 0.0066 \quad (55)$$

where Y is the absorbance and X is concentration (ppm)

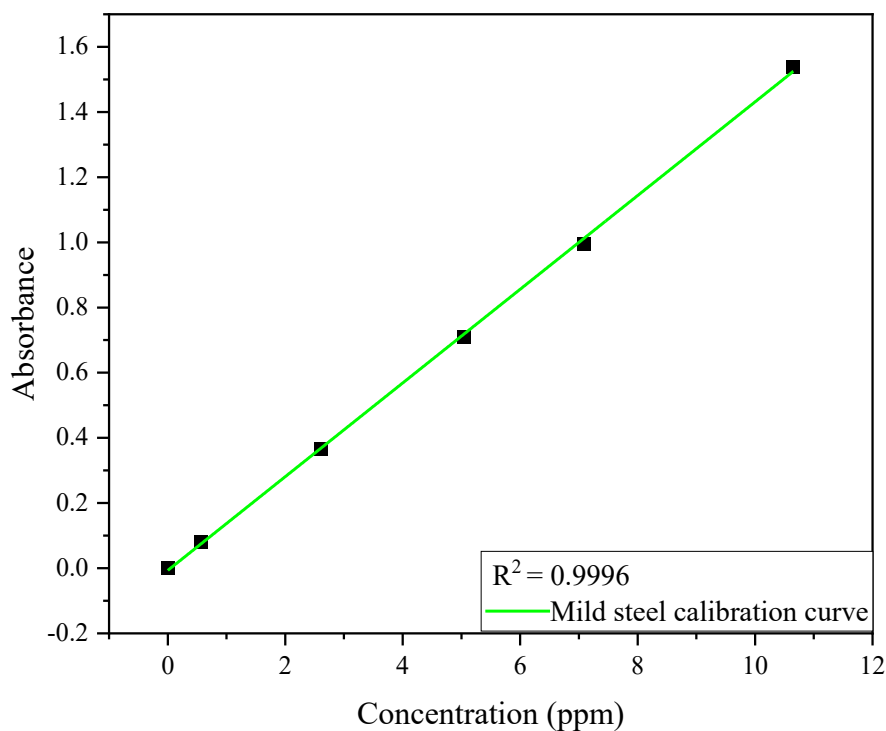


Figure 4.80: Absorbance against concentration calibration curve for mild steel.

The percentage inhibition efficiency ($\%IE_{AAS}$) of MQ6CA, Q6CA, and H2QCA was evaluated by measuring the mild steel ion in the solution with and without the inhibitors using the equation (56).

$$\%IE_{AAS} = \frac{C_{blank} - C_{inh}}{C_{blank}} \quad (56)$$

where C_{blank} and C_{inh} are the concentrations of mild steel ions in the absence and presence of the studied quinoxalines, respectively.

Table 4.23: Amount of dissolved mild steel present in 1.0 M HCl in the absence and presence of the studied quinoxalines.

Inhibitors	Mean absorbance	Concentration (ppm)	%IE _{AAS}
Blank	1.128	7.889	-
MQ6CA	0.184	1.323	83.23
Q6CA	0.223	1.598	79.74
H2QCA	0.536	3.771	52.20

Table 4.24: Amount of dissolved mild steel present in 1.0 M H₂SO₄ in the absence and presence of the studied quinoxalines.

Inhibitors	Mean absorbance	Concentration (ppm)	%IE _{AAS}
Blank	1.390	9.710	-
MQ6CA	0.374	2.648	72.73
Q6CA	0.429	3.001	69.09
H2QCA	0.688	4.832	50.24

Tables 4.23 and 4.24 reveal that in the blank solutions, the concentration of mild steel ions are relatively higher as compared to solutions when the quinoxalines were introduced. The decreases in the mild steel ions concentration on the inhibited solutions can be attributed to the availability of the adsorbing inhibitor molecules which forms a protective layer on mild steel surface, blocking the acids from further oxidation the metal. As seen in the weight loss measurement, this clearly shows that MQ6CA, Q6CA, and H2QCA protects mild steel from the corrosive media. The inhibition efficiencies were to vary in the order: MQ6CA>Q6CA>H2QCA. A similar order was observed in the weight loss measurements. Furthermore, the inhibition efficiency values obtained in this technique were lower than from weight loss measurements.

4.2.7 Fourier Transform Infrared Spectroscopy (FTIR)

The FTIR technique is an effective tool that has been utilized widely in studying the adsorption film resulting during the adsorption process [341]. In this study, FTIR was employed to gain more insight into the studied quinoxalines inhibitor's interaction with the mild steel surface in 1.0 M HCl and 1.0 M H₂SO₄. The FTIR spectra of the pure quinoxalines were compared to the adsorption film formed spectra that was scratched from the metal surface after weight loss measurements and are presented in figures 4.81 – 4.86. Quinoxalines exhibits several heteroatoms such as O and N, functional groups that have electron density. Reports in literature suggest that adsorption film between the vacant *d*-orbitals of metal and the inhibitor molecules is likely to form within these functional groups [299]. These functional groups together with their corresponding characteristic adsorption peaks from FTIR spectra of the studied quinoxalines in 1.0 M HCl and 1.0 M H₂SO₄ are presented in Tables 4.25 and 4.26, respectively.

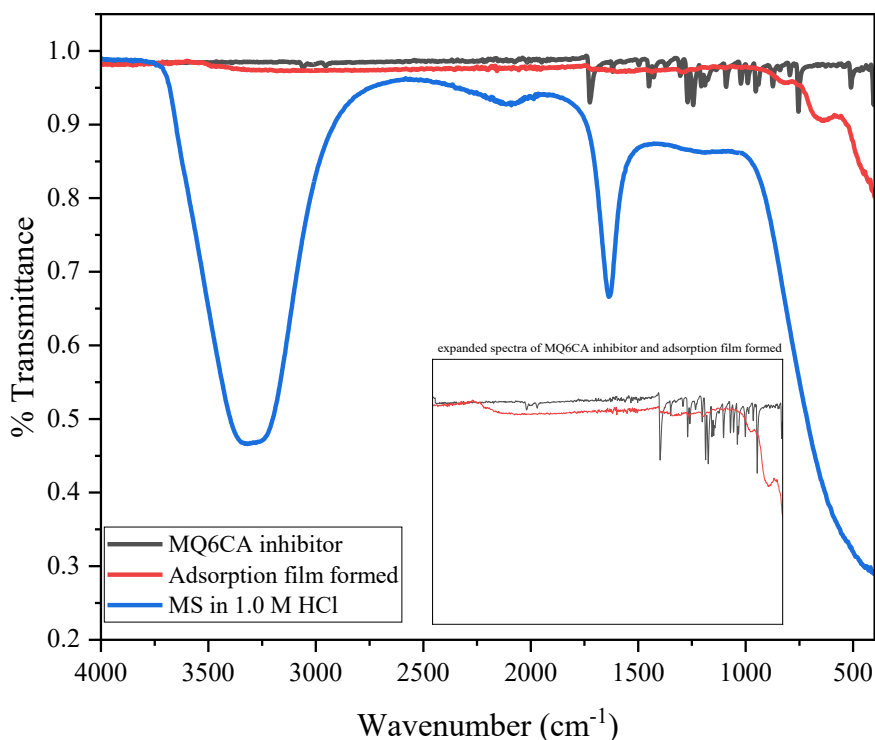


Figure 4.81: FTIR spectra of pure MQ6CA and the adsorption film formed on mild steel surface in 1.0 M HCl in the presence of MQ6CA.

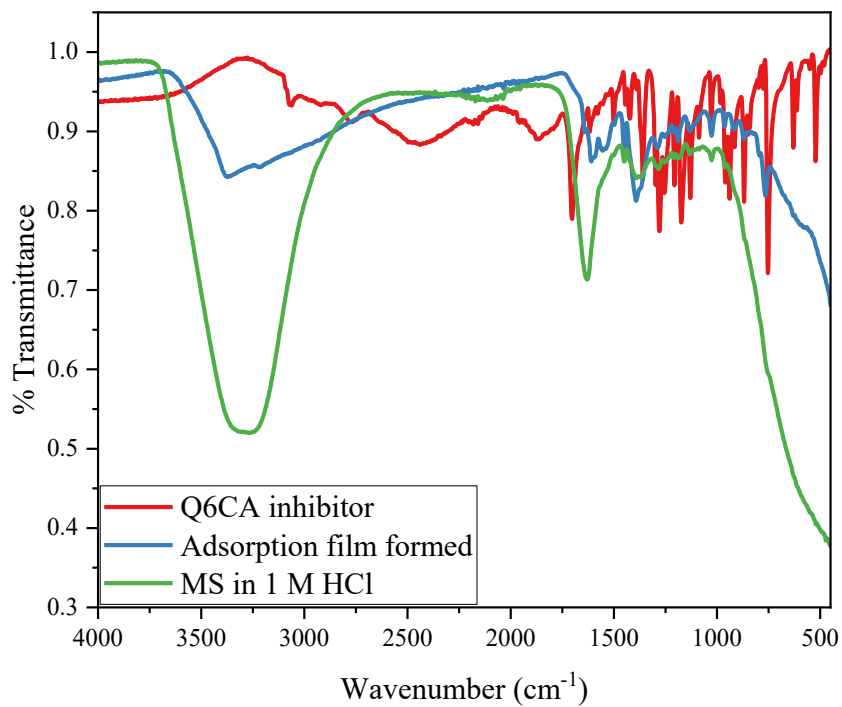


Figure 4.82: FTIR spectra of pure Q6CA and the adsorption film formed on mild steel surface in 1.0 M HCl in the presence of Q6CA.

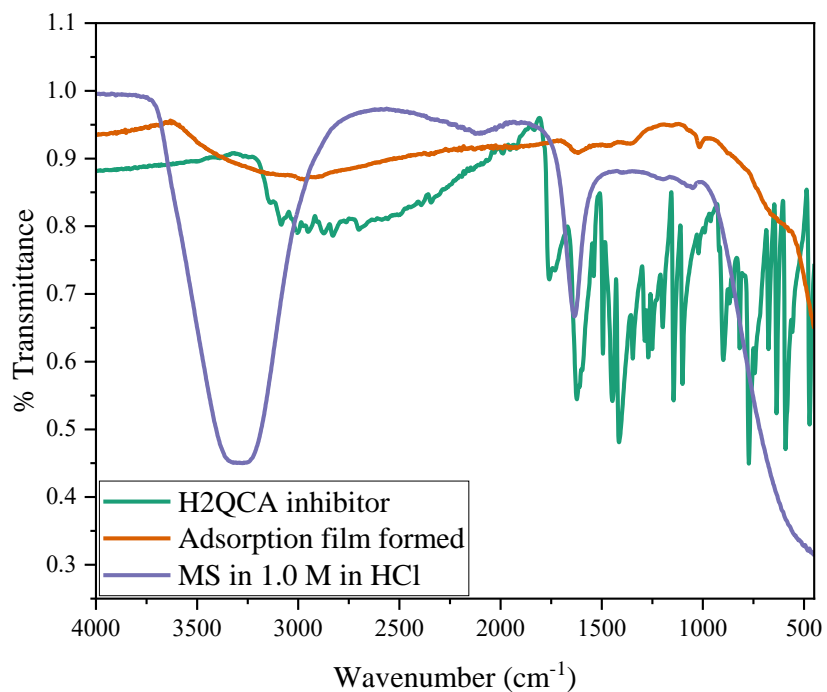


Figure 4.83: FTIR spectra of pure H2QCA and the adsorption film formed on mild steel surface in 1.0 M HCl in the presence of H2QCA.

Table 4.25: Peaks and identification from FTIR spectra of the studied quinoxalines and adsorption film formed on the mild steel in 1.0 M HCl.

Inhibitor-Mild steel	Functional Groups						
	Peaks from FTIR spectra (cm ⁻¹)						
	C=O	C-O	C-N	C=C	Aromatic C-H	O-H	γ-Fe ₂ O ₃
MQC6A	1717.89	1084.84	1271.78	1450.33	-	-	-
MQ6CA-MS	-	-	-	-	-	-	669.70
Q6CA	1706.61	1021.13	1276.07	-	3077.57	-	-
Q6CA-MS	1615.95	-	-	1404.95	-	3372.16	-
H2QCA	1719.22	-	1341.21	1457.35	3125.72	-	-
H2QCA-MS	-	-	-	-	-	3318.33	-

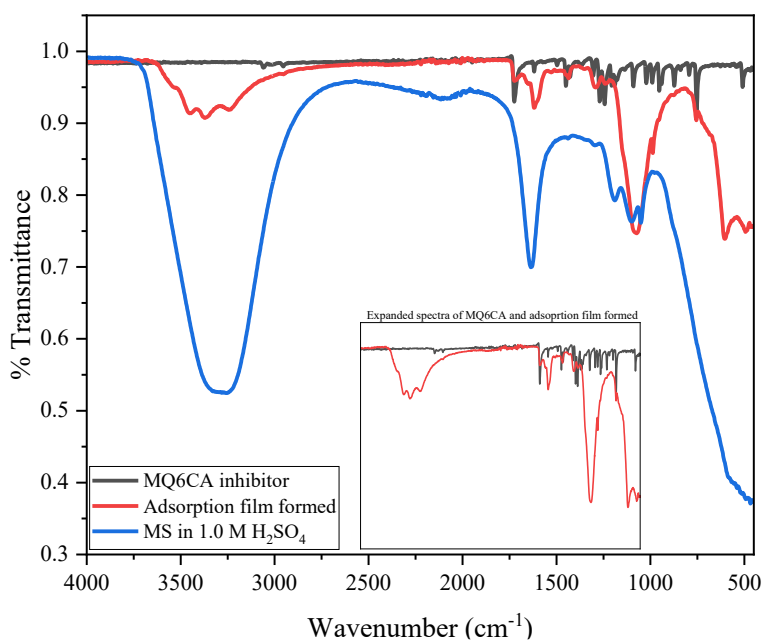


Figure 4.84: FTIR spectra of pure MQ6CA and the adsorption film formed on mild steel surface in 1.0 M H₂SO₄ in the presence of MQ6CA.

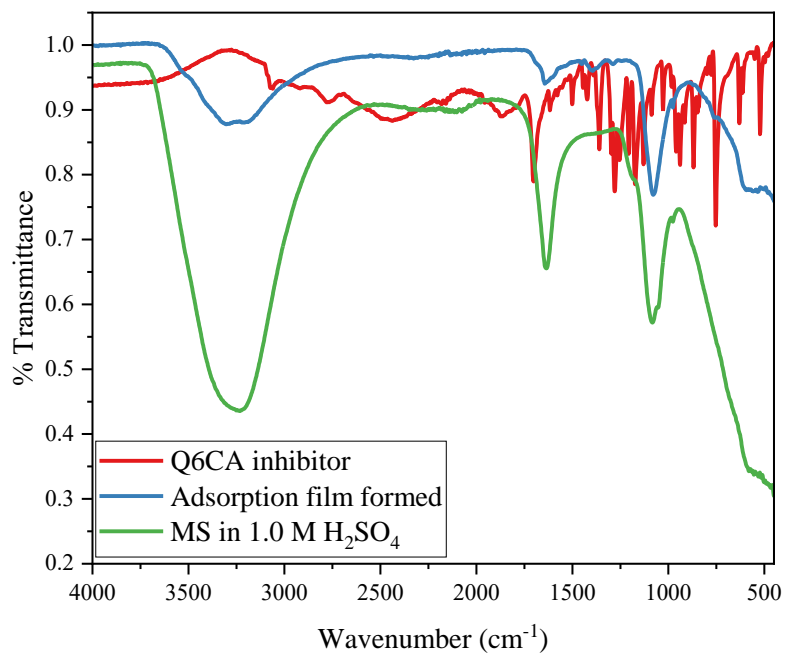


Figure 4.85: FTIR spectra of pure Q6CA and the adsorption film formed on mild steel surface in 1.0 M H₂SO₄ in the presence of Q6CA.

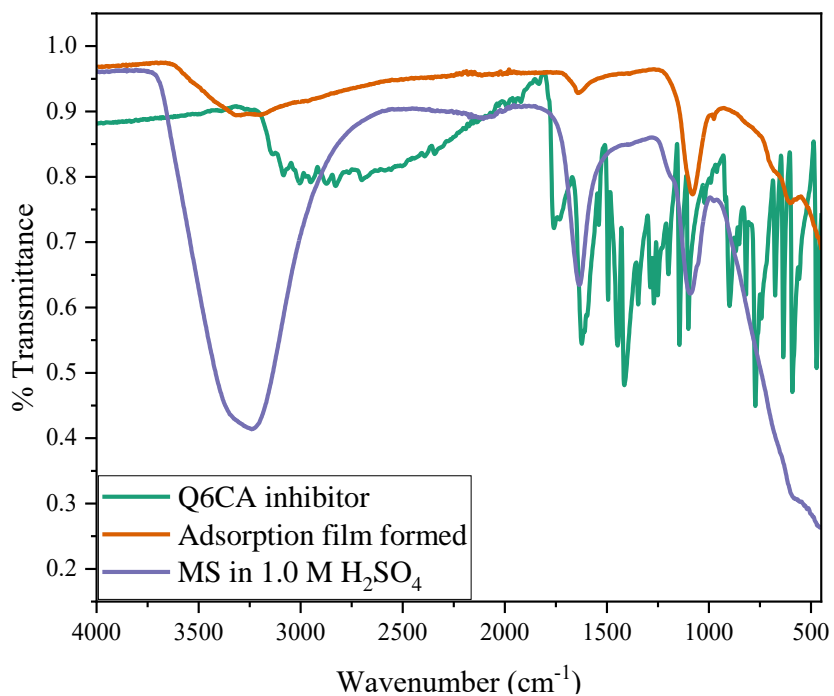


Figure 4.86: FTIR spectra of pure H₂QCA and the adsorption film formed on mild steel surface in 1.0 M H₂SO₄ in the presence of H₂QCA.

Table 4.26: Peaks and identification from FTIR spectra of the studied quinoxalines and adsorption film formed on the mild steel in 1.0 M H₂SO₄.

Inhibitor-Mild steel	Functional Groups						
	Peaks from FTIR spectra (cm ⁻¹)						
	C=O	C–O	C–N	C=C	Aromatic C–H	O–H	γ-Fe ₂ O ₃
MQC6A	1719.31	1089.09	1270.37	1450.21	-	-	-
MQ6CA-MS	-	1083.42	-	1443.15	-	3357.90	611.84
Q6CA	1705.20	1084.67	1276.07	-	-	-	-
Q6CA-MS	1651.40	1089.12	-	-	-	3302.00	610.42
H2QCA	1720.11	1084.12	1270.41	-	-	-	-
H2QCA-MS	-	1066.46	-	-	-	3339.58	625.99

Peaks corresponding to the stretching carbonyl C=O bond were observed at a range of 1720 – 1706 cm⁻¹ in all the studied quinoxalines. Strong peaks within wavelength range of 1085 – 1050 cm⁻¹ corresponding to the C–O stretch, 1342 – 1266 cm⁻¹ to C–N stretch, around 1600 – 1400 cm⁻¹ to conjugate C=C stretch, 3200 – 3000 cm⁻¹ to aromatic C–H stretch, 3300 – 2500 to O–H stretching [274]. A signal at around 670 cm⁻¹ corresponding to γ-Fe₂O₃. A similar discussion was utilized from all the studies quinoxalines as shown in figures 4.81 – 4.86 and presented in Tables 4.25 and 4.26. Inspection of the figures and tables, it can be seen that there was a disappearance of C=O peaks in the MQ6CA and H2QCA-Fe²⁺ spectra and a shift of peaks from 1706.61 cm⁻¹ to 1615.95 cm⁻¹ and 1705.20 cm⁻¹ to 1651.40 cm⁻¹ in the Q6CA-Fe²⁺ spectra in 1.0 M HCl and 1.0 H₂SO₄, respectively. The O atoms in this functional group could be responsible for donating the lone pairs to fill the partial or vacant *d*-orbital of the mild steel and thereby forming a chemical bond that could retard the corrosion rate of mild steel [7]. There was also a disappearance and shifts in the C–O and C–N in the inhibitor-Fe²⁺ complex spectra. An interesting observation was the new peak that appeared O–H peak at around 3300 cm⁻¹ for. The γ-Fe₂O₃ peak appeared in the MQ6CA- Fe²⁺

complex spectra in 1.0 M HCl, and in all the inhibitor-Fe²⁺ complex spectra in 1.0 M H₂SO₄. Literature suggests that this peak is indicative of a formation of iron oxide layers (γ -Fe₂O₃) which can further retard the rate of corrosion of mild steel [342–344]. Furthermore, the remarkable difference between the spectra of the pure studied quinoxalines and the adsorption film formed after immersion of mild steel in 1.0 M HCl and 1.0 M H₂SO₄ indicates that some chemical interaction occurred between the inhibitor molecules and the mild steel surface.

4.3 ZINC

4.3.1 Weight loss in the absence and presence of corrosion inhibitors

The weight loss of zinc in the absence and presence of various concentrations of MQ6CA, Q6CA, and H2QCA with and without KI in 1.0 M HCl and 1.0 M H₂SO₄ at various temperature of 303 – 333 K were studied. The data obtained are graphically presented in figures 4.87 – 4.94 and in Tables 4.27 and 4.28. MQ6CA and Q6CA were investigated at various concentrations of 0.5×10^{-3} , 1.0×10^{-3} , 2.0×10^{-3} , 3.0×10^{-3} , and 4.0×10^{-3} M for both acids. H2QCA was investigated at various concentration of 5.0×10^{-3} , 6.0×10^{-3} , 7.0×10^{-3} , 8.0×10^{-3} , and 9.0×10^{-3} M addition of potassium iodide (0.005 M) in the solution.

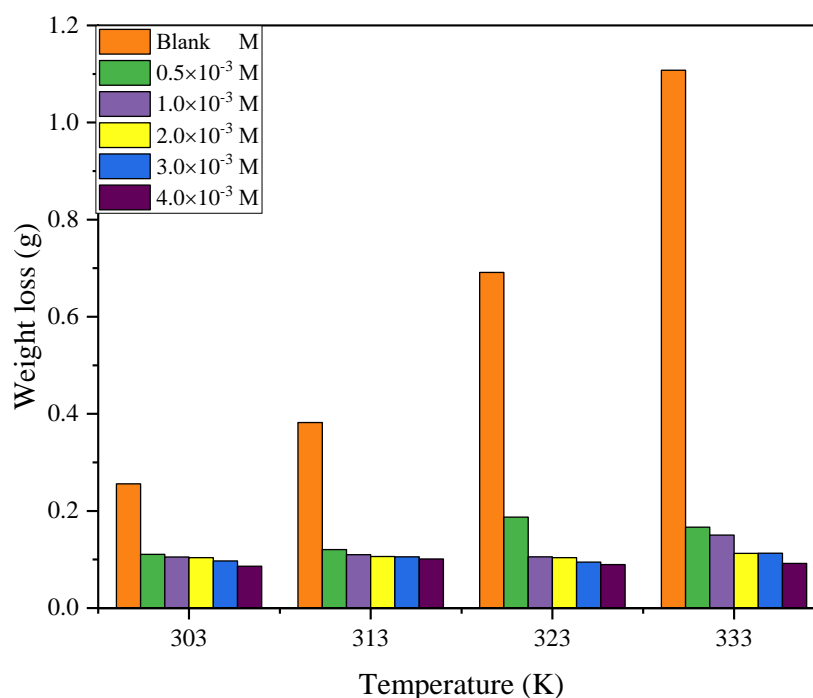


Figure 4.87: Weight loss measurements of zinc in the absence and presence of MQ6CA in 1.0 M HCl at different temperatures.

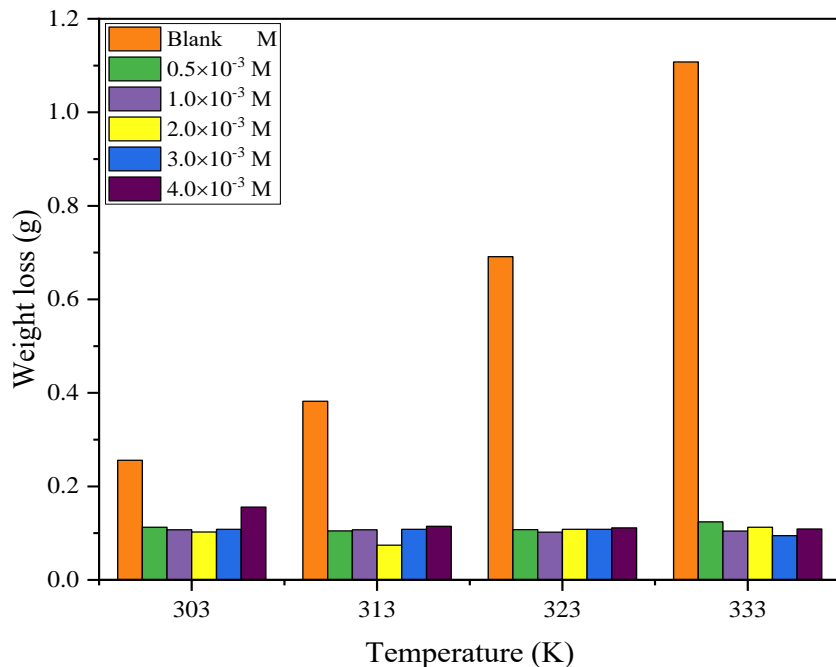


Figure 4.88: Weight loss measurements of zinc in the absence and presence of Q6CA in 1.0 M HCl at different temperatures.

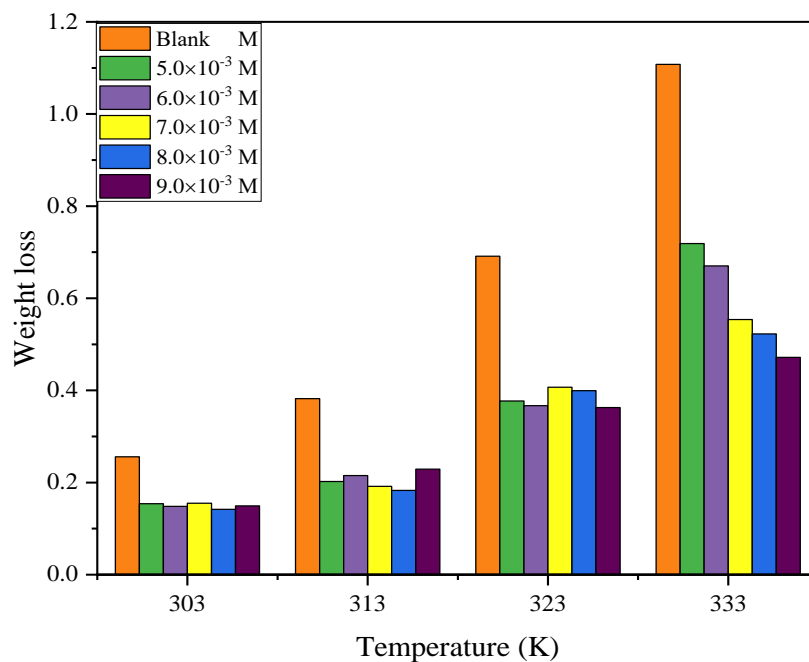


Figure 4.89: Weight loss measurements of zinc in the absence and presence of H2QCA without KI in 1.0 M HCl at different temperatures.

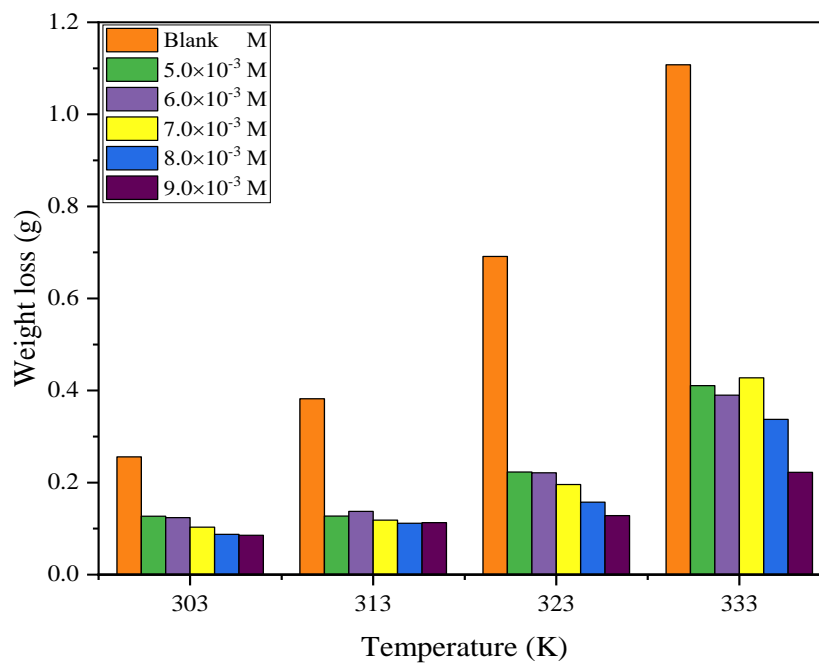


Figure 4.90: Weight loss measurements of zinc in the absence and presence of H₂QCA with KI in 1.0 M HCl at different temperatures.

Table 4.27: Weight loss measurements of in the absence and presence of MQ6CA, Q6CA and H2QCA in 1.0 M HCl obtained at different temperatures.

Inhibitor	Concentration ($\times 10^{-3}$ M)	Weight loss (g)			
		303 K	313 K	323 K	333 K
	0.000	0.2558	0.3832	0.6913	1.1077
MQ6CA	0.5	0.1105	0.1206	0.1874	0.1666
	1.0	0.1053	0.1101	0.1054	0.1502
	2.0	0.1038	0.1061	0.1040	0.1128
	3.0	0.0969	0.1054	0.0948	0.1129
	4.0	0.0861	0.1013	0.0896	0.0920
Q6CA	0.5	0.1126	0.1047	0.1075	0.1243
	1.0	0.1072	0.1073	0.1021	0.1044
	2.0	0.1025	0.0745	0.1082	0.1128
	3.0	0.1084	0.1084	0.1083	0.0948
	4.0	0.1556	0.1148	0.1112	0.1091
H2QCA without KI	5.0	0.1540	0.2022	0.3771	0.7188
	6.0	0.1483	0.2151	0.3670	0.6703
	7.0	0.1552	0.1916	0.4070	0.5539
	8.0	0.1420	0.1829	0.3994	0.5225
	9.0	0.1492	0.2292	0.3629	0.4718
H2QCA with KI	5.0	0.1269	0.1271	0.2229	0.4108
	6.0	0.1240	0.1375	0.2212	0.3900
	7.0	0.1031	0.1185	0.1958	0.4275
	8.0	0.0874	0.1115	0.1575	0.3375
	9.0	0.0855	0.1130	0.1282	0.2224

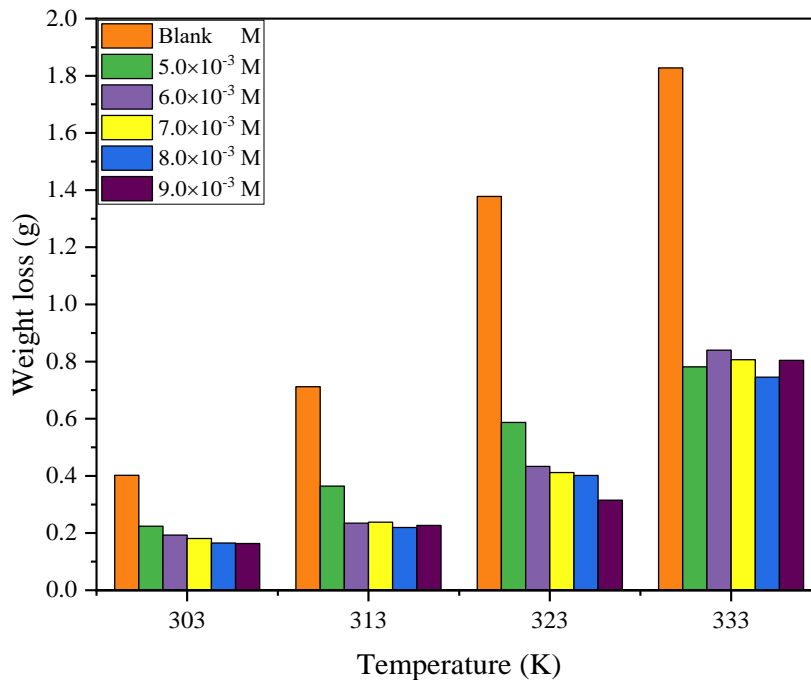


Figure 4.91: Weight loss measurements of zinc in the absence and presence of MQ6CA in 1.0 M H_2SO_4 at different temperatures.

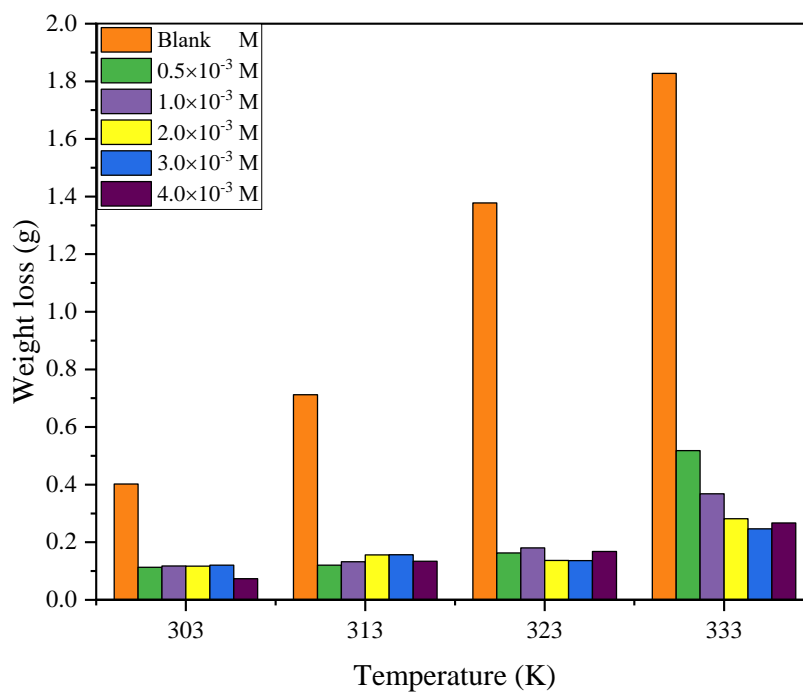


Figure 4.92: Weight loss measurements of zinc in the absence and presence of Q6CA in 1.0 M H_2SO_4 at different temperatures.

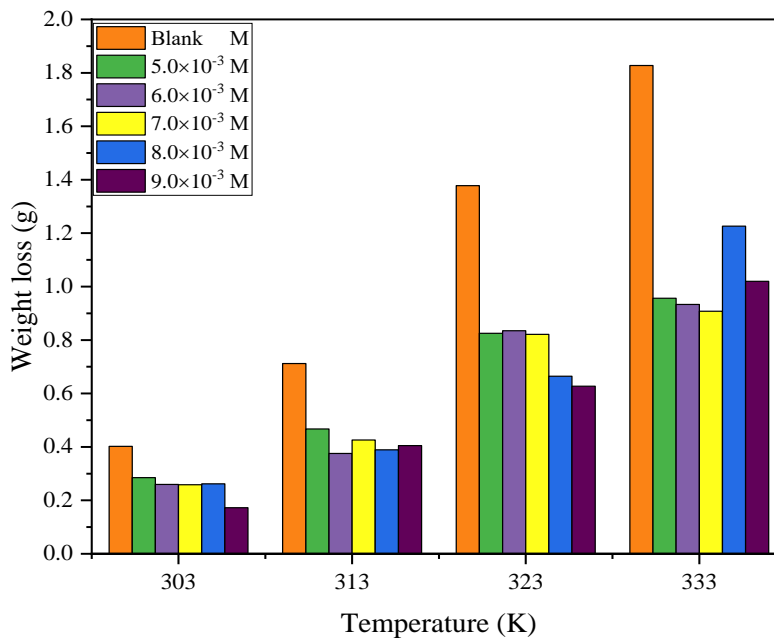


Figure 4.93: Weight loss measurements of zinc in the absence and presence of H2QCA without KI in 1.0 M H₂SO₄ at different temperatures.

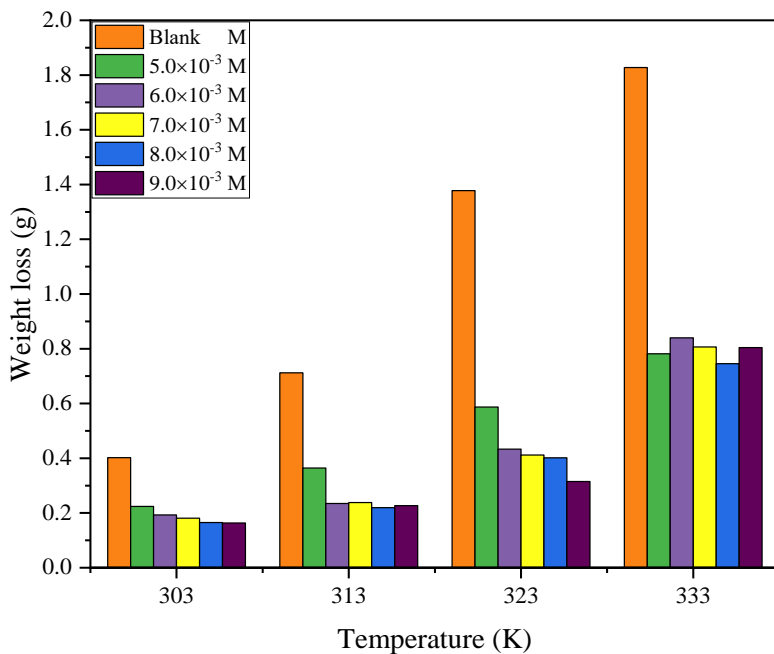


Figure 4.94: Weight loss measurements of zinc in the absence and presence of H2QCA with KI in 1.0 M H₂SO₄ at different temperatures.

Table 4.28: Weight loss measurements of zinc in the absence and presence of MQ6CA, Q6CA and H2QCA in 1.0 M H₂SO₄ obtained at different temperatures.

Inhibitor	Concentration ($\times 10^{-3}$ M)	Weight loss (g)			
		303 K	313 K	323 K	333 K
	0.000	0.4022	0.7123	1.3779	1.8276
MQ6CA	0.5	0.1147	0.1878	0.1760	0.1844
	1.0	0.1101	0.1294	0.1752	0.1815
	2.0	0.1101	0.1234	0.1660	0.1802
	3.0	0.1096	0.1196	0.1582	0.1694
	4.0	0.1004	0.1125	0.1480	0.1661
Q6CA	0.5	0.1134	0.1205	0.1630	0.5179
	1.0	0.1179	0.1322	0.1804	0.3680
	2.0	0.1170	0.1562	0.1370	0.2819
	3.0	0.1203	0.1567	0.1364	0.2467
	4.0	0.0736	0.1340	0.1682	0.2672
H2QCA without KI	5.0	0.2849	0.4672	0.8251	0.9567
	6.0	0.2594	0.3755	0.8350	0.9335
	7.0	0.2586	0.4261	0.8212	0.9080
	8.0	0.2616	0.3890	0.6647	1.2261
	9.0	0.1726	0.4048	0.6275	1.0200
H2QCA with KI	5.0	0.2240	0.3641	0.5873	0.7817
	6.0	0.1927	0.2350	0.4333	0.8400
	7.0	0.1810	0.2379	0.4119	0.8065
	8.0	0.1649	0.2197	0.4015	0.7453
	9.0	0.1636	0.2269	0.3152	0.8041

It is clear from the figures 4.87 – 4.94 that the weight loss of zinc drastically decreased as the concentration of the studied quinoxalines was increased. The Tables 4.27 and 4.28 reveal that weight loss values of zinc remarkably decreased in presence of the inhibitors as compared to in the blank solution (for both acids). For instance, in Table 4.27, the values of weight loss of zinc for the blank test were obtained to be 0.2558 g, 0.3832 g, 0.6913 g, and 1.1077 g at the temperatures of 303 K, 313 K, 323 K, and 333 K, respectively, in comparison to tests with an introduction of 0.5×10^{-3} M Q6CA which the weight loss of zinc was obtained to be 0.1126 g, 0.1047 g, 0.1075 g, and 0.1243 g at the temperature of 303 K, 313 K, 323 K, and 333 K, respectively. Inspection of these tables reveals that the addition of KI in H2QCA system tremendously reduced the weight loss of zinc in 1.0 M HCl and 1.0 M H₂SO₄. For instance, in Table 4.28, the concentration of 9.0×10^{-3} M H2QCA with KI, the weight loss of zinc was found to increase from 0.1726 g, 0.4048 g, 0.6275, then 1.0200 g at 303 K, 313 K, 323 K, and 333 K, respectively. However, in the presence of KI values enormously reduced to 0.1636 g, 0.2269 g, 0.3152 g, then 0.8041 g at the temperature of 303 K, 313 K, 323 K, and 333 K, respectively. A similar trend was also observed in all the studied concentrations of H2QCA, and also in Table 4.27. These findings are in agreement with fact that an increase in inhibitor concentration reduces the weight loss of zinc, eventually decreases the rate of corrosion [345]. Furthermore, these tables reveal that H₂SO₄ was more corrosive than HCl. This may be due to the fact that H₂SO₄ possesses a relatively higher concentration than HCl [294].

4.3.2 Corrosion rate and inhibition efficiency

The corrosion rate (C_R), surface coverage (θ), and percentage inhibition efficiency (% IE) obtained from weight loss measurement of zinc in 1.0 M HCl and 1.0 M H₂SO₄ in the absence and presence of various concentration of MQ6CA, Q6CA, and H₂QCA with and without KI at temperature 303 – 333 K are presented in the Tables 4.29 – 4.34 and figures 4.95 – 4.102.

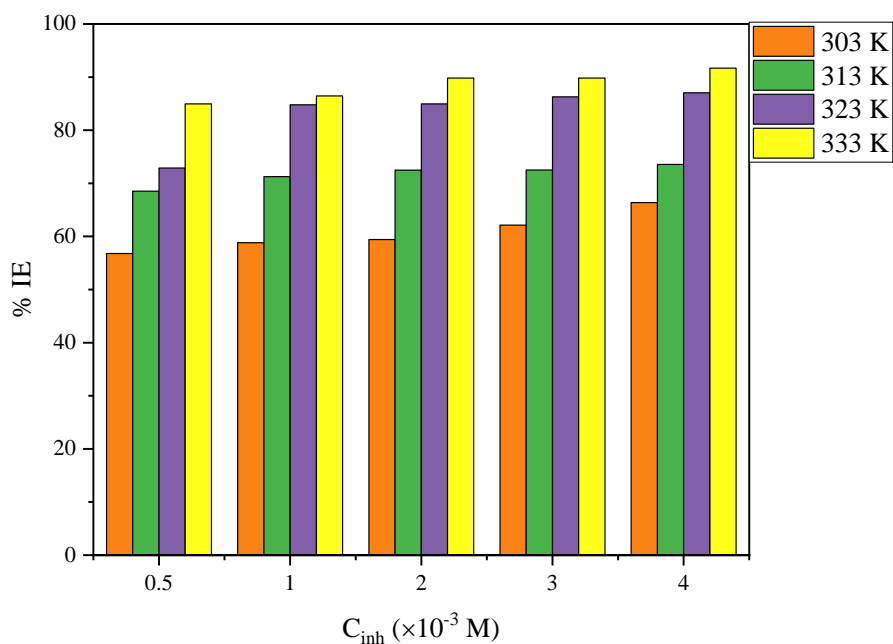


Figure 4.95: The variation of percentage inhibition efficiency with various concentration of MQ6CA at various temperatures in 1.0 M HCl.

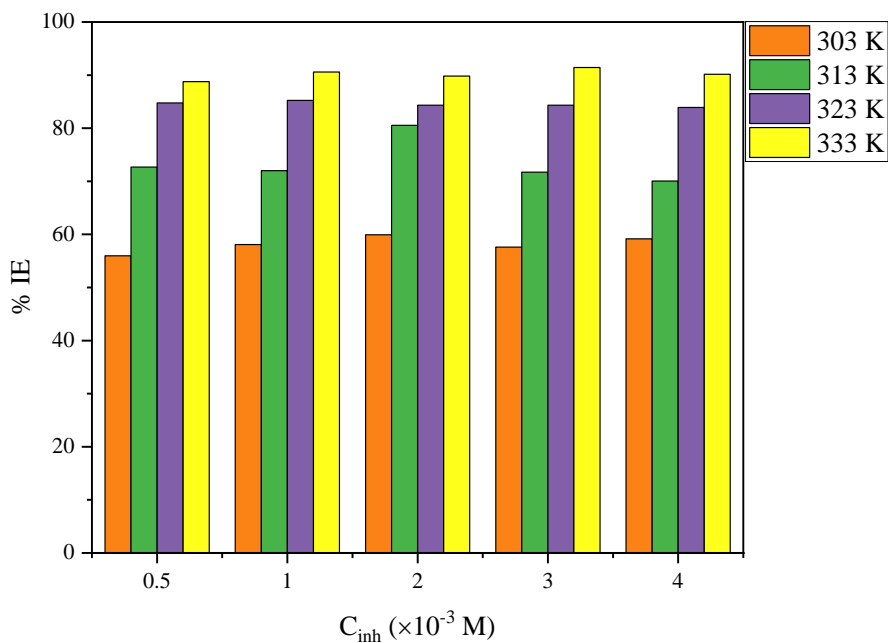


Figure 4.96: The variation of percentage inhibition efficiency with various concentration of Q6CA at various temperatures in 1.0 M HCl.

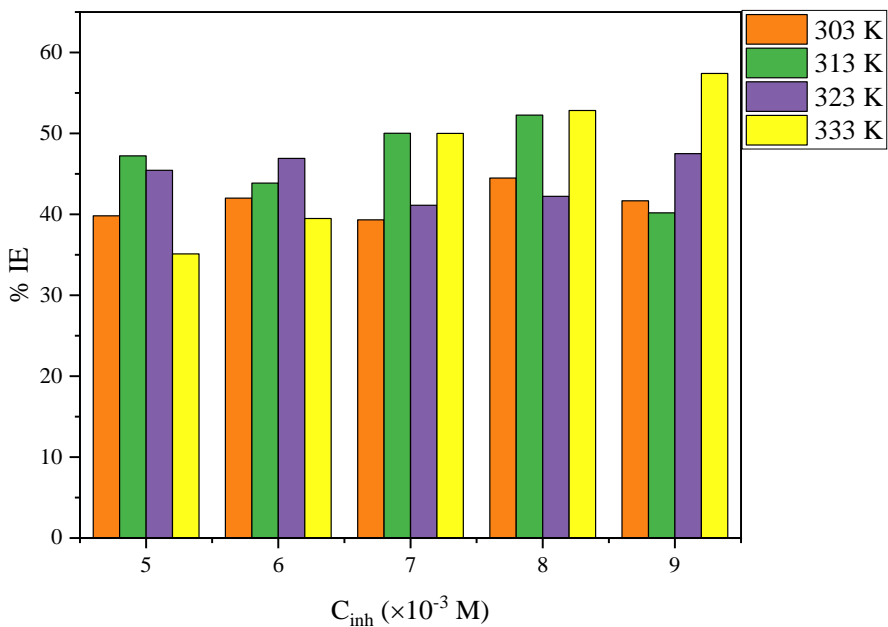


Figure 4.97: The variation of percentage inhibition efficiency with various concentration of H2QCA without KI at various temperatures in 1.0 M HCl.

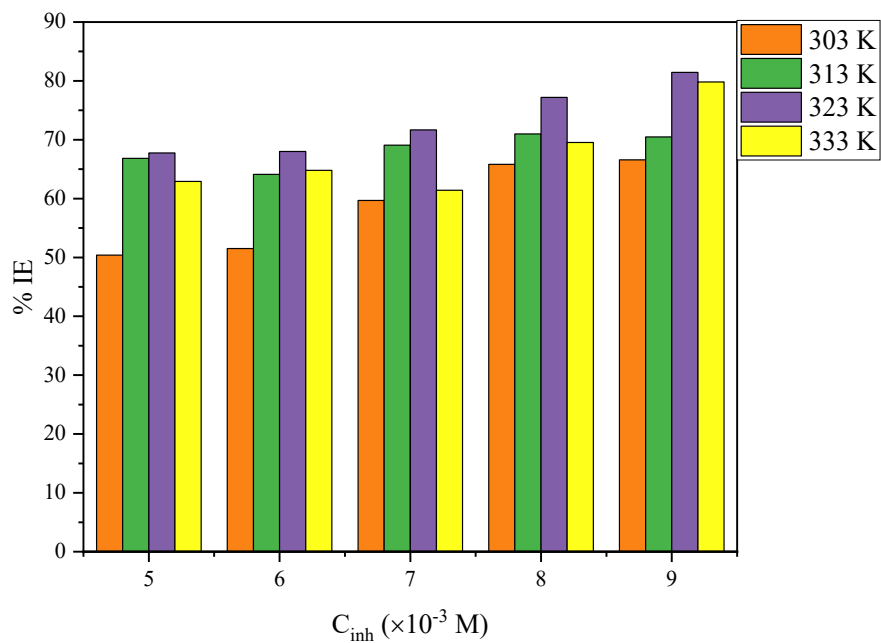


Figure 4.98: The variation of percentage inhibition efficiency with various concentration of H2QCA with KI at various temperatures in 1.0 M HCl.

Table 4.29: The corrosion parameters for zinc in 1.0 M HCl in the absence and presence of various concentrations of MQ6CA obtained from weight loss measurements at 303 – 333 K.

Inhibitor	Temperature (K)	Inhibior concentration ($\times 10^{-3}$ M)	Corrosion rate ($\text{g.cm}^{-2}.\text{h}^{-1}$)	Surface coverage (θ)	Inhibition efficiency (%)
MQ6CA	303	-	0.0060905	-	-
		0.5	0.0026310	0.5680	56.80
		1.0	0.0025071	0.5883	58.83
		2.0	0.0024714	0.5942	59.42
		3.0	0.0023071	0.6212	62.12
		4.0	0.0020500	0.6638	66.38
	313	-	0.0091238	-	-
		0.5	0.0028714	0.6852	68.52
		1.0	0.0026214	0.7127	71.27
		2.0	0.0025262	0.7249	72.49
		3.0	0.0025095	0.7250	72.50
		4.0	0.0024119	0.7356	73.56
	323	-	0.0164595	-	-
		0.5	0.0044619	0.7289	72.89
		1.0	0.0025095	0.8478	84.78
		2.0	0.0024762	0.8496	84.96
		3.0	0.0022571	0.8629	86.29
		4.0	0.0021333	0.8704	87.04
	333	-	0.0263738	-	-
		0.5	0.0039667	0.8496	84.96
		1.0	0.0035762	0.8644	86.44
		2.0	0.0026857	0.8981	89.81
		3.0	0.0026881	0.8982	89.82
		4.0	0.0021905	0.9169	91.69

Table 4.30: The corrosion parameters for zinc in 1.0 M HCl in the absence and presence of various concentrations of Q6CA obtained from weight loss measurements at 303 – 333 K.

Inhibitor	Temperature (K)	Inhibitor concentration ($\times 10^{-3}$ M)	Corrosion rate ($\text{g.cm}^{-2}.\text{h}^{-1}$)	Surface coverage (θ)	Inhibition efficiency (%)
Q6CA	303	-	0.0060904	-	-
		0.5	0.0026809	0.5598	55.98
		1.0	0.0025523	0.5808	58.08
		2.0	0.0024404	0.5992	59.92
		3.0	0.0258090	0.5762	57.62
		4.0	0.0037047	0.5917	59.17
	313	-	0.0091238	-	-
		0.5	0.0024928	0.7267	72.67
		1.0	0.0025547	0.7199	71.99
		2.0	0.0017738	0.8055	80.55
		3.0	0.0025809	0.7171	71.71
		4.0	0.0027333	0.7004	70.04
	323	-	0.0164595	-	-
		0.5	0.0025595	0.8444	84.44
		1.0	0.0024310	0.8523	85.23
		2.0	0.0025762	0.8434	84.34
		3.0	0.0025789	0.8433	84.33
		4.0	0.0026472	0.8391	83.91
	333	-	0.0263738	-	-
		0.5	0.0029595	0.8877	88.77
		1.0	0.0024857	0.9057	90.57
		2.0	0.0026857	0.8981	89.81
		3.0	0.0022571	0.9144	91.44
		4.0	0.0025976	0.9015	90.15

Table 4.31: The corrosion parameters for zinc in 1.0 M HCl in the absence and presence of various concentrations of H₂QCA with and without KI obtained from weight loss measurements at 303 – 333 K.

Inhibitor	Temperature (K)	Inhibior concentration ($\times 10^{-3}$ M)	Corrosion rate (g.cm ⁻² .h ⁻¹)	Surface coverage (θ)	Inhibition efficiency (%)
H ₂ QCA without KI	303	-	0.0060904	-	-
		5.0	0.0036667	0.3981	39.81
		6.0	0.0035310	0.4201	42.01
		7.0	0.0036952	0.3932	39.32
		8.0	0.0033810	0.4449	44.49
		9.0	0.0035523	0.4168	41.68
	313	-	0.0091238	-	-
		5.0	0.0481428	0.4722	47.22
		6.0	0.0051214	0.4386	43.86
		7.0	0.0045619	0.5001	50.01
		8.0	0.0043548	0.5227	52.27
		9.0	0.0054571	0.4019	40.19
	323	-	0.0164595	-	-
		5.0	0.0089787	0.4545	45.45
		6.0	0.0087380	0.4691	46.91
		7.0	0.0096048	0.4113	41.13
		8.0	0.0095095	0.4222	42.22
		9.0	0.0086405	0.4750	47.50
	333	-	0.0263738	-	-
		5.0	0.0171143	0.3511	35.11
		6.0	0.0231024	0.3949	39.49
		7.0	0.0138810	0.5000	50.00
		8.0	0.0124405	0.5283	52.83
		9.0	0.0112333	0.5741	57.41
303	-	0.0060904	-	-	
	5.0	0.0030214	0.5039	50.39	
	6.0	0.0029523	0.5152	51.52	
	7.0	0.0024548	0.5969	59.69	
	8.0	0.0020810	0.6581	65.81	
	9.0	0.0020357	0.6659	66.59	
	-	0.0091238	-	-	

H2QCA with KI	313	5.0	0.0030262	0.6683	66.83
		6.0	0.0032738	0.6411	64.11
		7.0	0.0028214	0.6907	69.07
		8.0	0.0026548	0.7098	70.98
		9.0	0.0026905	0.7049	70.49
	323	-	0.0164595	-	-
		5.0	0.0053071	0.6776	67.76
		6.0	0.0052667	0.6801	68.01
		7.0	0.0046619	0.7167	71.67
		8.0	0.00375	0.7721	77.21
		9.0	0.0030524	0.8145	81.45
	333	-	0.0263738	-	-
		5.0	0.0097810	0.6291	62.91
		6.0	0.0092857	0.6479	64.79
		7.0	0.0101786	0.6141	61.41
		8.0	0.0080357	0.6953	69.53
		9.0	0.0052952	0.7992	79.92

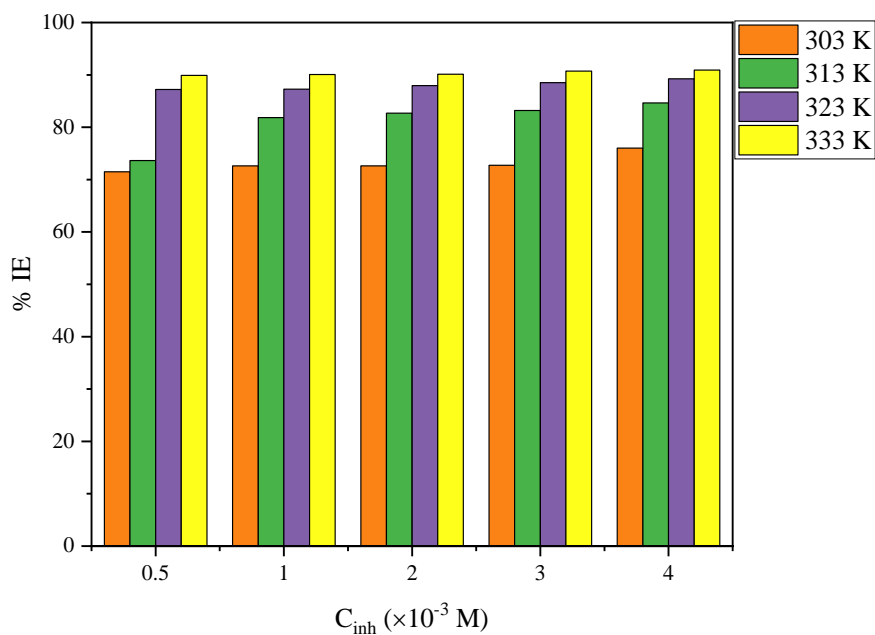


Figure 4.99: The variation of percentage inhibition efficiency with various concentration of MQ6CA at various temperatures in 1.0 M H₂SO₄.

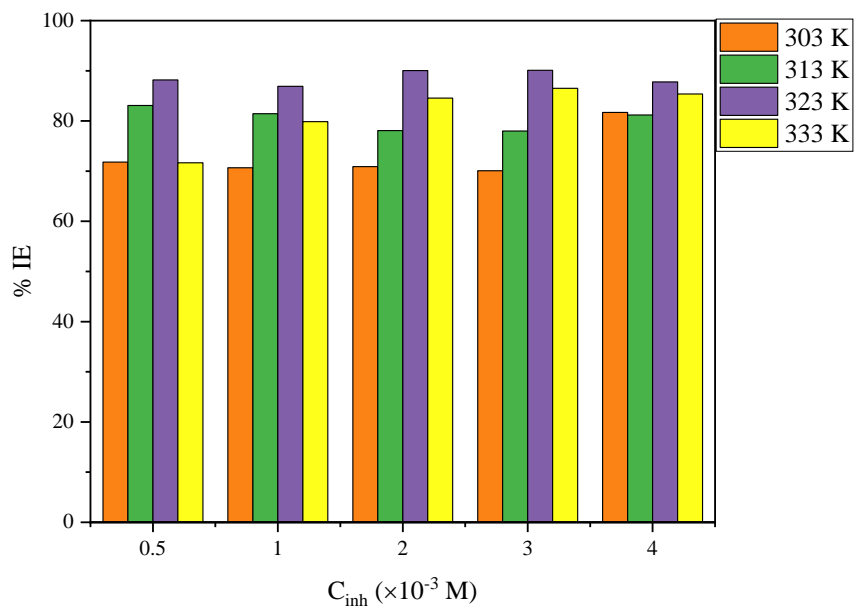


Figure 4.100: The variation of percentage inhibition efficiency with various concentration of Q6CA at various temperatures in 1.0 M H_2SO_4 .

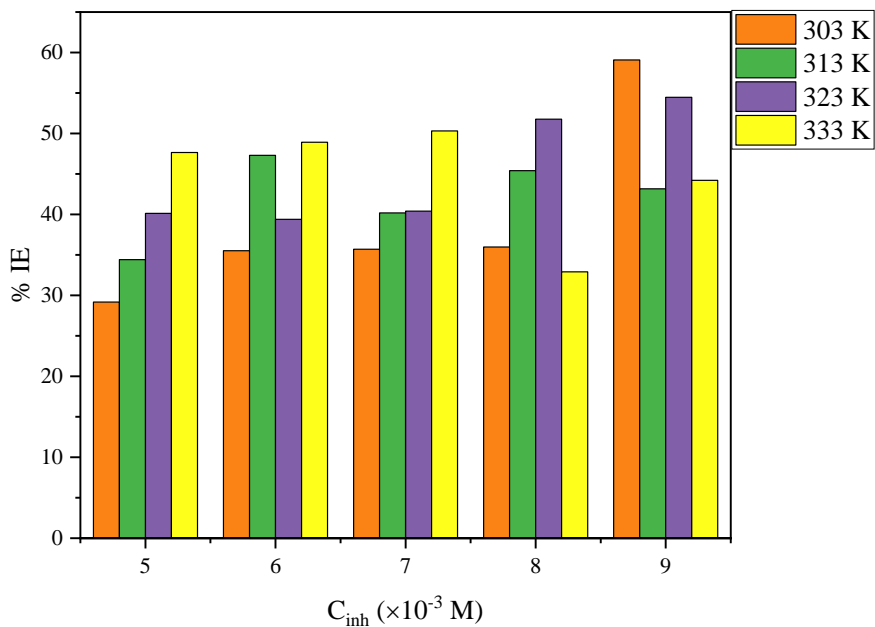


Figure 4.101: The variation of percentage inhibition efficiency with various concentration of H2QCA without KI at various temperatures in 1.0 M H_2SO_4 .

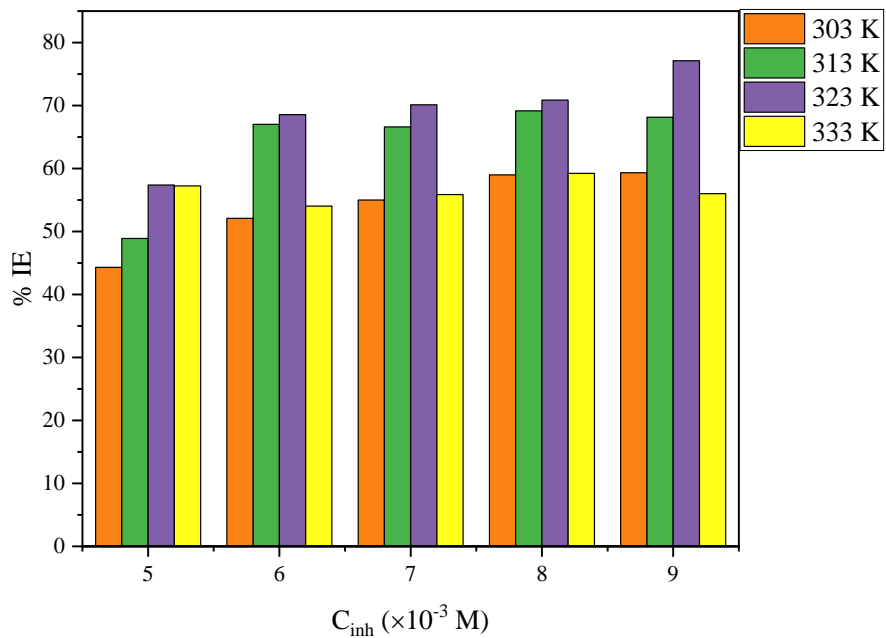


Figure 4.102: The variation of percentage inhibition efficiency with various concentration of H₂QCA with KI at various temperatures in 1.0 M H₂SO₄.

Table 4.32: The corrosion parameters for zinc in 1.0 M H₂SO₄ in the absence and presence of various concentrations of MQ6CA obtained from weight loss measurements at 303 – 333 K.

Inhibitor	Temperature (K)	Inhibior concentration ($\times 10^{-3}$ M)	Corrosion rate ($\text{g.cm}^{-2}.\text{h}^{-1}$)	Surface coverage (θ)	Inhibition efficiency (%)
MQ6CA	303	-	0.0095762	-	-
		0.5	0.0027310	0.7148	71.48
		1.0	0.0026214	0.7263	72.63
		2.0	0.0026214	0.7263	72.63
		3.0	0.0026095	0.7275	72.75
		4.0	0.0023905	0.7603	76.03
	313	-	0.0169595	-	-
		0.5	0.0447142	0.7363	73.63
		1.0	0.0030810	0.8183	81.83
		2.0	0.0029381	0.8268	82.68
		3.0	0.0028476	0.8321	83.21
		4.0	0.0026786	0.8463	84.63
	323	-	0.0328071	-	-
		0.5	0.0041905	0.8723	87.23
		1.0	0.0041714	0.8728	87.28
		2.0	0.0039524	0.8795	87.95
		3.0	0.0037667	0.8852	88.52
		4.0	0.0035238	0.8926	89.26
	333	-	0.0435142	-	-
		0.5	0.0043905	0.8991	89.91
		1.0	0.0043214	0.9007	90.07
		2.0	0.0042904	0.9014	90.14
		3.0	0.0040333	0.9073	90.73
		4.0	0.0039548	0.9091	90.91

Table 4.33: The corrosion parameters for zinc in 1.0 M H₂SO₄ in the absence and presence of various concentrations of Q6CA obtained from weight loss measurements at 303 – 333 K.

Inhibitor	Temperature (K)	Inhibior concentration ($\times 10^{-3}$ M)	Corrosion rate ($\text{g.cm}^{-2}.\text{h}^{-1}$)	Surface coverage (θ)	Inhibition efficiency (%)
Q6CA	303	-	0.0095762	-	-
		0.5	0.0027000	0.7180	71.80
		1.0	0.0028071	0.7068	70.68
		2.0	0.0027856	0.7090	70.90
		3.0	0.0028643	0.7008	70.08
		4.0	0.0017523	0.8170	81.70
	313	-	0.0169595	-	-
		0.5	0.0028690	0.8308	83.08
		1.0	0.0031476	0.8144	81.44
		2.0	0.0037190	0.7807	78.07
		3.0	0.0037309	0.7800	78.00
		4.0	0.0031905	0.8118	81.18
	323	-	0.0328000	-	-
		0.5	0.0038810	0.8817	88.17
		1.0	0.0042952	0.8690	86.90
		2.0	0.0032619	0.9005	90.05
		3.0	0.0032476	0.9010	90.10
		4.0	0.0040047	0.8779	87.79
	333	-	0.0435142	-	-
		0.5	0.0181238	0.7166	71.66
		1.0	0.0130476	0.7986	79.86
		2.0	0.0090857	0.8457	84.57
		3.0	0.0059100	0.8650	86.50
		4.0	0.0062904	0.8539	85.39

Table 4.34: The corrosion parameters for zinc in 1.0 M H₂SO₄ in the absence and presence of various concentrations of H₂QCA with and without KI obtained from weight loss measurements at 303 – 333 K.

Inhibitor	Temperature (K)	Inhibitor concentration ($\times 10^{-3}$ M)	Corrosion rate ($\text{g}\cdot\text{cm}^{-2}\cdot\text{h}^{-1}$)	Surface coverage (θ)	Inhibition efficiency (%)
H ₂ QCA without KI	303	-	0.0095762	-	-
		5.0	0.0067833	0.2917	29.17
		6.0	0.0061762	0.3551	35.51
		7.0	0.0061571	0.3570	35.70
		8.0	0.0062286	0.3497	34.97
		9.0	0.0041095	0.5908	59.08
	313	-	0.0169595	-	-
		5.0	0.0111238	0.3441	34.41
		6.0	0.0089405	0.4729	47.29
		7.0	0.0101452	0.4018	40.18
		8.0	0.0092619	0.4540	45.40
		9.0	0.0096381	0.4317	43.17
	323	-	0.0328000	-	-
		5.0	0.0196452	0.4012	40.12
		6.0	0.0198810	0.3940	39.40
		7.0	0.0195524	0.4040	40.40
		8.0	0.0158262	0.5176	51.76
		9.0	0.0149405	0.5446	54.46
	333	-	0.0435142	-	-
		5.0	0.0227786	0.4765	47.65
		6.0	0.0222262	0.4892	48.92
		7.0	0.0216190	0.5032	50.32
		8.0	0.0291929	0.3291	32.91
		9.0	0.0242857	0.4421	44.21
KI	303	-	0.0095762	-	-
		5.0	0.0053330	0.4431	44.31
		6.0	0.0045881	0.5210	52.10
		7.0	0.0043095	0.5499	54.99
		8.0	0.0039262	0.5900	59.00
		9.0	0.0038952	0.5932	59.32
	313	-	0.0169595	-	-
		5.0	0.0139833	0.4889	48.89

H2QCA with KI	313	6.0	0.0055952	0.6701	67.01
		7.0	0.0056643	0.6660	66.60
		8.0	0.0052310	0.6916	69.16
		9.0	0.0054024	0.6815	68.15
	323	-	0.0328000	-	-
		5.0	0.0139833	0.5738	57.38
		6.0	0.0103167	0.6855	68.55
		7.0	0.0098071	0.7011	70.11
		8.0	0.0095595	0.7086	70.86
		9.0	0.0075048	0.7712	77.12
	333	-	0.0435142	-	-
		5.0	0.0186119	0.5723	57.23
		6.0	0.0200000	0.5404	54.04
		7.0	0.0192024	0.5587	55.87
		8.0	0.0177452	0.5922	59.22
		9.0	0.0191452	0.5600	56.00

It is evident from these tables that the corrosion rate of zinc in the absence of the inhibitors was relatively high at all the studied temperatures. However, after introducing the three quinoxalines in the corrosion medium, the corrosion rate decreased. Tables 4.29 and 4.32 reveal that the percentage inhibition efficiency increased with increase in concentration of MQ6CA at all temperature. Moreover, the inhibition efficiency values of this compound are observed to increase with temperature of the corrosive environment. Table 4.29 show that the inhibition efficiency for MQ6CA was attained at concentration of 4×10^{-3} M. A similar trend was observed in Table 4.32. This can be ascribed to the availability of preferential adsorption inhibitor molecules at the metal/solution interface as the concentration is increased. Furthermore, the inhibition efficiency of this compound in 1.0 M HCl and 1.0 M H₂SO₄ was found to range from 56.80 – 91.69 % and 71.84 – 90.91 %, respectively.

The increase in inhibitor concentration is known to be associated with the reduction of corrosion rate and high inhibition efficiency values [300]. However, Tables 4.30 and 4.33 show no regular trend in the values of inhibition efficiency as the concentration of Q6CA and the temperature were increased. Although the tests were done in triplicates, no simple trend was observed. This observation can be attributed to the fact that corrosion is a highly complex process due to activities that lead to the alterations which includes the exchange of electrons and desorption of the inhibitor

among others [301]. Several researchers also reported similar findings [302–304]. Nevertheless, the introduction of various concentrations of Q6CA in 1.0 M HCl and 1.0 M H₂SO₄ solutions significantly reduced the corrosion rate of zinc. In 1.0 M HCl, the highest inhibition efficiency was obtained to be 91.44% at a concentration of 3×10^{-3} M and temperature 333 K. The lowest inhibition efficiency was obtained at a concentration of 0.5×10^{-3} M and temperature of 303 K to be 55.98 %. Even though there was no regular trend observed in the values of inhibition efficiency of Q6CA, looking closely at Table 4.30, it can be observed that inhibition efficiency values increased with an increase in temperature. At concentration of 303 K for instance, the values were obtained to be 55.89, 58.08, 59.92, 57.62, and 59.17 % at 0.5×10^{-3} , 1.0×10^{-3} , 2.0×10^{-3} , 3.0×10^{-3} , and 4.0×10^{-3} M, respectively. However, at 313 K, these values increased to 72.67, 71.99, 80.55, 71.71, and 70.04 % at 0.5×10^{-3} , 1.0×10^{-3} , 2.0×10^{-3} , 3.0×10^{-3} , and 4.0×10^{-3} M, respectively.

Tables 4.31 and 4.34 illustrate the inhibition efficiency values of H2QCA with and without the addition of KI. It is clear from these tables that without the addition of KI in the H2QCA systems there was no simple trend in the inhibition efficiency values. However, after the addition of KI the inhibition efficiency values increased with increase concentration of the inhibitor and increase in temperature of the corrosive environment. In both acids, H2QCA without KI performed poorly in retarding the rate of corrosion of zinc. For instance, in table 4.31, at a concentration of 5.0×10^{-3} M, the inhibition efficiency values were obtained to be 39.81, 47.22, 45.45, and 35.11 % at temperatures 303, 313, 323, and 333 K, respectively. At the same concentration with the addition of KI in the inhibitor solution, the inhibition efficiency value improved to 50.39, 66.83, 67.76, then 62.91 % at temperatures 303, 313, 323, and 333 K, respectively. Similar improvements in the inhibition efficiency values were also observed in table 4.34. Thus, it is clear that the addition of KI remarkably improved the percentage efficiency of H2QCA. Thus, clearly showed that the addition of KI in the H2QCA system remarkably improved the percentage efficiency of H2QCA.

The inhibition efficiency of the studied compound varied in the order: MQ6CA>Q6CA>H2QCA. As shown in figures 4.87 – 4.94 and in Tables 4.27 and 4.28, all the studied quinoxalines on zinc performed best at higher temperatures. This effect can be attributed to that as the temperature is increased the corrosion products of zinc becomes more dense, compact, and cohesive to the metal surface, thereby eventually forming a protective zinc film oxide on the metal surface. This type of

adsorption is classified as chemical adsorption. This is in accordance with the report by Raja and co-workers [346].

4.3.3 Impact of temperature and kinetic parameters

As seen from section 4.3.1, temperature is influential factor on the corrosion of zinc in acidic media. An increase in temperature of the corrosive environment was found to lessen the rate of corrosion of zinc. Therefore, temperature variation can be utilized to further understand the type of adsorption of the studied quinoxaline on zinc surface. The Arrhenius equation is often utilized to explain the reliance of the corrosion rate of metals on the temperature of the surrounding [313]. The type of Arrhenius equation [equation (46)] utilized to evaluate the activation energy (E_a) of zinc corrosion was shown earlier in section 4.2.3 [314, 315]. The values of activation energy of zinc corrosion in the absence and presence of various concentration of the studied quinoxalines were computed from the plot of $\log C_R$ against $1/T$ (figures 4.103 – 4.114) and are presented in Tables 4.35 and 4.36.

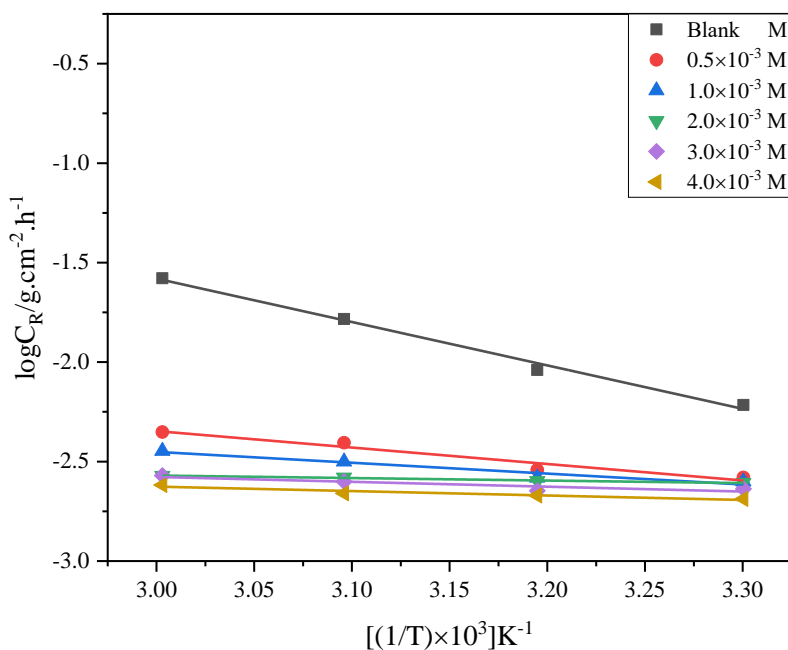


Figure 4.103: Arrhenius plots for zinc corrosion in 1.0 M HCl solution in the absence and presence of different concentrations of MQ6CA.

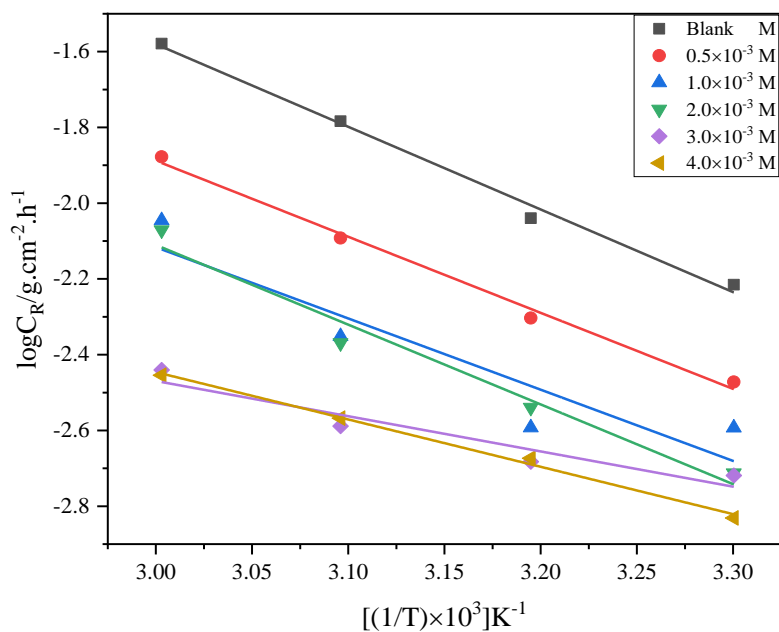


Figure 4.104: Arrhenius plots for zinc corrosion in 1.0 M HCl solution in the absence and presence of different concentrations of Q6CA.

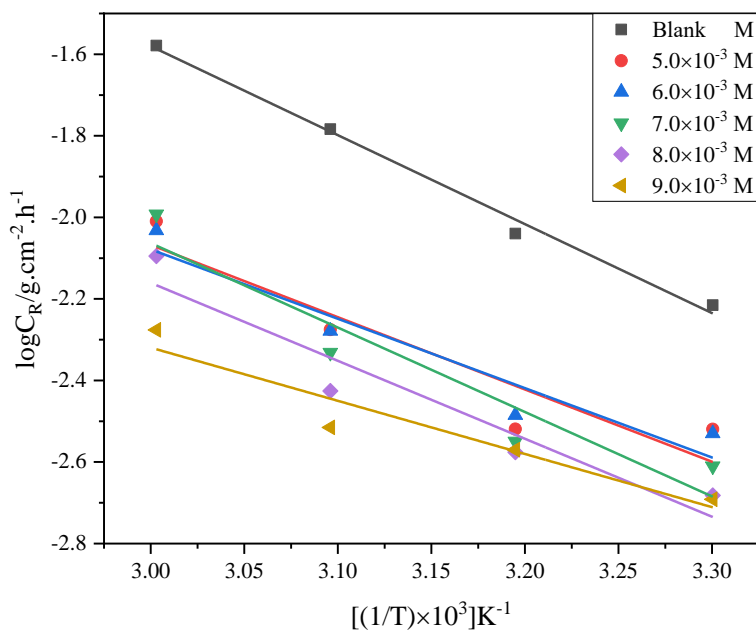


Figure 4.105: Arrhenius plots for zinc corrosion in 1.0 M HCl solution in the absence and presence of different concentrations of H2QCA with KI.

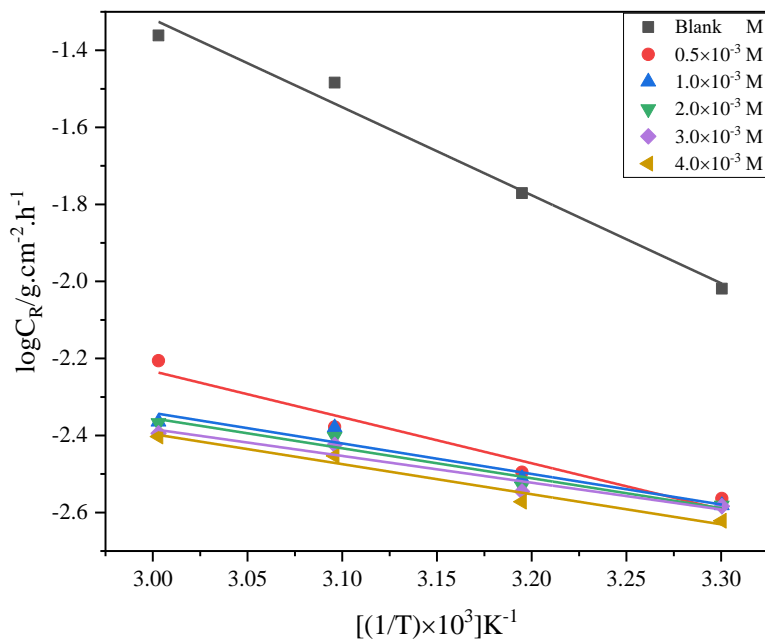


Figure 4.106: Arrhenius plots for zinc corrosion in 1.0 M H₂SO₄ solution in the absence and presence of different concentrations of MQ6CA.

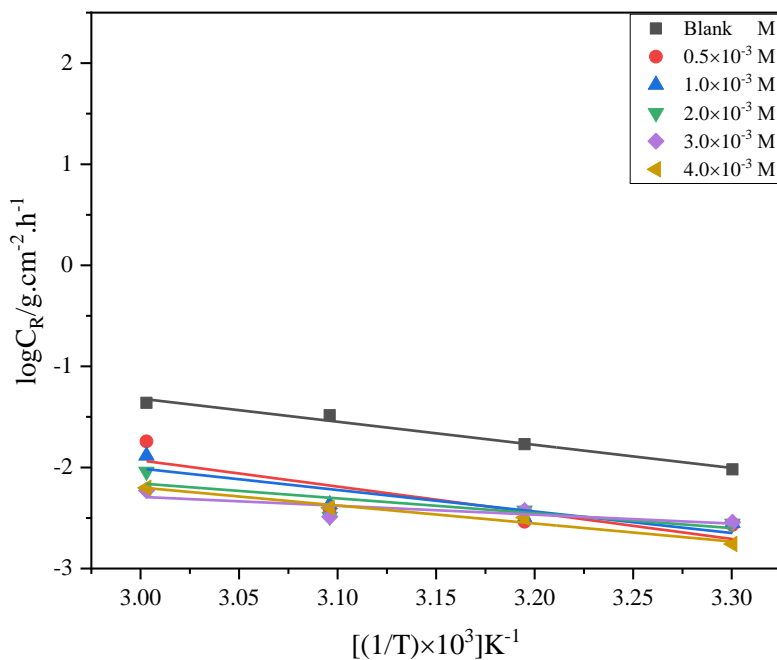


Figure 4.107: Arrhenius plots for zinc corrosion in 1.0 M H₂SO₄ solution in the absence and presence of different concentrations of Q6CA.

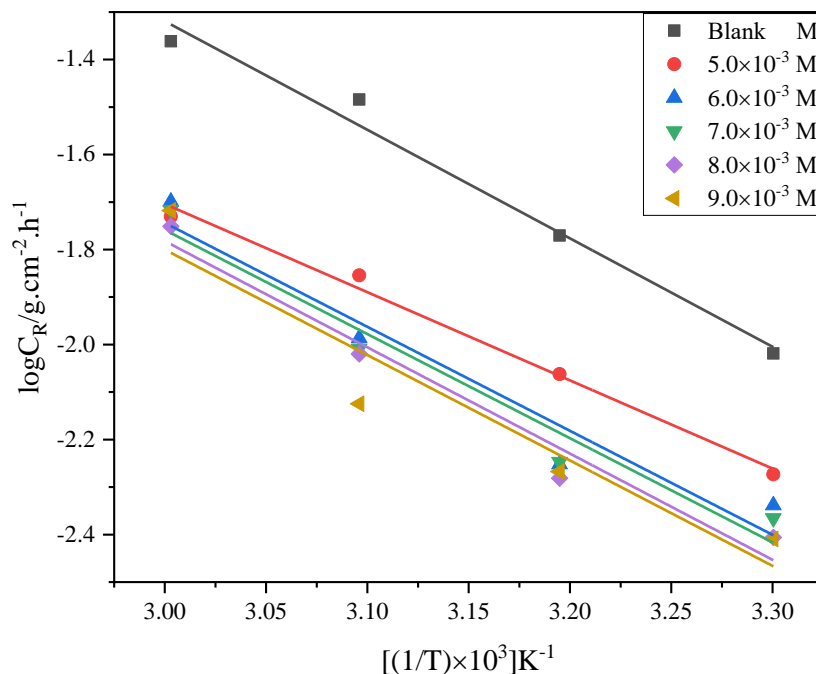


Figure 4.108: Arrhenius plots for zinc corrosion in 1.0 M H₂SO₄ solution in the absence and presence of different concentrations of H₂QCA with KI.

More information on the impact of temperature on the corrosion rate of zinc in 1.0 M HCl and 1.0 M H₂SO₄ can be derived from thermodynamic parameters such as enthalpy of activation (ΔH^*) and entropy of activation (ΔS^*). The rate of corrosion and temperature are related to these parameters through the transition-state equation (47) [314, 315]. Figures 4.124 – 4.129 present the plot of $\log(CR/T)$ against $(1/T)$ with the data best fitted having a slope $(-\Delta H^*/2.303R)$ and an intercept $[\log(R/Nh) + (\Delta S^*/2.303R)]$ which were utilized to compute the values of the standard enthalpy (ΔH^*) and entropy of activation (ΔS^*) in the absence and presence of various concentrations of the studied quinoxalines. Their values are presented in Tables 4.35 and 4.36.

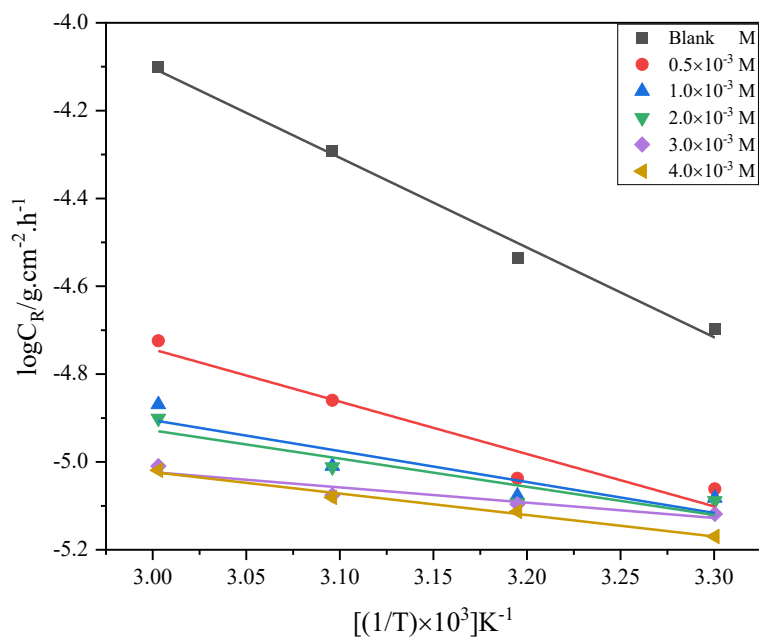


Figure 4.109: Transition state plots for zinc corrosion in 1.0 M HCl solution in the absence and presence of different concentrations of MQ6CA.

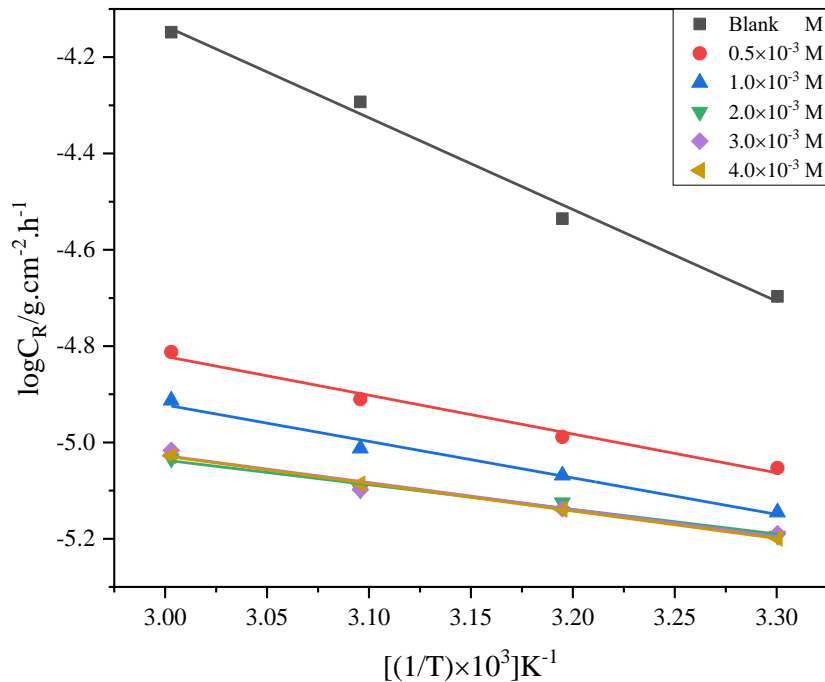


Figure 4.110: Transition state plots for zinc corrosion in 1.0 M HCl solution in the absence and presence of different concentrations of Q6CA.

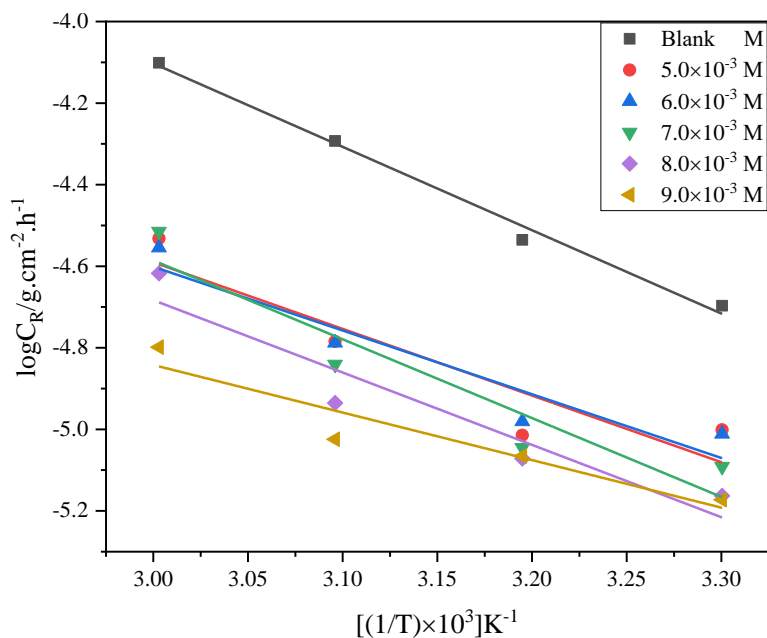


Figure 4.111: Transition state plots for zinc corrosion in 1.0 M HCl solution in the absence and presence of different concentrations of H2QCA with KI.

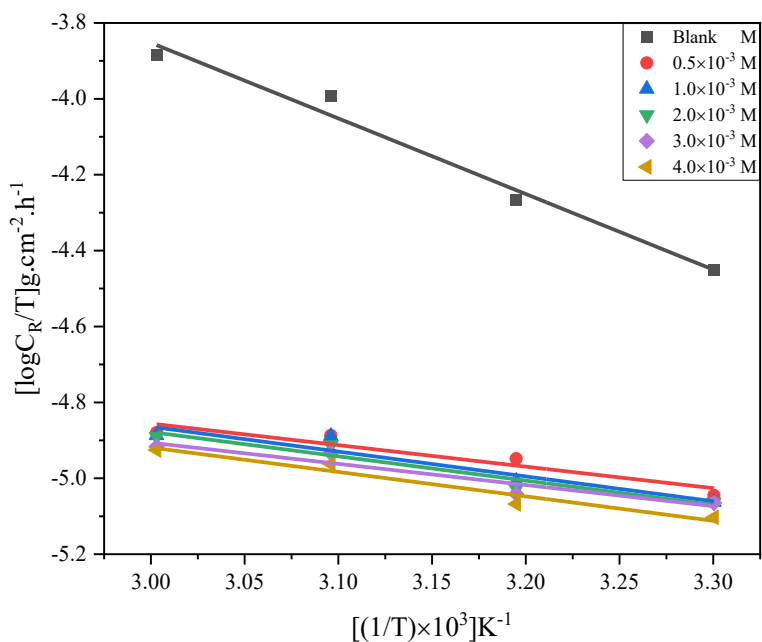


Figure 4.112: Transition state plots for zinc corrosion in 1.0 M H₂SO₄ solution in the absence and presence of different concentrations of MQ6CA.

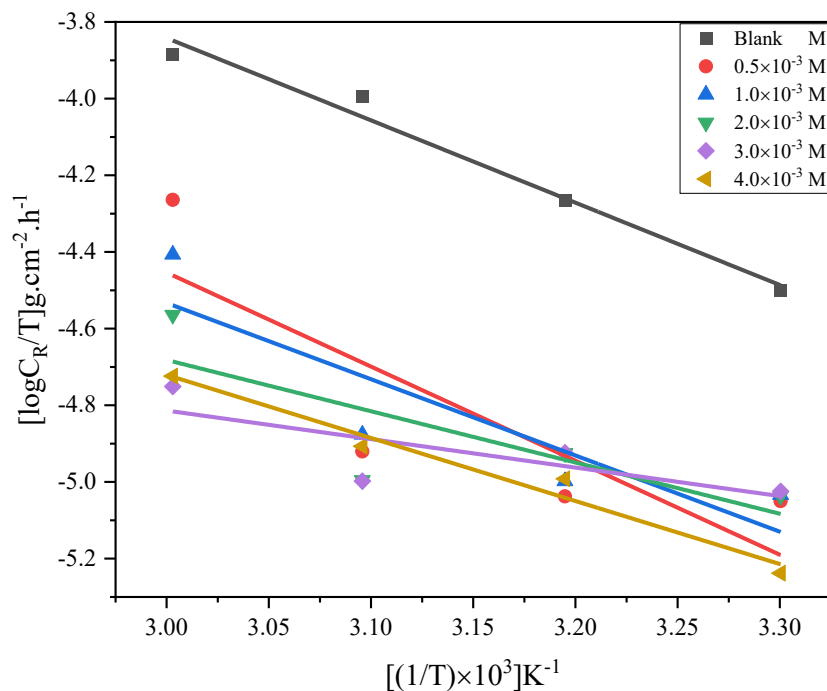


Figure 4.113: Transition state plots for zinc corrosion in 1.0 M H₂SO₄ solution in the absence and presence of different concentrations of Q6CA.

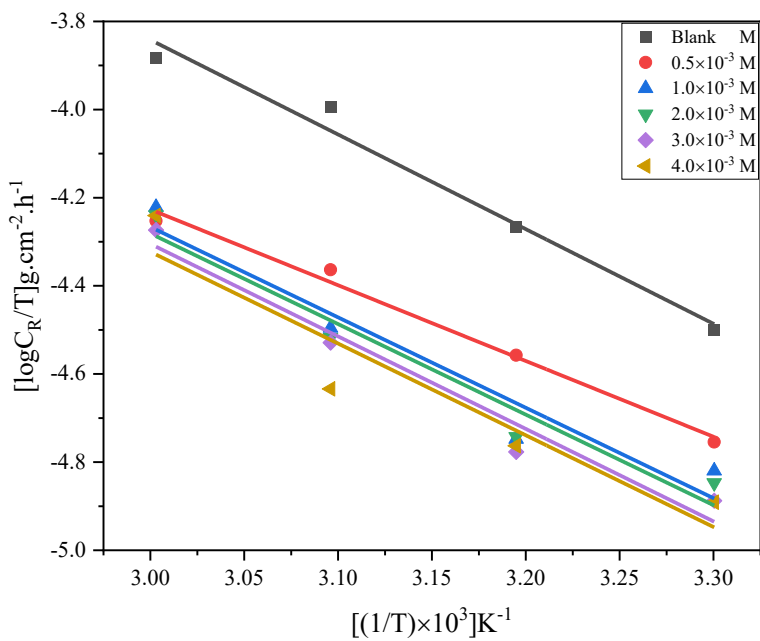


Figure 4.114: Transition state plots for zinc corrosion in 1.0 M H₂SO₄ solution in the absence and presence of different concentrations of H₂QCA with KI.

Higher values of the activation energy of a process in the presence of an inhibitor compared to that of a process in the absence of an inhibitor are generally associated with physical adsorption, while the opposite is associated with chemical adsorption. A closer look at Tables 4.35 and 4.36, shows that the activation energy values the quinoxalines were obtained less than for blank solution. This can be ascribed to an increase in adsorption of the preferential quinoxaline inhibitor molecules on zinc surface with increase in temperature of the corrosive surrounding. This effect suggests a chemical type of adsorption. A similar behavior was also reported in literature [347, 348]. An interesting observation in Table 4.36, the activation energy for Q6CA at concentration of 0.5×10^{-3} M was found to be higher than that of blank solution, suggesting that at low concentration the inhibitor molecules were adsorbed physically on zinc surface. These findings suggest that Q6CA is a mixed-type inhibitor.

This adsorption process of zinc and the studied quinoxaline can be classified into either endothermic or exothermic. Moreover, an exothermic process releases energy in a form of heat and may suggest either physical or chemical adsorption. An endothermic process requires an input of energy in a form of heat, and it suggests chemisorption entirely. From Tables 4.35 and 4.36, the calculated values of entropy of activation were obtained to be positive, suggesting that the adsorption of the studied quinoxalines on zinc surface is endothermic, which further implies that the dissolution of zinc is slow in the presence of the studied quinoxalines. Ogoko et. al. reported similar findings [349]. A review in literature reveals that the values of enthalpy of activation 40.86 kJ/mol indicate physical adsorption whereas enthalpy of activation values around 100.00 kJ/mol indicate chemical adsorption [322–324]. In the present study, the range of enthalpy of activation values (6.51 – 46.97 kJ/mol), suggesting that the studied quinoxalines are associated with a physical type of adsorption of zinc adsorption. It is also observed from Tables 4.35 and 4.36 that the values of activation energy and enthalpy of activation varied similarly, however, the enthalpy of activation values were a bit lower than those of the activation energy. This observation was also reported in the literature [325]. An increase in the concentration of the studied quinoxalines resulted in large and negative values of entropy of activation. This implies that there is a formation of an activated complex in the rate-determining step which represents association rather than dissolution of zinc, meaning that there is more disorder in the presence of the studied quinoxalines, which may be attributed to the desorption of the molecules from zinc surface. A similar observation was reported in the literature [349].

Table 4.35: Arrhenius and transition parameters for zinc in 1.0 M HCl in the absence and presence of various concentrations of the studied quinoxalines.

Inhibitor	Concentration of inhibitors ($\times 10^{-3}\text{M}$)	E_a ($\text{kJ}\cdot\text{mol}^{-1}$)	ΔH^* ($\text{kJ}\cdot\text{mol}^{-1}$)	$-\Delta S^*$ ($\text{J}\cdot\text{mol}^{-1}\cdot\text{K}^{-1}$)
	–	41.78	39.14	158.25
MQ6CA	0.5	15.85	22.83	193.43
	1.0	10.46	13.40	220.84
	2.0	2.43	12.25	224.38
	3.0	4.69	6.51	240.92
	4.0	4.28	9.34	233.78
Q6CA	0.5	38.43	15.41	199.52
	1.0	36.00	14.49	199.77
	2.0	40.36	9.78	200.62
	3.0	17.79	10.72	200.46
	4.0	28.91	10.91	200.43
H2QCA with KI	5.0	33.93	31.29	191.12
	6.0	32.57	29.93	195.44
	7.0	39.65	37.01	173.91
	8.0	36.61	33.97	184.88
	9.0	24.95	22.33	-219.33

Table 4.36: Arrhenius and transition parameters for zinc in 1.0 M H₂SO₄ in the absence and presence of various concentrations of the studied quinoxalines.

Inhibitor	Concentration of inhibitors ($\times 10^{-3}\text{M}$)	E_a ($\text{kJ}\cdot\text{mol}^{-1}$)	ΔH^* ($\text{kJ}\cdot\text{mol}^{-1}$)	$-\Delta S^*$ ($\text{J}\cdot\text{mol}^{-1}\cdot\text{K}^{-1}$)
	–	43.76	41.11	147.32
MQ6CA	0.5	22.88	10.87	257.47
	1.0	15.19	12.26	252.63
	2.0	14.93	12.54	253.75
	3.0	13.31	10.67	258.96
	4.0	14.96	12.32	254.33
Q6CA	0.5	49.59	46.97	141.46
	1.0	40.73	38.06	169.70
	2.0	28.18	25.58	209.96
	3.0	16.87	14.23	246.57
	4.0	34.12	31.40	193.06
H2QCA with KI	5.0	35.56	32.74	179.30
	6.0	41.93	39.25	160.97
	7.0	41.91	39.33	161.08
	8.0	42.83	40.17	159.00
	9.0	42.49	39.85	160.33

4.3.4 Adsorption isotherms and thermodynamic parameters

The adsorption isotherm can be utilized to understand the mechanism of the studied quinoxalines on zinc surface [327]. The adsorption of organic molecules at the metal/solution interface can occur as a result replacement of water molecules and adsorbed organic molecules in the aqueous solution. The adsorption of organic molecules at the metal/solution interface can be described as a result of replacement of water molecules and adsorbed organic molecules in the aqueous solution as represented by equation (48) [350]. It is important to know the suitable adsorption isotherm that can provide more information about the type of adsorption of the studied quinoxalines on zinc surface. Trials were made to fit the data to several known adsorption isotherms namely Langmuir, Frumkin, Freundlich, and Temkin. The plots of these adsorption isotherms are shown with descriptions in figures 4.115 – 4.138. Among all the fitted isotherms for zinc 1.0 M HCl and 1.0 M H₂SO₄ in the absence and presence of the studied quinoxaline, the Langmuir isotherm was obtained to the description of the adsorption behavior of the investigated compounds. This judgment was based on the regression coefficient values (R^2) that were found to be at/and near the unity. The regression coefficient values obtained in all the tested isotherms for zinc in this present study are presented in Tables 4.37 and 4.38. From this table, it is clear that all the other isotherms except for Langmuir isotherm are deviating from unity.

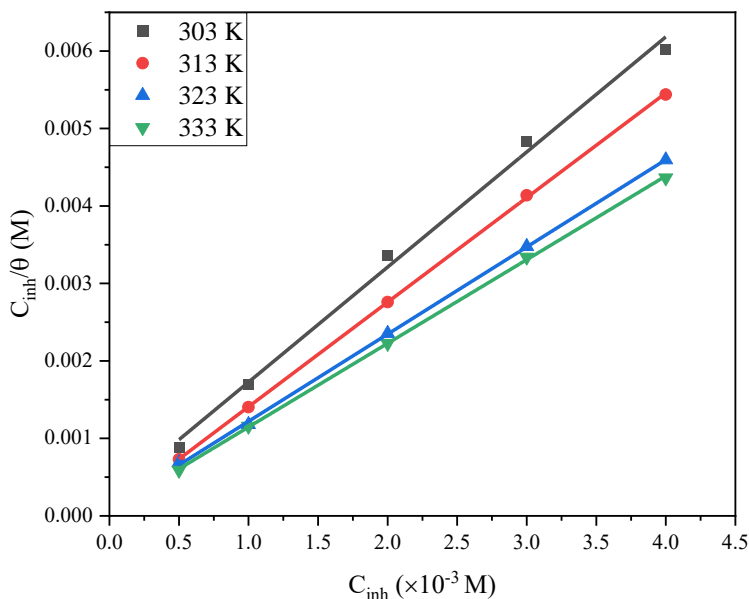


Figure 4.115: Langmuir adsorption isotherm plot for the adsorption of various concentrations of MQ6CA on the surface of zinc in 1.0 M HCl at various temperatures.

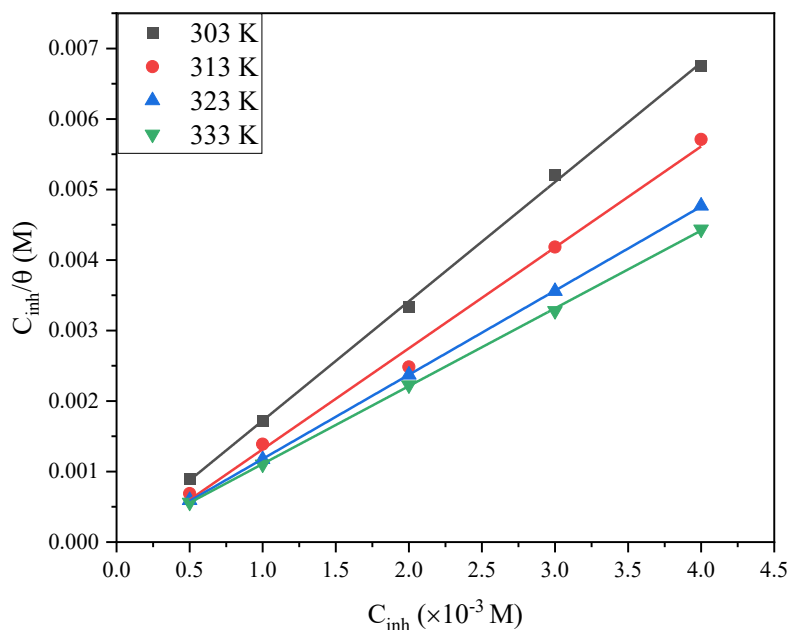


Figure 4.116: Langmuir adsorption isotherm plot for the adsorption of various concentrations of Q6CA on the surface of zinc in 1.0 M HCl at various temperatures.

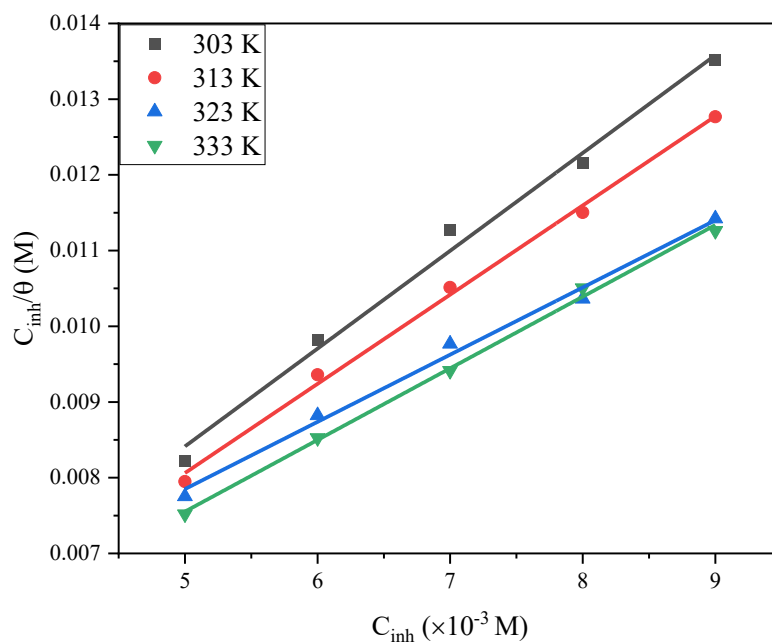


Figure 4.117: Langmuir adsorption isotherm plot for the adsorption of various concentrations of H2QCA with KI on the surface of zinc in 1.0 M HCl at various temperatures.

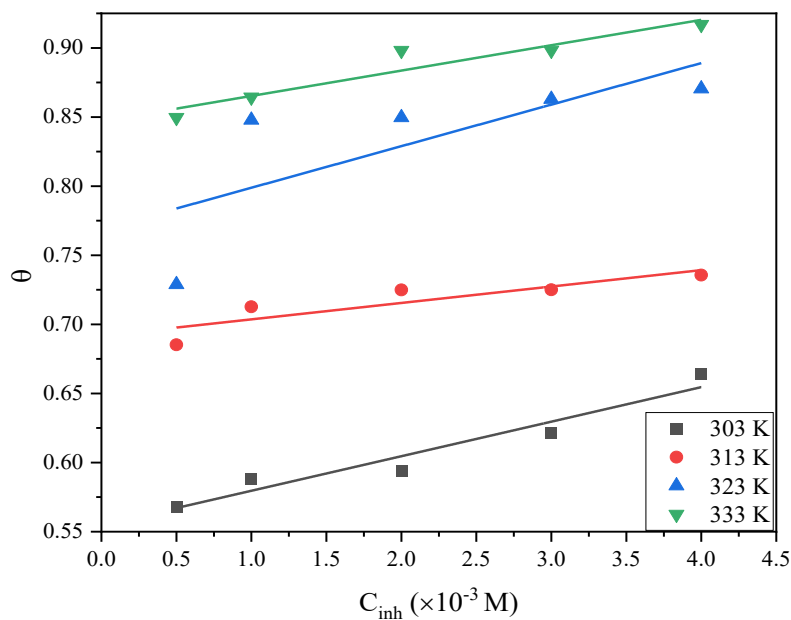


Figure 4.118: Frumkin adsorption isotherm plot for the adsorption of various concentrations of MQ6CA on the surface of zinc in 1.0 M HCl at various temperatures.

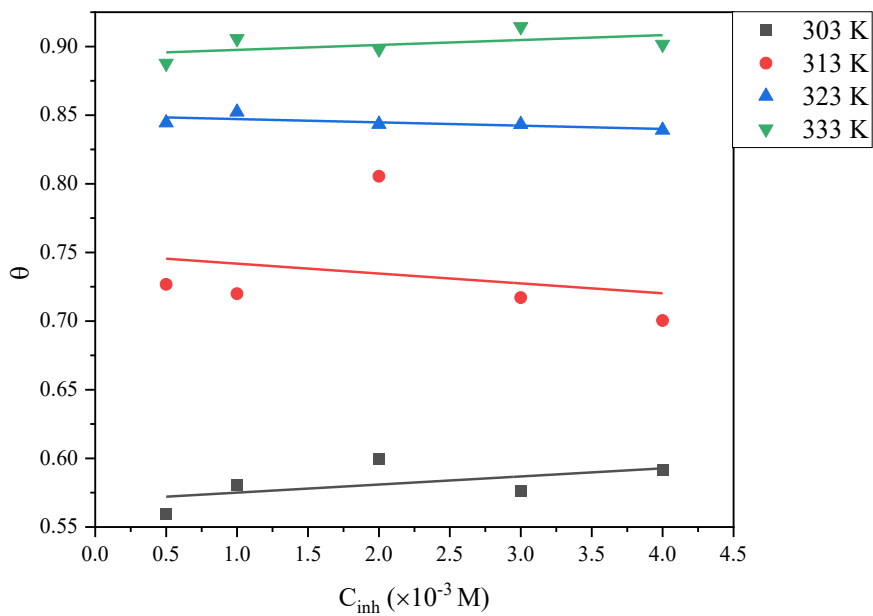


Figure 4.119: Frumkin adsorption isotherm plot for the adsorption of various concentrations of Q6CA on the surface of zinc in 1.0 M HCl at various temperatures.

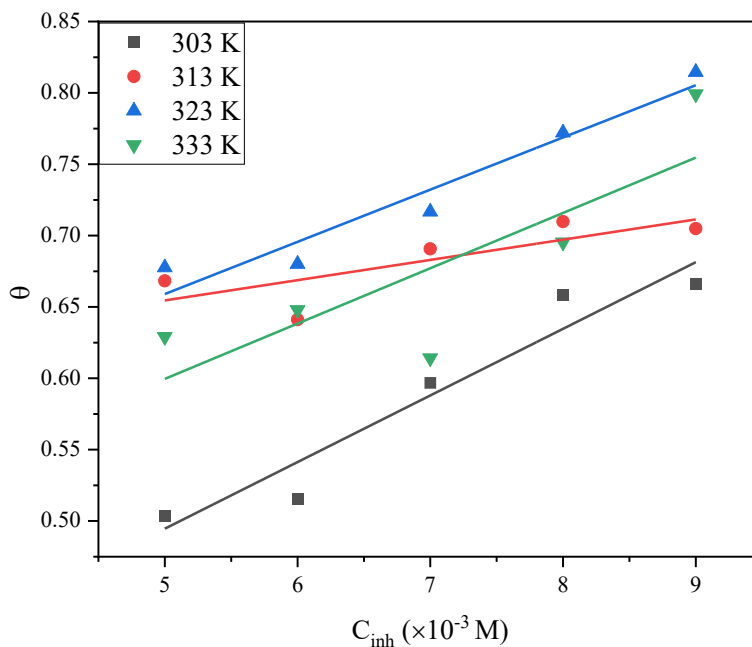


Figure 4.120: Frumkin adsorption isotherm plot for the adsorption of various concentrations of H2QCA with KI on the surface of zinc in 1.0 M HCl at various temperatures.

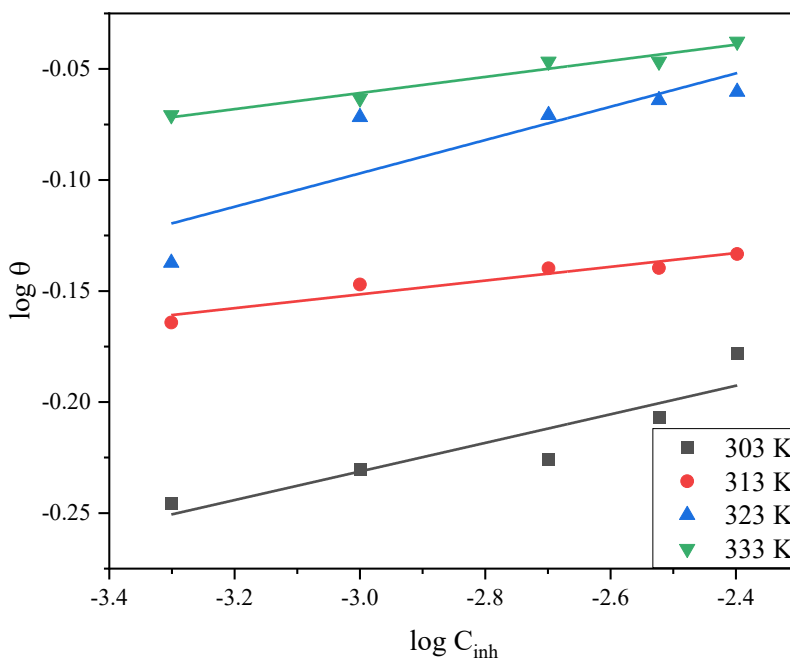


Figure 4.121: Freundlich adsorption isotherm plot for the adsorption of various concentrations of MQ6CA on the surface of zinc in 1.0 M HCl at various temperatures.

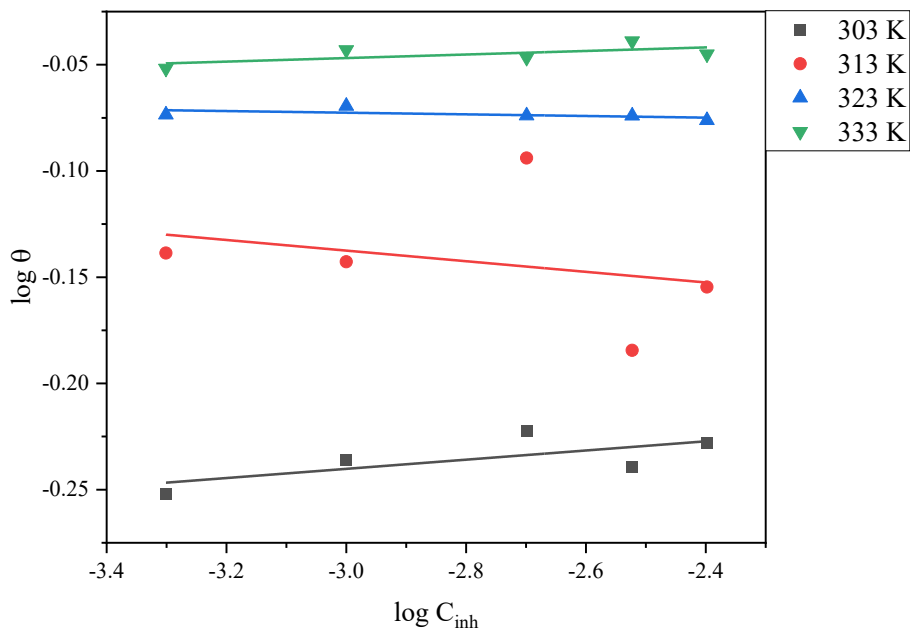


Figure 4.122: Freundlich adsorption isotherm plot for the adsorption of various concentrations of Q6CA on the surface of zinc in 1.0 M HCl at various temperatures.

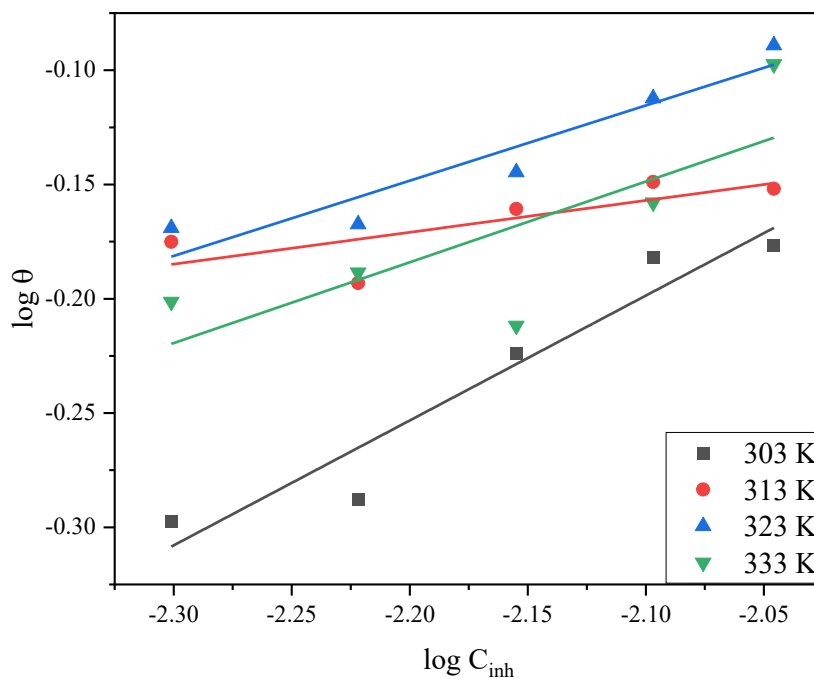


Figure 4.123: Freundlich adsorption isotherm plot for the adsorption of various concentrations of H2QCA with KI on the surface of zinc in 1.0 M HCl at various temperatures.

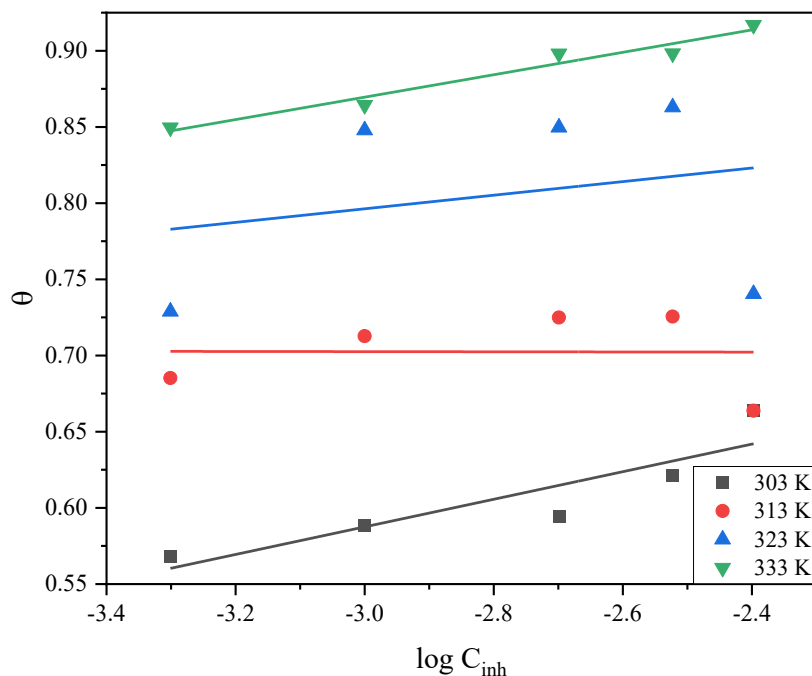


Figure 4.124: Temkin adsorption isotherm plot for the adsorption of various concentrations of MQ6CA on the surface of zinc in 1.0 M HCl at various temperatures.

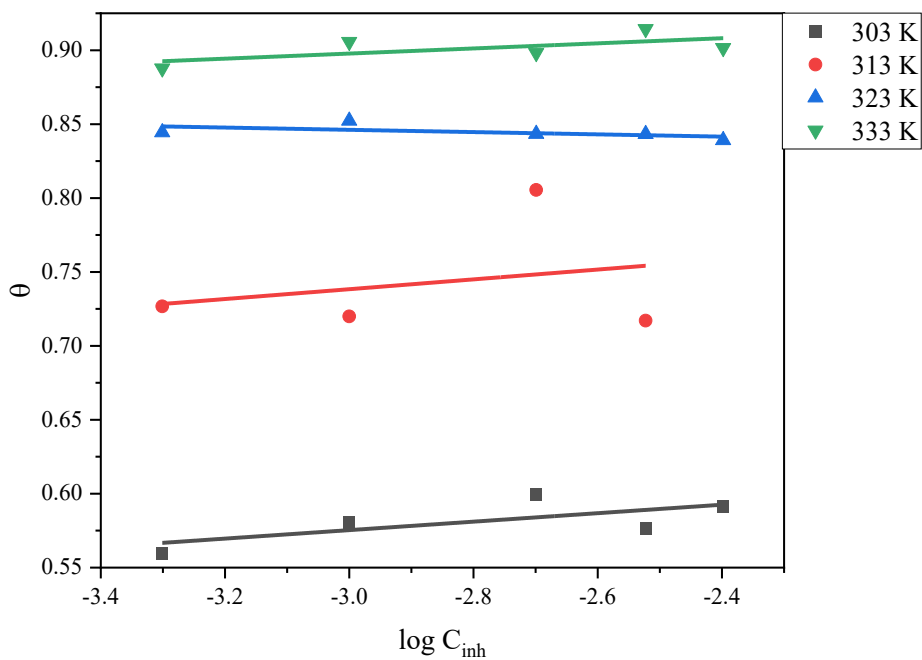


Figure 4.125: Temkin adsorption isotherm plot for the adsorption of various concentrations of Q6CA on the surface of zinc in 1.0 M HCl at various temperatures.

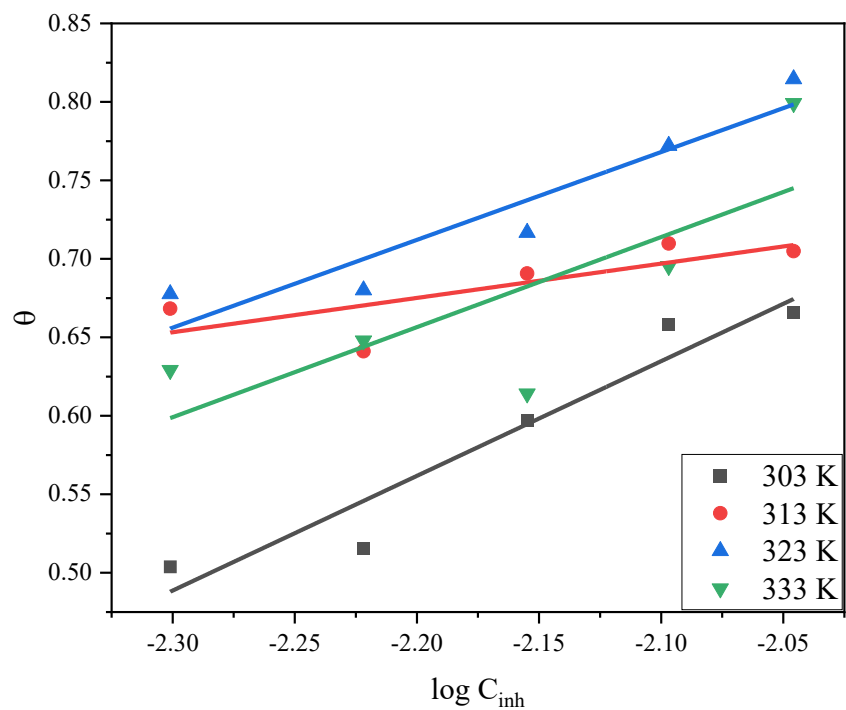


Figure 4.126: Temkin adsorption isotherm plot for the adsorption of various concentrations of H₂QCA with KI on the surface of zinc in 1.0 M HCl at various temperatures.

Table 4.37: The regression coefficient values obtained from different adsorption isotherms for zinc in 1.0 M HCl at various temperatures for the studied quinoxaline.

Inhibitor	Temperature (K)	Correlation coefficient (R ²)			
		Langmuir	Frumkin	Freundlich	Temkin
MQ6CA	303	0.9958	0.9378	0.8278	0.8085
	313	0.9999	0.7698	0.9194	5.07×10 ⁻⁵
	323	0.9998	0.5445	0.6578	0.0626
	333	0.9998	0.9084	0.9610	0.9595
Q6CA	303	0.9993	0.3107	0.4879	0.4823
	313	0.9945	0.0626	0.0782	0.0723
	323	0.9999	0.5082	0.3310	0.3410
	333	0.9999	0.2732	0.4191	0.4167
H2QCA with KI	303	0.9914	0.9302	0.9276	0.9270
	313	0.9968	0.6236	0.5919	0.6023
	323	0.9925	0.9357	0.8982	0.8905
	333	0.9976	0.6717	0.5994	0.5993

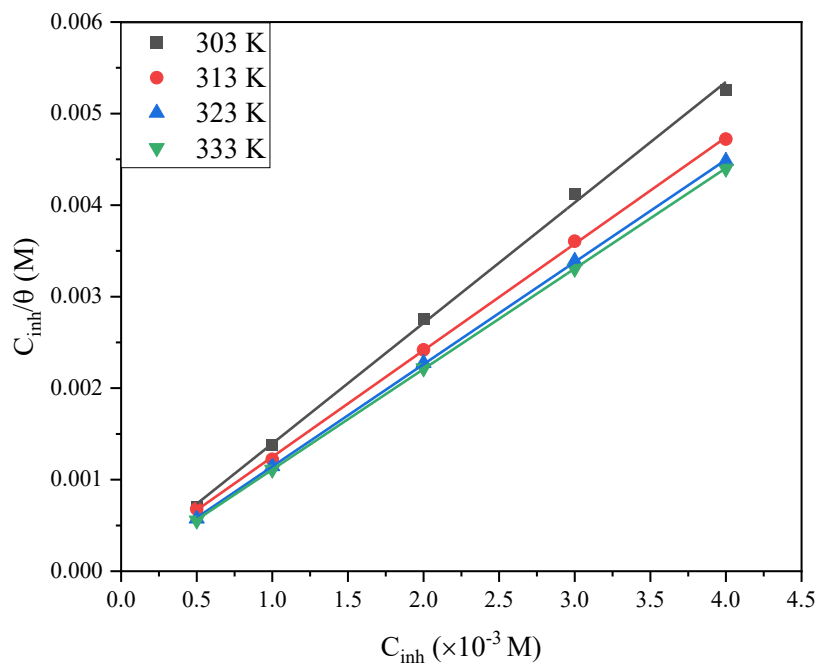


Figure 4.127: Langmuir adsorption isotherm plot for the adsorption of various concentrations of MQ6CA on the surface of zinc in 1.0 M H₂SO₄ at various temperatures.

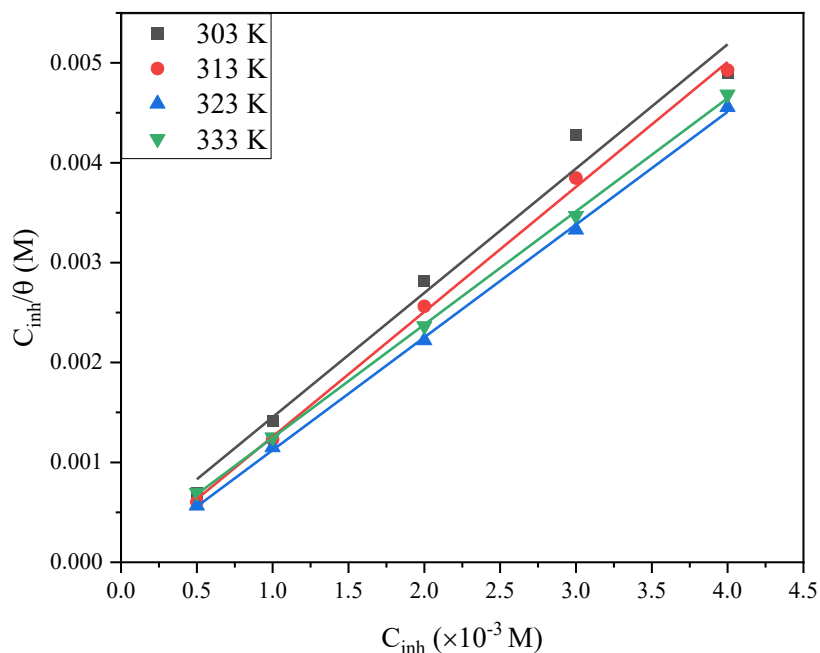


Figure 4.128: Langmuir adsorption isotherm plot for the adsorption of various concentrations of Q6CA on the surface of zinc in 1.0 M H₂SO₄ at various temperatures.

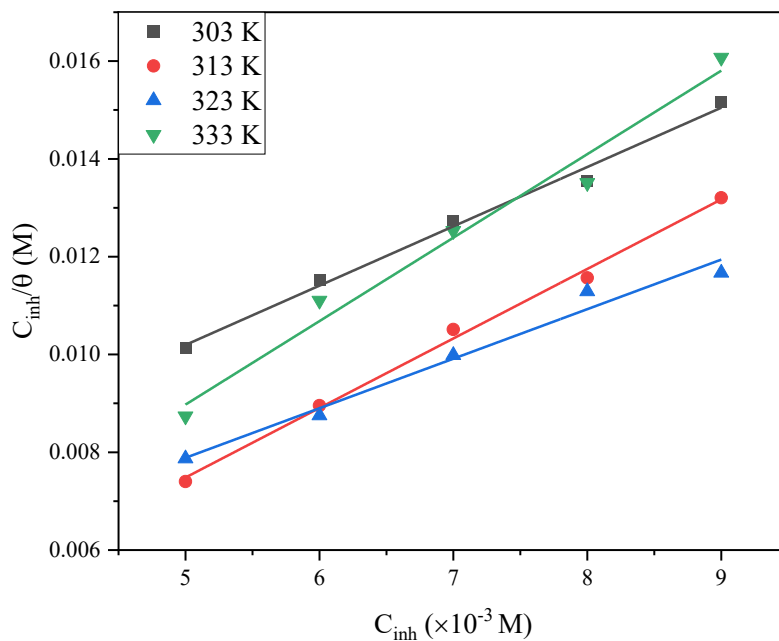


Figure 4.129: Langmuir adsorption isotherm plot for the adsorption of various concentrations of H2QCA with KI on the surface of zinc in 1.0 M H₂SO₄ at various temperatures.

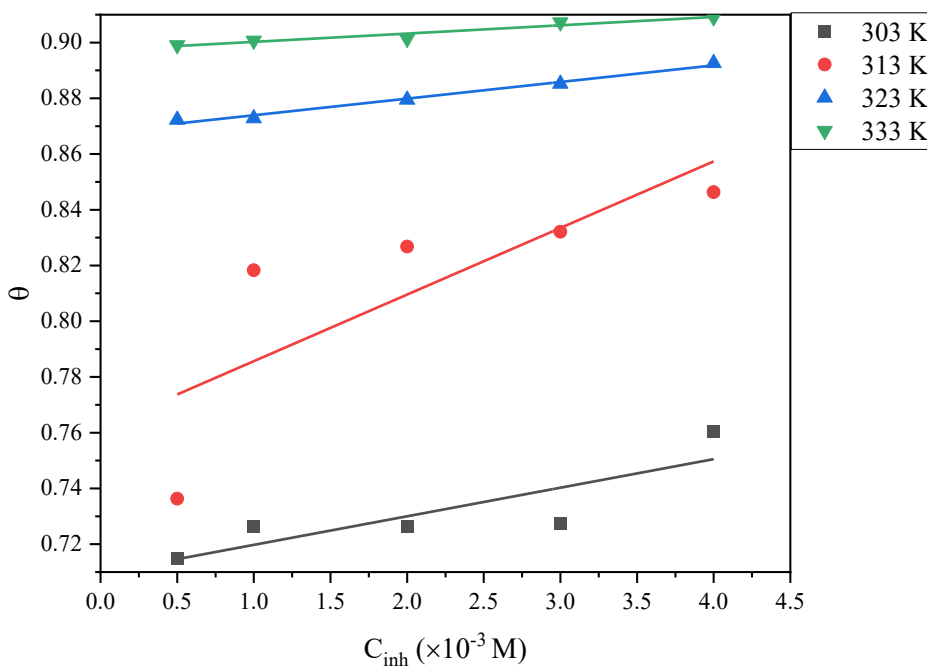


Figure 4.130: Frumkin adsorption isotherm plot for the adsorption of various concentrations of MQ6CA on the surface of zinc in 1.0 M H₂SO₄ at various temperatures.

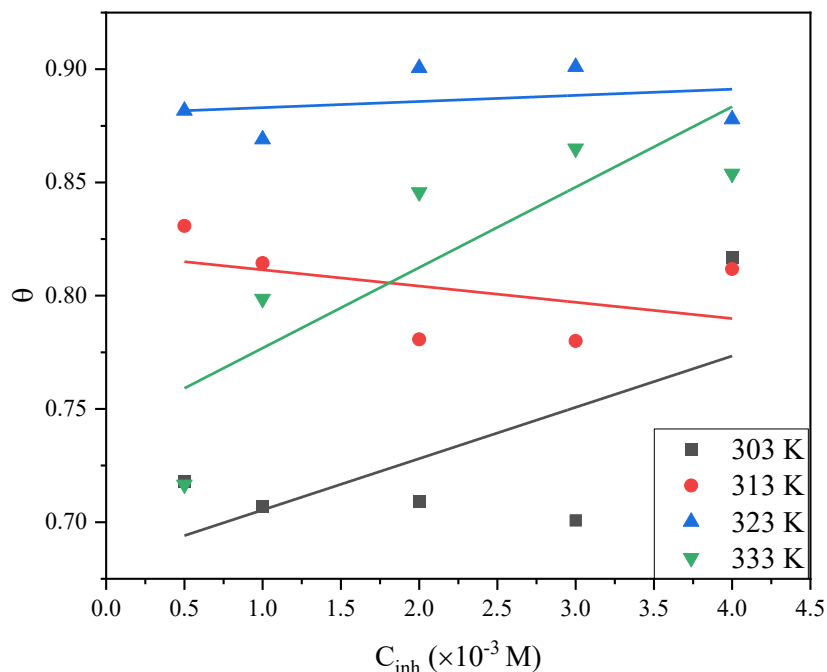


Figure 4.131: Frumkin adsorption isotherm plot for the adsorption of various concentrations of Q6CA on the surface of zinc in 1.0 M H_2SO_4 at various temperatures.

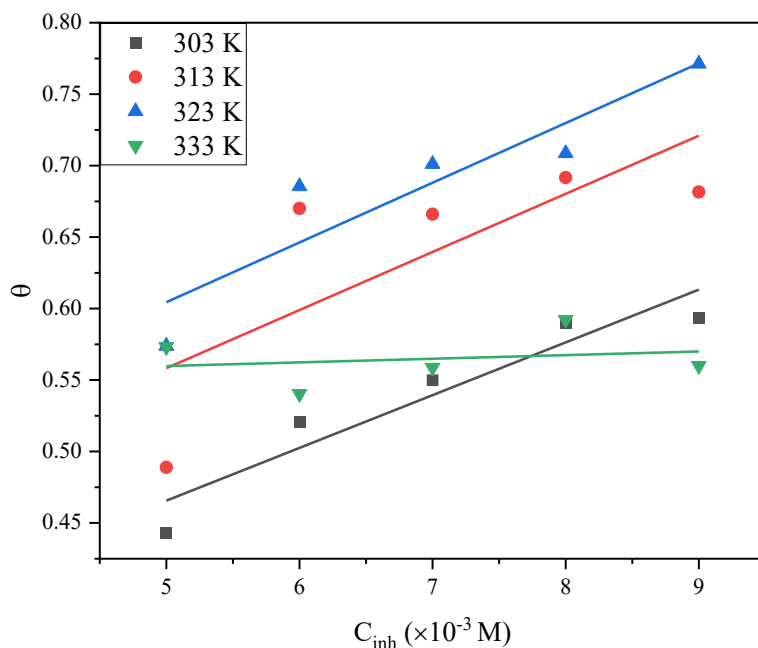


Figure 4.132: Frumkin adsorption isotherm plot for the adsorption of various concentrations of H2QCA with KI on the surface of zinc in 1.0 M H_2SO_4 at various temperatures.

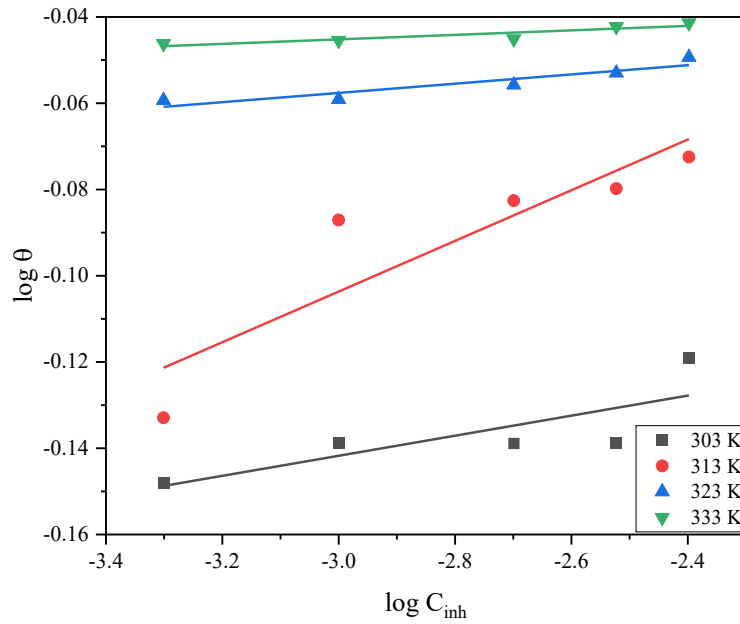


Figure 4.133: Freundlich adsorption isotherm plot for the adsorption of various concentrations of MQ6CA on the surface of zinc in 1.0 M H₂SO₄ at various temperatures.

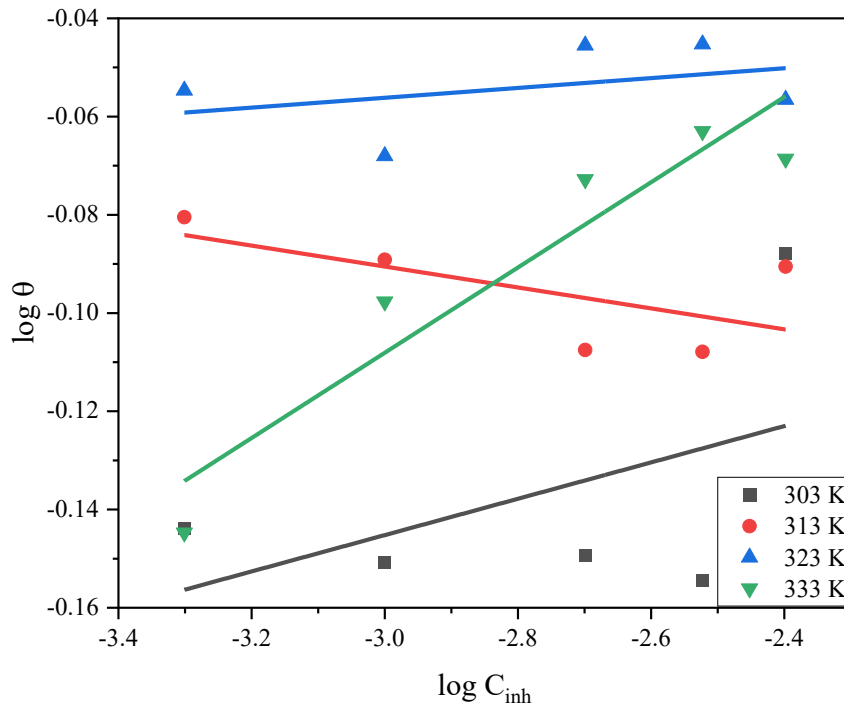


Figure 4.134: Freundlich adsorption isotherm plot for the adsorption of various concentrations of Q6CA on the surface of zinc in 1.0 M H₂SO₄ at various temperatures.

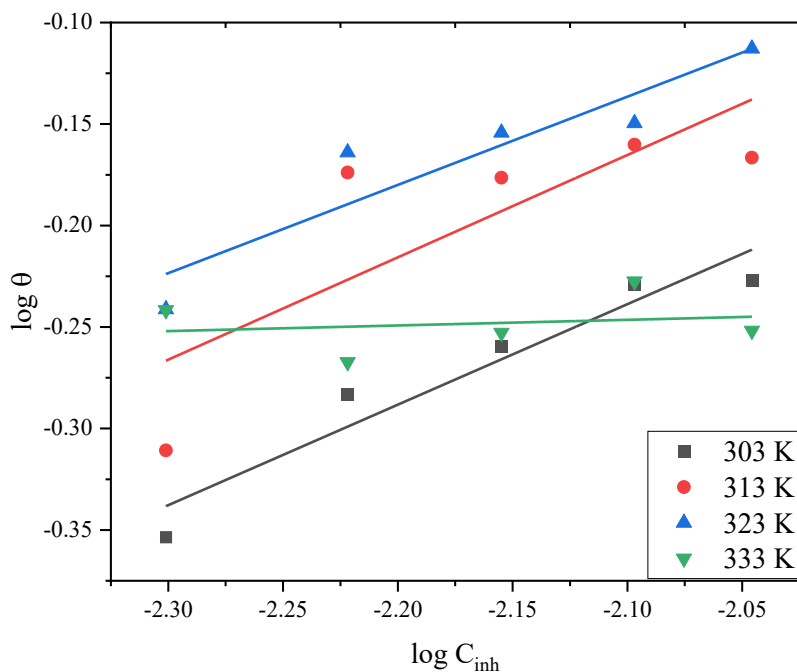


Figure 4.135: Freundlich adsorption isotherm plot for the adsorption of various concentrations of H2QCA with KI on the surface of zinc in 1.0 M H₂SO₄ at various temperatures.

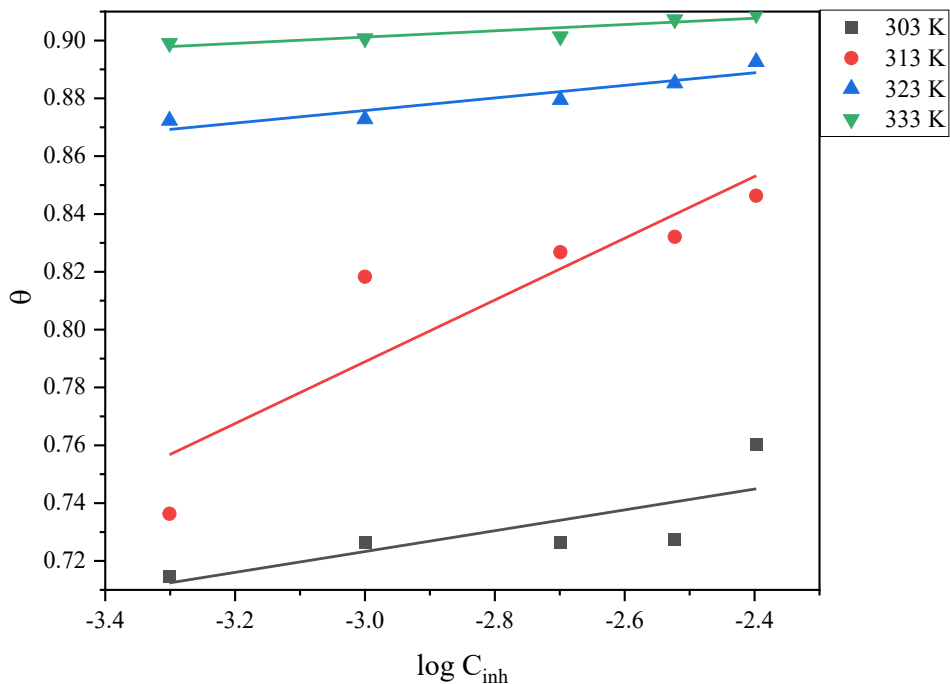


Figure 4.136: Temkin adsorption isotherm plot for the adsorption of various concentrations of MQ6CA on the surface of zinc in 1.0 M H₂SO₄ at various temperatures.

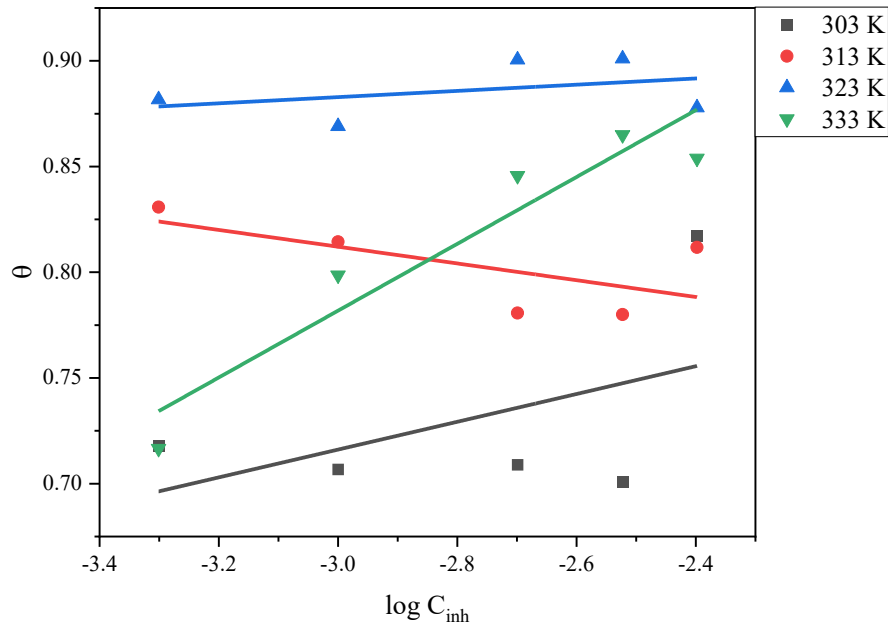


Figure 4.137: Temkin adsorption isotherm plot for the adsorption of various concentrations of Q6CA on the surface of zinc in 1.0 M H_2SO_4 at various temperatures.

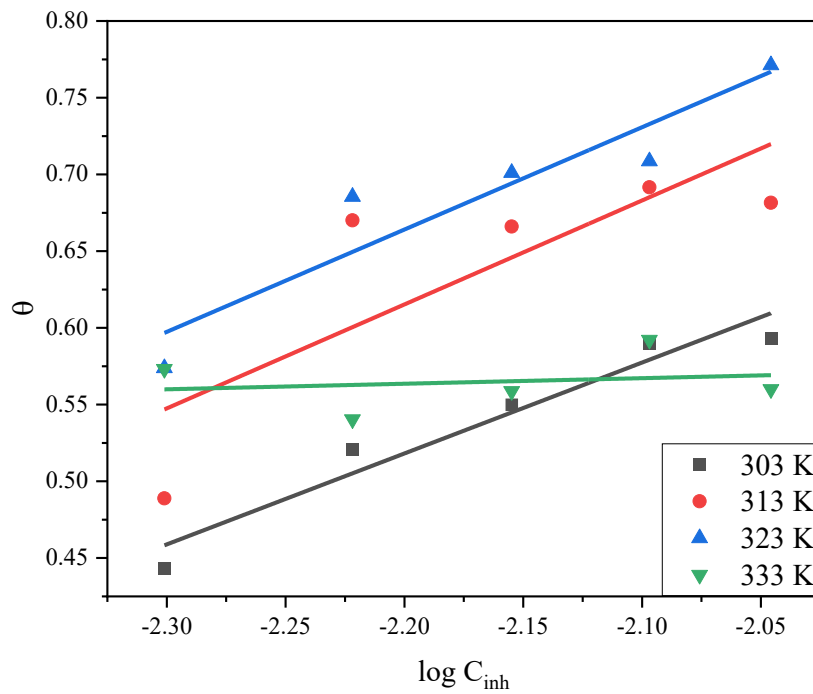


Figure 4.138: Temkin adsorption isotherm plot for the adsorption of various concentrations of H2QCA with KI on the surface of zinc in 1.0 M H_2SO_4 at various temperatures.

Table 4.38: The regression coefficient values obtained from different adsorption isotherms for zinc in 1.0 M H₂SO₄ at various temperatures for the studied quinoxaline.

Inhibitor	Temperature (K)	Correlation coefficient (R ²)			
		Langmuir	Frumkin	Freundlich	Temkin
MQ6CA	303	0.9982	0.7323	0.6366	0.5935
	313	0.9998	0.6187	0.8023	0.8119
	323	0.9999	0.9855	0.8629	0.8615
	333	0.9999	0.9372	0.8233	0.8228
Q6CA	303	0.9819	0.4413	0.2368	0.2438
	313	0.9985	0.2101	0.4163	0.4218
	323	0.9994	0.0746	0.1536	0.1440
	333	0.9996	0.6945	0.8643	0.9026
H2QCA with KI	303	0.9920	0.8981	0.9249	0.9415
	313	0.9962	0.5744	0.6389	0.6487
	323	0.9779	0.8492	0.8654	0.8798
	333	0.9775	0.0436	0.0362	0.0362

The surface coverage (θ) of the studied quinoxaline obtained from weight loss measurements on zinc surface and the variety of their concentration are best related by Langmuir isotherm given by equation (49). The values of K_{ads} were calculated from the intercept of the line from the aforementioned Langmuir plots. K_{ads} can be related to the free Gibbs energy of adsorption (ΔG°_{ads}) through equation (51). The K_{ads} and ΔG°_{ads} for zinc in 1.0 M HCl and 1.0 M H₂SO₄ in the absence and presence of the studied quinoxalines are listed in Tables 4.39 and 4.40, respectively.

The values of K_{ads} are representative of the strength between the inhibitor molecules and a surface of a metal. Moreover, literature shows that large values of K_{ads} signifies greater binding strength [330]. The large values of K_{ads} obtained in this present study suggest a strong adsorption of the quinoxaline inhibitors on the zinc surface. Hence appreciable inhibition efficiency obtained as reported earlier. The tables show no regular trend in the K_{ads} values. The free Gibbs energy of adsorption gives more information on the mode interaction occurring between the inhibitors and the metal surface. In the present study, the values of ΔG°_{ads} were obtained to be negative for all the studied inhibitors which indicated that the inhibition processes of zinc were spontaneous. Generally, the values of ΔG°_{ads} around -20 kJ/mol or lower are associated with physical adsorption and values of ΔG°_{ads} around -40 kJ/mol and more negative are associated with chemical adsorption [331]. In the presence study, the ΔG°_{ads} values for zinc in 1.0 M HCl and 1.0 M H₂SO₄ in the absence and presence of the studied quinoxalines were obtained to be in the range of -23.95 to -44.42 kJ/mol, indicating a mixed-typed of adsorption of the studied quinoxalines on zinc surface, however, with chemisorption dominant.

Table 4.39: Langmuir adsorption parameters for corrosion of zinc in 1.0 M HCl at various temperatures in the presence of the studied quinoxalines.

Inhibitor	Temperature (K)	K_{ads} (L/mol)	$-\Delta G^{\circ}_{ads}$ (kJ.mol ⁻¹)
MQ6CA	303	4153.39	31.11
	313	17017.95	35.80
	323	10578.99	35.67
	333	15011.30	37.74
Q6CA	303	32323.75	36.28
	313	8666.26	34.05
	323	74790.96	40.92
	333	167485.11	44.42
H2QCA with KI	303	512.82	25.84
	313	460.83	26.41
	323	293.26	26.04
	333	354.61	27.37

Table 4.40: Langmuir adsorption parameters for corrosion of zinc in 1.0 M H₂SO₄ at various temperatures in the presence of the studied quinoxalines.

Inhibitor	Temperature (K)	K_{ads} (L/mol)	$-\Delta G^{\circ}_{ads}$ (kJ.mol ⁻¹)
MQ6CA	303	4153.39	31.11
	313	17018.09	35.80
	323	10578.99	35.67
	333	15011.26	37.74
Q6CA	303	4785.90	31.46
	313	141536.00	41.32
	323	163791.04	43.03
	333	8774.24	36.26
H2QCA with KI	303	242.131	23.95
	313	2688.17	31.98
	323	354.61	26.55
	333	2293.58	32.54

4.3.5 Potentiodynamic polarization (PDP)

PDP experiments for the corrosion of zinc were conducted at room temperature (303 K) in 1.0 M HCl and 1.0 M H₂SO₄ in the absence and presence of the studied quinoxalines, as presented in figures 4.139 – 4.146. From these figures, it can be observed in both corrosive media the anodic and cathodic half-reactions of zinc corrosion were affected by the introduction of the studied quinoxalines. The corresponding potentiodynamic parameters such as corrosion current density (i_{corr}), corrosion potential (E_{corr}), polarization resistance (R_p), and anodic (β_a) and cathodic (β_c) Tafel slopes were successfully calculated from both the anodic and cathodic regions of the Tafel plots. These parameters are presented in Tables 4.41 and 4.42. The potentiodynamic polarization inhibition efficiency (%IE_{PDP}) was then evaluated from the measured i_{corr} value from equation (43).

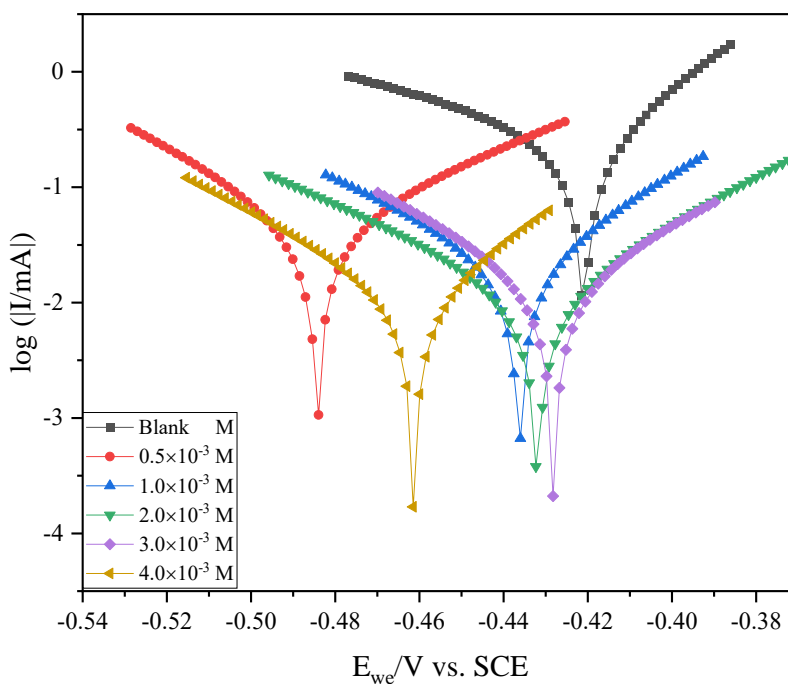


Figure 4.139: Tafel plots for zinc in 1.0 M HCl in the absence and presence of various concentrations of MQ6CA at 303 K.

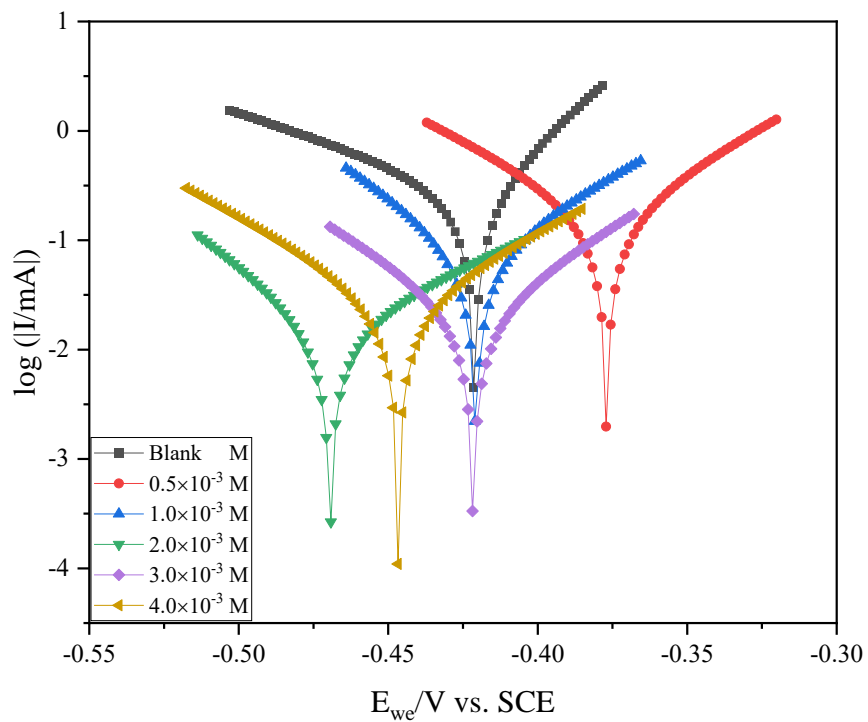


Figure 4.140: Tafel plots for zinc in 1.0 M HCl in the absence and presence of various concentrations of Q6CA at 303 K.

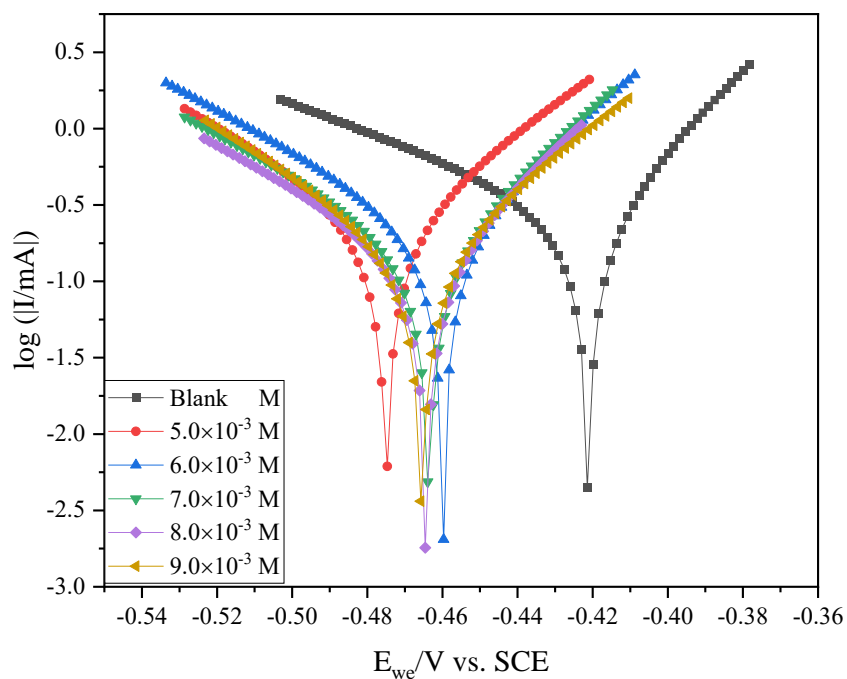


Figure 4.141: Tafel plots for zinc in 1.0 M HCl in the absence and presence of various concentrations of H2QCA without KI at 303 K.

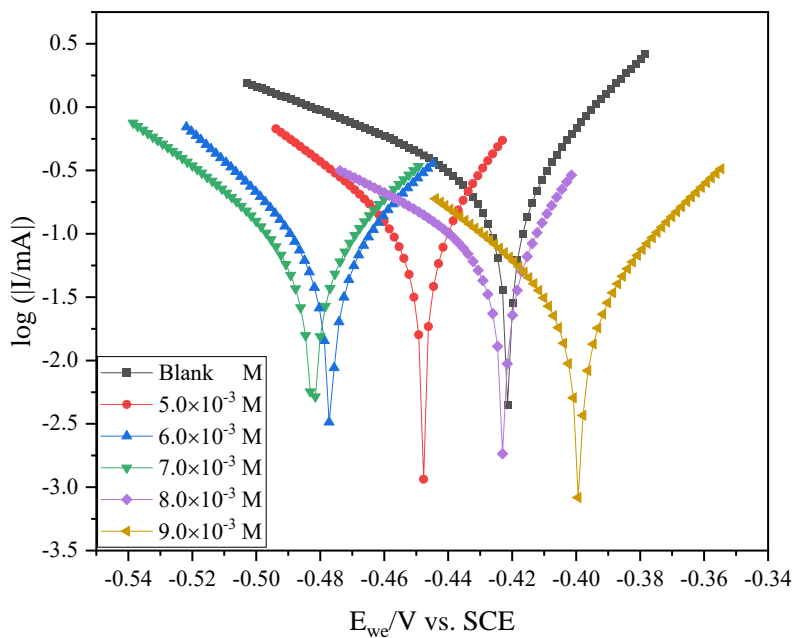


Figure 4.142: Tafel plots for zinc in 1.0 M HCl in the absence and presence of various concentrations of H₂QCA with KI at 303 K.

Table 4.41: Potentiodynamic Polarization (PDP) parameters such as corrosion current density (i_{corr}), corrosion potential (E_{corr}), polarization resistance (R_p), and anodic (β_a) and cathodic (β_c) Tafel slopes utilizing the studied quinoxalines in 1.0 M HCl.

Inhibitor	Conc. ($\times 10^{-3}$ M)	C_r /mpy	E_{corr} / mV vs. SCE	β_a / mV.dec ⁻¹	β_c / mV.dec ⁻¹	i_{corr} / μ A.cm ⁻²	R_p/Ω	%IE _{PDP}	% IE _{WL}
Blank	-	179.249	-421.293	45.1	115.7	298.585	31.50	-	-
MQ6CA	0.5	31.383	-483.511	65.5	57.4	53.167	227.00	82.19	56.80
	1.0	12.878	-436.395	46.2	57.9	21.818	192.00	92.69	58.83
	2.0	6.821	-432.670	49.9	57.2	11.556	-	96.01	59.42
	3.0	6.002	-430.233	41.1	32.6	10.173	-	96.59	62.12
	4.0	5.095	-465.610	37.9	33.2	8.632	637.00	97.11	66.38
Q6CA	0.5	48.087	-379.128	33.5	54.0	81.466	78.7	72.72	55.98
	1.0	18.888	-382.837	48.7	49.4	31.910	201.00	89.31	58.08
	2.0	14.478	-451.386	74.2	52.1	24.528	-	91.79	59.92
	3.0	11.663	-421.751	53.5	54.9	19.703	207.00	93.40	57.62
	4.0	7.323	-467.230	58.9	43.9	12.371	584.00	95.86	59.17
	5.0	133.536	-472.240	49.1	71.8	226.225	49.90	24.23	39.81
	6.0	125.742	-459.786	49.3	75.8	212.423	22.40	28.86	42.01
	7.0	101.405	-463.576	47.4	77.0	171.309	19.80	42.63	39.32

H2QCA without KI	8.0	85.088	-464.396	46.9	75.5	143.745	28.00	51.86	44.49
	9.0	92.140	-465.455	54.4	66.5	155.658	57.6	47.87	41.68
H2QCA with KI	5.0	59.688	-447.780	32.5	55.6	100.834	35.70	66.23	50.39
	6.0	43.627	-476.799	45.4	46.0	73.703	22.5	75.32	51.52
	7.0	39.426	-485.806	49.7	39.6	66.774	56.3	77.64	59.69
	8.0	38.096	-421.681	25.2	47.5	64.346	93.9	78.45	65.81
	9.0	17.853	-398.382	40.5	56.7	30.160	280.00	89.90	66.59

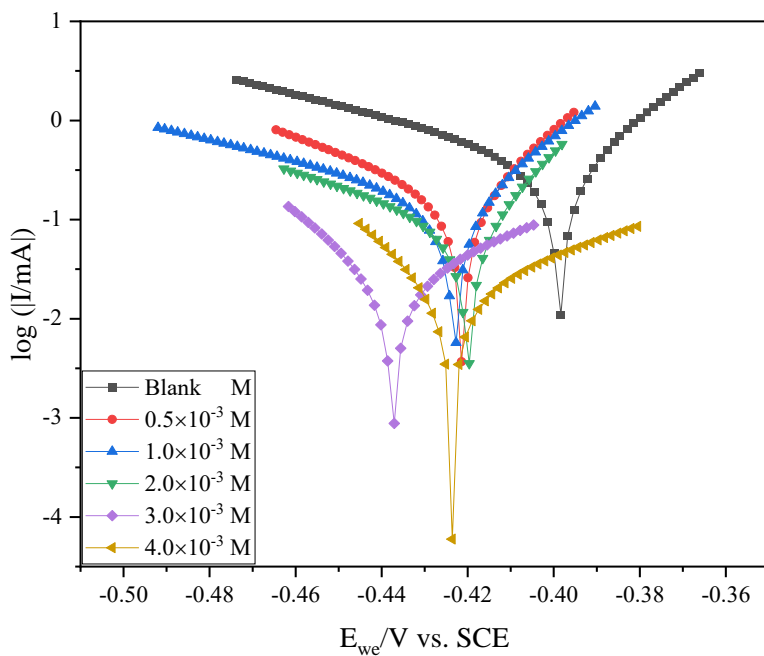


Figure 4.143: Tafel plots for zinc in 1.0 M H₂SO₄ in the absence and presence of various concentrations of MQ6CA at 303 K.

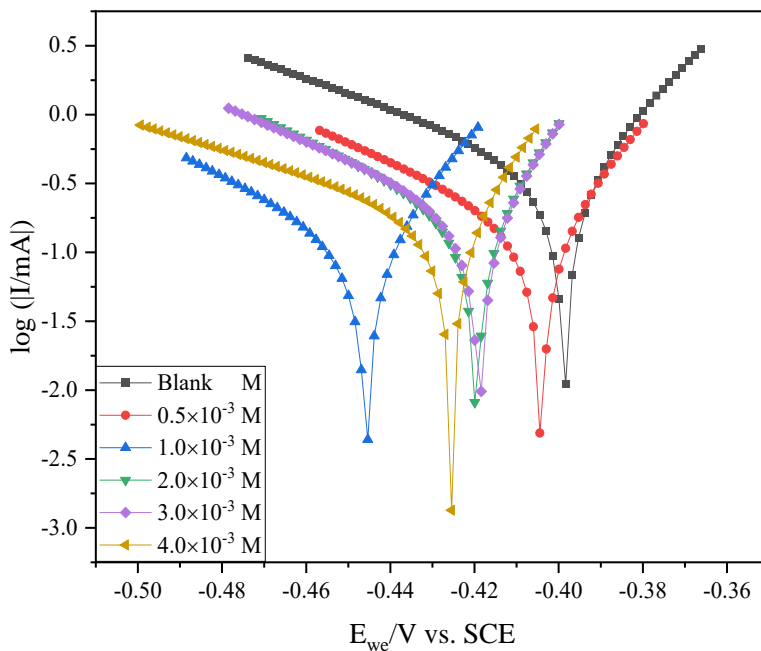


Figure 4.144: Tafel plots for zinc in 1.0 M H₂SO₄ in the absence and presence of various concentrations of Q6CA at 303 K.

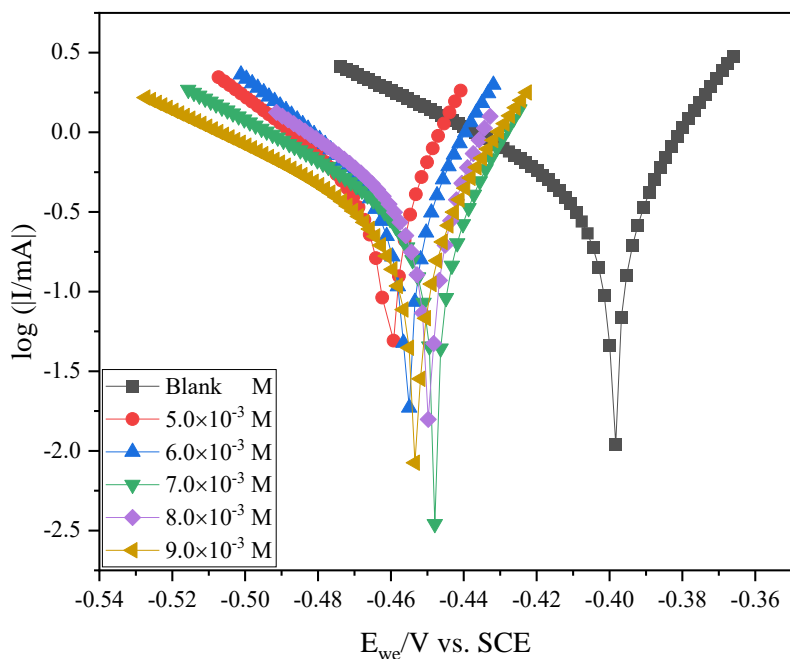


Figure 4.145: Tafel plots for zinc in 1.0 M H₂SO₄ in the absence and presence of various concentrations of H₂QCA without KI at 303 K.

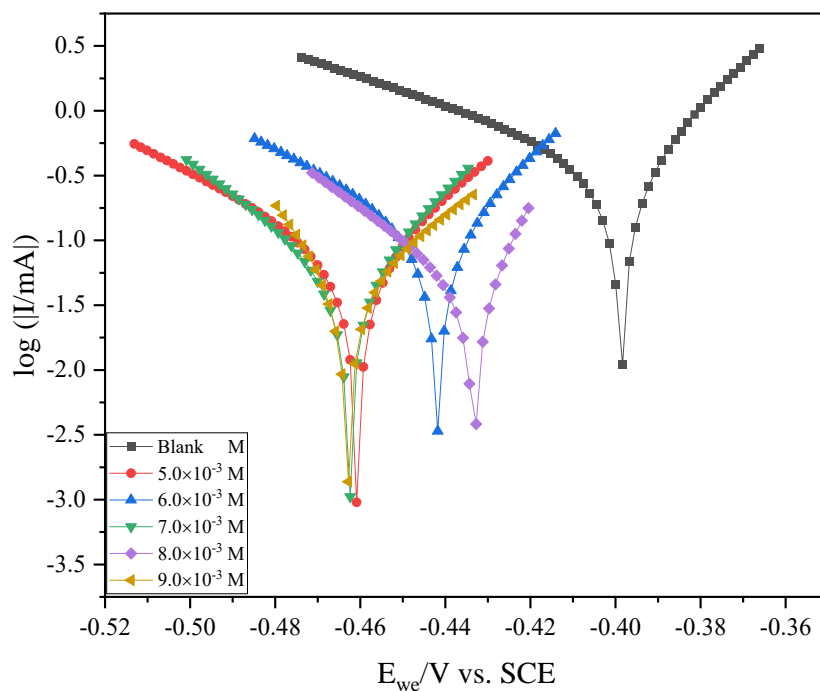


Figure 4.146: Tafel plots for zinc in 1.0 M H₂SO₄ in the absence and presence of various concentrations of H₂QCA with KI at 303 K.

Table 4.42: Potentiodynamic Polarization (PDP) parameters such as corrosion current density (i_{corr}), corrosion potential (E_{corr}), polarization resistance (R_p), and anodic (β_a) and cathodic (β_c) Tafel slopes utilizing the studied quinoxalines in 1.0 M H_2SO_4 .

Inhibitor	Conc. ($\times 10^{-3}$ M)	C_r /mpy	E_{corr} / mV vs. SCE	β_a / mV.dec ⁻¹	β_c / mV.dec ⁻¹	i_{corr} / $\mu A.cm^{-2}$	R_p/Ω	%IE _{PDP}	% IE _{WL}
Blank	-	236.989	-398.631	36.1	92.6	400.360	20.20	-	-
MQ6CA	0.5	101.25	-421.246	29.7	64.1	171.047	57.50	57.28	71.48
	1.0	99.824	-423.095	34.8	88.1	168.639	51.10	57.89	72.63
	2.0	59.397	-419.221	25.4	74.20	97.149	31.70	75.73	72.63
	3.0	20.610	-437.876	55.6	40.7	24.949	243.00	93.78	72.75
	4.0	12.506	-450.601	42.0	31.5	21.123	31.00	94.72	76.03
Q6CA	0.5	91.439	-302.824	28.4	79.3	154.322	64.30	61.45	71.80
	1.0	66.222	-445.725	30.1	66.8	111.874	42.30	72.06	70.68
	2.0	54.729	-422.201	18.4	33.0	92.458	31.70	76.91	70.90
	3.0	21.137	-436.590	22.1	73.4	35.708	58.50	91.08	70.08
	4.0	16.871	-425.509	28.5	53.1	27.3	167.00	93.18	81.70
	5.0	220.571	-460.289	26.6	60.5	372.624	12.00	6.92	29.17
	6.0	214.354	-455.401	30.6	56.8	362.121	10.80	9.55	35.51
	7.0	167.885	-447.821	31.4	83.1	283.618	14.90	29.16	35.70

H2QCA without KI	8.0	193.307	-449.387	25.7	68.4	326.565	15.3	18.43	34.97
	9.0	148.900	-453.165	33.4	87.7	251.545	21.9	37.17	59.08
H2QCA with KI	5.0	73.749	-441.821	36.7	61.9	124.589	57.90	68.88	44.31
	6.0	46.148	-460.706	41.1	61.3	77.994	102.00	80.51	52.10
	7.0	31.656	-462.534	33.1	42.6	53.326	102.00	86.70	54.99
	8.0	24.984	-433.258	19.0	42.4	42.207	99.40	89.46	59.00
	9.0	18.430	-464.016	28.4	12.1	31.135	-	92.22	59.32

The addition of various concentrations of the three studied inhibitors in the corrosive media resulted in the shift of polarization curves towards the low current density regions as compared to the blank system, suggesting an adsorption of the inhibitor molecules on the active sites of the zinc surface. Furthermore, this indicates that the inhibitor molecules reduced the anodic dissolution of zinc and also retarded the hydrogen evolution reaction [351]. Tables 4.41 and 4.42 reveal that the increase in concentrations of MQ6CA, Q6CA, and H2QCA with KI resulted in the reduction of corrosion rate and increase in the percentage inhibition efficiency. This observation can be ascribed to the progressive adsorption of inhibitor molecules on zinc surface with the increase in concentration. The highest inhibition efficiencies were attained at the optimum concentration for each studied inhibitor. A similar trend was also observed in the weight loss analysis. The values of E_{corr} in the uninhibited and inhibited systems can be utilized to give insight into the mode of inhibition. Based on the displacement of E_{corr} with respect to an inhibitor can be classified as cathodic, anodic or mixed-type. Literature reveals that if the displacement in E_{corr} values is greater than ± 85 mV with respect to the E_{corr} of the blank solution, then the inhibitor can be considered as a cathodic or anodic type [352]. In this present study, the maximum displacement in E_{corr} for zinc was found to be 64.571 mV and 65.385 in 1.0 M HCl and 1.0 M H₂SO₄, respectively. These findings imply that MQ6CA, Q6CA, and H2QCA with KI are mixed-type, that is, the studied quinoxaline retards both the anodic and cathodic half-reaction of the zinc corrosion process. The anodic and cathodic Tafel slope values can further be employed in confirming the mode of inhibition possessed by the studied quinoxalines. Tables 4.41 and 4.42 show no regular trend in the Tafel slope values as the concentration of the inhibitors were increased, this finding further indicated that the quinoxalines affected both the anodic and cathodic half-reactions, however, the effect was found to be more prominent on the cathodic half-reaction. From these findings it is evident that the studied quinoxalines inhibitors acted as mixed-type inhibitors on zinc surface. Moreover, the introduction of MQ6CA, Q6CA, and H2QCA with KI to the aggressive solution resulted in the polarization resistance (R_p). Tables 4.41 and 4.42 reveal that the R_p values increased with the increase in the concentration of the inhibitors. According to Nesane and co-workers [336], this effect suggests that further polarization of zinc was retarded by the barrier formed by the increasing population of the inhibitor molecules at the metal/solution interface. The %IE_{PDP} were not in agreement with those of weight loss analysis. According to

Weihua [353] this phenomenon may be ascribed to electrochemical measurements gives instantaneous corrosion rates, whereas the weight loss measurements give average corrosion rates.

4.3.6 Electrochemical impedance spectroscopy (EIS)

EIS provides insight regarding the kinetics of the corrosion process and simultaneously the mechanism of inhibition. In this study, EIS was employed to investigate the behavior of zinc corrosion in 1.0 M HCl and 1.0 M H₂SO₄ in the absence and presence of various concentrations of the studied quinoxalines at 303 K. The technique was conducted at the OCP after 3600 seconds of zinc immersion until a steady corrosion potential (E_{corr}) for all the working electrodes was established. Figures 4.147 – 4.160 show represent the obtained Nyquist plots and corresponding Bode plots. The Nyquist plots are represented by the imperfect semicircles capacitive loops which are indicative of a charge transfer process that controls the corrosion of zinc in acidic medium. These figures show that the diameter of these imperfect semicircles increases with increase in the concentration of the inhibitors. This can be attributed to the increase in the surface coverage of adsorptive quinoxaline molecules on zinc surface.

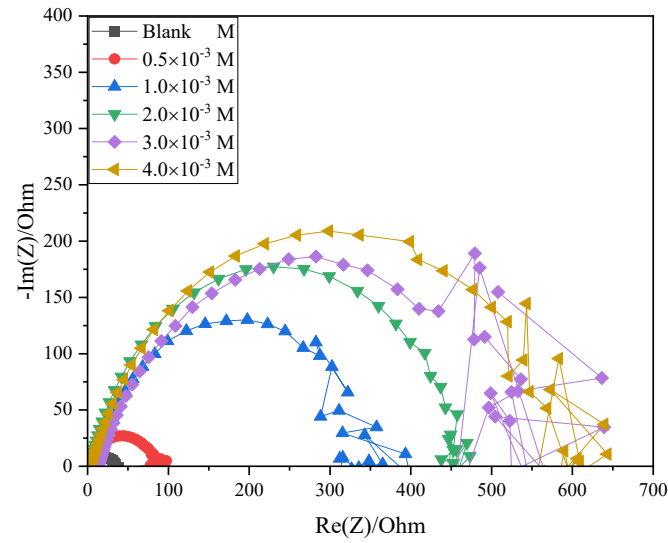


Figure 4.147: Nyquist plot of zinc in 1.0 M HCl in the presence and absence of various concentrations of MQ6CA.

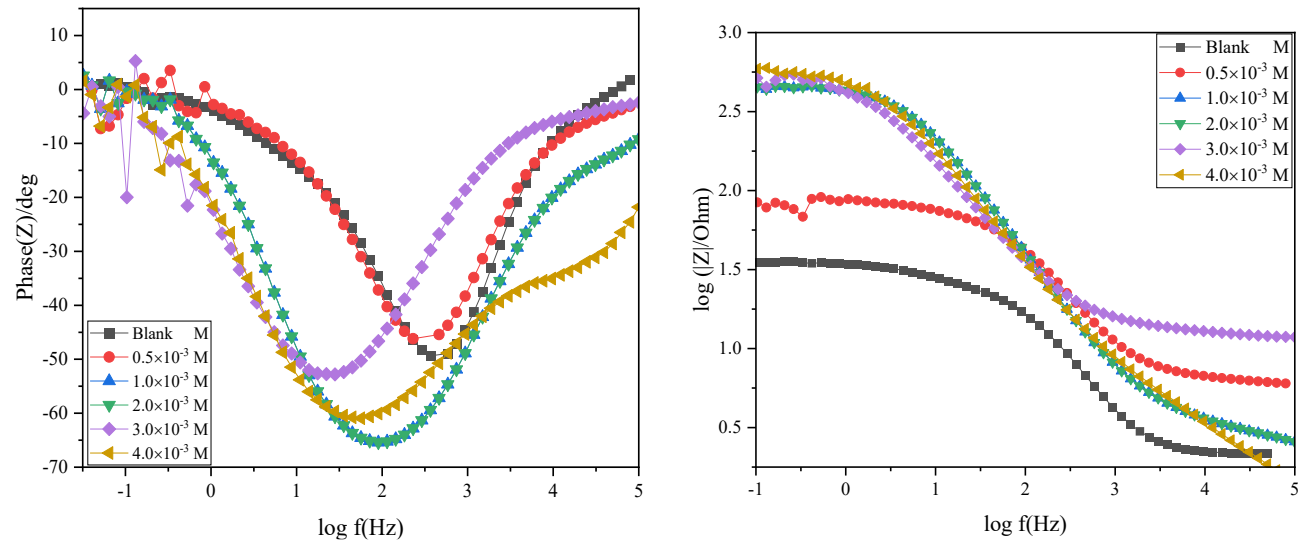


Figure 4.148: Bode plot of zinc in 1.0 M HCl in the presence and absence of various concentrations of MQ6CA.

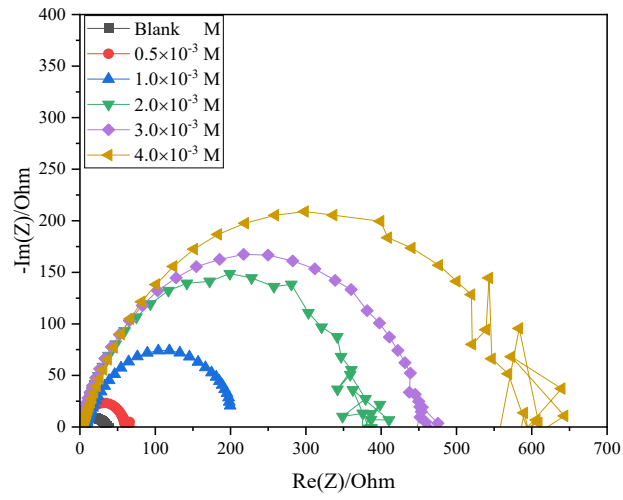


Figure 4.149: Nyquist plot of zinc in 1.0 M HCl in the presence and absence of various concentrations of Q6CA.

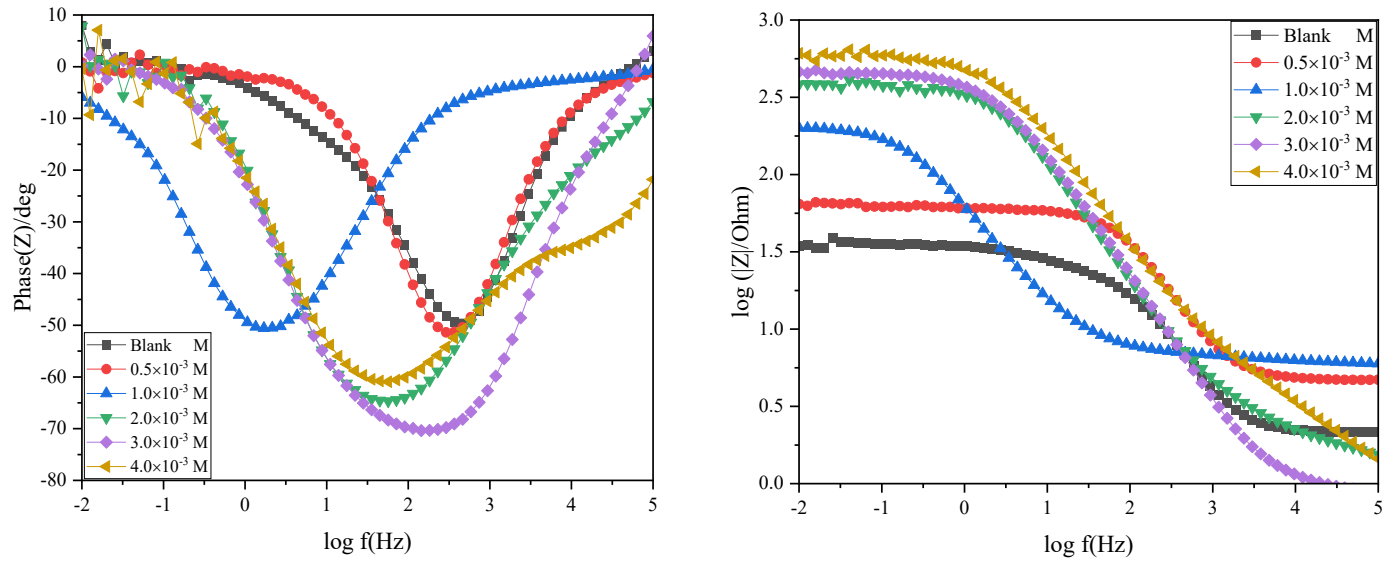


Figure 4.150: Bode plot of zinc in 1.0 M HCl in the presence and absence of various concentrations of Q6CA.

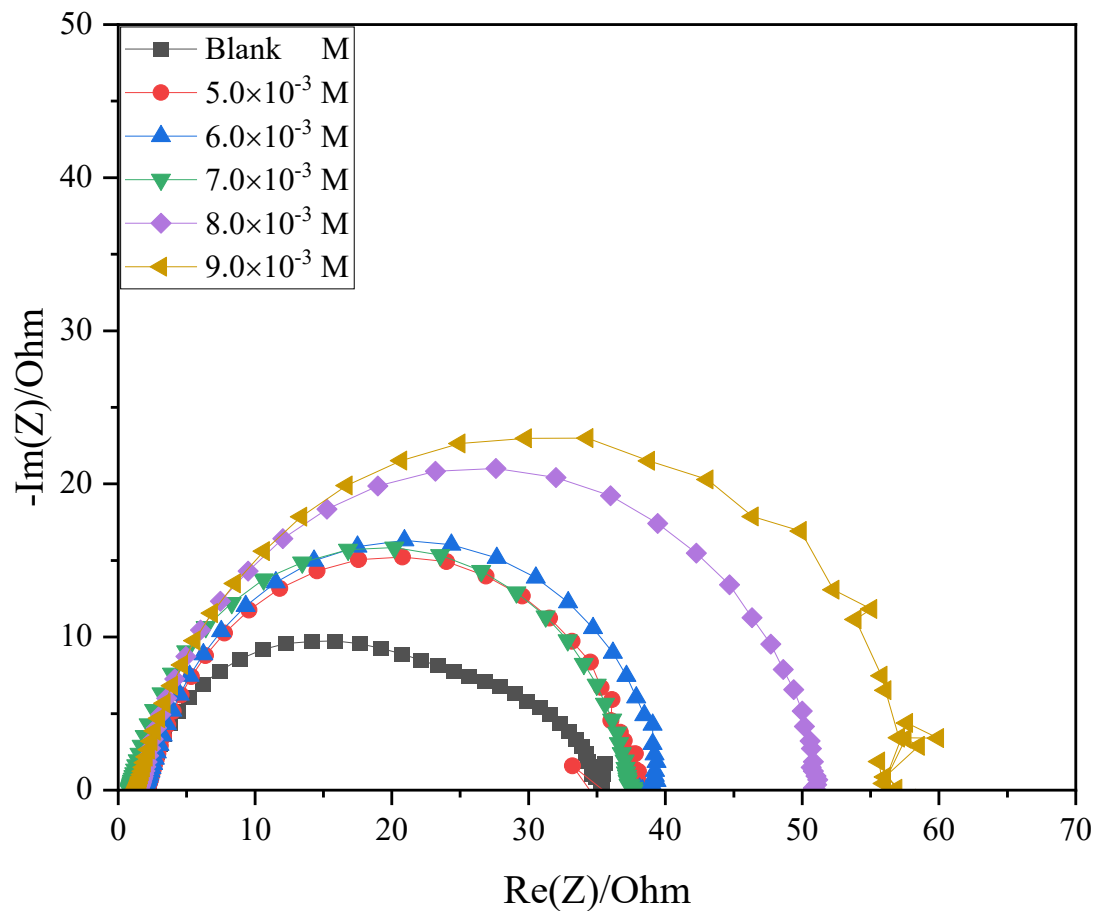


Figure 4.151: Nyquist plot of zinc in 1.0 M HCl in the presence and absence of various concentrations of H₂QCA without KI.

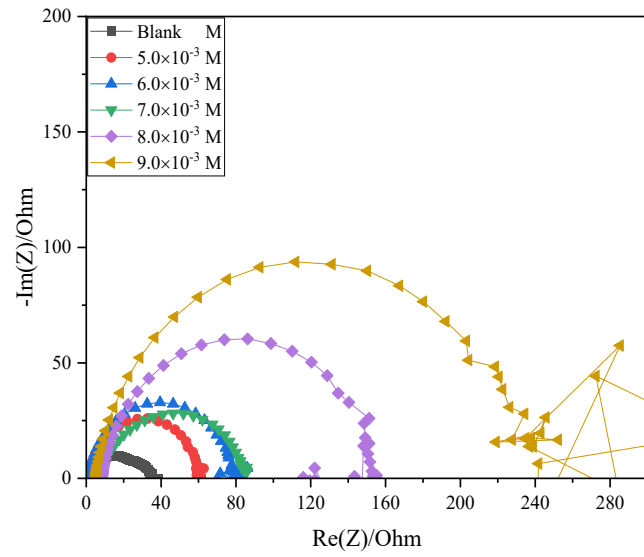


Figure 4.152: Nyquist plot of zinc in 1.0 M HCl in the presence and absence of various concentrations of H₂QCA with KI.

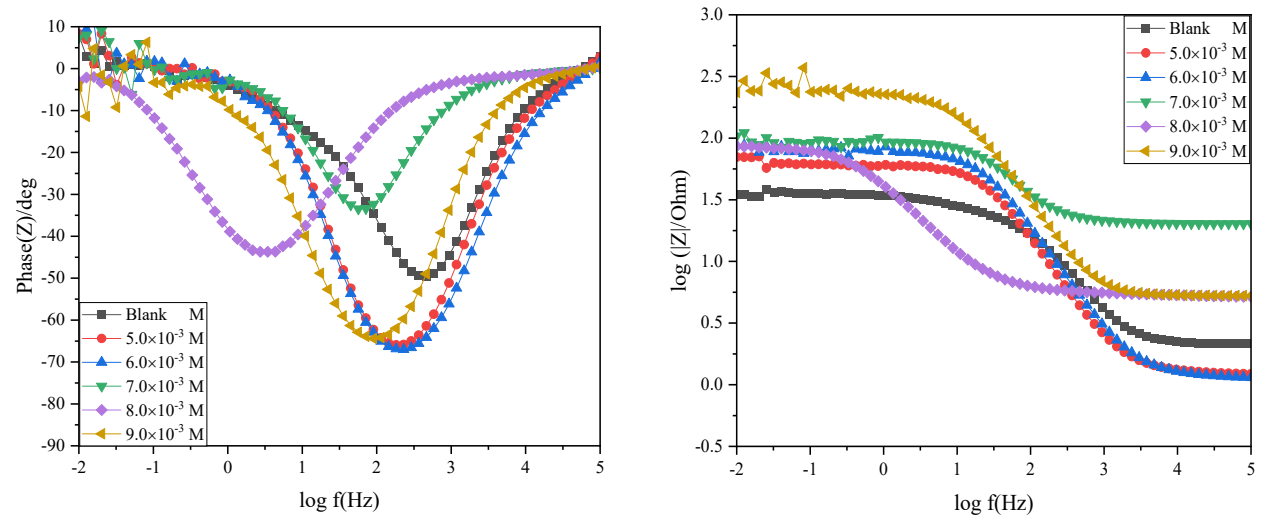


Figure 4.153: Bode plot of zinc in 1.0 M HCl in the presence and absence of various concentrations of H₂QCA with KI.

Table 4.43: Electrochemical impedance parameters such as the resistance of charge transfer (R_{ct}), constant phase element (CPE) and the CPE exponent (n) of zinc in the absence and presence of various concentrations of the studied quinoxalines in 1.0 M HCl.

Inhibitor	Conc. ($\times 10^{-3}$ M)	R_1/Ω	$Q_3/F.s^{(a-1)}$	R_2/Ω	C_1	R_3/Ω	n	θ	%IE _{EIS}	%IE _{PDP}	%IE _{WL}
Blank	-	2.189	1.114e-3	33.82	48.72e-6	12.180	0.538	-	-	-	-
MQ6CA	0.5	6.016	0.126e-3	78.21	6.602e-6	0.926	0.758	0.5676	56.76	82.19	56.80
	1.0	9.656	0.161e-3	330.30	7.717e-6	1.840	0.809	0.8976	89.76	92.69	58.83
	2.0	2.513	0.115e-3	461.10	4.713e-6	1.686	0.813	0.9267	92.67	96.01	59.42
	3.0	11.82	0.264e-3	538.80	3.459e-6	1.411	0.748	0.9372	93.72	96.59	62.12
	4.0	1.369	0.202e-3	604.30	3.691e6	3.434	0.751	0.9440	94.40	97.11	66.38
Q6CA	0.5	4.710	0.100e-6	57.66	20.94e-6	2.529	0.719	0.4135	41.35	72.72	55.98
	1.0	6.097	0.642e-3	211.30	48.29e-6	0.855	0.749	0.8399	83.99	89.31	58.08
	2.0	1.598	0.246e-3	386.40	10.77e-6	1.603	0.800	0.9125	91.25	91.79	59.92
	3.0	0.932	0.225e-3	459.10	17.46e-6	1.371	0.776	0.9263	92.63	93.40	57.62
	4.0	1.369	0.201e-3	604.30	3.691e-6	3.434	0.750	0.9440	94.40	95.86	59.17
H2QCA without KI	5.0	2.165	0.236e-3	35.98	-0.120e-15	17.78e-9	0.877	0.0600	06.00	24.23	39.81
	6.0	1.748	0.180e-3	37.54	24.44e-6	1.015	0.875	0.0991	09.91	28.86	42.01
	7.0	0.888	0.123e-3	37.10	45.37e-6	2.208	0.832	0.0884	08.84	42.63	39.32
	8.0	1.504	0.170e-3	50.42	32.23e-6	0.889	0.845	0.3292	32.92	51.86	44.49
	9.0	1.347	0.228e-3	57.18	32.03e-6	0.815	0.821	0.4085	40.85	47.87	41.68
H2QCA with KI	5.0	1.247	0.148e-3	60.66	54.53e-6	1.254	0.815	0.4425	44.25	66.23	50.39
	6.0	1.168	0.164e-3	78.94	0.457e-18	1.155	0.890	0.5716	57.16	75.32	51.52
	7.0	1.982	0.159e-3	82.41	81.63e-6	1.522	0.873	0.5896	58.96	77.64	59.69
	8.0	1.780	0.105e-3	136.50	0.140e-6	0.719	0.902	0.7522	75.22	78.45	65.81
	9.0	5.322	0.185e-3	250.6	40.78e-6	6.648	0.800	0.8650	86.50	89.90	66.59

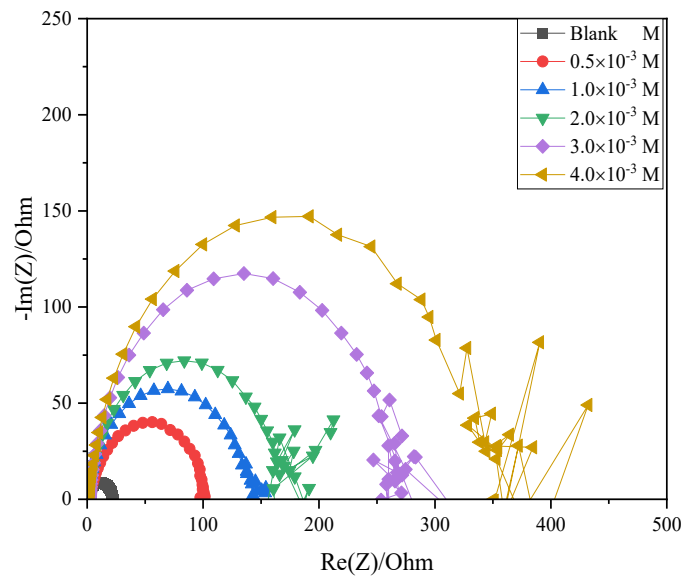


Figure 4.154: Nyquist plot of zinc in 1.0 M H_2SO_4 in the presence and absence of various concentrations of MQ6CA.

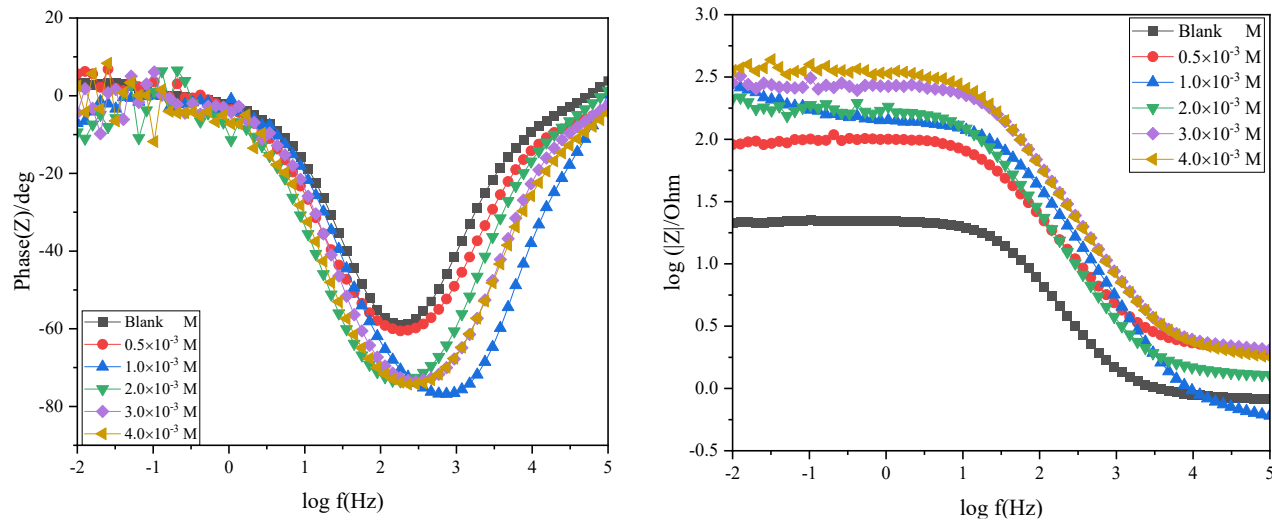


Figure 4.155: Bode plot of zinc in 1.0 M H_2SO_4 in the presence and absence of various concentrations of MQ6CA.

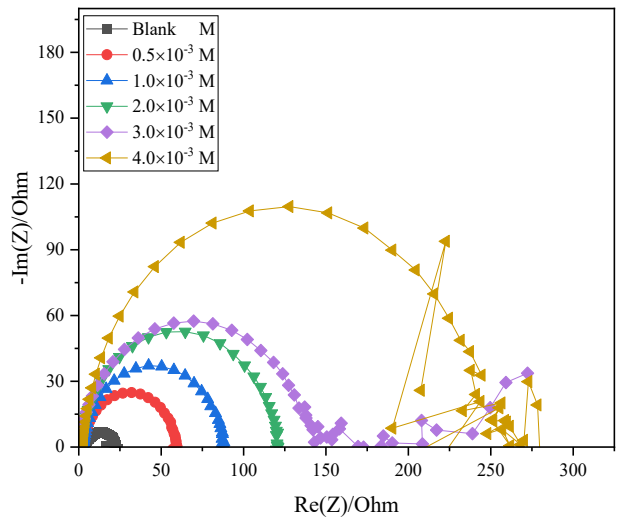


Figure 4.156: Nyquist plot of zinc in 1.0 M H_2SO_4 in the presence and absence of various concentrations of Q6CA.

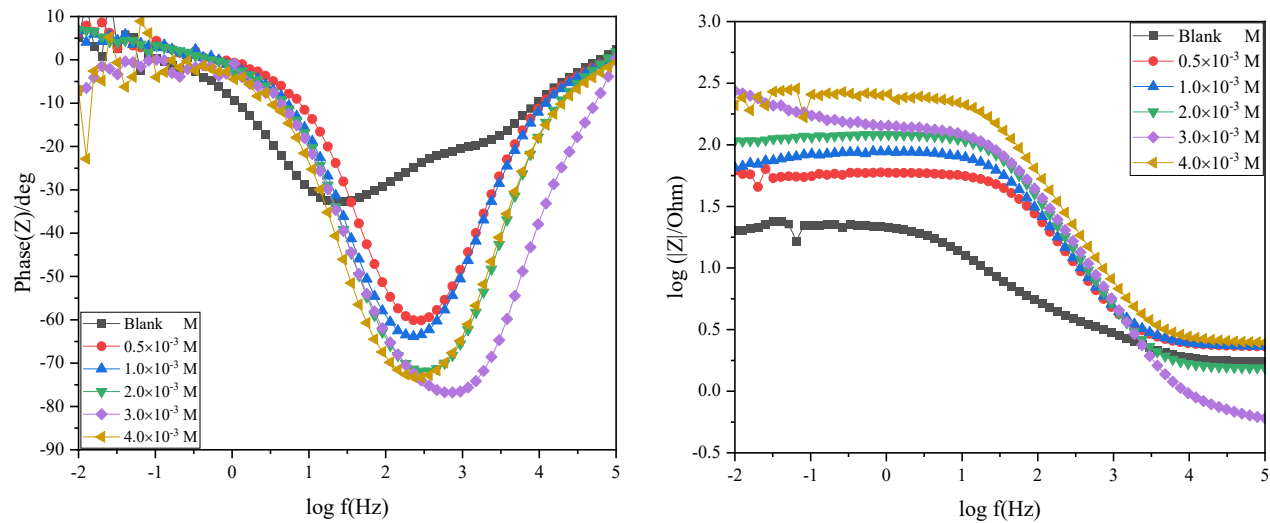


Figure 4.157: Bode plot of zinc in 1.0 M H_2SO_4 in the presence and absence of various concentrations of Q6CA.

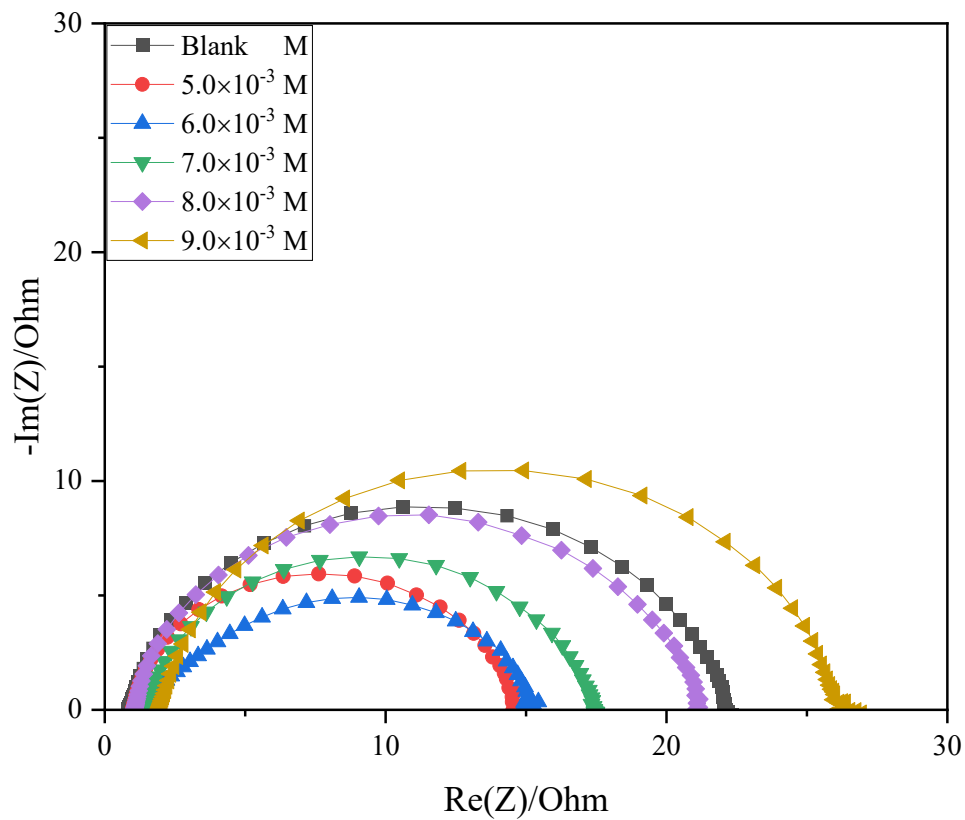


Figure 4.158: Nyquist plot of zinc in 1.0 M H₂SO₄ in the presence and absence of various concentrations of H₂QCA without KI.

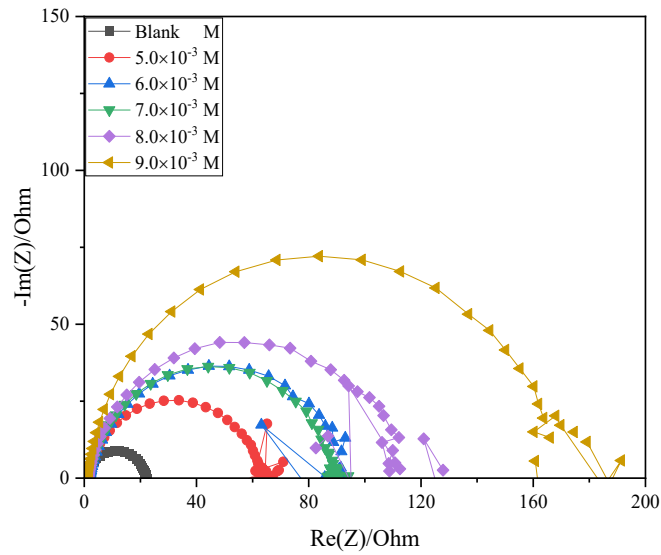


Figure 4.159: Nyquist plot of zinc in 1.0 M H_2SO_4 in the presence and absence of various concentrations of H₂QCA with KI.

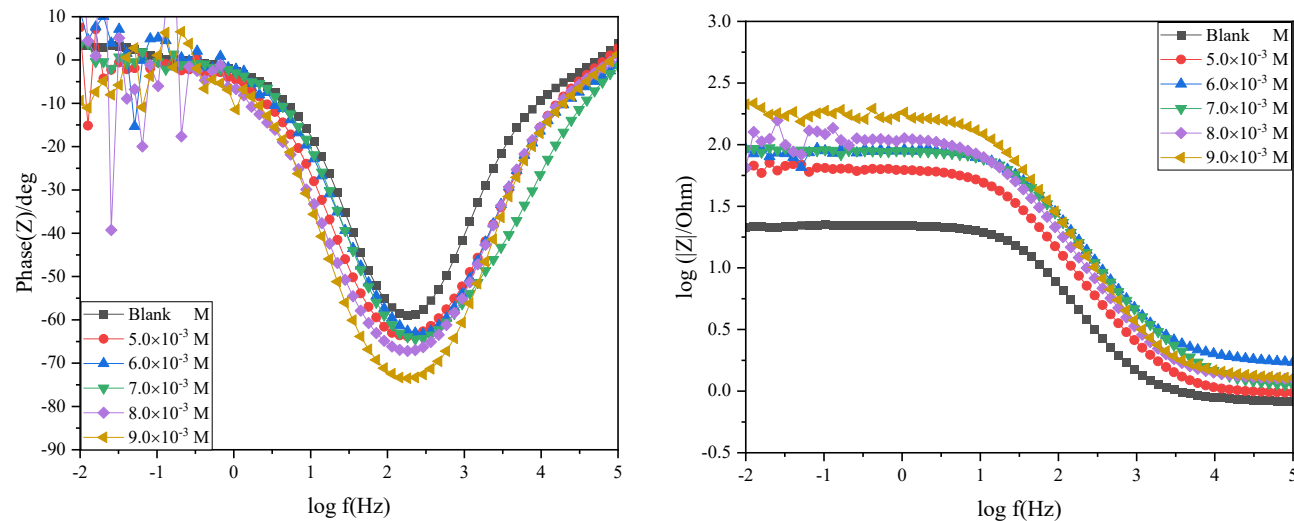


Figure 4.160: Bode plot of zinc in 1.0 M H_2SO_4 in the presence and absence of various concentrations of H₂QCA with KI.

Table 4.44: Electrochemical impedance parameters such as the resistance of charge transfer (R_{ct}), constant phase element (CPE) and the CPE exponent (n) of zinc in the absence and presence of various concentrations of the studied quinoxalines in 1.0 M H_2SO_4 .

Inhibitor	Conc. ($\times 10^{-3} M$)	R_1/Ω	$Q_3/F.s^{(a-1)}$	R_2/Ω	C_1	R_3/Ω	n	θ	%IE _{EIS}	%IE _{PDP}	%IE _{WL}
Blank	-	0.843	0.339e-3	21.15	97.24e-3	0.616	0.833	-	-	-	-
MQ6CA	0.5	1.927	0.153e-3	97.31	9.938e-6	0.530	0.832	0.7827	78.27	57.28	71.48
	1.0	1.662	88.57e-6	144.80	25.73e-6	1.844	0.685	0.8539	85.39	57.89	72.63
	2.0	1.316	81.46e-6	173.40	32.38e-6	1.173	0.836	0.8780	87.80	75.73	72.63
	3.0	2.212	0.111e-6	278.50	20.11e-6	0.096	0.885	0.9241	92.41	93.78	72.75
	4.0	1.804	39.33e-6	354.60	9.339e-6	1.179	0.863	0.9404	94.04	94.72	76.03
Q6CA	0.5	2.338	54.05e-6	55.14	33.74e-6	4.890	0.862	0.6164	61.64	61.45	71.80
	1.0	2.358	40.75e-6	78.92	32.13e-6	6.855	0.889	0.7320	73.20	72.06	70.68
	2.0	1.416	57.69e-6	114.80	13.10e-6	0.128	0.945	0.8158	81.58	76.91	70.90
	3.0	1.658	72.85e-6	141.70	24.99e-6	1.593	0.723	0.8507	85.07	91.08	70.08
	4.0	2.505	23.93e-6	237.70	16.96e-6	2.692	0.856	0.9110	91.10	93.18	81.70
H2QCA without KI	5.0	1.037	-0.440	13.13	96.33e-6	0.157e9	0.850	-0.6108	-61.20	6.92	29.17
	6.0	1.497	0.628e-3	13.60	81.07e-6	2.865	0.801	-0.5551	-55.51	9.55	35.51
	7.0	1.373	0.167e-3	16.04	43.06e-6	1.078	0.817	-0.3186	-31.86	29.16	35.70
	8.0	0.968	0.167e-3	19.53	-76.91e-9	0.088	0.902	-0.0829	-8.29	18.43	34.97
	9.0	1.929	0.153e-3	24.44	76.52e-18	0.039	0.904	0.1346	13.46	37.17	59.08
H2QCA with KI	5.0	0.962	0.277e-3	63.17	0.889e-9	0.012	0.855	0.6652	66.52	68.88	44.31
	6.0	1.729	0.110e-3	86.01	18.75e-6	0.955	0.832	0.7541	75.41	80.51	52.10
	7.0	1.150	0.109e-6	88.51	21.94e-6	2.836	0.829	0.7610	76.10	86.70	54.99
	8.0	1.379	0.166e-6	105.5	75.98e-6	1.061	0.717	0.7995	79.95	89.46	59.00
	9.0	1.329	82.46e-6	175.4	35.65e-6	1.759	0.856	0.8794	87.94	92.22	59.32

The Nyquist plots presented in this study consists of a capacitive loop at high-frequency regions which is an indicative of the charge transfer resistance and a double layer capacitance (C_{dl}). The similar shapes observed in these plots indicate that the three studied inhibitors retard the rate of corrosion in a similar mechanism [336]. The model of the equivalent circuit utilized to fit the experimental data in 1.0 M HCl and 1.0 M H_2SO_4 in the presence and absence of various concentrations of the studied quinoxalines is shown in figure 4.161. This circuit consists of a charge transfer resistance (R_{ct}), solution resistance (R_s), and constant phase element (CPE).

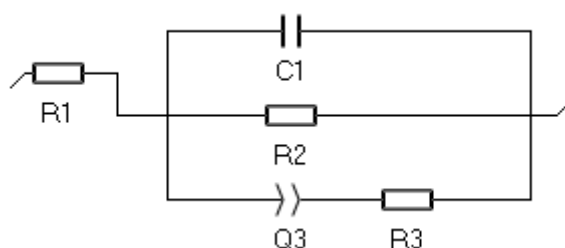


Figure 4.161: Equivalent circuit utilized to fit the impedance spectra obtained for zinc corrosion in 1.0 M HCl and 1.0 M H_2SO_4 in the absence and presence of various concentrations of the studied quinoxalines.

where R_1 , R_2 , R_3 , Q_2 , and C_1 are the solution resistance (R_s), charge transfer resistance (R_{ct}), charge transfer after the formation of the film layer, constant phase element (CPE) and capacitor, respectively.

The electrochemical impedance parameters for zinc corrosion in 1.0 M HCl and 1.0 M H_2SO_4 in the absence and presence of the studied quinoxalines are illustrated in Tables 4.43 and 4.44, respectively. It is clear from these tables that the charge transfer resistance increased with the increase in concentration of MQ6CA, Q6CA, and H2QCA, which resulted in the increase in the inhibition efficiency. There was no regular trend in the obtained values of CPE, however, the tables reveal that as the inhibitors were introduced in the corrosive solution, there was a decrease in the values of CPE. This decrease in CPE values may be ascribed to the adsorption film layer formed by the increasing population of the inhibitor molecules on zinc surface, or perhaps the decrease in local dielectric constant. The increase in the values of n in the inhibited system as compared to the uninhibited system is an indication that the adsorbed quinoxaline molecules on zinc surface

resulted in the improvement of inhomogeneity of the metal. The results obtained from EIS were reasonably in agreement with those of PDP.

4.3.7 Atomic absorption spectroscopy

Graphite furnace atomic absorption spectroscopy (GFAAS) has been widely utilized for the analysis of small concentrations of metal in aqueous solutions [354, 355]. In this study, GFAAS was employed to measure the concentrations of the zinc ions that passed into the in 1.0 M HCl and 1.0 M H₂SO₄ due to zinc corrosion. A calibration curve for zinc was prepared from known standard concentrations before the analysis of the samples. The concentration of all the samples having zinc ions were evaluated from the attained calibration curve through the relationship given by equation (57). The inhibition efficiency of the studied quinoxalines towards the corrosion of zinc was evaluated using equation (55), and the results are listed in Tables 4.45 and 4.46

$$Y = 0.0283X - 0.0148 \quad (57)$$

where Y is the absorbance and X is concentration (ppm)

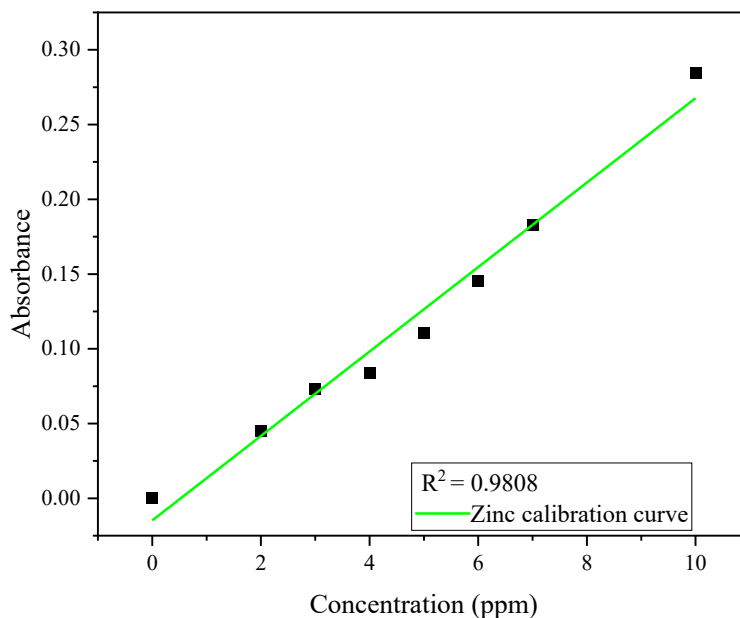


Figure 4.162: Absorbance against concentration calibration curve for zinc.

Table 4.45: Amount of dissolved zinc present in 1.0 M HCl in the absence and presence of the studied quinoxalines.

Inhibitors	Mean absorbance	Concentration (ppm)	%IE _{AAS}
Blank	0.098	3.984	-
MQ6CA	0.009	0.840	78.92
Q6CA	0.014	1.003	74.82
H2QCA	0.037	1.840	53.81

Table 4.46: Amount of dissolved zinc present in 1.0 M H₂SO₄ in the absence and presence of the studied quinoxalines.

Inhibitors	Mean absorbance	Concentration (ppm)	%IE _{AAS}
Blank	0.143	5.567	-
MQ6CA	0.035	1.770	68.20
Q6CA	0.055	2.484	55.45
H2QCA	0.053	2.390	57.07

Tables 4.45 and 4.46 reveal the concentration of zinc ions were higher in the blank solution as compared to the solutions when the quinoxalines were introduced. The decreases in the zinc ions concentration in the solution containing the studied quinoxalines can be attributed to the availability of the adsorbing inhibitor molecules which forms a protective layer on zinc surface, consequently blocking the acids from further oxidation the metal. As observed in the weight loss measurement, MQ6CA, Q6CA, and H2QCA protects zinc from further dissolution in the corrosive media. The inhibition efficiencies were to vary in the order: MQ6CA>Q6CA>H2QCA. A similar order was observed in the weight loss measurements.

4.3.8 Fourier Transform Infrared Spectroscopy (FTIR)

FTIR technique was utilized to gain more insight into the interactions between the studied quinoxalines and zinc surface in 1.0 M HCl and 1.0 M H₂SO₄. The FTIR spectra of the pure quinoxalines were compared to the adsorption film formed spectra that was scratched from the metal surface after weight loss measurements. These spectra are presented in figures 4.163 – 4.168. Quinoxalines exhibits several heteroatoms such as O and N, functional groups that have electron density. Reports in literature suggests that adsorption film between the vacant *d*-orbitals of metal and the inhibitor molecules is likely to form within these functional groups [299]. These functional groups together with their corresponding characteristic adsorption peaks from FTIR spectra of the studied quinoxalines in 1.0 M HCl and 1.0 M H₂SO₄ are presented in Tables 4.47 and 4.48, respectively.

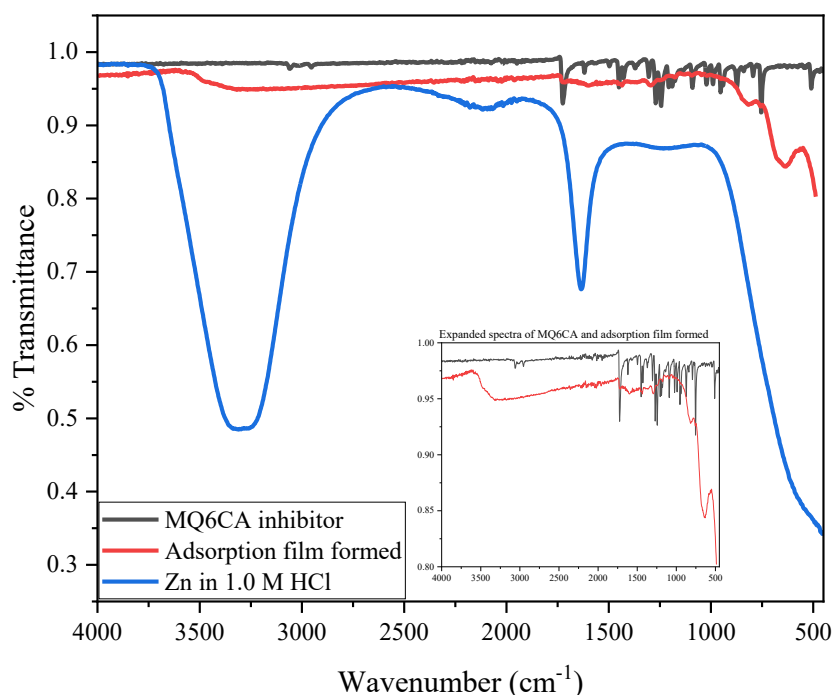


Figure 4.163: FTIR spectra of pure MQ6CA and the adsorption film formed on zinc surface in 1.0 M HCl in the presence of MQ6CA.

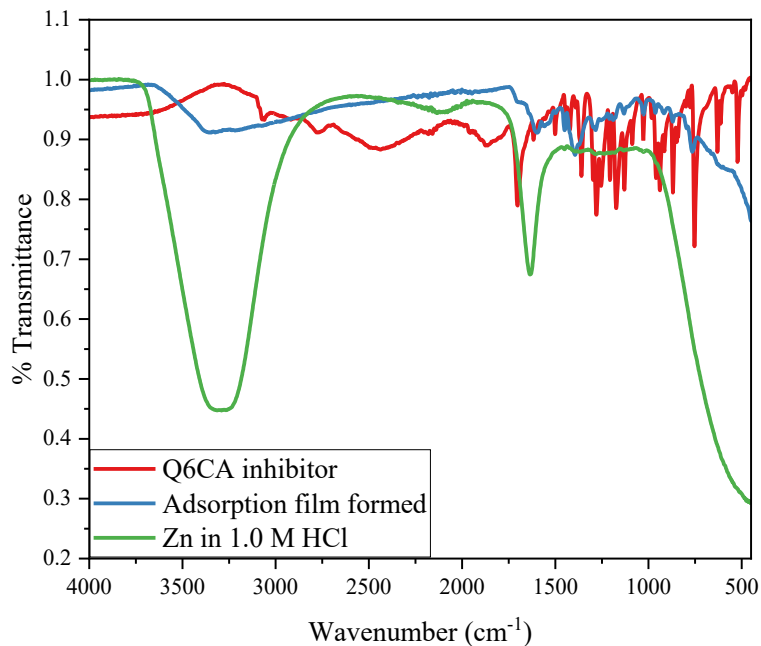


Figure 4.164: FTIR spectra of pure Q6CA and the adsorption film formed on zinc surface in 1.0 M HCl in the presence of Q6CA.

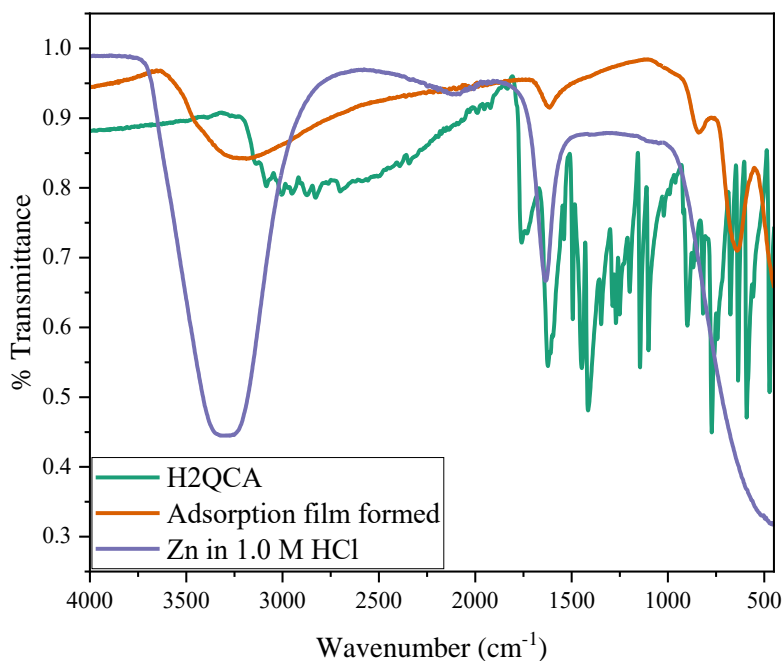


Figure 4.165: FTIR spectra of pure H2QCA and the adsorption film formed on zinc surface in 1.0 M HCl in the presence of H2QCA.

Table 4.47: Peaks and identification from FTIR spectra of the studied quinoxalines and adsorption film formed on the Zinc in 1.0 M HCl.

Inhibitor-Zinc	Functional Groups					
	Peaks from FTIR spectra (cm ⁻¹)					
	C=O	C-O	C-N	C=C	Aromatic C-H	O-H
MQC6A	1717.90	1087.67	1271.78	-	-	-
MQ6CA-Zn	-	-	-	-	-	3322.91
Q6CA	1706.61	-	1281.73	-	-	-
Q6CA-Zn	1613.14	-	-	-	-	3387.73
H2QCA	1727.86	1099.61	1270.40	1607.47	-	-
H2QCA-Zn	-	-	-	-	-	3253.19

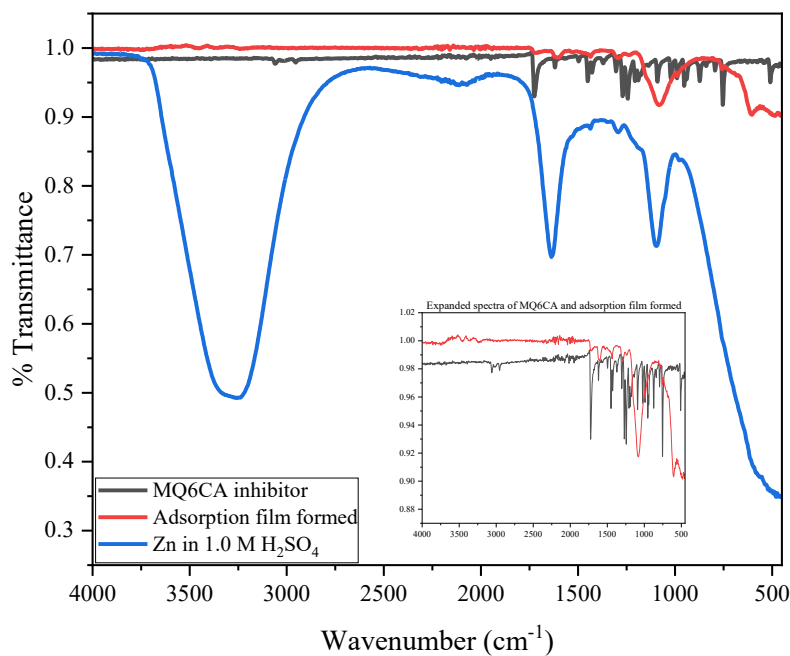


Figure 4.166: FTIR spectra of pure MQ6CA and the adsorption film formed on zinc surface in 1.0 M H₂SO₄ in the presence of MQ6CA.

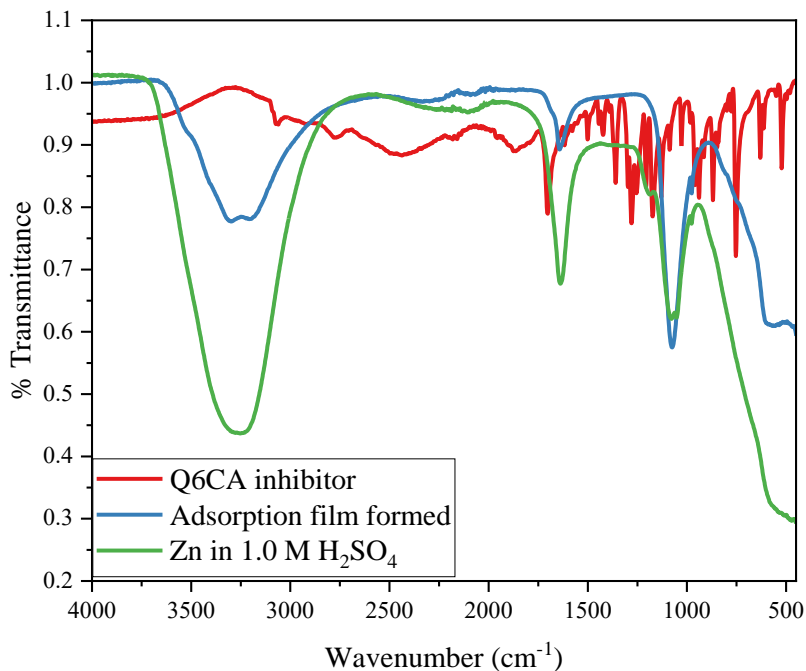


Figure 4.167: FTIR spectra of pure Q6CA and the adsorption film formed on zinc surface in 1.0 M H₂SO₄ in the presence of Q6CA.

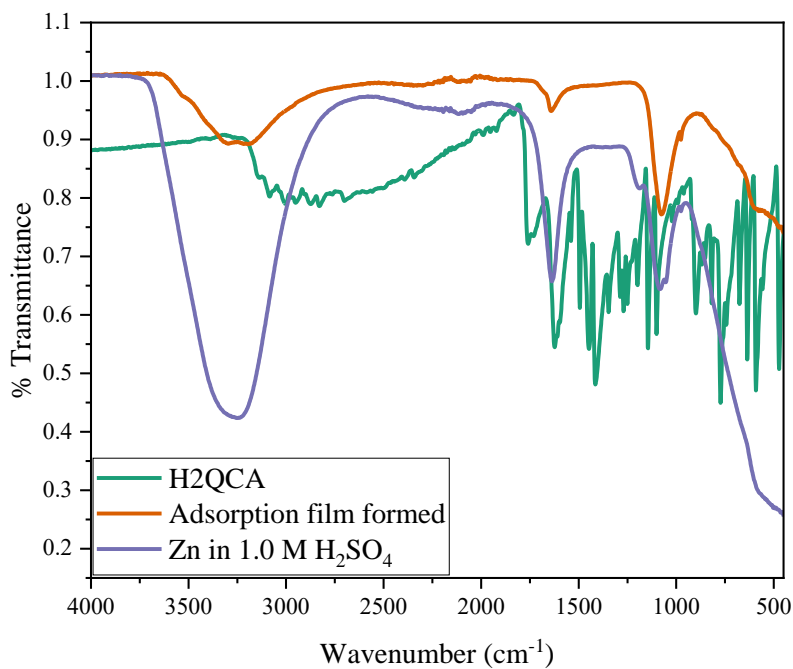


Figure 4.168: FTIR spectra of pure H2QCA and the adsorption film formed on zinc surface in 1.0 M H₂SO₄ in the presence of H2QCA.

Table 4.48: Peaks and identification from FTIR spectra of the studied quinoxalines and adsorption film formed on the zinc in 1.0 M H₂SO₄.

Inhibitor- Zinc	Functional Groups					
	Peaks from FTIR spectra (cm ⁻¹)					
	C=O	C-O	C-N	C=C	Aromatic C-H	O-H
MQC6A	1717.89	1087.67	1271.78	-	-	-
MQ6CA-Zn	-	1060.60	-	-	-	-
Q6CA	1708.03	-	1283.15	-	-	-
Q6CA-Zn	1648.55	1083.45	-	-	-	3299.93
H2QCA	1720.44	-	1271.82	1606.66	-	-
H2QCA-Zn	-	1087.70	-	-	-	3260.27

Tables 4.47 and 4.48 show the peaks corresponding to the adsorption preferential functional groups on the zinc surface suggested by Literature [350]. Examining these tables, one can observe that there was a disappearance of C=O peaks in the MQ6CA-Zn²⁺ and H2QCA-Zn²⁺ complex spectra and a shift of peaks from 1706.61 cm⁻¹ to 1613.14 cm⁻¹ and 1708.08 cm⁻¹ to 1648.55 cm⁻¹ in the Q6CA-Zn²⁺ complex spectra in 1.0 M HCl and 1.0 H₂SO₄, respectively. The disappearance of these spectra can be attributed to the lone pairs of the O atom in this functional group that may be involved in the formation of a protective layer of zinc surface. Table 4.47 reveals a disappearance of C-O and C-N in the adsorption film formed spectra and appearance of peaks within the wavenumber 3387.73 – 3253.19 cm⁻¹ corresponding to O-H stretch for the carboxylic acid. Figures 4.166 and 4.167 show an appearance of intense peaks in the adsorption film spectra around 1087.67 corresponding to the C-O group, which is one of the possible electron-donor group. Table 4.48 also reveals an appearance of a peak at 1606.66 cm⁻¹ corresponding to the C=C vibration. The changes between the spectra of the pure studied quinoxalines and the adsorption film formed after the 7 hours immersion of zinc in 1.0 M HCl and 1.0 M H₂SO₄ are symbolic that some chemical interaction occurred between the inhibitor molecules and the zinc surface.

4.4 Aluminium

4.4.1 Potentiodynamic polarization (PDP)

PDP measurements were conducted at room temperature (303 K) in 0.5 M HCl in the absence and presence of various concentrations of MQ6CA, Q6CA, and H2QCA with KI in order to get more insight into the corrosion mechanism process of aluminium. Figures 4.169 – 4.171 show the obtained Tafel plots. Inspection of these figures one can observe that in both corrosive media the anodic and cathodic half-reactions of aluminium corrosion were altered by the introduction of the studied quinoxalines. The corresponding potentiodynamic parameters such as corrosion current density (i_{corr}), corrosion potential (E_{corr}), polarization resistance (R_p), and anodic (β_a) and cathodic (β_c) Tafel slopes were successfully evaluated from both the anodic and cathodic regions of the Tafel plots. These parameters are listed in Table 4.49. The potentiodynamic polarization inhibition efficiency (%IE_{PDP}) was then evaluated from the measured i_{corr} value from equation (43).

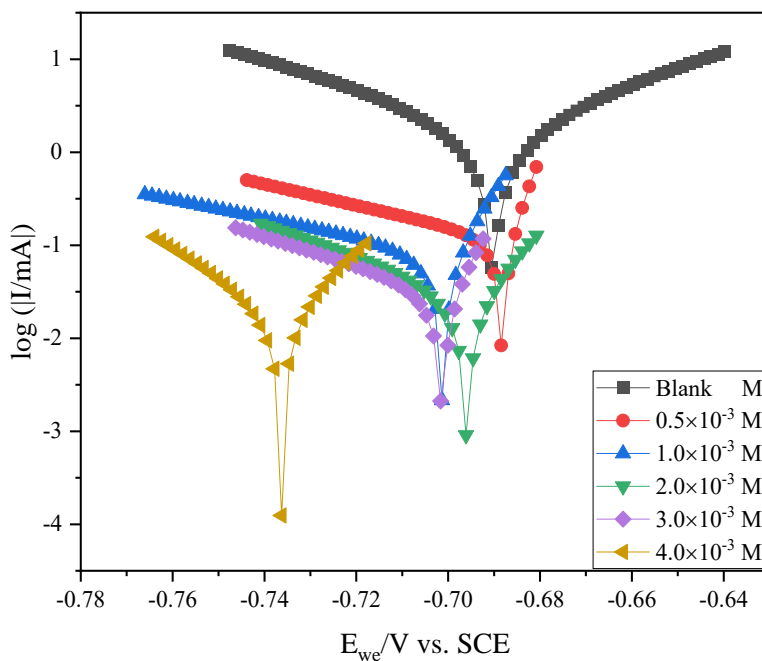


Figure 4.169: Tafel plots for zinc in 0.5 M HCl in the absence and presence of various concentrations of MQ6CA at 303 K.

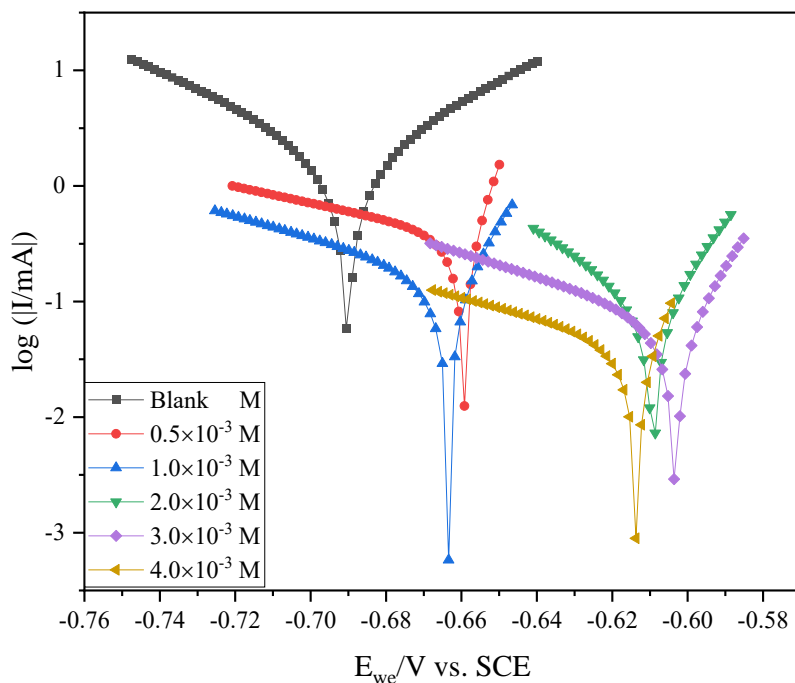


Figure 4.170: Tafel plots for zinc in 0.5 M HCl in the absence and presence of various concentrations of Q6CA at 303 K.

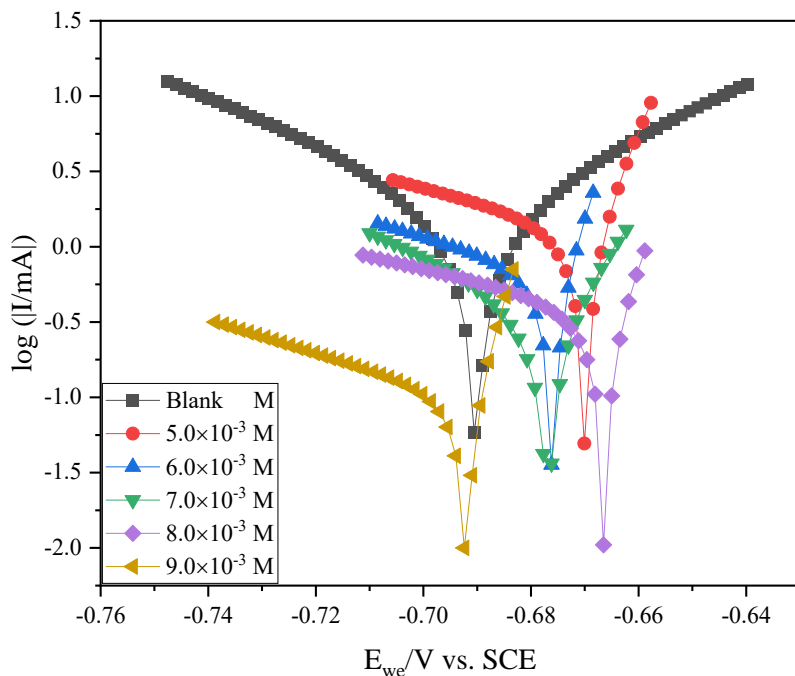


Figure 4.171: Tafel plots for zinc in 0.5 M HCl in the absence and presence of various concentrations of H2QCA with KI at 303 K.

Table 4.49: Potentiodynamic Polarization (PDP) parameters such as corrosion current density (i_{corr}), corrosion potential (E_{corr}), polarization resistance (R_p), and anodic (β_a) and cathodic (β_c) Tafel slopes utilizing the studied quinoxalines in 0.5 M HCl.

Inhibitor	Conc. ($\times 10^{-3}$ M)	C_R /mpy	E_{corr} / mV vs. SCE	β_a / mV.dec ⁻¹	β_c / mV.dec ⁻¹	i_{corr} / $\mu\text{A.cm}^{-2}$	R_p/Ω	%IE _{PDP}
Blank	-	905.018	-690.136	35.2	73.4	2 110.307	4.67	-
MQ6CA	0.5	49.361	-688.173	8.9	87.4	115.729	11.50	94.52
	1.0	34.248	-701.179	15.3	100.6	79.859	52.30	96.22
	2.0	13.573	-695.899	22.9	61.3	31.650	163.00	98.50
	3.0	13.309	-701.290	20.47	64.7	31.081	201.00	98.53
	4.0	8.366	-636.288	24.6	34.3	19.508	209.00	99.08
Q6CA	0.5	156.10	-659.393	13.5	139.8	363.991	7.52	82.75
	1.0	71.540	-663.406	24.7	109.9	166.821	43.30	92.09
	2.0	42.50	-659.159	26.2	49.4	99.106	44.10	95.30
	3.0	29.70	-613.246	23.9	98.2	69.265	98.50	96.72
	4.0	18.29	-613.573	18.8	115.3	42.655	142.00	97.99
H2QCA with KI	5.0	550.531	-669.868	13.6	107.2	1 283.300	2.89	39.19
	6.0	275.347	-675.917	11.6	93.8	642.112	4.88	69.57
	7.0	179.079	-676.856	25.5	69.5	417.615	34.60	80.21
	8.0	161.111	-666.355	14.3	121.4	375.500	47.70	82.21
	9.0	41.036	-691.988	9.6	89.9	95.688	41.06	95.47

Figures 4.169 – 4.171 show that the introduction of the inhibitors in the corrosive media resulted in the shift of the polarization curves to the lower current region as compared to the blank counterparts. This shift in the polarization curves can be ascribed to the adsorbed quinoxaline molecules on the aluminium surface. Table 4.49 shows that inhibition efficiency with KI increased with an increase in the concentration of all the studied quinoxalines. This response can be assigned to the increasing population of the inhibitor molecules, covering a larger aluminium surface as the concentration was increased, thereby, minimizing the effect of the acid species on the metal's surface. A similar trend was also recently reported by Ihora and co-workers [356]. As reported in the literature [357], anodic and cathodic inhibitors can be defined by the displacement in the E_{corr} values. Thus, if the displacement in E_{corr} values is greater than ± 85 mV with respect to the E_{corr} of the blank solution, then the inhibitor can be considered as a cathodic or anodic type. In this present study, the maximum displacement in E_{corr} for aluminium was attained to be 76.56 mV, suggesting that the studied quinoxalines are mixed-type.

No simple trend was observed in values of the Tafel slopes as the concentration of the inhibitor was increased. The changes in the Tafel slopes further confirmed that both the anodic and cathodic half-reactions were affected, however, the effect was found to be more prominent on the cathodic half-reaction. Moreover, the addition of the inhibitors into the aggressive solution resulted in polarization resistance (R_p). Tables 4.49 shows that the R_p values increased with the increase in the concentration of the inhibitors. According to Nesane and co-workers [336], this effect suggests that further polarization of aluminium was retarded by the barrier formed as a result of the increasing population of the inhibitor molecules at the metal/solution interface.

4.4.2 Electrochemical impedance spectroscopy (EIS)

The EIS technique was employed to get more insight into the behavior of aluminium in 0.5 M HCl in the absence and presence of various concentrations of the studied quinoxalines at 303 K. the measurements were carried out at the OCP after 3600 seconds of aluminium immersion until a steady corrosion potential (E_{corr}) for all the working electrodes was established. Figures 4.172 – 4.177 show the obtained Nyquist plots and their corresponding Bode plots.

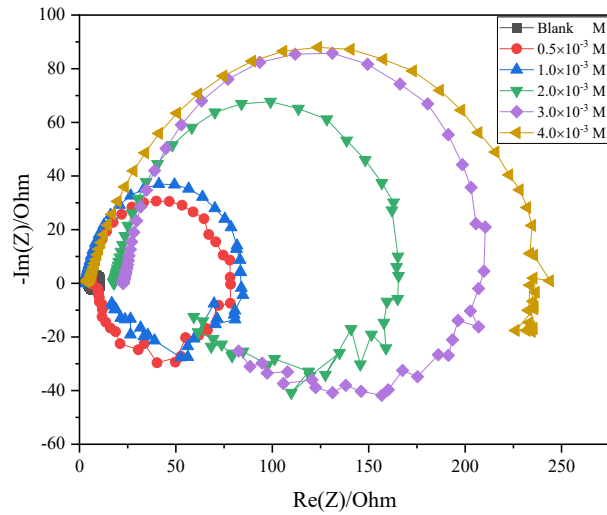


Figure 4.172: Nyquist plot of aluminium in 0.5 M HCl in the presence and absence of various concentrations of MQ6CA.

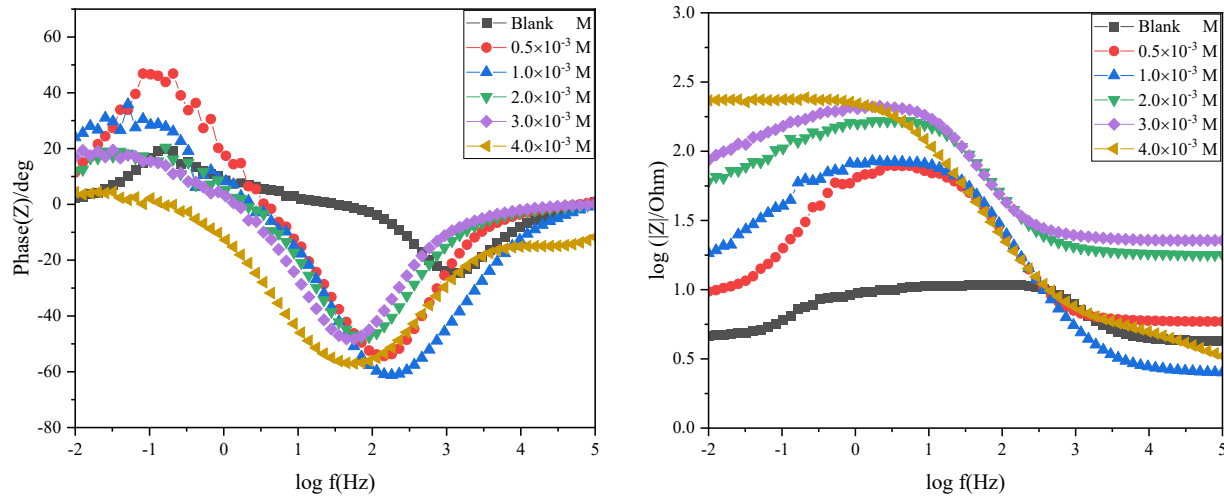


Figure 4.173: Bode plot of aluminium in 0.5 M HCl in the presence and absence of various concentrations of MQ6CA.

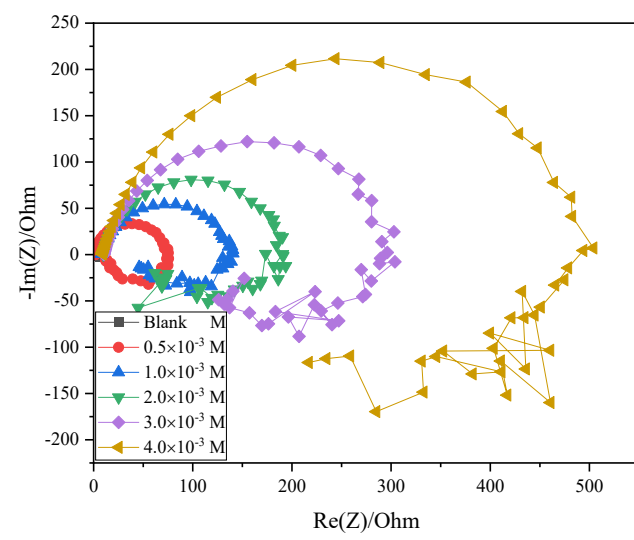


Figure 4.174: Nyquist plot of aluminium in 0.5 M HCl in the presence and absence of various concentrations of Q6CA.

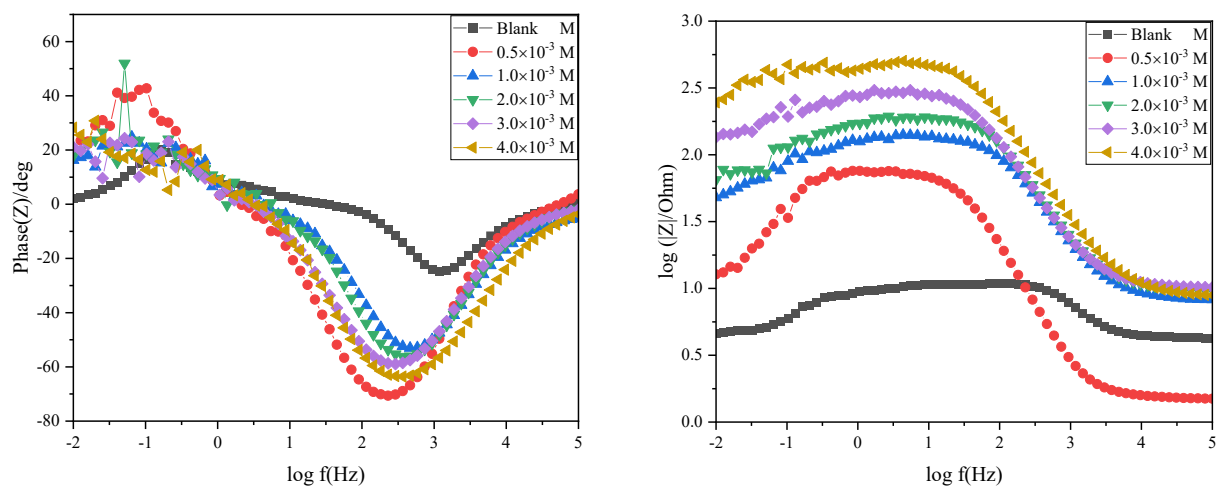


Figure 4.175: Bode plot of aluminium in 0.5 M HCl in the presence and absence of various concentrations of Q6CA.

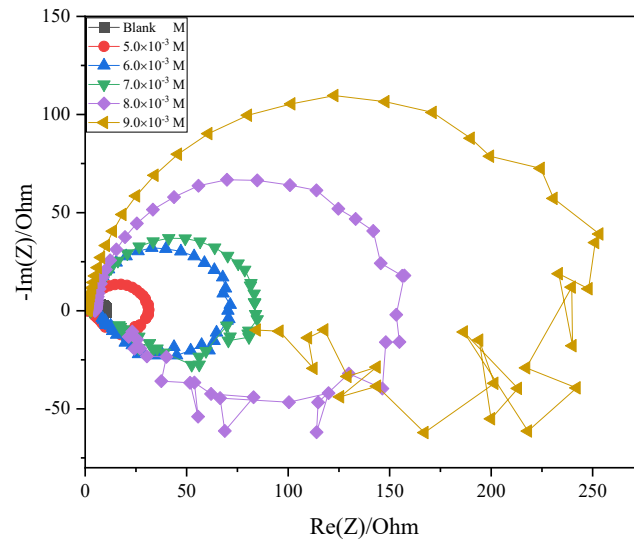


Figure 4.176: Nyquist plot of aluminium in 0.5 M HCl in the presence and absence of various concentrations of H2QCA with KI.

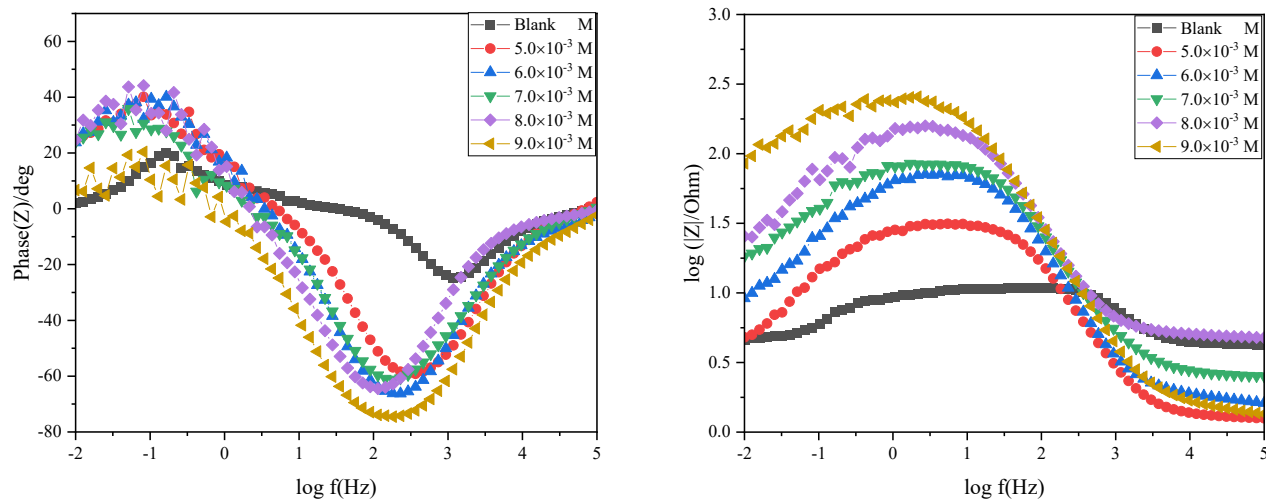


Figure 4.177: Bode plot of aluminium in 0.5 M HCl in the presence and absence of various concentrations of H2QCA with KI.

Table 4.50: Electrochemical impedance parameters such as the resistance of charge transfer (R_{ct}), constant phase element (CPE) and the CPE exponent (n) of aluminium in the absence and presence of various concentrations of the studied quinoxalines in 0.5 M HCl.

Inhibitor	Conc. ($\times 10^{-3}$ M)	R_1/Ω	$Q_1/F.s^{(a-1)}$	L_1/H	R_2	n	R_3/Ω	θ	%IE _{EIS}
Blank	-	4.322	28.73e-6	3.739	6.082	1	0.6153	-	-
MQ6CA	0.5	5.937	85.20e-6	26.51	66.60	0.951	4.19	0.9087	90.87
	1.0	8.626	0.104e-3	96.88	77.99	0.892	20.44	0.9220	92.20
	2.0	18.34	59.46e-6	239.3	140.70	0.933	71.82	0.9568	95.68
	3.0	23.17	65.58e-6	515.80	177.70	0.942	107.80	0.9658	96.58
	4.0	36.22	87.35e-6	743.02	240.70	0.855	183.01	0.9747	97.47
Q6CA	0.5	1.529	91.52e ⁻⁶	82.17	72.48	0.963	13.6	0.9161	91.61
	1.0	8.349	23.47e ⁻⁶	203.6	124.3	0.8846	64.32	0.9511	95.11
	2.0	9.958	17.2e ⁻⁶	268.6	170.9	0.9114	76.22	0.9644	96.44
	3.0	10.35	22.2e ⁻⁶	663.6	275.0	0.8904	209.7	0.9710	97.10
	4.0	9.129	14.23e ⁻⁶	3765	455.9	0.8843	276.2	0.9780	97.80
H2QCA with KI	5.0	1.294	0.129e-3	24.67	28.28	0.924	4.373	0.7849	78.49
	6.0	1.798	0.101e-3	42.85	64.33	0.936	9.578	0.9055	90.55
	7.0	2.626	0.104e-3	98.66	76.31	0.844	21.08	0.9203	92.03
	8.0	5.01	69.57e-6	131.50	137.90	0.949	22.77	0.9559	95.59
	9.0	1.468	83.48e-6	618.30	236.00	0.919	190.00	0.9742	97.42

The imperfect semicircles exhibit the same shape in the absence or presence of the studied inhibitors. This observation suggests that all the three inhibitors adsorbed in a similar mechanism on aluminium surface. The diameter of the blank imperfect circles was observed to be significantly smaller than those of the inhibited system. These figures reveal that the diameter of these semicircles increased with the increase in concentrations of the studied quinoxalines. Figure 4.187 shows a slight shift of the Nyquist plots from the origin at concentration of 2×10^{-3} M and 3×10^{-3} M, this response was due to the more availability of the inhibitor molecules in the corrosive medium providing a better coverage on the metal's surface. The impedance spectra in figures 4.172 – 4.177 are represented by the imperfect semicircles capacitive loops which are indicative of a charge transfer process that controls the corrosion of aluminium in an acidic medium and a double layer capacitance (C_{dl}), and low inductive loop that is related to the bulk relaxation process. The inductive loop may also be related to the adsorption or desorption equilibrium of active species of the surface of the metal during the impedance measurement [358]. The model of the equivalent circuit utilized to fit the experimental data in 0.5 M HCl in the presence and absence of various concentrations of the studied quinoxalines is shown in figure 4.178. This circuit consists of a charge transfer resistance (R_{ct}), solution resistance (R_s), and constant phase element (CPE).

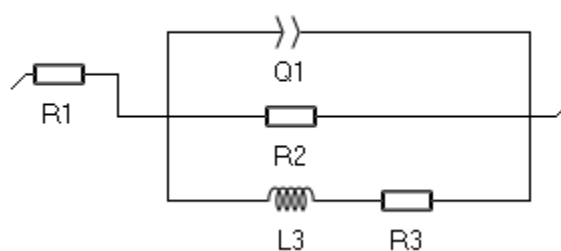


Figure 4.178: Equivalent circuit utilized to fit the impedance spectra obtained for aluminium corrosion in 0.5 M HCl in the absence and presence of various concentrations of the studied quinoxalines.

where R1 is the solution resistance (R_s), R2 charge transfer resistance (R_{ct}), R3 charge transfer after the formation of the film layer, Q1 constant phase element (CPE), and L3 inductive element.

The electrochemical impedance parameters for aluminium corrosion in 0.5 M HCl and in the absence and presence of the studied quinoxalines are illustrated in Tables 4.50.

The inhibition efficiency at various concentrations of the inhibitor was calculated using equation (44). It is clear from these Table 4.50 that the charge transfer resistance increased with the increase in the concentration of MQ6CA, Q6CA, and H2QCA, which resulted in the increase in the inhibition efficiency. No regular trend in the obtained values of CPE, however, the table reveals that the addition of the inhibitors in the corrosive solution resulted in the decrease in the values of CPE. This decrease in CPE values can also be due to the decrease in local dielectric constant and/or the increases in the thickness of the protective layer formed by the adsorbed inhibitor molecules on aluminium surface. Moreover, the value of n for the blank solution was at unity, however, as various concentrations of the inhibitors were added in the corrosive medium, there was a deviation in the n values, indicating that the adsorption process of the inhibitor molecules brought about a certain inhomogeneity on aluminum surface.

4.4.3 Adsorption isotherm

Important information on the mode of mechanism occurring during the adsorption process between the inhibitor and the metal can be attained through adsorption isotherms. The values of surface coverage (θ) were obtained at various concentrations of the inhibitors from PDP and EIS measurements. The data were fitted to several known adsorption isotherms namely Langmuir, Frumkin, Freundlich, and Temkin. The plots of these adsorption isotherms. Among all the fitted isotherms for aluminium 0.5 M HCl in the absence and presence of the studied quinoxaline, the Langmuir isotherm was obtained to describe the adsorption behavior of the investigated compounds. This judgment was based on the regression coefficient values (R^2) that were found to be at/and near the unity. The Langmuir adsorption isotherm plots are shown with descriptions in Figures 4.179 – 4.181.

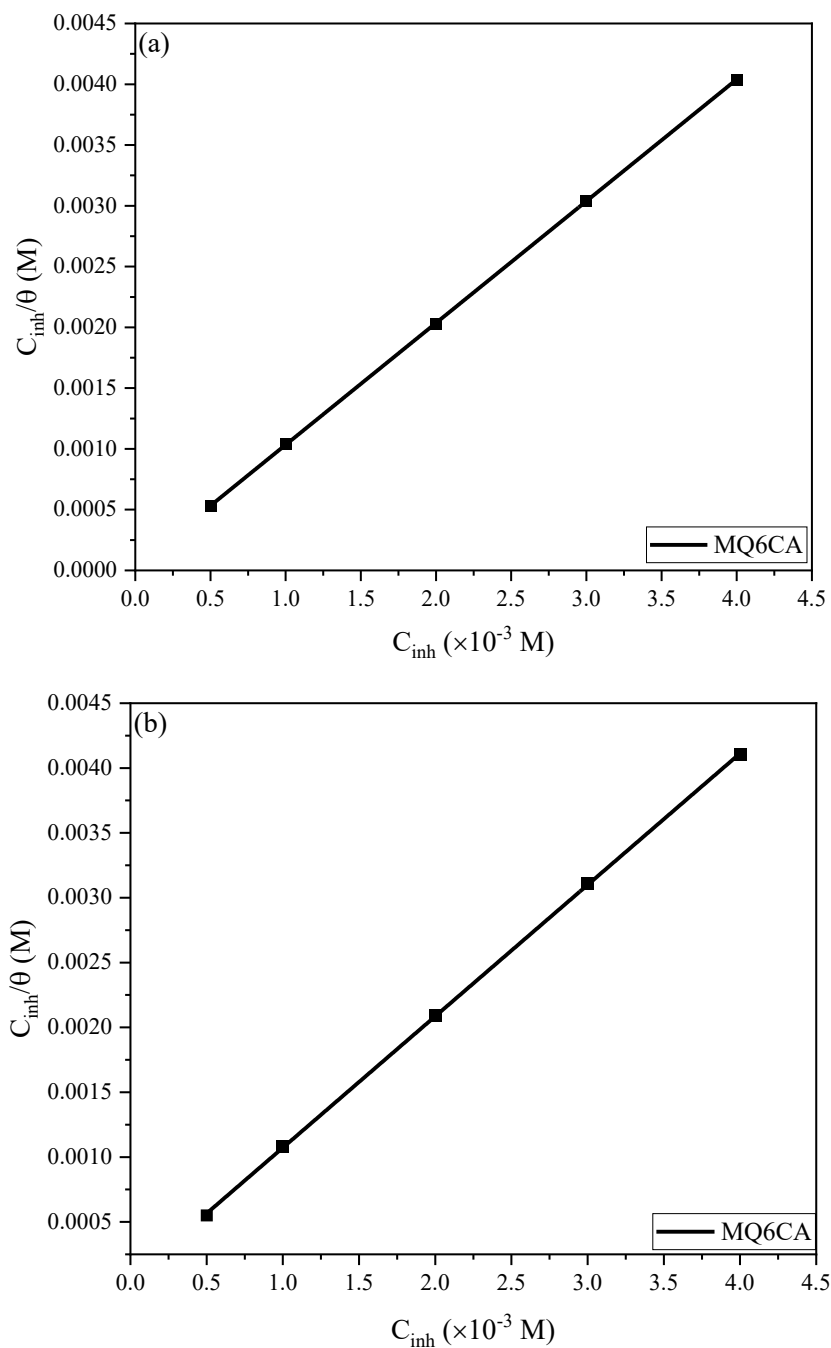


Figure 4.179: Langmuir adsorption isotherm plot for the adsorption of various concentrations of MQ6CA on the aluminium in 0.5 M HCl at 303 K (a) PDP and (b) EIS.

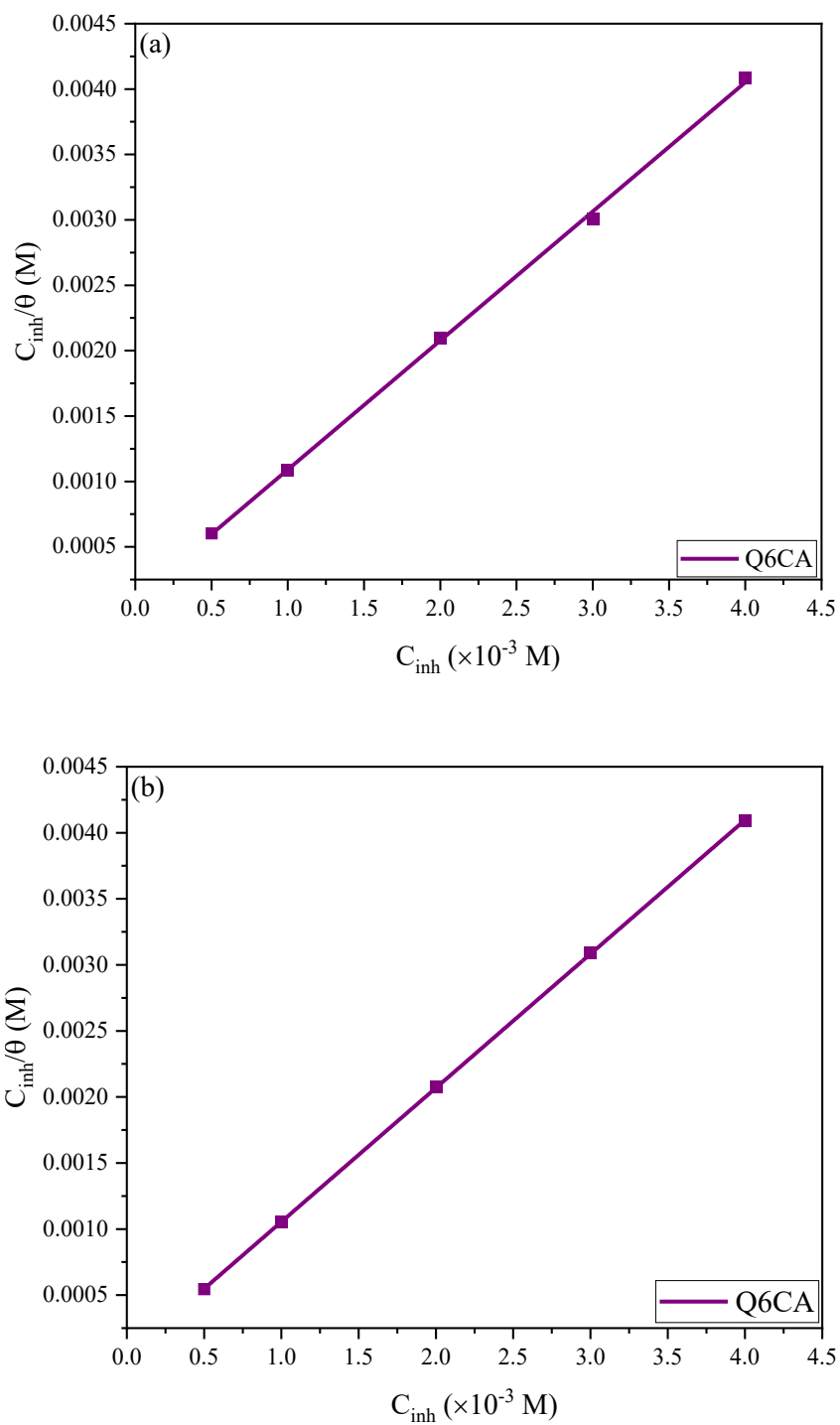


Figure 4.180: Langmuir adsorption isotherm plot for the adsorption of various concentrations of Q6CA on the aluminium in 0.5 M HCl at 303 K (a) PDP and (b) EIS.

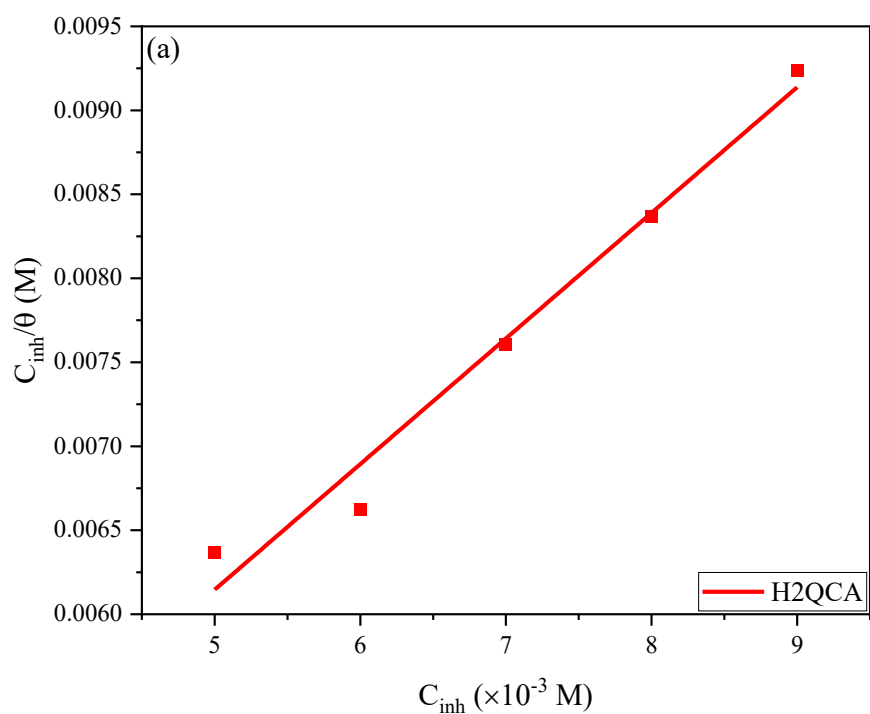
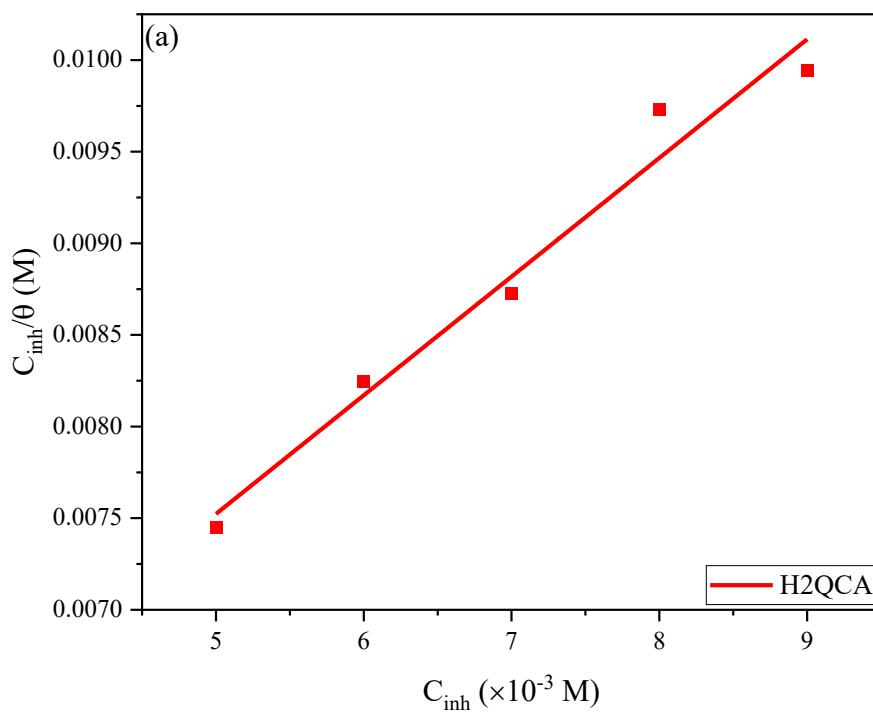


Figure 4.181: Langmuir adsorption isotherm plot for the adsorption of various concentrations of Q6CA on the aluminium in 0.5 M HCl at 303 K (a) PDP and (b) EIS.1

The surface coverage (θ) of the studied quinoxaline obtained from PDP and EIS on aluminium surface and the variety of their concentration are best related by Langmuir isotherm given by equation (49). The values of K_{ads} were calculated from the intercept of the line from the Langmuir plots. K_{ads} can be related to the free Gibbs energy of adsorption (ΔG°_{ads}) through equation (51). The K_{ads} and ΔG°_{ads} for aluminium in 0.5 M HCl in the absence and presence of the studied quinoxalines are listed in Table 4.51.

Table 4.51: Langmuir adsorption parameters for corrosion of aluminium in 0.5 M HCl at 303 K in the presence of the studied quinoxalines.

Inhibitor	PDP		EIS	
	K_{ads} (L/mol)	$-\Delta G^{\circ}_{ads}$ (kJ/mol)	K_{ads} (L/mol)	$-\Delta G^{\circ}_{ads}$ (kJ/mol)
MQ6CA	31926.44	36.24	17022.75	34.66
Q6CA	9676.05	33.34	24494.73	35.58
H2QCA with KI	233.64	23.86	414.94	25.30

The high K_{ads} values obtained indicate a strong adsorption of the studied quinoxalines on aluminium surface. As reported on literature, values of ΔG°_{ads} around -20 kJ/mol or less are related to physical adsorption, whereas values of ΔG°_{ads} around -40 kJ/mol and more negative are related to chemical adsorption [359]. In this present study, the values of ΔG°_{ads} were attained to within the range 23.86 – 36.24 kJ/mol, indicating that the studied quinoxaline acted as mixed-type inhibitors on aluminium surface, however, with domination of chemical adsorption. Moreover, the negative values of signified the adsorption of the studied quinoxalines on aluminium surface was a spontaneous process. It is worth stating that the experimental work for the corrosion of aluminum in sulphuric acid as corrosive medium were performed. However, the inhibitors did not produce satisfactory results hence the results are not presented in this current report.

4.5 THEORETICAL ANALYSIS

4.5.1 Validation of the calculation method

The method selected for the calculations were first validated by using results of the molecules for which the binding energies are known from literature. The selected molecules utilized for the validation of the methods include water, ammonia, nitric oxide and benzene. The experimental and theoretical results on some of the molecules provided in literature are reproduced in Table 4.52 along with the results reported in this work using the methodology suggested in chapter 3.

Table 4.52: Binding energies for selected molecules on the Al (111) surface built with three layers, two on the bottom fixed and one on top relaxed.

Molecule	Site	Energy data from this work (kcal/mol)	Energy data from literature (kcal/mol)
Water	Top	8.784	9.178 [360] 7.818 [362]
	Hallow	8.698	7.864 [362] 9.224 [360]
	bridge	39.420	-
Ammonia	Top	20.178	18.450 [363]
	Hallow	20.111	-
	bridge	20.105	-
Nitric oxide	N end-ON	40.1484	41.510 [364]
Benzene	Top	3.32072	2.767 [365]

Wei et. al. [360] utilized the density functional theory (DFT) to conduct the calculations of the binding energy of water molecule on Al (111) surface using MedeA-VASP 5.4 software [361]. Their calculations were conducted on 6-layer slabs of Al(111), separated by 20 Å of vacuum along the c-axis direction. In this present study three possible sites were considered, however, only the Top and hallow site are available on literature. The values of the binding energy obtained in this

present study were 8.784 and 8.698 kcal/mol on the top and hallow site, respectively, and they were in good agreement with the experimentally measured values (8.698 and 9.224 kcal/mol) [360], at respective sites. The percentage error between the values obtained from this study and the Wei and co-workers was attained to be 4.29 % and 5.70 % at top and hallow sites, respectively. F.Y. Guo et. al. [362], also utilized the DFT to conduct their calculations of water molecule on Al (111) surface, they utilized the GGA and Perdew and Wang (PW91) functionals to correct the gradient and values of adsorption energy that they obtained were also comparable with the values obtained in this present study. Hermann et. al. [363], utilized the *Ab initio* Hartree-Fock – LCAO method to calculate the binding energy of ammonia molecule on the top site. In this present study three possible site were considered as shown in Table 4.52. The binding energy value obtained in the present study was (20.178 kcal/mol) no significant difference from the value they obtained (18.450 kcal/mol), with percentage error of 8.56 %. Komrowski et al. [364], performed calculations of the adsorption energy of nitric oxide on the N end NO site using the DFT method and they obtained a value of 41.510 kcal/mol, which was also comparable with the value 40.148 kcal/mol that was obtained from this present study (percentage error of 3.28 %). Blomqvist and Salo [365], utilized Vienna ab initio simulation package (VASP) [361], in studying the adsorption energy of benzene on Al (111). They obtained a value of 2.7673 kcal/mol and in this present study the binding energy value was found to be 3.32072 kcal/mol. The minor differences in the binding energies between the results calculated in this work on the selected molecules and that reported in literature suggest that the methodology selected for study of the selected molecules in this study can be considered to be reliable enough and therefore it is reasonable for utilization in the study of the interactions between the inhibitor molecule and the metal surfaces.

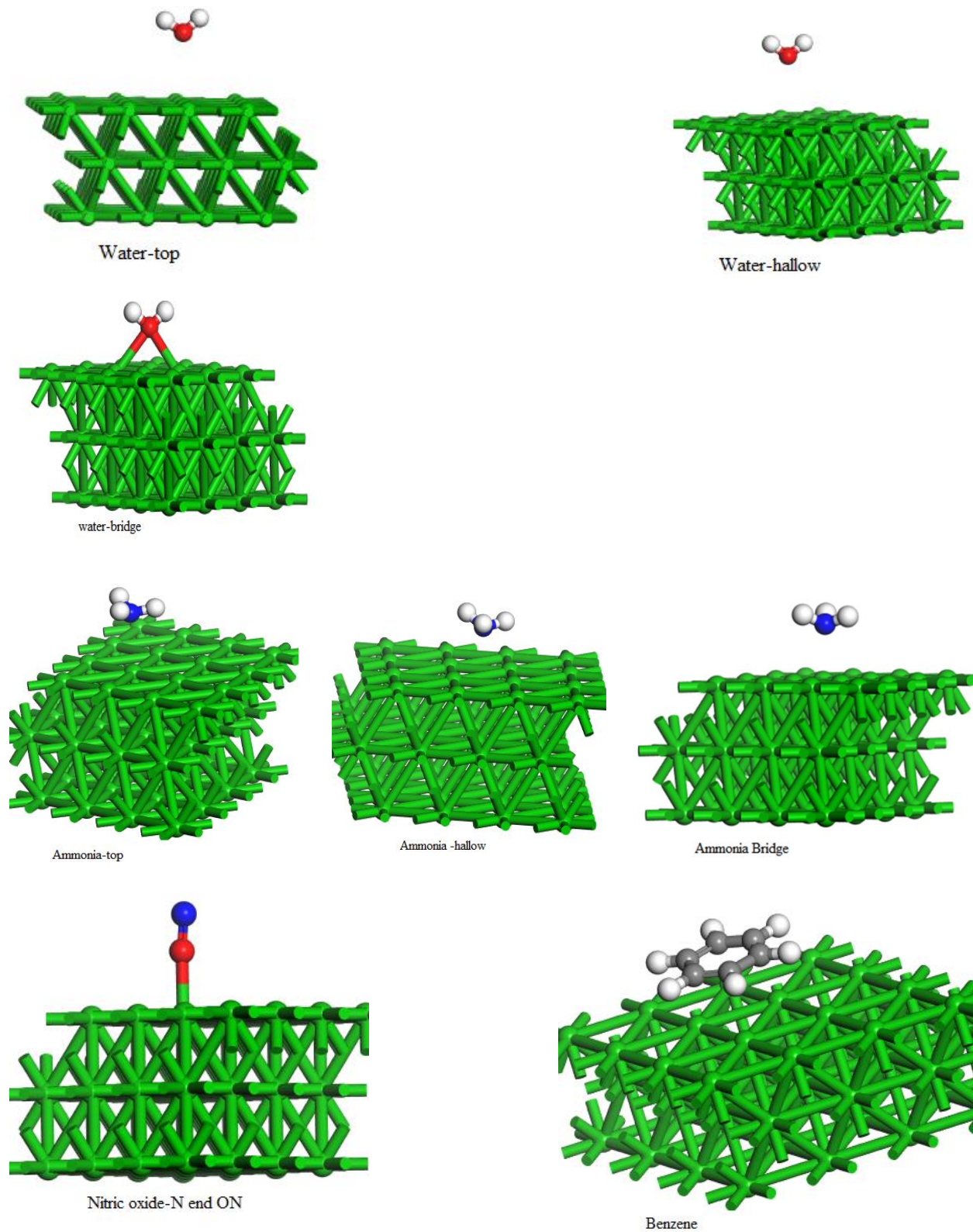
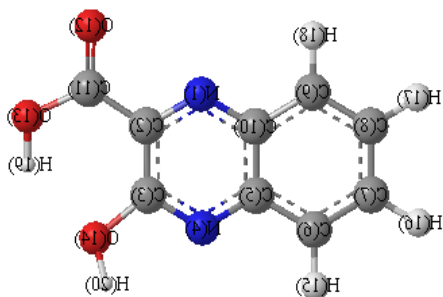
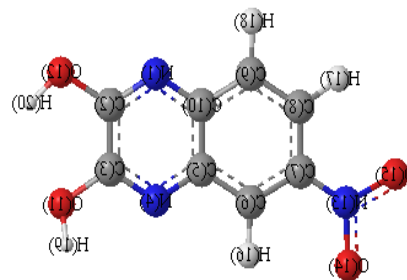


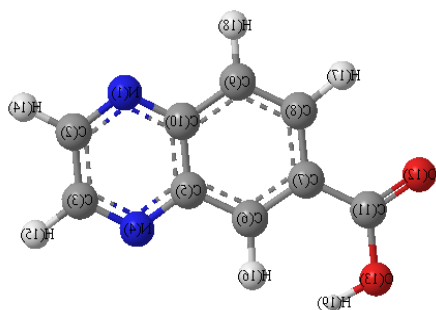
Figure 4.182: Selected molecules with different orientation studied for the verification the method utilized in the current study.



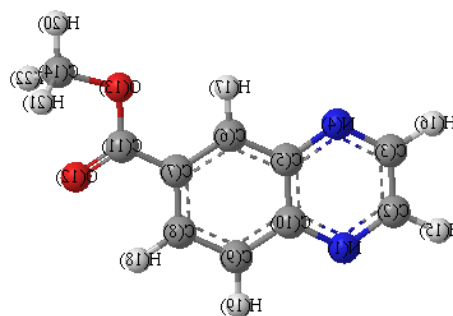
3-Hydroxy-2-quinoxalinecarboxylic acid (H2QCA)



6-Nitro-2,3-dihydroxyquinoxaline (6NDQ)



Quinoxaline-6-carboxylic acid (Q6CA)



methyl quinoxaline-6-carboxylate (MQ6CA)

Figure 4.183: Selected molecules to be studied with atom numbering.

4.5.2 Results of the study on the interaction between selected quinoxaline derivatives on the Al surface

Various binding sites of the selected quinoxalines on the Al (111) were optimized. The results related to H2QCA are presented in figure 4.184, related to 6NDQ are presented in figure 4.185, related to Q6CA are presented in figure 4.186, and related to MQ6CA are presented in figure 4.187.

Analysis of the results related to the binding of H2QCA on Al (111) surface suggest that five different possible arrangements of the molecule preferred binding on the Al surface. The most preferred arrangement was the one in which the interaction between H2QCA and Al (111) was about 167.562 kJ/mol. In this arrangement, the H2QCA interacted with the Al (111) surface by bonding to through the carbonyl oxygen of the carboxylic group which is one of the possible electron donors functional groups. The bond distance between O12 and Al was obtained to be about 1.889 Å, which represent a very strong interaction. In fact, the covalent interaction between Al and an oxygen atom in Al₂O₃ is about 1.86–1.98 Å. Ustinova and Shcheka also reported similar observation [366]. In this way, the interaction involving H2QCA, and Al are suggestive of the covalent interaction. In other words, it suggests that the H2QCA...Al bond distance is an indicative of chemical interaction between the inhibitor and the Al surface.

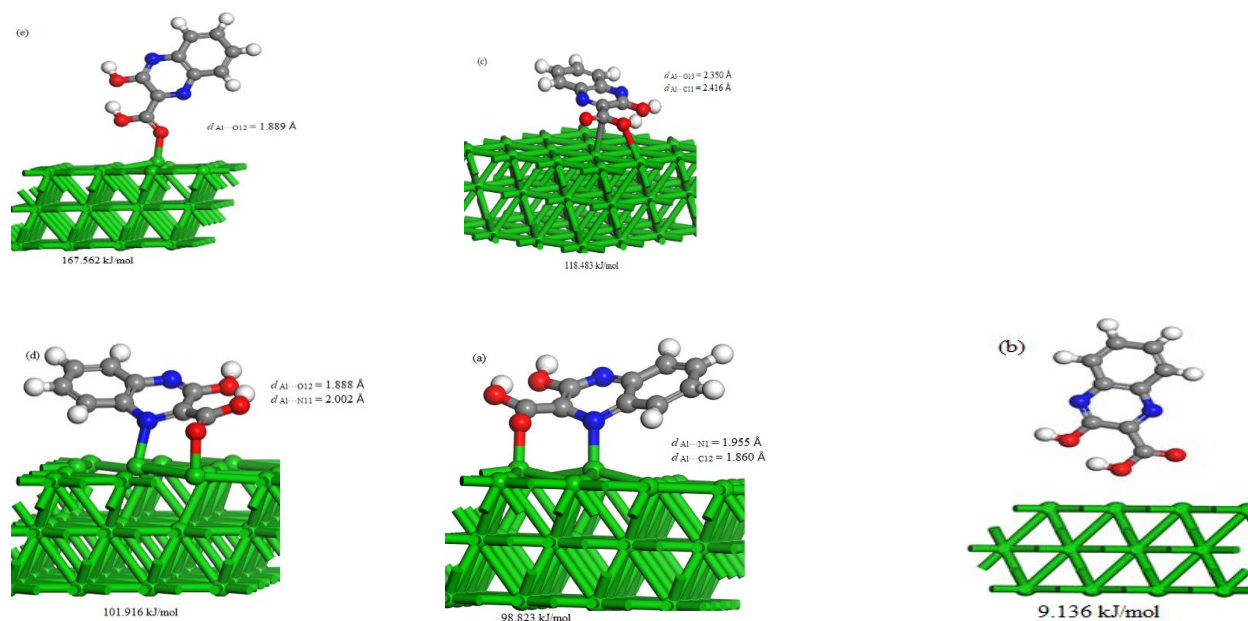


Figure 4.184: Selected structure, bond lengths and binding energy at different positions for Al (111) interacting with 3-Hydroxy-2-quinoxalinecarboxylic acid. The structures are arranged in order of decreasing binding energies.

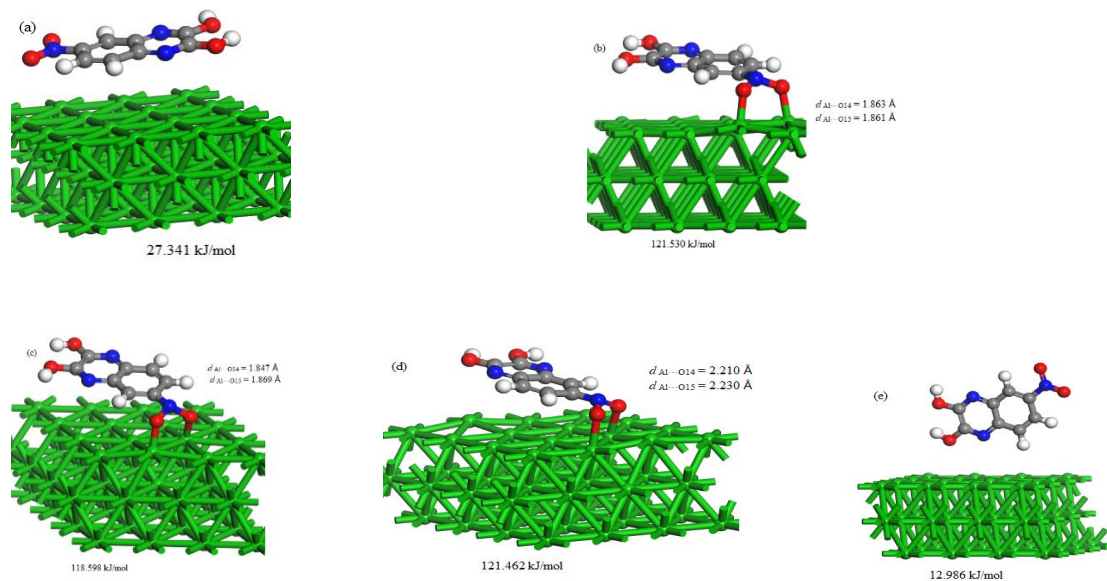


Figure 4.185: Selected structure, bond distances and binding energy at different positions for Al (111) interacting with 6-Nitro-2,3-dihydroxyquinoxaline.

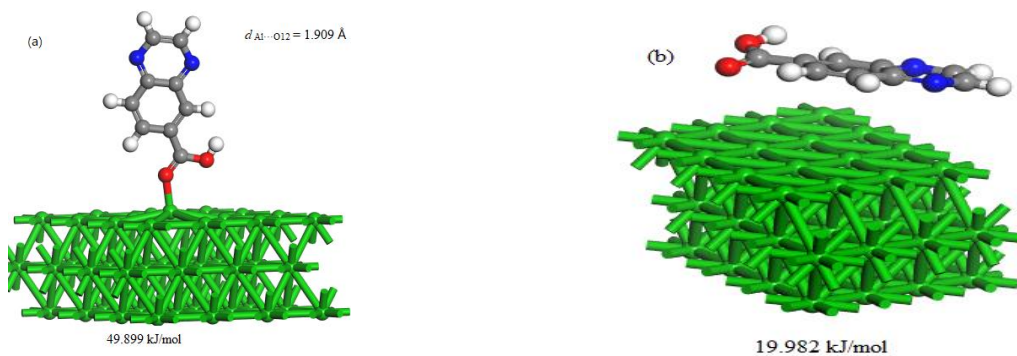


Figure 4.186: Selected structures, bond distances and binding energy at different positions for Al (111) interacting with quinoxaline-6-carboxylic acid.

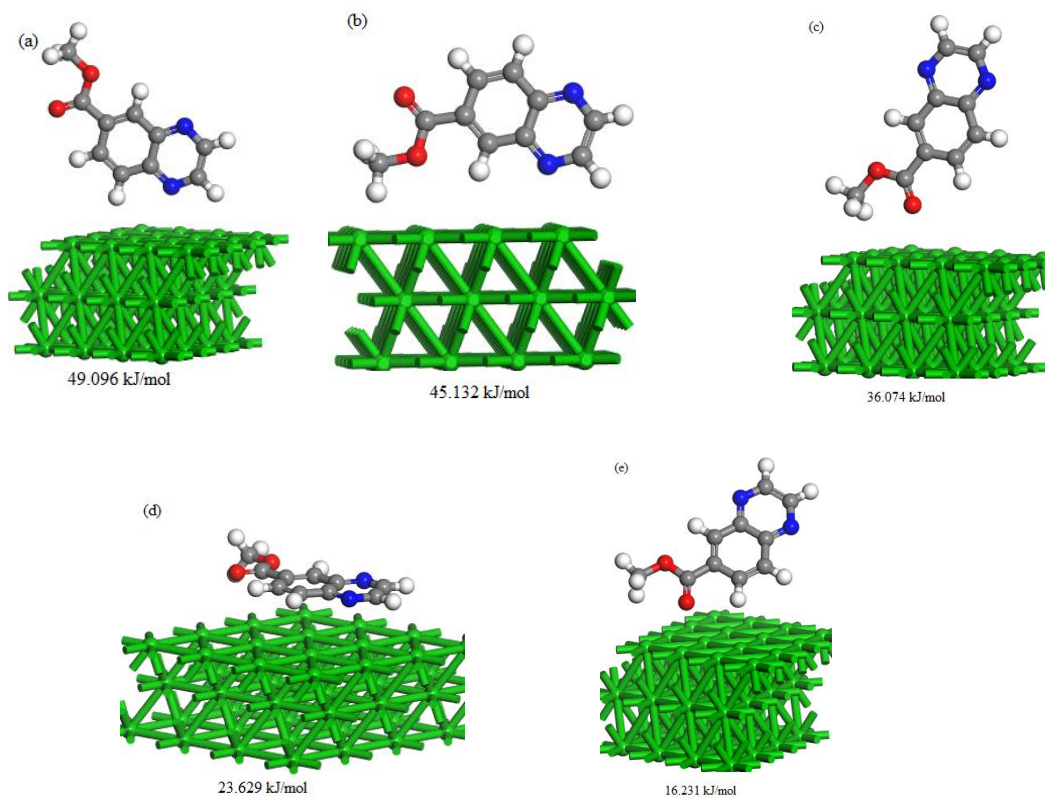


Figure 4.187: Selected structures, bond distances and binding energy at different positions for Al (111) interacting with methyl quinoxaline-6-carboxylate.

The structure with the second highest binding energy (118.483 kJ/mol) corresponded to the interaction of H2QCA with Al (111) surface through the C11 and O13 atoms. Although the interaction energy is significantly high, the bond distances between Al and C11 or between Al and O13 are significantly large, and it is possible that the geometry arrangement in this case corresponds to covalent interactions rather than chemical interactions. In other words, the geometry criteria could have a stronger role in determining the type of interaction within this configuration. In the third configuration, in terms of interaction energy, the H2QCA molecule interacted with the Al surface through the O12 and N1 atom. In this case, it was noted that the Al...O12 bond distance was within covalent range and also the Al...N1 bond distances was about 2.001 Å. The bond distance of the covalent interaction between Al and N was previously reported in literature to have a value of 1.80 Å [367]. This suggests that the bond distance of Al with N1 in H2QCA molecule is longer than the literature value, in other words, the bonding in the configuration suggests a combination of chemical and physical interactions at different sites of the molecule, that is, chemical interaction at the O12 and physical interaction at N1.

The arrangement of all the three molecules in figures 4.184 (b), 4.185 (e), 4.186 (b), and 4.187 (e) resulted in the smallest values of binding energies of 9.136, 12.986, 19.982, and 16.231 kJ/mol, respective. These physical interactions can be attributed to that there were no bonds formed and only intermolecular forces between all molecules and Al surface. The adsorption energy in the configuration in figure 4.185 (a) was obtained to be 27.341 kJ/mol. Studies also suggest that if the distortion of the molecule is small and there is no dissociation in any part of the molecule during the adsorption process, physical adsorptions are likely to be observed [368].

The configurations in figures 4.184(a), (c), (d),(e), 4.185 (b), (c), (d) and 4.186 (a) shows that all the three molecules shifted towards their respective surfaces, and the adsorptions in all the cases led to the formation of Al — O bond, with values of the bond length ranging from 1.86 to 1.90 Å which was smaller than the sum of the ionic radii, hence chemical adsorption was observed. These bond length values agree with the corresponding literature value of 1.86 Å [360, 369].

In some cases, the adsorption of H2QCA on the Al surface led to the formation of Al — C bond [figure 4.184 (c)] with the bond length of 2.416 Å and formation of the Al — N [figure 4.184 (d)] bond with bond length in the range of 1.955 – 2.002 Å. Chaichao et. al. [11] also obtained similar bond length values. The calculated adsorption energies for the configurations in figure 4.184 (a),

(c), (d), and (e) were obtained to be 98.823, 118.483, 101.916, and 167.562 kJ/mol, respectively. It was also observed that the electrostatic interactions of H2QCA onto Al (111) surface were higher only when the Al — O12 bond is formed than in cases when other atoms such as nitrogen and carbon are involved in bonding. Configurations in figure 4.185 (b), (c), and (b) shows that both oxygen atoms O14 and O15 of the nitro group bonded with the Al surface which resulted in strong interaction with the calculated adsorption energies of 121.530, 118.598, and 121.462 kJ/mol, respectively. Another Al — O12 was observed in the evaluation of Q6CA interacting with Al (111), however, the calculated adsorption was low as compared to the cases of H2QCA and 6NDQ when the Al — O12 bonds were observed. The calculated adsorption energies for the configurations in figures 4.187 (a), (b), (c), and (d) were obtained to be 46.096, 45.132, 36.074, and 23.629 kJ/mol, respectively. Indicating both physical and chemical adsorptions, however, a domination of chemisorption.

4.5.3 Results of the study on the interaction between selected quinoxaline derivatives on the Zn surface.

The arrangement of all the three molecules interacting with Zn (110) shown in figures 4.188 (b) and (c), figure 4.189 (c) and (f), and figures 4.190 (a) and (d), resulted in physical adsorption with adsorption energy ranging from 21.871– 37.591 kJ/mol. These small values of adsorption energy can be attributed to the that there were no bonds formed between the selected molecules and the Zn surface. In addition, the arrangement of Q6CA in figure 4.189 (a) resulted in the adsorption energy of 37.591 kJ/mol which was close to the chemical adsorption region, this observation can be attributed to the fact that the molecule contain conjugated double bonds and the sp² carbon which are considered to be major adsorption centers because they have high electron density [370].

The adsorption in the configuration shown in figure 4.188 (a) resulted to the formation of three bonds which are: Al — O12, Al — N1, and Al — C7 with the bond lengths of 2.050, 2.173, and 2.592 Å, respectively. The calculated adsorption energy was found to be 93.080 kJ/mol. Another three cases were studied, and are represented in figures 4.189 (a), (b), and (e). In all three cases, the molecule did not dissociate, however, chemical adsorptions were observed with corresponding adsorption energies of 100.511, 81.705, and 71.631 kJ/mol. For configurations in Figure 4.190 (b) and (c), Al — O bonds formed in both cases, however, the interaction between O12 and Al surface

resulted in stronger interaction (36.865 kJ/mol) as compared to the interaction between O13 and Al (18.647 kJ/mol). The calculated adsorption energies for the configurations in figure 4.191 (a) – (f) were obtained to be 73.971, 61.095, 38.647, 35.879, 35.707, and 35.404 kJ/mol, respectively. Indicating strong chemical adsorptions.

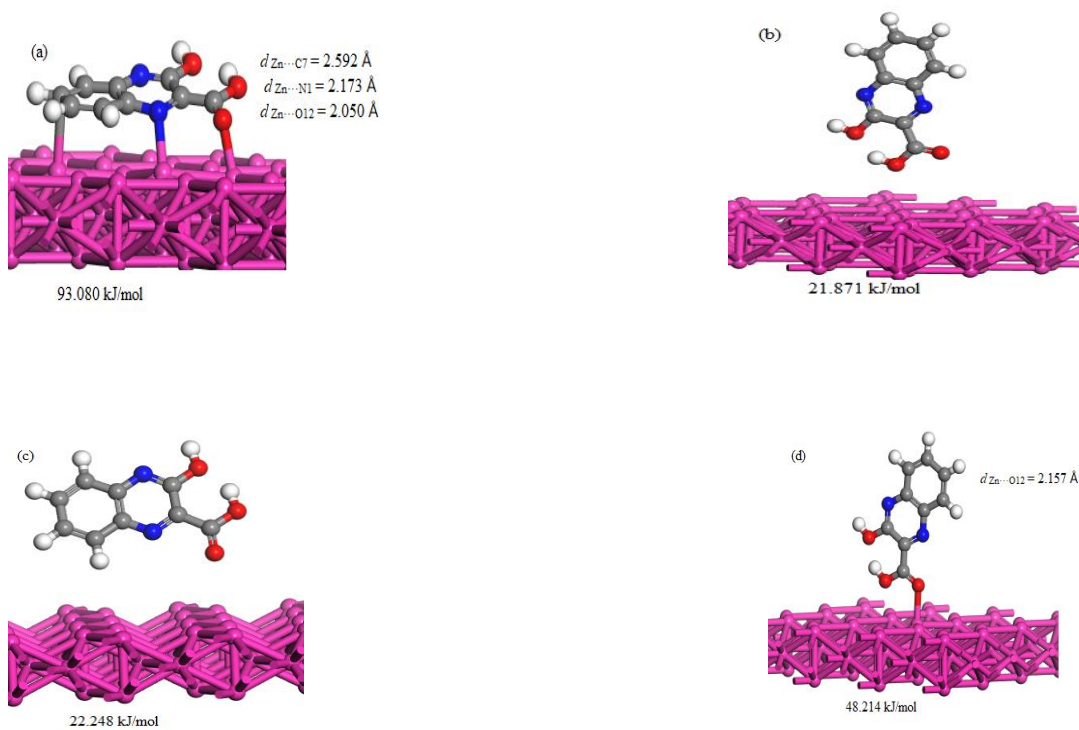


Figure 4.188: Selected structure, bond lengths and binding energy at different positions for Zn interacting with 3-Hydroxy-2-quinoxalinecarboxylic acid.

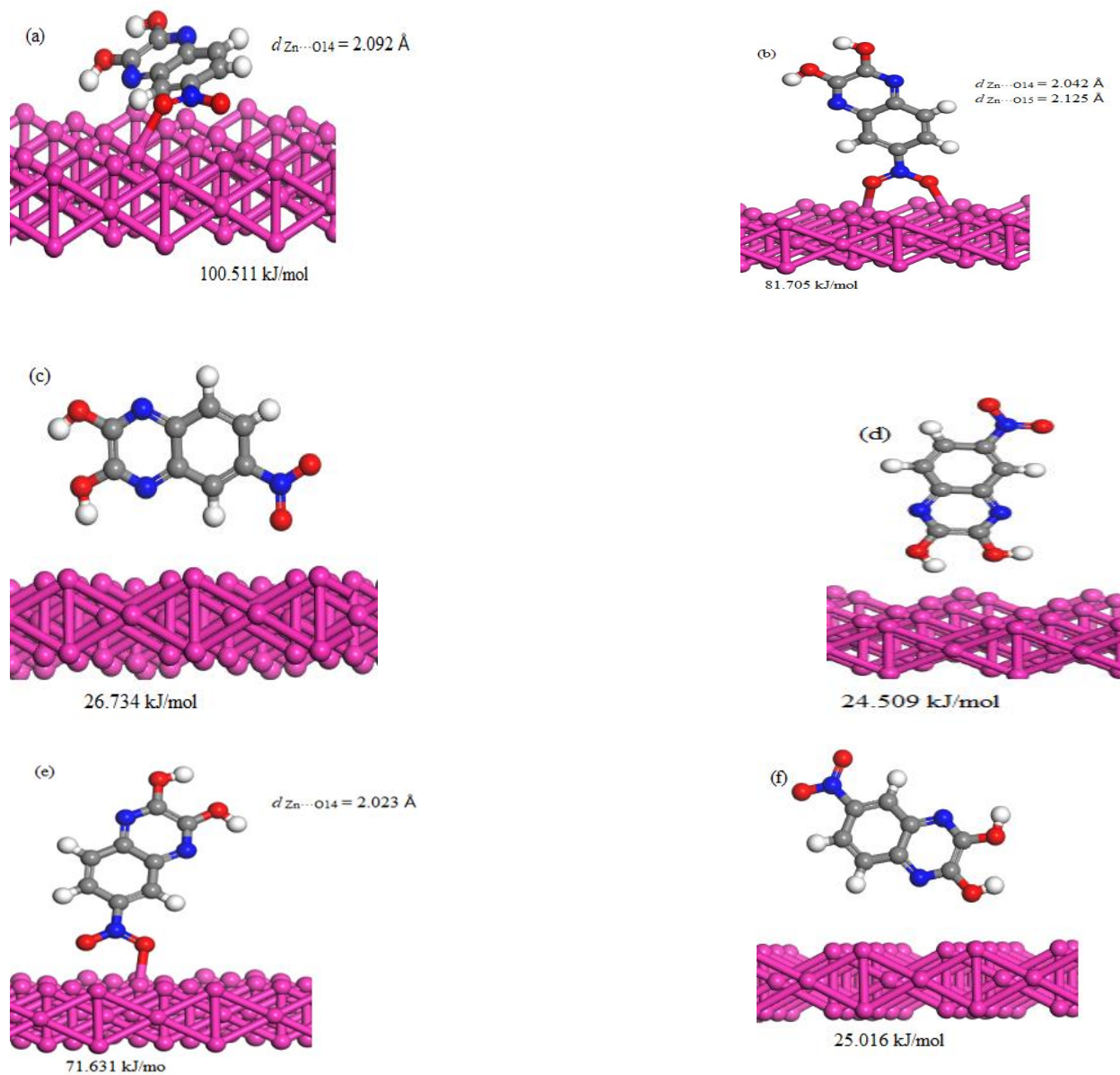


Figure 4.189: Selected structure, bond lengths and binding energy at different positions for Zn interacting with 6-Nitro-2,3-dihydroxyquinoxaline.

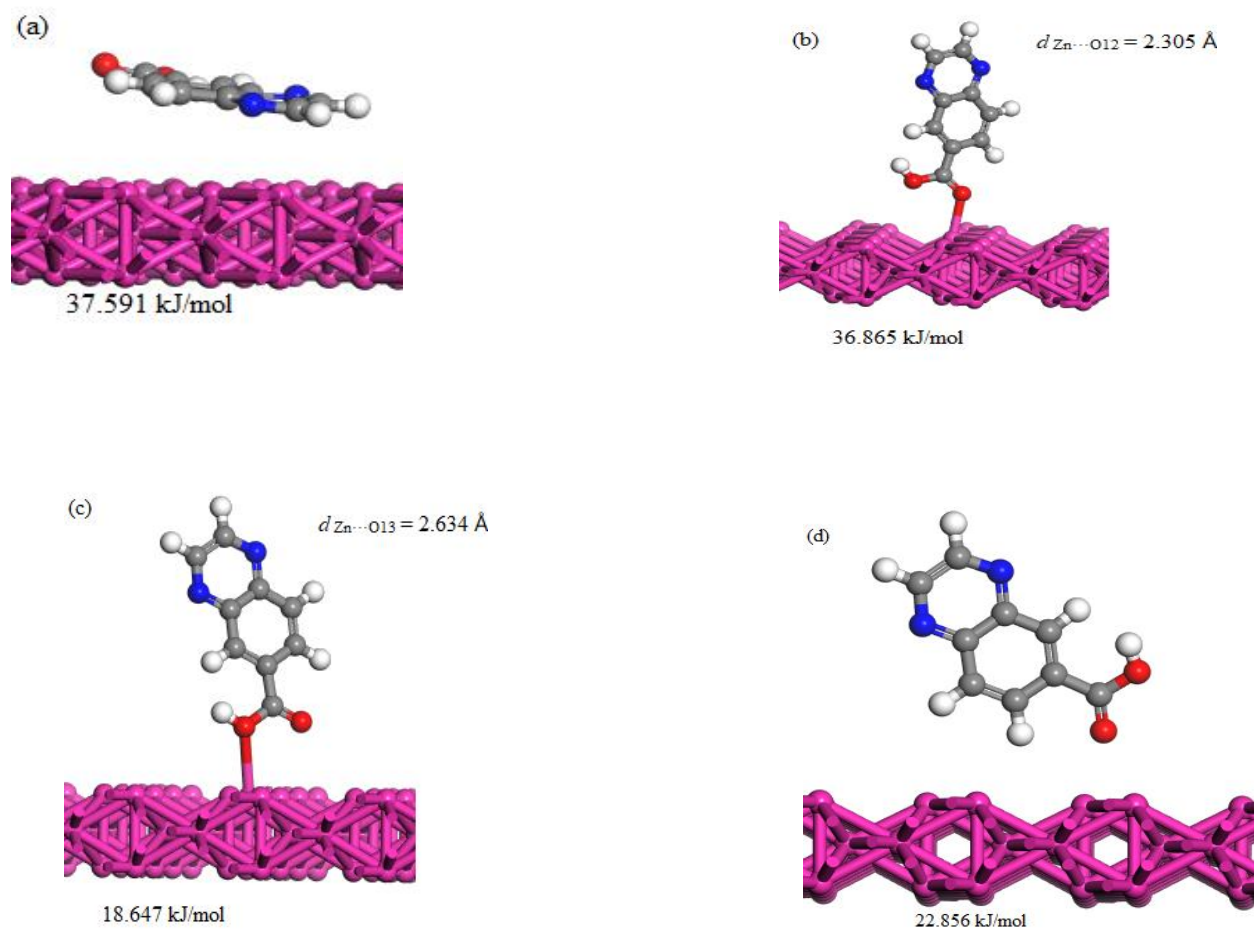


Figure 4.190: Selected structure, bond lengths and binding energy at different positions for Zn interacting with quinoxaline-6-carboxylic acid.

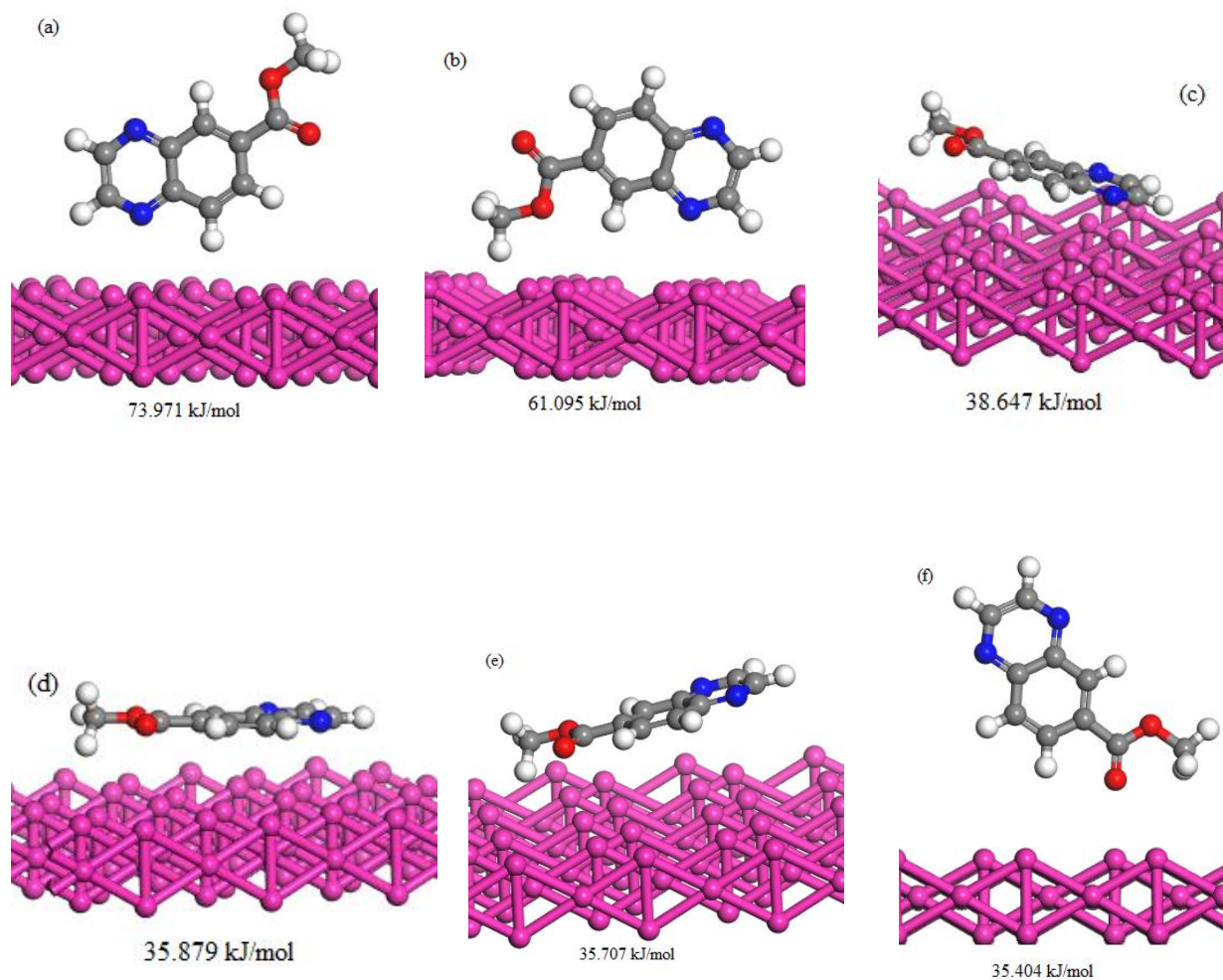


Figure 4.191: Selected structure, bond lengths and binding energy at different positions for Zn interacting with methyl quinoxaline-6-carboxylate.

For all the above-mentioned configurations, the adsorption energy of all the selected molecules interacting with Al (111) or Zn (110) they were found to depend on the initial arrangement in which the molecule was placed. In addition, in the vertical adsorption configurations where the sp^2 oxygen atom was oriented above and on-top site to both the surfaces the adsorptions were found to be chemisorption and their adsorption energies were relatively high. In cases where the selected molecules were initially oriented horizontally to both the surfaces only physical adsorption was observed because the aromatic rings did not strongly interact with the surfaces. In all the arrangement of the four selected molecules, it was observed that the molecules interact better with

Al (111) surface as compared to Zn (110) surface. This observation can be attributed to the fact that the Zn has an electron configuration of $1s^2, 2s^2, 2p^6, 3d^{10}$, therefore not readily accepting electrons because of its filled d subshells and that as indicated by its position in the electromotive force series, Al is a thermodynamically reactive metal that Zn. The computational data obtained are in good agreement with the experimental findings, which also suggest that the studied quinoxalines interact with zinc and aluminium surfaces through both physical and chemical type of interaction, that, the quinoxalines are mixed-type inhibitors. A similar observation was also reported in literature [371].

CHAPTER 5:

CONCLUSIONS

AND

RECOMMENDATIONS

This chapter provides the summary of the results obtained in this study. In essence, it responds on the aim and the objectives that were set in undertaking this study. It also provides recommendations on other aspects that can be explored in future.

5.1 CONCLUSIONS

The adsorption behavior and corrosion properties of three quinoxaline derivatives, namely; quinoxalone-6-carboxylic acid (Q6CA), 3-hydroxy-2-quinoxaline carboxylic acid (H2QCA), and Methyl quinoxaline-6-carboxylate (MQ6CA) were studied for mild steel and zinc in 1.0 M HCl and 1.0 M H₂SO₄ solutions at 303 – 333 K using the gravimetric technique, electrochemical methods (PDP and EIS), Atomic Absorption Spectroscopy (AAS), Fourier Transform Infrared spectrometry (FTIR), and chemical/theoretical techniques. The inhibitors were also investigated on aluminum using electrochemical techniques in 0.5 M HCl solutions at 303 K, and chemical/theoretical techniques.

The studied quinoxaline derivatives showed excellent inhibition on mild steel, zinc, and aluminium against the acidic species. The gravimetric analysis revealed that inhibition efficiency of these compounds on mild steel was found to increase with an increase of their concentration and decreased with the increase in temperature of the corrosive environment. On the other hand, for zinc, the inhibition efficiency was obtained to increase with the increase in the concentration of the inhibitors and also with the increase in temperature of the corrosive environment. H2QCA without KI showed poor performance in reducing the corrosion rate of mild steel and zinc in both acidic media, however, the addition of KI in the system improved the inhibition efficiency of the compound. Among the studied compounds, MQ6CA exhibited the highest inhibition efficiencies in both acidic media and on both metals.

Further manipulation of the gravimetric data revealed that the inhibition of the quinoxaline derivatives on mild steel and zinc in both investigated corrosive media was an endothermic process, suggesting that the dissolution of these metals was slow in the presence of the studied quinoxalines. The adsorption mechanism of the studied inhibitors was found to be both the combination of physical and chemical adsorption, which is also known as mixed-type adsorption, however, the chemical adsorption was dominant. From the surface coverage values obtained from gravimetric measurements, various known adsorption isotherms were fitted. The isotherm that was found best fit to describe the adsorption process of the studied quinoxalines on mild steel and zinc was Langmuir isotherm, that is, all the three inhibitors obeyed Langmuir adsorption isotherm. The negative of the free Gibbs energy of adsorption (ΔG°_{ads}) indicated that the adsorption processes of these inhibitors were spontaneous. Moreover, the ΔG°_{ads} were obtained to be within the range

of 23.95 – 42.05 kJ/mol, further indicating a mixed-type adsorption mechanism, with the domination of chemical adsorption process.

PDP analysis reveals that all the three studied inhibitors reduced the anodic dissolution and also suppressed the hydrogen evolution reaction of mild steel, zinc, and aluminum. The inhibition efficiency increased with an increase in the inhibitor concentration. The corrosion parameters (E_{corr} , i_{corr} , β_a , and β_c) obtained from this analysis revealed that studied quinoxalines are mixed-type inhibitors, that is, are both anodic and cathodic inhibitors. The Nyquist plots exhibited imperfect semicircle capacitive loops for the metal of interest. These semicircles are indicative of a charge transfer process that controls the mild steel, zinc, and aluminium corrosion in acidic media. The increase of concentration concentration of the inhibitors increased the charge transfer resistance, consequently increasing in inhibition efficiency of the studied inhibitors. The increase in the concentration of the inhibitors resulted in a decrease in the CPE values. This decrease in the CPE values is attributed to the increase in the thickness of the electrical double which is indicative that the quinoxalines molecules electrostatically adsorbed on the investigated metals.

The FTIR spectra confirmed the formation of the inhibitor- Fe^{2+} and inhibitor- Zn^{2+} complexes. The analysis of the functional groups showed the O atom from the C=O and the N atom from the C–N functional groups from the studied quinoxalines are the most preferential sites for the interaction with mild steel and zinc surfaces. There was a formation of iron oxide layers (γ - Fe_2O_3) at the peak around 650 cm^{-1} wavenumbers. The remarkable difference between the spectra of the pure studied quinoxalines and the adsorption film formed after immersion of mild steel and zinc in 1.0 M HCl and 1.0 M H_2SO_4 confirmed that some chemical interaction occurred between the inhibitor molecules and metal surfaces. The AAS analysis revealed a decrease in the concentration of iron and zinc ions in the presence of the studied inhibitors as compared to the blank solutions. The inhibition efficiency increased with an increase in the concentration of the inhibitors. DFT technique was employed in the theoretical study. The obtained adsorption energies further confirm the weight loss measurements findings, that is, the studied quinoxalines exhibit a mixed-type adsorption mechanism, with the domination of the chemisorption process. Thus, a conclusion can be drawn that the aim of this study was realized.

5.2 Recommendations

The study presented in this dissertation champions the use of MQ6CA, Q6CA, and H2QCA as corrosion inhibitors of mild steel, zinc, and aluminum in acidic media. Therefore, future study will focus on the test of these inhibitors in neutral and basic media. Surface analysis such as scanning electron microscopy (SEM) will be employed to gain more insight into the surface morphology of the corrosion of the studied metals in the presence and absence of the compounds of interest. Future work will also focus in studying the corrosion aluminum in 0.5 M HCl as corrosive medium utilizing gravimetric, FTIR and AAS techniques. This study will be extended to further computation aspects such as MD simulations to it give even more conceptual framework.

REFERENCES

1. Talbot DE, Talbot JD. *Corrosion science and technology*. CRC press; 2018.
2. McCafferty E. *Introduction to corrosion science*. Springer Science & Business Media; 2010.
3. Roberge PR. *Corrosion engineering*. McGraw-Hill Education; 2008.
4. Von Baeckmann W, Schwenk W, Prinz W. *Handbook of cathodic corrosion protection*. Elsevier; 1997.
5. Fontana MG, Greene ND. *Corrosion Engineering*; 1967.
6. Ahmad Z. *Principles of corrosion engineering and corrosion control*. Elsevier; 2006.
7. Murulana LC. *Adsorption, thermodynamic and density functional theory investigation of some sulphonamides as corrosion inhibitors for some selected metals in acidic medium*. [Thesis]. North-West University; 2015.
8. Hussin MH, Kassim MJ. *The corrosion inhibition and adsorption behavior of Uncaria gambir extract on mild steel in 1 M HCl*. Materials Chemistry and Physics. 2011;125(3):461-8.
9. Walsh FC. *Faraday and his laws of electrolysis: an appreciation*. Bulletin of Electrochemistry. 1992;7(11):481-4.
10. Revie RW. *Corrosion and corrosion control: an introduction to corrosion science and engineering*. John Wiley & Sons; 2008.
11. Sastri VS. *Challenges in corrosion costs, causes, consequences, and control*. John Wiley & Sons; 2015.
12. National Research Council. *Research opportunities in corrosion science and engineering*. National Academies Press; 2011.
13. Evert DD. *During: Corrosion Atlas*; 2018.
14. Uhlig HH, Revie RW. *Corrosion and corrosion control*; 1985.
15. Philip AS, Schweitzer PE. *Fundamentals of corrosion: Mechanisms, causes, and preventative methods*; 2009.
16. Koch GH, Brongers MP, Thompson NG, Virmani YP, Payer JH. *Corrosion cost and preventive strategies in the United States*; 2002.
17. Nesane T. *Corrosion inhibition exploration of synthesized carboxylic acid and amino esters on selected metals in acid medium*. [Master's thesis]. University of Venda; 2020

18. McEwan JJ. *Corrosion Control in Southern Africa*. Corrosion Institute of Southern Africa, Johannesburg, South Africa; 2004.
19. Oki M, Adediran AA, Anawe PA. *Corrosion monitoring in the oil pipeline industry*. Journal of Multidisciplinary Engineering Science and Technology (JMEST). 2013;2(1).
20. Groysman A. *Corrosion for everybody*. Springer Science & Business Media; 2009.
21. Jones RH, editor. *Stress-corrosion cracking, materials performance and evaluation*. ASM international; 2017.
22. Durning ED, editor. *Corrosion atlas: A collection of illustrated case histories*. Elsevier; 2018.
23. Roberge PR, Eng P. *Corrosion engineering*. Principles and Practice; 2005.
24. Fontana MG, Greene ND. *Corrosion engineering*. McGraw-hill; 2018.
25. Poston RW, West JS. *Investigation of the Charlotte Motor Speedway bridge collapse*. In Structures Congress 2005: Metropolis and Beyond 2005.
26. Surendranath A. *Corrosion Inhibiting Non-Toxic Calcium Silicate Based Pigments*. [Doctoral dissertation]. University of Cincinnati; 2011.
27. Kelly RG, Scully JR, Shoesmith D, Buchheit RG. *Electrochemical techniques in corrosion science and engineering*. CRC Press; 2002.
28. McEwan JJ. *Corrosion Control in Southern Africa*. Corrosion Institute of Southern Africa, Johannesburg, South Africa; 2004.
29. Bardgett WE, Stanners JF. *The Delhi pillar-a study of the corrosion aspects*. NML Technical Journal; 1963;5(1).
30. Wranglén G. *The "rustless" iron pillar at Delhi*. Corrosion Science. 1970;10(10):761-70.
31. White RE. *Comprehensive treatise of electrochemistry*. Bockris JO, Conway BE, Yeager E, editors. New York: Plenum press; 1980.
32. Jones DA. *Principles and prevention of corrosion*; 1996.
33. Schultz, M.P. "OCE-4518 Protection of Marine Materials Class Notes", Florida Institute of Technology; 1197.
34. Swain GW. *OCE-4518 Protection of Marine Materials Class Notes*. Florida Institute of Technology; 1996.
35. Newton Jr LE, Hausler RH. *Methodology to Study Cost of Corrosion*. Corrosion Engineering, Science and Technology. 2005;40(4).

36. Nesic S, Wang S, Cai J, Xiao Y. *Integrated CO₂ corrosion-multiphase flow model*. In SPE International Symposium on Oilfield Corrosion; 2004.
37. Ailor WH, ed. *Handbook on Corrosion Testing and Evaluation*. New York: John Wiley & Sons, 1971; 697–730.
38. Steele BC. *Survey of materials selection for ceramic fuel cells II. Cathodes and anodes*. Solid State Ionics. 1996;86:1223-34.
39. Taiwade RV, Patil AP, Ghugal RD, Patre SJ, Dayal RK. *Corrosion Engineering Corrosion Engineering* 78, 2005. ISIJ international. 2013 Jan 15;53(1):102-9.
40. Stroud EG, Vernon WH. *The prevention of corrosion in packaging. III. Vapour-phase inhibitors*. Journal of Applied Chemistry. 1952 Apr;2(4):178-84.
41. Ehrlich, G.; Turnbull, D. *Physical Metallurgy of Stress Corrosion Fracture; In terscience*: New York and London; 1959.
42. Nkuna A. *Investigation of anticorrosive properties of some ionic liquids on selected metals*. [Master’s thesis]. University of Venda; 2018.
43. Brown PW, Masters LW, Ailor WJ. *Atmospheric Corrosion*. New York; 1982.
44. Grossman PR. *Investigation of atmospheric exposure factors that determine time-of-wetness of outdoor structures. In Atmospheric factors affecting the corrosion of engineering metals*. ASTM International; 1978 .
45. Black HL, Lherbier LW. *Metal corrosion in the atmosphere*. ASTM STP. 1968;435(3).
46. Barton K. *Protection Against Atmospheric Corrosion*, English Translation, ed. by JR Ducan.
47. Hatch JE. *Aluminum: Properties and physical metallurgy: ASM International*. Materials Park N, Ohio. 1984;1-24.
48. Ruhl AS, Kranzmann A. *Corrosion behavior of various steels in a continuous flow of carbon dioxide containing impurities*. International Journal of Greenhouse Gas Control. 2012;9:85-90.
49. Allam IM, Arlow JS, Saricimen H. *Initial stages of atmospheric corrosion of steel in the Arabian Gulf*. Corrosion Science. 1991;32(4):417-32.
50. Naeemi AH, Albrecht P. *Atmospheric Corrosion of Weathering Steel*. International Congress on Metallic Corrosion; 1984.
51. Money KL. *Metals Handbook Corrosion*. Metals Park, Ohio, ASM International. 1987;204.

52. Leygraf C, Wallinder IO, Tidblad J, Graedel T. *Atmospheric corrosion*. John Wiley & Sons; 2016.
53. Seinfeld JH. Effects of air pollution. *Atmospheric Chemistry and Physics of Air Pollution*; 1986.
54. Morcillo M. *Atmospheric corrosion in Ibero-America: the MICAT project*. In *Atmospheric corrosion*. ASTM International; 1995.
55. Revie RW, editor. *Uhlig's corrosion handbook*. John Wiley & Sons; 2011;1-299.
56. Logan KH. *Soil-corrosion studies, 1934-Rates of loss of weight and pitting of ferrous specimens*. Journal of research of the national bureau of standards. 1936;16(5):432.
57. Handbook M. Vol. 13. *Corrosion*, ASM International, Metals Park, OH. 1987: 487–494, 893–906.
58. Bardal E. *Engineering Materials and Processes. Corrosion and Protection*. Springer-Verlag, London Berlin Heidelberg. 2004:1-259.
59. Bahadori A. *Corrosion and materials selection: a guide for the chemical and petroleum industries*. John Wiley & Sons; 2014:125-155.
60. Altayaran AM, Madany IM. *Impact of a desalination plant on the physical and chemical properties of seawater, Bahrain*. *Water Research*. 1992; 26(4):435-441.
61. Al-Fozan SA, Malik AU. *Effect of seawater level on corrosion behavior of different alloys*. *Desalination*. 2008;228(1-3):61-67.
62. Evans UR, Winterbottom AB. *Metallic corrosion, passivity and protection*; 1948.
63. La Que FL, Copson HR. *Corrosion Resistance of Metals and Alloys Reinhold*. New York. 1963;332.
64. Fink FW. *Corrosion of metals in sea water*. 1960;2.
65. Ferster BS, Subrahmanyam B. *A Comparison of Satellite-Derived Sea Surface Salinity and Salt Fluxes in the Southern Ocean*. *Remote Sensing in Earth Systems Sciences*. 2018;1(1):1-13.
66. Forch C. *Berichte über die Konstantenbestimmungen zur Aufstellung der hydrographischen Tabellen*. Bianco Lunos Bogtr; 1902.
67. Williams WD, Sherwood JE. *Definition and measurement of salinity in salt lakes*. *International Journal of Salt Lake Research*. 1994;3(1):53-63.

68. Uhlig HH, Triadis DN, Stern M. *Effect of oxygen, chlorides, and calcium ion on corrosion inhibition of iron by polyphosphates*. Journal of the Electrochemical Society. 1955;102(2):59-66.
69. Hertzberg RW. *Deformation and fracture mechanics of engineering materials*. Journal of Materials Education. 1997;19: 227-32.
70. Davis JR, editor. *Corrosion: Understanding the basics*. ASM International; 2000.
71. Crolet JL. *Mechanisms of uniform corrosion under corrosion deposits*. Journal of materials science. 1993;28(10):2589-606.
72. Cicek V. *Corrosion engineering and cathodic protection handbook: with extensive question and answer section*. John Wiley & Sons; 2017.
73. Kruger J, Long GG, Kuriyama M, Goldman AJ. *Passivity of Metals and Semiconductors*. Elsevier Science Publishers: Amsterdam. 1983;163.
74. Strehblow HH, Marcus P. *Mechanisms of pitting corrosion*. Corrosion technology-New York and Basel; 2002.
75. Wallen B, Andersson T. *Galvanic corrosion of copper alloys in contact with a highly alloyed stainless steel in seawater*; 1986.
76. Uhlig HH, Revie RW. *Corrosion and corrosion control*; 1985.
77. Lees DJ, DJ L. *Characteristics of stress-corrosion fracture initiation and propagation*. 1982;29–38.
78. Hatch JE. *Aluminum: Properties and Physical Metallurgy, Metals Park*. American Society for Metals. 1984.
79. Combrade P. *Crevice corrosion of metallic materials*. Corrosion technology-New York and Basel; 2002.
80. Ijsseling FP. *Survey of literature on crevice corrosion (1979-1998): Mechanisms, test methods and results, practical experience, protective measures and monitoring*. Maney Publishing; 2000.
81. Schweitzer PA. *Corrosion Engineering Handbook: Fundamentals of Metallic Corrosion*; 2006.
82. Levy AV. *Solid particle erosion and erosion-corrosion of materials*. Asm International; 1995.
83. Bardal E. *Corrosion and protection*. Springer Science & Business Media. 2007; 135-136.

84. Srinath KV. *Corrosion and its inhibition studies on branded steel and brass of industrial importance*. Davis JR, editor. *Corrosion: Understanding the basics*. ASM International; 2000.
85. Pourbeix M. *Atlas of Electrochemical Equilibria in Aqueous Solution*. Corrosion Science; 1966.
86. Perez N. *Electrochemistry and corrosion science*. Boston: Kluwer academic publishers; 2004.
87. Murthy SK, Sharma AK, Choo C, Birgersson E. *Analysis of concentration overpotential in an all-vanadium redox flow battery*. *Journal of The Electrochemical Society*. 2018;165(9): A1746.
88. Yaro AS, Wael RK, Khadom AA. *Reaction kinetics of corrosion of mild steel in phosphoric acid*. *Journal of the University of Chemical Technology and Metallurgy*. 2010;45(4):443-8.
89. Okeremi AO. *The Effect of Nitrite on Pitting and Stress Corrosion Cracking of Corrosion Resistant Alloys (CRA) under Oil Field Conditions*. The University of Manchester (United Kingdom); 2011.
90. Atkin R, Craig VS, Biggs S. *Adsorption kinetics and structural arrangements of cationic surfactants on silica surfaces*. *Langmuir*. 2000;16(24):9374-9380.
91. Xu J, Wang Y, Zhang Z. *Potential and concentration dependent electrochemical dealloying of Al₂Au in sodium chloride solutions*. *The Journal of Physical Chemistry C*. 2012 ;116(9):5689-99.
92. Zheng X, Zhang S, Li W, Gong M, Yin L. *Experimental and theoretical studies of two imidazolium-based ionic liquids as inhibitors for mild steel in sulfuric acid solution*. *Corrosion science*. 2015; 95:168-79.
93. Pasha T. *Phthalocyanine compounds as corrosion inhibitors for metals in corrosive environment*. [Doctoral thesis]; 2018.
94. Otieno M, Beushausen H, Alexander M. *Prediction of corrosion rate in reinforced concrete structures—a critical review and preliminary results*. *Materials and Corrosion*. 2012;63(9):777-90.
95. ABD ALAMEER NA. *The effect of temperature and pH on the corrosion rate of carbon steel in 1 M NaCl*. *Journal of Techniques*. 2011;24(3).

96. Živica V. *Significance and influence of the ambient temperature as a rate factor of steel reinforcement corrosion*. Bulletin of Materials Science. 2002;25(5):375-379.
97. Khadom AA, Yaro AS, Kadum AA, AlTaie AS, Musa AY. *The effect of temperature and acid concentration on corrosion of low carbon steel in hydrochloric acid media*. American Journal of Applied Sciences. 2009;6(7):1403.
98. Hashim NZ, Kassim K. *The effect of temperature on mild steel corrosion in 1 M HCl by Schiff bases*. Malaysian Journal of Analytical Sciences. 2014;18(1):28-36.
99. Hackerman N. *Effect of temperature on corrosion of metals by water*. Industrial & Engineering Chemistry. 1952;44(8):1752-5.
100. Hackerman N. *Effect of temperature on corrosion of metals by water*. Industrial & Engineering Chemistry. 1952;44(8):1752-5
101. Skaperdas GT, Uhlig HH. *Corrosion of steel by dissolved carbon dioxide and oxygen*. Industrial & Engineering Chemistry. 1942;34(6):748-54.
102. Speller FN. *Corrosion (Causes and Prevention)*. McGraw-Hill Book Company Inc. New York. 1951.
103. Fernandes JS, Montemor F. *Corrosion*. Materials for Construction and Civil Engineering 2015 (pp. 679-716). Springer, Cham.
104. Kaesche H. *Corrosion of metals: physicochemical principles and current problems*. Springer Science & Business Media; 2003.
105. Dehri I, Erbil ME. *The effect of relative humidity on the atmospheric corrosion of defective organic coating materials: an EIS study with a new approach*. Corrosion science. 2000 ;42(6):969-78.
106. White BS. *Influence of humidity on corrosion rate*. Anti-Corrosion Methods and Materials. 1992;39(8):4-5.
107. Jones DA. *Principles and prevention of corrosion.*;1996.
108. McIntyre NS, Chen C. *Role of impurities on Mg surfaces under ambient exposure conditions*. Corrosion Science. 1998;40(10):1697-1709.

109. Ralston KD, Fabijanic D, Birbilis N. *Effect of grain size on corrosion of high purity aluminium*. *Electrochimica acta*. 2011;56(4):1729-1736.
110. McNulty RE, Hanawalt JD. *Some corrosion characteristics of high purity magnesium alloys*. *Transactions of The Electrochemical Society*. 1942;81(1):423.
111. Copson HR. *Effects of velocity on corrosion*. *Corrosion*. 1960;16(2):86t-92t.
112. Copson HR. *Effects of velocity on corrosion by water*. *Industrial & Engineering Chemistry*. 1952;1745-1752.
113. Li Z, Zhang J, Cheng J. *The influence of critical flow velocity on corrosion of stainless steel*. *Journal of Failure Analysis and Prevention*. 2017;17(6):1234-1240.
114. Foroulis ZA, Uhlig HH. *Effect of velocity and oxygen on corrosion of iron in sulfuric acid*. *Journal of The Electrochemical Society*. 1964;111(1):13.
115. Yang Y, Cheng YF. *Parametric effects on the erosion–corrosion rate and mechanism of carbon steel pipes in oil sands slurry*. *Wear*. 2012; 276:141-148.
116. Chexal B, Horowitz J, Dooley B. *Flow-accelerated corrosion in power plants. Revision 1*. *Electric Power Research Inst.*; 1998.
117. Ayeni FA, Madugu IA, Sukop P, Ihom AP, Alabi OO, Okara R, Abdulwahab M. *Effect of aqueous extracts of bitter leaf powder on the corrosion inhibition of Al-Si alloy in 0.5 M caustic soda solution*. *Journal of Minerals and Materials characterization and Engineering*. 2012;11(7):667-670.
118. Bouyanzer, A., B. Hammouti, and L. Majidi, *Pennyroyal oil from Mentha pulegium as corrosion inhibitor for steel in 1 M HCl*. *Materials Letters*. 2006;2840-2843.
119. Satapathy AK, Gunasekaran G, Sahoo SC, Amit K, Rodrigues PV. *Corrosion inhibition by Justicia gendarussa plant extract in hydrochloric acid solution*. *Corrosion science*. 2009 ;51(12):2848-2856.
120. Sastri VS. *Challenges in corrosion: costs, causes, consequences, and control*. John Wiley & Sons; 2015.

121. Uhlig HH. *The cost of corrosion to the United States*. Chemical and Engineering News. 1949; 27:2764.
122. Hoar TP. *Report of the Committee on Corrosion and Protection*. Department of Trade and Industry; 1971.
123. Bosoku G. *Report of the Committee on Corrosion and Protection*. A survey of the cost of corrosion to Japan. Corrosion Engineering Journal. 1977;26(7):401-28.
124. Koch GH, Brongers MP, Thompson NG, Virmani YP, Payer JH. *Cost of corrosion in the United States*. In Handbook of environmental degradation of materials 2005 Jan 1. William Andrew Publishing.
125. Chin KR, Dalury DF, Zurakowski D, Scott RD. *Intraoperative measurements of male and female distal femurs during primary total knee arthroplasty*. Journal of Knee Surgery. 2002; 15:213–217.
126. Guy SP, Farndon MA, Sidhom S, Al-Lami M, Bennett C, London NJ. *Gender differences in distal femoral morphology and the role of gender specific implants in total knee replacement: a prospective clinical study*. The Knee. 2012;19(1):28-31.
127. Kim JM, Kim SB, Kim JM, Lee DH, Lee BS, Bin SI. *Results of gender-specific total knee arthroplasty: comparative study with traditional implant in female patients*. Knee surgery & Related Research. 2015;27(1):17.
128. Kalman L. *3D printing of a novel dental implant abutment*. Journal of Dental Research, Dental Clinics, Dental Prospects. 2018;12(4):299.
129. Brown BF. *Stress corrosion cracking control measures*. American University Washington DC Department of Chemistry; 1977.
130. Hansson CM. *The impact of corrosion on society*. Metallurgical and Materials Transactions A. 2011;42(10):2952-2962.
131. Peterson MJ. Case Study: *Bhopal Plant Disaster*. International Dimensions of Ethics Education in Science and Engineering; 2009.

132. Andrew W, James R, Handfield M. *Royal Commission of Inquiry into the Sinking of Mv Princess Ashika*. 2010;629.
133. Bardal E. *Corrosion and protection*. Springer Science & Business Media. 2007.
134. Landrum RJ. *Fundamentals of designing for corrosion control: a corrosion aid for the designer*. R. J. Landrum published 1989 by NACE, 350. 1989.
135. Shreir LL, editor. *Corrosion: corrosion control*. Newnes; 2013.
136. Saeedikhani M, Wijesinghe S, Blackwood DJ. *Moving boundary simulation and mechanistic studies of the electrochemical corrosion protection by a damaged zinc coating*. *Corrosion Science*. 2020; 163:108296.
137. Edavan RP, Kopinski R. *Corrosion resistance of painted zinc alloy coated steels*. *Corrosion Science*. 2009;51(10):2429-2442.
138. Harbi JA, Hussein FI, Sabri LA. *Monitoring and Control on Impressed Current Cathodic Protection for Oil Pipelines*. *Al-Nahrain Journal for Engineering Sciences*. 2017;20(4):807-814.
139. Craig BD. *Fundamental aspects of corrosion films in corrosion science*. Springer Science & Business Media; 1991.
140. Putilova IN, Balezin SA, Barannik VP. *Metallic corrosion inhibitors*. Pergamon Press; 1960.
141. TrabANELLI G, Carassiti V. *Advances in corrosion science and technology*. Plenum Press, New York. 1970; 1:147.
142. Sanyal B. *Organic compounds as corrosion inhibitors in different environments-a review*. *Progress in Organic Coatings*. 1981;9(2):165-236.
143. Tabanelli G, Zucchi F. *Reviews on Coatings and Corrosion*. *Reviews. Coating. Corrosion*. 1973;1(2):97-100.
144. Rozenfel'd IL., *Corrosion inhibitors*. New York, McGraw-Hill; 1981.
145. Kemkhadze VS, Balezin SA, Bregman VJ. *Corrosion Inhibitors*. MacMillans, New York. 1963:192.

146. Collie MJ. *Corrosion inhibitors: Developments since 1980*. Noyes Data Corporation, New Jersey, USA; 1983.
147. Hausler RH. *Corrosion inhibition: Proceedings of the International Conference on Corrosion Inhibition, May 16-20, 1983, Dallas, Texas; 1988*.
148. Bregman JI. *Corrosion inhibitors: Principles and application*. John Wiley & Sons, New York; 1998.
149. Guo L, Dong W, Zhang S. *Theoretical challenges in understanding the inhibition mechanism of copper corrosion in acid media in the presence of three triazole derivatives*. RSC advances. 2014;4(79):41956-41967.
150. Boffardi BP. *Control of environmental variables in water-recirculating systems*. ASM Handbook. 1987; 13:487-497.
151. Awad MK, Mustafa MR, Elnga MM. *Computational simulation of the molecular structure of some triazoles as inhibitors for the corrosion of metal surface*. Journal of Molecular Structure: Theochem. 2010;959(1-3):66-74.
152. Deng S, Li X. *Inhibition by Ginkgo leaves extract of the corrosion of steel in HCl and H₂SO₄ solutions*. Corrosion Science. 2012; 55:407-415.
153. Roy P, Pal A, Sukul D. *Origin of the synergistic effect between polysaccharide and thiourea towards adsorption and corrosion inhibition for mild steel in sulphuric acid*. RSC advances. 2014;4(21):10607-10613.
154. Song P, Guo XY, Pan YC, Shen S, Sun Y, Wen Y, Yang HF. *Insight in cysteamine adsorption behaviors on the copper surface by electrochemistry and Raman spectroscopy*. Electrochemical Acta. 2013; 89:503-509.
155. Ebenso EE, Kabanda MM, Murulana LC, Singh AK, Shukla SK. *Electrochemical and quantum chemical investigation of some azine and thiazine dyes as potential corrosion inhibitors for mild steel in hydrochloric acid solution*. Industrial & engineering chemistry research. 2012;51(39):12940-12958.

156. Lin B, Zuo Y. *Inhibition of Q235 carbon steel by calcium lignosulfonate and sodium molybdate in carbonated concrete pore solution*. *Molecules*. 2019;24(3):518.
157. Yang Z, Fischer H, Polder R. *Synthesis and characterization of modified hydrotalcites and their ion exchange characteristics in chloride-rich simulated concrete pore solution*. *Cement and Concrete Composites*. 2014; 47:87-93.
158. Obot IB, Solomon MM, Umoren SA, Suleiman R, Elanany M, Alanazi NM, Sorour AA. *Progress in the development of sour corrosion inhibitors: Past, present, and future perspectives*. *Journal of Industrial and Engineering Chemistry*. 2019; 79:1-18.
159. Cao F, Wei J, Dong J, Ke W. *The corrosion inhibition effect of phytic acid on 20SiMn steel in simulated carbonated concrete pore solution*. *Corrosion Science*. 2015; 100:365-376.
160. Tang F, Wang X, Xu X, Li L. *Phytic acid doped nanoparticles for green anticorrosion coatings*. *Colloids and Surfaces A: Physicochemical and Engineering Aspects*. 2010;369(1-3):101-105.
161. Mohamed HA. *Eco-friendly zero VOC anticorrosive paints for steel protection*. *Journal of Applied Polymer Science*. 2012;125(3):1790-1795.
162. Qu Q, Li L, Bai W, Jiang S, Ding Z. *Sodium tungstate as a corrosion inhibitor of cold rolled steel in peracetic acid solution*. *Corrosion Science*. 2009;51(10):2423-2428.
163. Robertson WD. *Molybdate and tungstate as corrosion inhibitors and the mechanism of inhibition*. *Journal of The Electrochemical Society*. 1951;98(3):94.
164. Bansod AV, Patil AP, Suranshe S, Dahiwal A. *Pitting corrosion behavior of Cr–Mn austenitic stainless steel with addition of molybdate and tungstate under stagnant and flow condition in NaCl solution*. *Journal of Failure Analysis and Prevention*. 2017;17(6):1241-1250.
165. Kumari VA, Sreevalsan K, Shibli SM. *Sodium molybdate for the effective protection of steel: A comprehensive review*. *Corrosion Prevention & Control*. 2001;48(3):83.
166. Mu G, Li X, Qu Q, Zhou J. *Molybdate and tungstate as corrosion inhibitors for cold rolling steel in hydrochloric acid solution*. *Corrosion Science*. 2006;48(2):445-459.

167. Zhou Y, Zuo Y. *The inhibitive mechanisms of nitrite and molybdate anions on initiation and propagation of pitting corrosion for mild steel in chloride solution*. Applied Surface Science. 2015; 353:924-932.
168. Cheng TP, Lee JT, Tsai WT. *Passivation of titanium in molybdate-containing sulphuric acid solution*. Electrochemical Acta. 1991;36(14):2069-2076.
169. Alentejano CR, Aoki IV. *Localized corrosion inhibition of 304 stainless steel in pure water by oxyanions tungstate and molybdate*. Electrochemical Acta. 2004;49(17-18):2779-2785.
170. Wu S, Zhang Q, Sun D, Luan J, Shi H, Hu S, Tang Y, Wang H. *Understanding the synergistic effect of alkyl polyglucoside and potassium stannate as advanced hybrid corrosion inhibitor for alkaline aluminum-air battery*. Chemical Engineering Journal. 2020; 383:123162.
171. Zeng XX, Wang JM, Wang QL, Kong DS, Shao HB, Zhang JQ, Cao CN. *The effects of surface treatment and stannate as an electrolyte additive on the corrosion and electrochemical performances of pure aluminum in an alkaline methanol–water solution*. Materials Chemistry and Physics. 2010;121(3):459-464.
172. Thomaz TR, Weber CR, Pelegrini Jr T, Dick LF, Knörnschild G. *The negative difference effect of magnesium and of the AZ91 alloy in chloride and stannate-containing solutions*. Corrosion Science. 2010;52(7):2235-2243.
173. Gao YB, Hu J, Zuo J, Liu Q, Zhang H, Dong SG, Du RG, Lin CJ. *Synergistic inhibition effect of sodium tungstate and hexamethylene tetramine on reinforcing steel corrosion*. Journal of The Electrochemical Society. 2015;162(10):C555-C562.
174. Mustafa CM, Shahinoor Islam Dulal SM. *Molybdate and nitrite as corrosion inhibitors for copper-coupled steel in simulated cooling water*. Corrosion. 1996;52(1):16-22.
175. Javidi M, Omidvar R. *Synergistic inhibition behavior of sodium tungstate and penicillin G as an eco-friendly inhibitor on pitting corrosion of 304 stainless steel in NaCl solution using Design of Experiment*. Journal of Molecular Liquids. 2019; 291:111330.
176. Lin B, Zuo Y. *Corrosion inhibition of carboxylate inhibitors with different alkylene chain lengths on carbon steel in an alkaline solution*. RSC Advances. 2019;9(13):7065-7077.

177. Zhou Y, Zuo Y, Lin B. *The compounded inhibition of sodium molybdate and benzotriazole on pitting corrosion of Q235 steel in NaCl+ NaHCO₃ solution*. Materials Chemistry and Physics. 2017; 192:86-93.
178. Antonijevec MM, Petrovic MB. *Copper corrosion inhibitors*. A review. International Journal of Electrochemical Science. 2008;3(1):1-28.
179. Groth VJ, Hafsten RJ. *Corrosion of refinery equipment by sulfuric acid and sulfuric acid sludges*. Corrosion. 1954;10(11):368-90.
180. Bockris JO, Conway BE. *Hydrogen Overpotential and the Partial Inhibition of the Corrosion of Iron*. The Journal of Physical Chemistry. 1949;53(4):527-539.
181. Premkumar P, Kannan K, Natesan M. *Effect of menthol coated craft paper on corrosion of copper in HCl environment*. Bulletin of Materials Science. 2010;33(3):307-311.
182. Kumar PP, Kannan K, Natesan M. *Natural thyme as volatile corrosion inhibitor for mild steel in HCl environment*. Journal of Metallurgy and Materials Science. 2008;50(4):227-234.
183. Rafiquee MZ, Khan S, Saxena N, Quraishi MA. *Influence of some thiadiazole derivatives on corrosion inhibition of mild steel in formic and acetic acid media*. Portugaliae Electrochemical Acta. 2007;25(4):419-434.
184. Subramanian A, Gopalakrishnan R, Boopathi C, Balakrishnan K, Vasudevan T, Natesan M, Rengaswamy NS. *Morpholine and its derivatives as vapour phase corrosion inhibitors for mild steel*. Bulletin of electrochemistry. 1998;14(10):289-290.
185. McConnell R. *Volatile corrosion inhibitors offer effective protection for processing and shipment of metal-based products*. Metal finishing. 2008;106(9):23-27.
186. Da-quan ZH. *Application and Development of Volatile Corrosion Inhibition Materials*. Corrosion & Protection. 2007:07.
187. Ash M, Ash I. *Handbook of corrosion inhibitors*; 2011
188. Mercer AD. *Corrosion inhibition: Principles and practice*. Butterworth-Heinemann. In Corrosion 1994; 17-10.

189. Amira WE, Rahim AA, Osman H, Awang K, Raja PB. *Corrosion inhibition of mild steel in 1 M HCl solution by Xylopiya ferruginea leaves from different extract and partitions*. International Journal of Electrochemical Science. 2011;6(7):2998-3016.
190. Shaju KS, Thomas KJ, Raphael VP, Paul A. *Synergistic effect of KI on corrosion inhibition of mild steel by polynuclear Schiff base in sulphuric acid*. International Scholarly Research Notice; 2012.
191. Foley RT. *Role of the chloride ion in iron corrosion*. Corrosion. 1970;26(2):58-70.
192. Ebenso EE, Alemu H, Umoren SA, Obot IB. *Inhibition of mild steel corrosion in sulphuric acid using alizarin yellow GG dye and synergistic iodide additive*. International Journal of Electrochemical Science. 2008;3(12):1325-1339.
193. Umoren SA, Eduok UM, Oguzie EE. *Corrosion inhibition of mild steel in 1 M H₂SO₄ by polyvinyl pyrrolidone and synergistic iodide additives*. Portugaliae Electrochemical Acta. 2008;26(6):533-546.
194. Quraishi MA, Rawat J. *Influence of iodide ions on inhibitive performance of tetraphenyl-dithia-octaaza-cyclotetradeca-hexaene (PTAT) during pickling of mild steel in hot sulfuric acid*. Materials Chemistry and Physics. 2001;70(1):95-99.
195. Desimone MP, Grundmeier G, Gordillo G, Simison SN. *Amphiphilic amido-amine as an effective corrosion inhibitor for mild steel exposed to CO₂ saturated solution: polarization, EIS and PM-IRRAS studies*. Electrochemical Acta. 2011;56(8):2990-2998.
196. Shetty P. *Corrosion inhibition behaviour of thiourea derivatives in acid media against mild steel deterioration: An overview*. Surface Engineering and Applied Electrochemistry. 2017;53(6):587-91.
197. Kinniburgh DG. *General purpose adsorption isotherms*. Environmental science & technology. 1986;20(9):895-904.
198. Babić-Samardžija K, Khaled KF, Hackerman N. *N-heterocyclic amines and derivatives as corrosion inhibitors for iron in perchloric acid*. Anti-Corrosion Methods and Materials; 2005.

199. Ayawei N, Ebelegi AN, Wankasi D. *Modelling and interpretation of adsorption isotherms*. Journal of Chemistry; 2017.
200. Donohue MD, Aranovich GL. *Classification of Gibbs adsorption isotherms*. Advances in colloid and interface science. 1998; 76:137-152.
201. Lecloux A, Pirard JP. *The importance of standard isotherms in the analysis of adsorption isotherms for determining the porous texture of solids*. Journal of Colloid and Interface Science. 1979;70(2):265-281.
202. Langmuir I. *The adsorption of gases on plane surfaces of glass, mica and platinum*. Journal of the American Chemical Society. 1918;40(9):1361-1403.
203. Azizian S, Eris S, Wilson LD. *Re-evaluation of the century-old Langmuir isotherm for modeling adsorption phenomena in solution*. Chemical Physics. 2018; 513:99-104.
204. Rudzinski W, Lee SL, Yan CC, Panczyk T. *A fractal approach to adsorption on heterogeneous solid surfaces. 1. The relationship between geometric and energetic surface heterogeneities*. The Journal of Physical Chemistry B. 2001;105(44):10847-10856.
205. Markin VS, Volkova-Gugeshashvili MI, Volkov AG. *Adsorption at liquid interfaces: the generalized Langmuir isotherm and interfacial structure*. The Journal of Physical Chemistry B. 2006;110(23):11415-11420.
206. Zhou L, Zhang J, Zhou Y. *A simple isotherm equation for modeling the adsorption equilibria on porous solids over wide temperature ranges*. Langmuir. 2001;17(18):5503-5507.
207. Al-Duri B, McKay G. *Prediction of binary systems for kinetics of batch adsorption using basic dyes onto activated carbon*. Chemical Engineering Science. 1991;46(1):193-204.
208. Freundlich H, Heller W. *The adsorption of cis-and trans-azobenzene*. Journal of the American Chemical Society. 1939;61(8):2228-2230.
209. Kumar KV, de Castro MM, Martinez-Escandell M, Molina-Sabio M, Rodriguez-Reinoso F. *A site energy distribution function from Toth isotherm for adsorption of gases on heterogeneous surfaces*. Physical Chemistry Chemical Physics. 2011;13(13):5753-5759.

210. Freundlich H. *Kapillarchemie, eine Darstellung der Chemie der Kolloide und verwandter Gebiete*. akademische Verlagsgesellschaft; 1922.
211. Shahbeig H, Bagheri N, Ghorbanian SA, Hallajisani A, Poorkarimi S. *A new adsorption isotherm model of aqueous solutions on granular activated carbon*. World Journal of Modelling and Simulation. 2013;9(4):243-254.
212. Vijayaraghavan K, Padmesh TV, Palanivelu K, Velan M. *Biosorption of nickel (II) ions onto Sargassum wightii: application of two-parameter and three-parameter isotherm models*. Journal of Hazardous Materials. 2006;133(1-3):304-8.
213. Davis JR, editor. *Corrosion of aluminum and aluminum alloys*. ASM International; 1999.
214. Vargel C. *Corrosion of aluminium*. Elsevier. 2020.
215. Nayak P. *Aluminum: impacts and disease*. Environmental Research. 2002;89(2):101-115.
216. Lecka K, Antonczak A. *The influence of fiber laser radiation on the corrosion resistance of aluminium alloy*.
217. Kliškić M, Radošević J, Gudić S, Katalinić V. *Aqueous extract of Rosmarinus officinalis L. as inhibitor of Al–Mg alloy corrosion in chloride solution*. Journal of applied electrochemistry. 2000;30(7):823-30.
218. Vargel C. *Corrosion of Aluminium*, Elsevier. 2004.
219. Bryan JM. *The mechanism of the corrosion of aluminium*. Chemistry and Industry; 1948.
220. Foley RT, Nguyen TH. *The chemical nature of aluminum corrosion: V. Energy transfer in aluminum dissolution*. Journal of the Electrochemical Society. 1982;129(3):464.
221. Craddock PT. *The early history of zinc*. Endeavour. 1987;11(4):183-91.
222. Habashi F. *Zinc, the metal from the east*. Metall (Berlin, West). 2002;56(6):389-394.
223. Kropschot SJ, Doebrich JL. *Zinc-The key to preventing corrosion*. US Geological Survey; 2011.

224. Pistofidis N, Vourlias G, Konidaris S, Pavlidou E, Stergiou A, Stergioudis G. *Microstructure of zinc hot-dip galvanized coatings used for corrosion protection*. Materials Letters. 2006;60(6):786-9.
225. Doerre M, Hibbitts L, Patrick G, Akafuah NK. *Advances in automotive conversion coatings during pretreatment of the body structure: A review*. Coatings. 2018;8(11):405.
226. Sorour N, Zhang W, Ghali E, Houlachi G. *A review of organic additives in zinc electrodeposition process (performance and evaluation)*. Hydrometallurgy. 2017;171:320-32.
227. Maniam KK, Paul S. *Corrosion Performance of Electrodeposited Zinc and Zinc-Alloy Coatings in Marine Environment*. Corrosion and Materials Degradation. 2021;2(2):163-189.
228. Schweitzer PA. *Metallic materials: physical, mechanical, and corrosion properties*. CRC Press; 2003.
229. Thirumoolan D, Katkar VA, Gunasekaran G, Kanai T, Basha KA. *Hyperbranched poly (cyanurateamine): a new corrosion inhibitor for mild steel in hydrochloric acid medium*. Progress in Organic Coatings. 2014;77(8):1253-63.
230. Fahlman M, Jasty S, Epstein AJ. *Corrosion protection of iron/steel by emeraldine base polyaniline: an X-ray photoelectron spectroscopy study*. Synthetic Metals. 1997;85(1-3):1323-6.
231. Patidar AK, Jeyakandan M, Mobiya AK, Selvam G. *Exploring potential of quinoxaline moiety*. International Journal of PharmTech Research. 2011;3(1):386-392.
232. Ganapaty S, Ramalingam P, Rao CB. *Antibacterial, antifungal and antitubercular screening of some novel condensed bridgehead nitrogen heterocycles of quinoxalines*. Indian Journal of Heterocyclic Chemistry. 2007;16(3):283-286.
233. Refaat HM, Moneer AA, Khalil OM. *Synthesis and antimicrobial activity of certain novel quinoxalines*. Archives of Pharmacal Research. 2004;27(11):1093-1098.

234. Badran M.M., Abouzid K.A.M. and Hussein M.H.M. *Synthesis of certain substituted quinoxalines as anti-microbial agents, Part II*. Archives of Pharmacal Research., 2003;26,107–113.
235. Nasr MN. *Synthesis and Antibacterial Activity of Fused 1, 2, 4-Triazolo [4, 3-a] quinoxaline and Oxopyrimido [2', 1': 5, 1] -1, 2, 4-triazolo [4, 3-a] quinoxaline Derivatives*. Archiv der Pharmazie: An International Journal Pharmaceutical and Medicinal Chemistry. 2002 ;335(8):389-94.
236. El-Hawash SA, Habib NS, Fanaki NH. *Quinoxaline derivatives. Part II: Synthesis and antimicrobial testing of 1, 2, 4-triazolo [4, 3-a] quinoxalines, 1, 2, 4-triazino [4, 3-a] quinoxalines and 2-pyrazolylquinoxalines*. Die Pharmazie. 1999;54(11):808-813.
237. El-Gendy AA, El-Meligie S, El-Ansary AK, Ahmedy AM. *Synthesis of some quinoxaline derivatives containing indoline-2, 3-dione or thiazolidinone residue as potential antimicrobial agents*. Archives of Pharmacal Research. 1995;18(1):44-47.
238. Richard JK. *Preparation of quinoxalines, dihydropyrazines, pyrazines and piperazines using tandem oxidation processes*. Chemical communications. 2003(18):2286-2287.
239. Dell A, Williams DH, Morris HR, Smith GA, Feeney J, Roberts GC. *Structure revision of the antibiotic echinomycin*. Journal of the American Chemical Society. 1975;97(9):2497-2502.
240. Seitz LE, Suling WJ, Reynolds RC. *Synthesis and antimycobacterial activity of pyrazine and quinoxaline derivatives*. Journal of medicinal chemistry. 2002;45(25):5604-5606.
241. Ganapaty S, Ramalingam P, Rao CB. *Antibacterial, antifungal and antitubercular screening of some novel condensed bridgehead nitrogen heterocycles of quinoxalines*. Indian Journal of Heterocyclic Chemistry. 2007;16(3):283-286.
242. Obafemi CA, Akinpelu DA. *Synthesis and antimicrobial activity of some 2 (1H)-quinoxalinone-6-sulfonyl derivatives*. Phosphorus, Sulfur, and Silicon and the Related Elements. 2005;180(8):1795-807.
243. Badran MM, Abouzid KA, Hussein MH. *Synthesis of certain substituted quinoxalines as antimicrobial agents (part II)*. Archives of Pharmacal Research. 2003;26(2):107-113.

244. Nasr MN. *Synthesis and Antibacterial Activity of Fused 1, 2, 4-Triazolo [4, 3-a] quinoxaline and Oxopyrimido [2', 1': 5, 1] -1, 2, 4-triazolo [4, 3-a] quinoxaline Derivatives*. *Archiv der Pharmazie: An International Journal Pharmaceutical and Medicinal Chemistry*. 2002;335(8):389-394.
245. Tandon VK, Yadav DB, Maurya HK, Chaturvedi AK, Shukla PK. *Design, synthesis, and biological evaluation of 1, 2, 3-trisubstituted-1, 4-dihydrobenzo [g] quinoxaline-5, 10-diones and related compounds as antifungal and antibacterial agents*. *Bioorganic & Medicinal Chemistry*. 2006;14(17):6120-6126.
246. Sanna P, Carta A, Loriga M, Zanetti S, Sechi L. *Preparation and biological evaluation of 6/7-trifluoromethyl (nitro)-, 6, 7-difluoro-3-alkyl (aryl)-substituted-quinoxalin-2-ones. Part 3. II* *Farmaco*. 1999;54(3):169-177.
247. El-Sayed HA, Said SA, Moustafa AH, Baraka MM, Abdel-Kader RT. *Synthesis and Biological Evaluation of 2-Oxo/Thioxoquinoxaline and 2-Oxo/Thioxoquinoxaline-Based Nucleoside Analogues*. *Nucleosides, Nucleotides and Nucleic Acids*. 2016;35(1):16-31.
248. Refaat HM, Moneer AA, Khalil OM. *Synthesis and antimicrobial activity of certain novel quinoxalines*. *Archives of Pharmacal Research*. 2004;27(11):1093-1098.
249. Carta A, Sanna P, Gherardini L, Usai D, Zanetti S. *Novel functionalized pyrido [2, 3-g] quinoxalinones as antibacterial, antifungal and anticancer agents. II* *Farmaco*. 2001;56(12):933-8.
250. Blache Y, Gueiffier A, Elhakmaoui A, Viols H, Chapat JP, Chavignon O, Teulade JC, Grassy G, Dauphin G, Carpy A. *Synthesis and reactivity of pyrrolo [1, 2- α] quinoxalines. Crystal structure and AM1 calculation*. *Journal of Heterocyclic Chemistry*. 1995;32(4):1317-1324.
251. Hassan SY, Khattab SN, Bekhit AA, Amer A. *Synthesis of 3-benzyl-2-substituted quinoxalines as novel monoamine oxidase A inhibitors*. *Bioorganic & Medicinal Chemistry Letters*. 2006;16(6):1753-1756.
252. Sarges R, Howard HR, Browne RG, Lebel LA, Seymour PA, Koe BK. *4-Amino [1, 2, 4] triazolo [4, 3-a] quinoxalines. A novel class of potent adenosine receptor antagonists and*

- potential rapid-onset antidepressants*. Journal of Medicinal Chemistry. 1990;33(8):2240-2254.
253. Olayiwola G, Obafemi CA, Taiwo FO. *Synthesis and neuropharmacological activity of some quinoxalinone derivatives*. African Journal of Biotechnology. 2007;6(6):777-786.
254. Kobylyanskii EV, Vasil'kevich IM, Dvorko GF. *Dihydro-1, 2, 3-tricarbalcoxycyclopenta [b] quinoxalines*. Chemistry of Heterocyclic Compounds. 1975;11(7):874-6.
255. Wagle S, Adhikari AV, Kumari NS. *Synthesis of some new 2-(3-methyl-7-substituted-2-oxoquinoxaliny)-5-(aryl)-1, 3, 4-oxadiazoles as potential non-steroidal anti-inflammatory and analgesic agents*.
256. Ries UJ, Pripke HW, Huel NH, Handschuh S, Mihm G, Stassen JM, Wienen W, Nar H. *Heterocyclic thrombin inhibitors. Part 2: quinoxalinone derivatives as novel, potent antithrombotic agents*. Bioorganic & Medicinal Chemistry Letters. 2003;13(14):2297-302.
257. Varano F, Catarzi D, Colotta V, Cecchi L, Filacchioni G, Galli A, Costagli C. *Synthesis of a set of ethyl 1-carbamoyl-3-oxoquinoxaline-2-carboxylates and of their constrained analogue imidazo [1, 5-a] quinoxaline-1, 3, 4-triones as glycine/NMDA receptor antagonists*. European Journal of Medicinal Chemistry. 2001;36(2):203-9.
258. Li JJ. *Synthesis of novel 3-substituted pyrrolo [2, 3-b] quinoxalines via an intramolecular heck reaction on an aminoquinoxaline scaffold*. The Journal of Organic Chemistry. 1999;64(22):8425-7.
259. Zarranz B, Jaso A, Aldana I, Monge A, Maurel S, Deharo E, Jullian V, Sauvain M. *Synthesis and antimalarial activity of new 3-arylquinoxaline-2-carbonitrile derivatives*. Arzneimittelforschung. 2005;55(12):754-61.
260. Ramalingam P, Ganapaty S, Rao CB. *In vitro antitubercular and antimicrobial activities of 1-substituted quinoxaline-2, 3 (1H, 4H)-diones*. Bioorganic & Medicinal Chemistry Letters. 2010;20(1):406-8.
261. El-Sayed HA, Said SA, Moustafa AH, Baraka MM, Abdel-Kader RT. *Synthesis and Biological Evaluation of 2-Oxo/Thioxoquinoxaline and 2-Oxo/Thioxoquinoxaline-Based Nucleoside Analogues*. Nucleosides, Nucleotides and Nucleic Acids. 2016;35(1):16-31.
262. Kleim JP, Bender R, Billhardt UM, Meichsner C, Riess G, Rösner M, Winkler I, Paessens A. *Activity of a novel quinoxaline derivative against human immunodeficiency virus type 1*

- reverse transcriptase and viral replication*. Antimicrobial agents and chemotherapy. 1993 ;37(8):1659-64..
263. Mamedov VA. *Quinoxalines: Synthesis, Reactions, Mechanisms and Structure*. Springer; 2016.
264. Mamedov VA. *Quinoxalines: Synthesis, Reactions, Mechanisms and Structure*. Springer; 2016.
265. Eicher T, Hauptmann S, Speicher A. *The chemistry of heterocycles: structures, reactions, synthesis, and applications*. John Wiley & Sons; 2013.
266. Hinsberg O. *Ueber quinoxaline*. Chemische Berichte. 1887;17(1):318–323.
267. Körner G. *Ueber einige umwandlungen des orthonitranilins und der orthodiamine*. Chemische Berichte. 1884;17(2):572–573.
268. Saranya J, Sounthari P, Kiruthuka A, Parameswari K, Chitra S. *The inhibiting effect of some quinoxaline derivative towards mild steel corrosion in acid media: chemical, electrochemical and theoretical studies*. Journal of Materials and Environmental Science. 2015;6(2):425-44.
269. Atkins PW, Friedman RS. *Molecular quantum mechanics*. Oxford university press; 2011.
270. Boyd DB. *Quantum mechanics in drug design: Methods and applications*. Drug Information Journal. 1983;17(3):121-31.
271. Cramer, C.J. *Essentials of Computational Chemistry; Theories and Models*. 2nd ed, Wiley; 2004.
272. Olasunkanmi, L.O. *Theoretical study of the molecular geometry, electronic and thermodynamic properties of novel 1,10-phenanthroline[5,6-f]1,10-phenanthroline and its selected transition metal complexes*. [Master's thesis]. Obafemi Awolowo University, Ile-Ife, Nigeria, 2012.
273. Hellman A. *Nonadiabaticity in the initial oxidation of Mg (0001): First-principles density-functional calculations*. Physical Review B. 2005 Nov 18;72(20):201403.
274. Jensen F. *Introduction to computational chemistry*. John wiley & sons; 2017.
275. Dewar MJ, Thiel W. *Ground states of molecules. 38. The MNDO method. Approximations and parameters*. Journal of the American Chemical Society. 1977;99(15):4899-907.
276. Young D. *Computational chemistry: a practical guide for applying techniques to real world problems*. John Wiley & Sons; 2004.

277. Stewart JJ. *Optimization of parameters for semiempirical methods. III Extension of PM3 to Be, Mg, Zn, Ga, Ge, As, Se, Cd, In, Sn, Sb, Te, Hg, Tl, Pb, and Bi.* Journal of Computational Chemistry. 1991;12(3):320-41.
278. Kabanda M.M., Morulana L.C., Ozcan M., Karadag F., Dehri I., Obot I.B., Ebenso E.E. *Quantum chemical studies on the corrosion inhibition of Mild steel by some triazoles and benzimidazole derivatives in acidic medium.* International Journal of Electrochemical Science. 2012; 7(5035):e5056.
279. Allen LC, Karo AM. *Basis functions for Ab Initio calculations.* Reviews of Modern Physics. 1960;32(2):275.
280. Lotrich VF, Bartlett RJ, Grabowski I. *Intermolecular potential energy surfaces of weakly bound dimers computed from ab initio density functional theory: the right answer for the right reason.* Chemical Physics Letters. 2005;405(1-3):43-8.
281. Townsend JS. *A modern approach to quantum mechanics.* University Science Books; 2000.
282. Otukile KP. Reactions of phloroglucinols with radical species, a theoretical study in different media.[Doctoral dissertation], North-West University; 2020.
283. Obayes HR, Al-Amiery AA, Alwan GH, Abdullah TA, Kadhun AA, Mohamad AB. *Sulphonamides as corrosion inhibitor: experimental and DFT studies.* Journal of Molecular Structure. 2017; 1138:27-34.
284. Biovia DS. *Materials Studio. R2 (Dassault Systèmes BIOVIA, San Diego. 2017.*
285. Sharma S, Kumar P, Chandra R. *Applications of BIOVIA materials studio, LAMMPS, and GROMACS in various fields of science and engineering.* Molecular Dynamics Simulation of Nanocomposites Using BIOVIA Materials Studio, Lammmps and Gromacs. 2019:329-41.
286. Gupta RK, Malviya M, Ansari KR, Lgaz H, Chauhan DS, Quraishi MA. *Functionalized graphene oxide as a new generation corrosion inhibitor for industrial pickling process: DFT and experimental approach.* Materials Chemistry and Physics. 2019; 236:121727.
287. Benabid S, Douadi T, Issaadi S, Penverne C, Chafaa S. *Electrochemical and DFT studies of a new synthesized Schiff base as corrosion inhibitor in 1 M HCl.* Measurement. 2017; 99:53-63.
288. Liu W, Dai X, Bai Z, Wang Y, Yang Z, Zhang L, Xu L, Chen L, Li Y, Gui D, Diwu J. *Highly sensitive and selective uranium detection in natural water systems using a luminescent mesoporous metal–organic framework equipped with abundant Lewis basic sites: a combined*

- batch, X-ray absorption spectroscopy, and first principles simulation investigation. Environmental Science & Technology. 2017;51(7):3911-21.*
289. Lynch ME, Folz DC, Clark DE. *Use of FTIR reflectance spectroscopy to monitor corrosion mechanisms on glass surfaces. Journal of Non-crystalline Solids. 2007;353(27):2667-74.*
290. Manamela KM, Murulana LC, Kabanda MM, Ebenso EE. *Adsorptive and DFT studies of some imidazolium based ionic liquids as corrosion inhibitors for zinc in acidic medium. vol. 2014; 9:3029-46.*
291. Olasunkanmi LO, Obot IB, Kabanda MM, Ebenso EE. *Some quinoxalin-6-yl derivatives as corrosion inhibitors for mild steel in hydrochloric acid: experimental and theoretical studies. The Journal of Physical Chemistry C. 2015;119(28):16004-19.*
292. Kabanda MM, Murulana LC, Ozcan M, Karadag F, Dehri I, Obot IB, Ebenso EE. *Quantum chemical studies on the corrosion inhibition of mild steel by some triazoles and benzimidazole derivatives in acidic medium. International Journal of Electrochemical Science. 2012;7(5035): e5056.*
293. Wang J, Wang J, Ming H, Zhang Z, Han EH. *Effect of temperature on corrosion behavior of alloy 690 in high temperature hydrogenated water. Journal of Materials Science & Technology. 2018;34(8):1419-27.*
294. Loto RT, Tobilola O. *Corrosion inhibition properties of the synergistic effect of 4-hydroxy-3-methoxybenzaldehyde and hexadecyltrimethylammoniumbromide on mild steel in dilute acid solutions. Journal of King Saud University-Engineering Sciences. 2018;30(4):384-90.*
295. Li W, He Q, Pei C, Hou B. *Experimental and theoretical investigation of the adsorption behaviour of new triazole derivatives as inhibitors for mild steel corrosion in acid media. Electrochimica Acta. 2007;52(22):6386-94.*
296. Zhang S, Tao Z, Li W, Hou B. *The effect of some triazole derivatives as inhibitors for the corrosion of mild steel in 1 M hydrochloric acid. Applied Surface Science. 2009;255(15):6757-63.*
297. Adardour K, Kassou O, Tourir R, Ebn Touhami M, El Kafsaoui H, Benzeid H, El Essassi M, Sfaira M. *Study of the influence of new quinoxaline derivatives on corrosion inhibition of mild steel in hydrochloric acidic medium. Journal of Materials and Environmental Science. 2010;1(2):129-38.*

298. Karzazi Y, Belghiti ME, El-Hajjaji F, Hammouti B. *Density functional theory modeling and monte carlo simulation assessment of N-substituted quinoxaline derivatives as mild steel corrosion inhibitors in acidic medium*. Journal of Materials and Environmental Science. 2016;7:3916-29.
299. Nkuna AA, Akpan ED, Obot IB, Verma C, Ebenso EE, Murulana LC. *Impact of selected ionic liquids on corrosion protection of mild steel in acidic medium: experimental and computational studies*. Journal of Molecular Liquids. 2020; 314:113609.
300. Noor EA. *Temperature effects on the corrosion inhibition of mild steel in acidic solutions by aqueous extract of fenugreek leaves*. International Journal of Electrochemical Science. 2007;2(12).
301. Quraishi MA, Jamal D. *Dianils as new and effective corrosion inhibitors for mild steel in acidic solutions*. Materials chemistry and physics. 2003;78(3):608-13.
302. Soror TY, El-Ziady MA. *Effect of cetyl trimethyl ammonium bromide on the corrosion of carbon steel in acids*. Materials Chemistry and Physics. 2003;77(3):697-703.
301. Soltani N, Behpour M, Ghoreishi SM, Naeimi H. *Corrosion inhibition of mild steel in hydrochloric acid solution by some double Schiff bases*. Corrosion Science. 2010;52(4):1351-61.
302. Obi-Egbedi NO, Obot IB, El-Khaiary MI, Umoren SA, Ebenso EE. *Computational simulation and statistical analysis on the relationship between corrosion inhibition efficiency and molecular structure of some phenanthroline derivatives on mild steel surface*. International Journal of Electrochemical Science. 2011;6(1):5649-75.
303. Saratha R, Priya SV, Thilagavathy P. *Investigation of Citrus aurantiifolia leaves extract as corrosion inhibitor for mild steel in 1 M HCl*. E-Journal of Chemistry. 2009;6(3):785-95.
304. Zhang S, Tao Z, Li W, Hou B. *The effect of some triazole derivatives as inhibitors for the corrosion of mild steel in 1 M hydrochloric acid*. Applied Surface Science. 2009;255(15):6757-63.
305. Çalışkan N, Bilgic S. *Effect of iodide ions on the synergistic inhibition of the corrosion of manganese-14 steel in acidic media*. Applied Surface Science. 2000;153(2-3):128-33.
306. Bouklah M, Hammouti B, Aouniti A, Benkaddour M, Bouyanzer A. *Synergistic effect of iodide ions on the corrosion inhibition of steel in 0.5 M H₂SO₄ by new chalcone derivatives*. Applied Surface Science. 2006;252(18):6236-42.

307. Feng Y, Siow KS, Teo WK, Hsieh AK. *The synergistic effects of propargyl alcohol and potassium iodide on the inhibition of mild steel in 0.5 M sulfuric acid solution*. Corrosion Science. 1999;41(5):829-52.
308. Chitra S, Parameswari K, Vidhya M, Kalishwari M, Selvaraj A. *Evaluation of quinoxalines as corrosion inhibitors for mild steel in acid environment*. International Journal of Electrochemical Science. 2011;6(10):4593-613.
309. Yin ZF, Feng YR, Zhao WZ, Bai ZQ, Lin GF. *Effect of temperature on CO₂ corrosion of carbon steel*. Surface and Interface Analysis. 2009 Jun;41(6):517-23.
310. Murulana LC, Singh AK, Shukla SK, Kabanda MM, Ebenso EE. *Experimental and quantum chemical studies of some bis (trifluoromethyl-sulfonyl) imide imidazolium-based ionic liquids as corrosion inhibitors for mild steel in hydrochloric acid solution*. Industrial & Engineering Chemistry Research. 2012;51(40):13282-99.
311. Alamiery AA. *Anticorrosion effect of thiosemicarbazide derivative on mild steel in 1 M hydrochloric acid and 0.5 M sulfuric Acid: Gravimetric and theoretical studies*. Materials Science for Energy Technologies. 2021; 4:263-73.
312. Nesane T, Mnyakeni-Moleele SS, Murulana LC. *Exploration of synthesized quaternary ammonium ionic liquids as unharmed anti-corrosives for aluminium utilizing hydrochloric acid medium*. Heliyon. 2020;6(6): e04113.
313. Singh AK, Quraishi MA. *Effect of 2, 2' benzothiazolyl disulfide on the corrosion of mild steel in acid media*. Corrosion Science. 2009;51(11):2752-60.
314. Korde R, Verma CB, Ebenso EE, Quraishi MA. *Electrochemical and Thermo Dynamical Investigation of 5-ethyl 4-(4-methoxyphenyl)-6-methyl-2-thioxo-1, 2, 3, 4 tetrahydropyrimidine-5-carboxylate on Corrosion Inhibition Behavior of Aluminium in 1M Hydrochloric Acid Medium*. International Journal of Electrochemical Science. 2015; 10:1081-93.
315. Yadav M, Kumar S, Sinha RR, Bahadur I, Ebenso EE. *New pyrimidine derivatives as efficient organic inhibitors on mild steel corrosion in acidic medium: electrochemical, SEM, EDX, AFM and DFT studies*. Journal of Molecular Liquids. 2015; 211:135-45.
316. Ojo FK, Adejoro IA, Akpomie KG, Ogunyemi BT, Oyeka EE. *Effect of Iodide Ions on the Inhibitive Performance of O-, M-, P-Nitroaniline on Mild Steel in Hydrochloric Acid Solution*. Journal of Applied Sciences and Environmental Management. 2018;22(5):775-82.

317. Abouchane M, El Bakri M, Touir R, Rochdi A, Elkhatabi O, Touhami ME, Forssal I, Mernari B. *Corrosion inhibition and adsorption behavior of triazoles derivatives on mild steel in 1 M H₂SO₄ and synergistic effect of iodide ions*. Research on Chemical Intermediates. 2015;41(4):1907-23.
318. Damaskin BB, Petrii OA, Batrakov VV, Uvarov EB, Parsons R. *Adsorption of organic compounds on electrodes*. New York: Plenum Press; 1971.
319. Dubey RK, Gupta N, Nafees SM, Kalpana S. *Inhibition of Mild Steel Corrosion in Hydrochloric Acid Solution by Leaves of Ziziphus jujuba*. Nature Environment and Pollution Technology. 2020;19(2):799-807.
320. Kokalj A. *Corrosion inhibitors: physisorbed or chemisorbed?* Corrosion Science. 2021:109939.
321. Hmamou DB, Salghi R, Zarrouk A, Zarrok H, Hammouti B, Al-Deyab SS, Bouachrine M, Chakir A, Zougagh M. *Alizarin red: an efficient inhibitor of C38 steel corrosion in hydrochloric acid*. International Journal of Electrochemical Science. 2012;7(6):5716.
322. Ekop AS, Eddy NO. *Inhibitive and Adsorptive Properties of Orphenadrine for the Corrosion of*. Australian Journal of Basic and Applied Sciences. 2008;2(4):1258-63.
323. Dahiya S, Pahuja P, Lgaz H, Chung IM, Lata S. *Advanced quantum chemical and electrochemical analysis of ravage drugs for corrosion inhibition of mild steel*. Journal of Adhesion Science and Technology. 2019;33(10):1066-89.
324. Saranya J, Sounthari P, Kiruthika A, Saranya G, Yuvarani S, Parameswari K, Chitra S. *Experimental and Quantum chemical studies on the inhibition potential of some Quinoxaline derivatives for mild steel in acid media*. Oriental Journal of Chemistry. 2014;30(4):1719.
325. Danaee I, Bahramipannah N. *Thermodynamic and adsorption behavior of N₂O₄ schiff base as a corrosion inhibitor for API-5L-X65 steel in HCl solution*. Russian Journal of Applied Chemistry. 2016;89(3):489-99.
326. Kumar R, Chahal S, Dahiya S, Dahiya N, Kumar S, Lata S. *Experimental and theoretical approach to exploit the corrosion inhibition activity of 3-formyl chromone derivatives on mild steel in 1 M H₂SO₄*. Corrosion Reviews. 2017;35(2):95-110.
327. Kumar R, Chahal S, Kumar S, Lata S, Lgaz H, Salghi R, Jodeh S. *Corrosion inhibition performance of chromone-3-acrylic acid derivatives for low alloy steel with theoretical modeling and experimental aspects*. Journal of Molecular Liquids. 2017;243:439-50.

328. Baertschi SW, Dorman DE, Oocolowitz JL, Spangle LA, Collins MW, Wildfeuer ME, Lorenz LJ. *Isolation and structure elucidation of a novel product of the acidic degradation of cefaclor*. Journal of pharmaceutical sciences. 1993;82(6):622-6.
329. Hmamou DB, Zarrouk A, Salghi R, Zarrok H, Ebenso EE, Hammouti B, Kabanda MM, Benchat N, Benali O. *Experimental and Theoretical Studies of the Adsorption and Corrosion Inhibition of 6-phenylpyridazine-3 (2H)-thione on Carbon Steel in 2.0 M H₃PO₄ M solution*. International Journal of Electrochemical Science. Sci. 2014; 9:120-38.
330. Obot IB, Ebenso EE, Kabanda MM. *Metronidazole as environmentally safe corrosion inhibitor for mild steel in 0.5 M HCl: experimental and theoretical investigation*. Journal of Environmental Chemical Engineering. 2013;1(3):431-9.
331. Akinbulumo OA, Odejobi OJ, Odekanle EL. *Thermodynamics and adsorption study of the corrosion inhibition of mild steel by Euphorbia heterophylla L. extract in 1.5 M HCl*. Results in Materials. 2020; 5:100074.
332. Jafari H, Danaee I, Eskandari H, RashvandAvei M. *Electrochemical and theoretical studies of adsorption and corrosion inhibition of N, N'-bis (2-hydroxyethoxyacetophenone)-2, 2-dimethyl-1, 2-propanediimine on low carbon steel (API 5L Grade B) in acidic solution*. Industrial & Engineering Chemistry Research. 2013;52(20):6617-32.
333. Shukla SK, Quraishi MA. *The effects of pharmaceutically active compound doxycycline on the corrosion of mild steel in hydrochloric acid solution*. Corrosion Science. 2010 ;52(2):314-21.
334. Mahdavian M, Attar MM. *Electrochemical behaviour of some transition metal acetylacetonate complexes as corrosion inhibitors for mild steel*. Corrosion Science. 2009;51(2):409-14.
335. Nasser AJ, Sathiq MA. *Comparative study of N-[(4-methoxyphenyl) (morpholin-4-yl) methyl] acetamide (MMPA) and N- [morpholin-4-yl (phenyl) methyl] acetamide (MPA) as corrosion inhibitors for mild steel in sulfuric acid solution*. Arabian Journal of Chemistry. 2017;10: S261-73.
336. Jacob KS, Parameswaran G. *Corrosion inhibition of mild steel in hydrochloric acid solution by Schiff base furoin thiosemicarbazone*. Corrosion Science. 2010 Jan 1;52(1):224-8.
337. Verma C, Hussain CM. *Polyethylene glycol and its derivatives as environmentally sustainable corrosion inhibitors: A literature survey*. Environmentally Sustainable Corrosion Inhibitors. 2022:321-33.

338. Cen H, Wu C, Chen Z. *Polydopamine functionalized graphene oxide as an effective corrosion inhibitor of carbon steel in HCl solution*. Journal of Materials Science. 2022;1-23.
339. Jorcin JB, Orazem ME, Pébère N, Tribollet B. *CPE analysis by local electrochemical impedance spectroscopy*. Electrochemical Acta. 2006;51(8-9):1473-9.
340. Solmaz R, Altunbaş E, Kardaş G. *Adsorption and corrosion inhibition effect of 2-((5-mercapto-1, 3, 4-thiadiazol-2-ylimino) methyl) phenol Schiff base on mild steel*. Materials Chemistry and Physics. 2011;125(3):796-801.
341. Gerengi H, Sahin HI. *Schinopsis lorentzii extract as a green corrosion inhibitor for low carbon steel in 1 M HCl solution*. Industrial & Engineering Chemistry Research. 2012;51(2):780-7.
342. Abu-Dalo MA, Othman AA, Al-Rawashdeh NA. *Exudate gum from acacia trees as green corrosion inhibitor for mild steel in acidic media*. International Journal of Electrochemical Science. 2012;7(10):9303-24.
343. Saraswat V, Kumari R, Yadav M. *Novel carbon dots as efficient green corrosion inhibitor for mild steel in HCl solution: Electrochemical, gravimetric and XPS studies*. Journal of Physics and Chemistry of Solids. 2022;160:110341.
344. Nwankwo HU, Akpan ED, Olasunkanmi LO, Verma C, Al-Mohaimeed AM, Al Farraj DA, Ebenso EE. *N-substituted carbazoles as corrosion inhibitors in microbiologically influenced and acidic corrosion of mild steel: Gravimetric, electrochemical, surface and computational studies*. Journal of Molecular Structure. 2021;1223:129328.
345. Thomas S, Birbilis N, Venkatraman MS, Cole IS. *Corrosion of zinc as a function of pH*. Corrosion, The Journal of Science and Engineering. 2012;68(1):015009-1.
346. Raja PB, Sethuraman MG. *Inhibitive effect of black pepper extract on the sulphuric acid corrosion of mild steel*. Materials Letters. 2008;62(17-18):2977-9.
347. Ikpi ME, Abeng FE, Obono OE. *Adsorption and Thermodynamic Studies for Corrosion Inhibition of API 5L X-52 Steel in 2 M HCl Solution by Moxifloxacin*. World News of Natural Sciences. 2017;9.
348. Singh AK, Ebenso EE. *Effect of Ceftezole on the corrosion of mild steel in HCl solution*. International journal of Electrochemical Science. 2012; 7:2349-60.
349. Ogoko EC, Odoemelum SA, Ita BI, Eddy NO. *Adsorption and inhibitive properties of clarithromycin for the corrosion of Zn in 0.01 to 0.05 M H₂SO₄*. Portugaliae Electrochemical Acta. 2009;27(6):713-24.

350. Guruprasad AM, Sachin HP, Swetha GA, Prasanna BM. *Adsorption and inhibitive properties of seroquel drug for the corrosion of zinc in 0.1 M hydrochloric acid solution*. International Journal of Industrial Chemistry. 2019;10(1):17-30.
351. Harvey TJ, Walsh FC, Nahlé AH. *A review of inhibitors for the corrosion of transition metals in aqueous acids*. Journal of Molecular Liquids. 2018; 266:160-75.
352. Prabhu RA, Venkatesha TV, Praveen BM, Chandrappa KG, Abd Hamid SB. *Inhibition effect of Azadirachta indica, a natural product, on the corrosion of zinc in hydrochloric acid solution*. Transactions of the Indian Institute of Metals. 2014;67(5):675-9.
353. Hebbar N, Praveen BM, Prasanna BM, Venkatesha VT. *Inhibition effect of an anti-HIV drug on the corrosion of zinc in acidic medium*. Transactions of the Indian Institute of Metals. 2015;68(4):543-51.
354. Nasab SG, Yazd MJ, Semnani A, Kahkesh H, Rabiee N, Rabiee M, Bagherzadeh M. *Natural corrosion inhibitors*. Synthesis Lectures on Mechanical Engineering. 2019;14(1):1-96.
355. Salih AO, Zakria BA, Salah IM, Taha M, Mohammed BA. *Determination the Effective of Grain Size on Gold Recovery by Integral of Sieve Analysis and Atomic Absorption Spectroscopy Methods*. Science. 2018;6(2):12-20.
356. Iroha NB, Maduelosi NJ. *Corrosion inhibitive action and adsorption behaviour of justicia secunda leaves extract as an eco-friendly inhibitor for aluminium in acidic media*. Biointerface Research in Applied Chemistry. 2021;11:13019-30.
357. El-Haddad MN, Fouda AS. *Electroanalytical, quantum and surface characterization studies on imidazole derivatives as corrosion inhibitors for aluminum in acidic media*. Journal of Molecular Liquids. 2015; 209:480-6.
358. Ashassi-Sorkhabi H, Asghari E. *Electrochemical corrosion behavior of Al7075 rotating disc electrode in neutral solution containing l-glutamine as a green inhibitor*. Journal of Applied Electrochemistry. 2010;40(3):631-7.
359. Mostafa MA, Ashmawy AM, Reheim MA, Bedair MA, Abuelela AM. *Molecular structure aspects and molecular reactivity of some triazole derivatives for corrosion inhibition of aluminum in 1 M HCl solution*. Journal of Molecular Structure. 2021; 1236:130292.
360. Wei X, Dong C, Chen Z, Xiao K, Li X. *A DFT study of the adsorption of O₂ and H₂O on Al (111) surfaces*. RSC Advances. 2016;6(61):56303-12.
361. Kresse G, Furthmuller J. *VASP the Guide*. Vienna University of Technology, Vienna; 2001.

362. Guo FY, Long CG, Zhang J, Zhang Z, Liu CH, Yu K. *Adsorption and dissociation of H₂O on Al (1 1 1) surface by density functional theory calculation*. Applied Surface Science. 2015; 324:584-9.
363. Hermann K, Bagus PS, Bauschlicher Jr CW. *Adsorption of ammonia on the Al (111) surface: Theoretical studies*. Physical Review B. 1985;31(10):6371.
364. Komrowski AJ, Ternow H, Razaznejad B, Berenbak B, Sexton JZ, Zoric I, Kasemo B, Lundqvist BI, Stolte S, Kleyn AW, Kummel AC. *Dissociative adsorption of NO upon Al (111): Orientation dependent charge transfer and chemisorption reaction dynamics*. The Journal of Chemical Physics. 2002;117(18):8185-9.
365. Blomqvist J, Salo P. *Adsorption of benzene, phenol, propane and carbonic acid molecules on oxidized Al (111) and α -Al₂O₃ (0001) surfaces: A first-principles study*. Journal of Physics: Condensed Matter. 2009;21(22):225001.
366. Ustinova EA, Shcheka OL, Ustinov AY. *Theoretical study of aluminum oxide interaction with CO*. Pacific Science Review. 2012;14(3):308-12.
367. Kandalam AK, Pandey R, Blanco MA, Costales A, Recio JM, Newsam JM. *First principles study of polyatomic clusters of AlN, GaN, and InN. 1. Structure, stability, vibrations, and ionization*. The Journal of Physical Chemistry B. 2000;104(18):4361-7.
368. Kubicki JD, Apitz SE. *Molecular cluster models of aluminum oxide and aluminum hydroxide surfaces*. American Mineralogist. 1998;83(9-10):1054-66.
369. Ye C, Ju X, Zhao F, Xu S. *Adsorption and Decomposition Mechanism of 1, 1-Diamino-2, 2-dinitroethylene on Al (111) Surface by Periodic DFT Calculations*. Chinese Journal of Chemistry. 2012;30(10):2539-48.
370. Ebenso EE, Obot IB, Murulana LC. *Quinoline and its derivatives as effective corrosion inhibitors for mild steel in acidic medium*. International Journal of Electrochemistry. 2010; 5:1574-86.
371. Murulana LC, Nesane T, Kabanda MM, Olasunkanmi LO, Ebenso EE. *Electrochemical And DFT Investigations of Anticorrosive Potentials of Selected Sulphonamides Based on Adsorption at Aluminium/Aqueous Acid Interface*.